

**MULTIPLE INTRUSION AND DEFORMATION WITHIN  
THE NORTHWESTERN QUADRANT OF THE PLUTONIC  
COMPLEX, TROODOS OPHIOLITE, CYPRUS**

**CENTRE FOR NEWFOUNDLAND STUDIES**

**TOTAL OF 10 PAGES ONLY  
MAY BE XEROXED**

**(Without Author's Permission)**

**SHERRY MARY DUNSWORTH, B.Sc.Honours**





National Library  
of Canada

Bibliothèque nationale  
du Canada

Canadian Theses Service

Service des thèses canadiennes

Ottawa, Canada  
K1A 0N4

## NOTICE

The quality of this microform is heavily dependent upon the quality of the original thesis submitted for microfilming. Every effort has been made to ensure the highest quality of reproduction possible.

If pages are missing, contact the university which granted the degree.

Some pages may have indistinct print especially if the original pages were typed with a poor typewriter ribbon or if the university sent us an inferior photocopy.

Reproduction in full or in part of this microform is governed by the Canadian Copyright Act, R.S.C. 1970, c. C-30, and subsequent amendments.

## AVIS

La qualité de cette microforme dépend grandement de la qualité de la thèse soumise au microfilmage. Nous avons tout fait pour assurer une qualité supérieure de reproduction.

S'il manque des pages, veuillez communiquer avec l'université qui a conféré le grade.

La qualité d'impression de certaines pages peut laisser à désirer, surtout si les pages originales ont été dactylographiées à l'aide d'un ruban usé ou si l'université nous a fait parvenir une photocopie de qualité inférieure.

La reproduction, même partielle, de cette microforme est soumise à la Loi canadienne sur le droit d'auteur, S.R.C. 1970, c. C-30, et ses amendements subséquents.



National Library  
of Canada

Bibliothèque nationale  
du Canada

Canadian Theses Service    Service des thèses canadiennes

Ottawa, Canada  
K1A 0N4

The author has granted an irrevocable non-exclusive licence allowing the National Library of Canada to reproduce, loan, distribute or sell copies of his/her thesis by any means and in any form or format, making this thesis available to interested persons.

The author retains ownership of the copyright in his/her thesis. Neither the thesis nor substantial extracts from it may be printed or otherwise reproduced without his/her permission.

L'auteur a accordé une licence irrévocable et non exclusive permettant à la Bibliothèque nationale du Canada de reproduire, prêter, distribuer ou vendre des copies de sa thèse de quelque manière et sous quelque forme que ce soit pour mettre des exemplaires de cette thèse à la disposition des personnes intéressées.

L'auteur conserve la propriété du droit d'auteur qui protège sa thèse. Ni la thèse ni des extraits substantiels de celle-ci ne doivent être imprimés ou autrement reproduits sans son autorisation.

ISBN 0-315-59234-6

Canada



MULTIPLE INTRUSION AND DEFORMATION WITHIN THE  
NORTHWESTERN QUADRANT OF THE PLUTONIC COMPLEX,  
TROODOS OPHIOLITE, CYPRUS

BY

Copyright © Sherry Mary Dunsworth, B.Sc. Honours

A thesis submitted to the School of Graduate

Studies in partial fulfillment of the

requirements of the degree of

Masters of Science

Department of Earth Sciences

Memorial University of Newfoundland

January, 1989

St. John's

Newfoundland



### FRONTISPIECE

View south from the village of Kakopetria towards Mount Olympus and the north end of the Troodos study area. The Cyprus weather and communications station is visible at the right hand side of the photograph.

**ABSTRACT**

Detailed geological mapping (1:5,000) of a 16 sq. km. area was completed within the northwestern quadrant of the Troodos plutonic complex, Cyprus. The plutonic complex incorporates an older, high-temperature deformed sequence of harzburgite, dunite, transition zone orthopyroxenite and layered olivine and hypersthene gabbro that is intruded and truncated/disrupted by a series of post-kinematic ultramafic-mafic (i.e.: wehrlite, feldspathic-wehrlite, lherzolite, feldspathic-lherzolite, clinopyroxenite, websterite and pyroxene-hornblende gabbro) plutons. Post-kinematic mafic dikes intrude both the older and younger magmatic suites, marking the final stage of magmatism within this section of the ophiolite.

A penetrative, steep to subvertical regional  $S_1$  foliation, traced intermittently from the harzburgite tectonite into portions of the layered olivine gabbro tectonite, is coaxial to large scale infolding of the dunite-harzburgite boundary. An equant granoblastic to porphyroclastic microfabric prevails in the harzburgite, dunite and transition zone lithologies whereas the layered gabbro exhibits both primary cumulate igneous and secondary ductile deformation textures. The structurally highest position of the high-temperature ductile deformation, termed the deformation front and marked by the transition from ductile to brittle deformation mechanisms, occurs within the layered olivine gabbro of the Troodos plutonic complex.

The plutons of the younger suite represent variable sized, spatially and temporally distinct, fault-controlled magma chambers that are focused primarily along the transition zone of the older suite. Most of the older suite transition zone orthopyroxenite and part of both the dunite and layered gabbro have been removed through faulting and intrusion of the younger suite plutons.

The fractional crystallization sequence of the older suite layered gabbro and the younger suite ultramafic-mafic lithologies is olivine -> clinopyroxene -> orthopyroxene -> plagioclase -> +/- hornblende (+/- quartz). Textural features

#### IV

indicate simultaneous crystallization of the pyroxene phases within the gabbroic units. Electron microprobe studies indicate that the younger and older suites cannot be distinguished on the basis of their respective mineral chemistry, that fractionation trends occur within both the younger and older suites and that cryptic chemical layering cannot be detected over a 20 m section of the layered olivine gabbro. The mafic dikes exhibit a tholeiitic affinity (island-arc tholeiite) and an extremely depleted, Mg-rich and Ti-poor chemistry correlative with the depleted upper pillow lava suite and indicative of derivation from a residual mantle source that had undergone previous partial melting and melt extraction event(s).

A dynamic crustal accretionary history consisting of multiple intrusion and ductile-brittle deformation is established for the Troodos plutonic complex. The geometrical relations between the penetrative regional foliation, infolding along the paleo-Moho and orientation of the enveloping surface of this folded dunite-harzburgite boundary at a high-angle to the regional foliation suggest that the Troodos ophiolite may represent a segment of diapirically flowing asthenosphere in an ancient ocean spreading region.



## ACKNOWLEDGMENTS

I would like to take this opportunity to thank a number of people who have helped me during the course of this study.

My sincere thanks to Drs. J. Malpas and T. Calon of Memorial University; for the geological discussions, financial assistance and critical reviews of draft versions of the thesis.

My gratitude is extended to Dr. Costas Xenophontas and Costas Stravides of the Cyprus Geological Survey Department for their friendship and dependable assistance with the logistics of the field work.

Funding for the project was provided by the Cyprus Crustal Study Project and a Memorial University Graduate Student Fellowship.

Thanks are also extended to Dr. Henry Longerich and Dave Press for instruction in the use of the analytical equipment; Wilf Marsh for assistance with the photographic reproduction; Brenda Jones for typing of the Appendices; and Ingrid Penney for help with the drafting of the figures. Kathy Gillis and Gunter Suhr are thanked for the helpful discussions and suggestions. Most sincere thanks and good wishes are extended to the special people of Mitsero village who made me feel warm and welcome in their homes and community. My stay in Cyprus a very special experience which I will always treasure.

My deepest thanks are reserved for my dear friend and husband, Jamie Meyer; who offered unlimited support and encouragement throughout the "ups and downs" of the project. Thanks Jamie!

## Table of Contents

<b>1. <u>INTRODUCTION</u></b>	<b>1</b>
1.1. <u>A Geographical and Political Perspective</u>	1
1.2. <u>Regional Geology of Cyprus</u>	1
1.2.1. The Kyrenia Range	4
1.2.2. The Mesaoria Plain	5
1.2.3. The Troodos Ophiolite Complex, The Limassol Forest and The Akamas Peninsula	6
1.2.4. The Mamonia Complex	10
1.3. <u>Regional Tectonic Setting of the Troodos Ophiolite</u>	13
1.4. <u>Review of Previous Work for the Troodos Ophiolite</u>	15
1.4.1. Origin and Formational Setting	15
1.4.2. Emplacement and Tectonic Disruption	17
1.4.3. The Plutonic Complex	19
1.4.4. The Volcanic Sequence	22
1.4.5. Solid State Deformation	23
1.4.6. Metamorphism	24
1.4.7. Geophysics	25
1.5. <u>Aims and Logistics of the Present Study</u>	26
<b>2. <u>FIELD RELATIONS</u></b>	<b>29</b>
2.1. <u>The Northwestern Quadrant of the Plutonic Complex : A Geological         Overview</u>	29
2.2. <u>The Older Suite</u>	32
2.2.1. Upper Mantle-Lower Metacumulate Units	33
2.2.1.1. Harzburgite Tectonite	37
2.2.1.2. Chromitite	40
2.2.1.3. Dunite	42
2.2.2. The Transition Zone	45
2.2.3. The Older Suite Gabbros	47
2.2.3.1. Layered Olivine Gabbro	49
2.2.3.2. Layered to Massive Hypersthene Gabbros	52
2.2.3.3. High Level-Massive Gabbros	52
2.3. <u>The Younger Intrusive Suite(s)</u>	57
2.3.1. Primary Features of the Younger Suites	57
2.3.2. Spatial Distribution and Contact Relations Between the Older and Younger Magmatic Suites	61

2.3.3. Spatial and Temporal Relations of Multiple Intrusion within the Younger Suites	66
2.3.4. Fault Controlled Intrusion of the Younger Suite in Relation to the Deformation Front	72
2.3.5. The Mafic Dikes	74
2.4. <u>Summary and Discussion</u>	75
<b>3. <u>STRUCTURE: MEGA-, MESO- AND MICROSCOPIC FEATURES</u></b>	<b>81</b>
3.1. <u>Introduction</u>	81
3.2. <u>Megascopic Structural Trends</u>	82
3.3. <u>Mesosopic Structural Features of the Older Suite</u>	86
3.3.1. Harzburgite	86
3.3.2. Dunite and Transition Zone Orthopyroxenite	88
3.3.3. High Temperature Deformation Features of the Layered Gabbros	88
3.4. <u>Position of the Ductile-Brittle Transition within the Layered Gabbros</u>	93
3.5. <u>Microfabrics and Mechanisms of High-Temperature, Ductile Deformation within Ultramafic-Mafic Rocks under Upper-Mantle/Lower Crustal Conditions : An Overview.</u>	97
3.5.1. Introduction	97
3.5.2. Ductile Deformation Theory	98
3.5.3. Microfabrics of the Principal Mineral Phases within Plastically Deformed Ultramafic-Mafic Rocks	101
3.6. <u>Microscopic Textural Features and Terminology of the Cumulate Mafic-Ultramafic Rocks</u>	103
3.7. <u>Microfabrics of the Tectonized Older Suite Lithologies</u>	107
3.7.1. Upper Mantle - Lower Crustal Peridotite Tectonites	108
3.7.2. Transition Zone Peridotites : A Case for Recrystallization via Subgrain Rotation Mechanism	110
3.8. <u>Layered Mafic Cumulates/Metacumulates</u>	116
3.8.1. Layered Olivine Gabbro	116
3.8.2. Layered Hypersthene Gabbro	121
3.8.3. Tectonized versus Undeformed Layered Gabbro	122
3.8.4. Fractional Crystallization Sequence for the Layered Gabbros	127
3.9. <u>Microscopic Evidence of Multiple Intrusion within the Troodos Plutonic Complex</u>	129
3.10. <u>Summary</u>	132
<b>4. <u>PETROGRAPHY AND CHEMISTRY</u></b>	<b>136</b>
4.1. <u>Petrography of the Younger Suite Intrusives</u>	136
4.1.1. The Ultramafic Cumulates	136
4.1.2. The Mafic Cumulates	141
4.1.3. Fractional Crystallization Sequence of the Younger Suite Intrusives	142

4.2. <u>Mineral Chemistry</u>	142
4.2.1. Fractionation Trends within the Younger Suite Plutons	143
4.2.2. Fractionation Trends within the Older Suite Gabbro	144
4.2.3. Geochemical Comparison of the Older and Younger Suites	146
4.2.4. Summary and Discussion	154
4.3. <u>Petrography and Geochemistry of the Mafic Dikes</u>	156
4.4. <u>Mineral Chemistry of a Section through the Layered Olivine Gabbro</u>	168
5. <u>SUMMARY OF CONCLUSIONS</u>	180
<u>BIBLIOGRAPHY</u>	192
<u>APPENDICES</u>	212
A. <u>Layered Olivine Gabbro Section - Microprobe Analyses</u>	
A.1 Clinopyroxene	212
A.2 Orthopyroxene	217
A.3 Plagioclase	218
A.4 Olivine	222
A.5 Zoning Data	224
B. <u>Microprobe Analyses of Mineral Phases from the Older Suite Layered Olivine and Hypersthene Gabbro and Transition Zone</u>	
B.1 Layered Olivine Gabbro	
B.1.1 Clinopyroxene	226
B.1.2 Orthopyroxene	229
B.1.3 Olivine	230
B.1.4 Plagioclase	232
B.2 Layered Hypersthene Gabbro	
B.2.1 Clinopyroxene	233
B.2.2 Orthopyroxene	238
B.2.3 Plagioclase	240
B.3 Transition Zone	
B.3.1 Orthopyroxene	241
B.3.2 Olivine	244
B.3.3 Clinopyroxene	245
C. <u>Microprobe analyses of Mineral Phases from the Younger Suite Wehrlite-Lherzolite, Pyroxenite and Gabbro</u>	
C.1 Wehrlite-Lherzolite	
C.1.1 Olivine	246
C.1.2 Clinopyroxene	249
C.1.3 Orthopyroxene	254
C.1.4 Plagioclase	256
C.2 Pyroxenite	
C.2.1 Clinopyroxene	257
C.2.2 Orthopyroxene	260
C.2.3 Olivine	262
C.2.4 Plagioclase	263



C.3 Gabbro	
C.3.1 Plagioclase	264
C.3.2 Clinopyroxene	265
C.3.3 Orthopyroxene	266
C.3.4 Hornblende	267
D. <u>Microprobe Analyses of Amphibolite Phase from the Mafic Dikes</u>	268
E. <u>Major and Trace Element Analyses of the Mafic Dikes</u>	
E.1 Major Elements	269
E.2 Trace Elements	271
F. <u>Analytical Equipment</u>	274

## List of Figures

<b>Figure 1-1:</b>	Location map for the island of Cyprus, situated within the eastern extremity of the Mediterranean Sea.	2
<b>Figure 1-2:</b>	Geographical distribution of the four major, east-west trending lithotectonic zones which comprise the island of Cyprus.	3
<b>Figure 1-3:</b>	Distribution of Tethyan ophiolite massifs along the more than 8,700 km long, east-west trending Tethyan Belt (after Searle, 1980).	14
<b>Figure 1-4:</b>	Schematic model for the formation of the Troodos ophiolite in a short spreading segment above a subduction zone and a collision with a small microcontinent (after Moores <i>et al.</i> 1984).	18
<b>Figure 2-1:</b>	The 45° east-dipping, normal fault contact between west-dipping older suite layered gabbro (LG) and east-dipping sheeted dikes (SD) in the Esso-Galata region.	34
<b>Figure 2-2:</b>	Fold hinge of isoclinally folded chromite layer along the harzburgite-dunite boundary near Kokkinorotsos. A strong axial planar $S_1$ is defined by elongate chromite grains.	36
<b>Figure 2-3:</b>	Compositional layering in harzburgite defined by metamorphic segregation of the olivine and orthopyroxene phases into bands orientated parallel to the regional foliation. Elongate/flattened orthopyroxene grains define the $S_1$ fabric.	38
<b>Figure 2-4:</b>	Coarse to pegmatitic isotropic pyroxene gabbro vein invading harzburgite near the harzburgite-dunite boundary.	39
<b>Figure 2-5:</b>	Angular harzburgite breccia fragments within a magnesite matrix in outcrop exposed along the chromite mine road.	41
<b>Figure 2-6:</b>	Massive to nodular "leopard type" chromite hosted by massive dunite located northeast of Kokkinorotsos.	42
<b>Figure 2-7:</b>	Clinopyroxene oikocrysts enclosing partially resorbed and rounded olivine chadacrysts within undeformed (younger suite) clinopyroxene-dunite.	43
<b>Figure 2-8:</b>	Layered orthopyroxenite of the older suite transition zone exposed in roadcut along Pine Road.	46

- Figure 2-9:** A dike of coarse to pegmatitic, undeformed clinopyroxenite (CPX) of the younger intrusive suite invading and truncating the  $S_0/S_1$  of the older suite transition zone (TZ) orthopyroxenite. 48
- Figure 2-10:** Prominent rhythmic phase layering of olivine and minor hypersthene gabbro exposed in roadcut to the north of the Eso Galata River. The  $S_0/S_1$  dips consistently  $35^\circ$ - $45^\circ$  to the southwest. View structural down-section. 50
- Figure 2-11:** Primary flow structures in layered olivine gabbro. Note the well preserved cross laminations and truncation of the phase layering. 51
- Figure 2-12:** Primary magmatic flow structures in layered hypersthene gabbro showing well preserved cross laminations and truncation of phase layering. 53
- Figure 2-13:** Vari-textured gabbros of the older suite showing abrupt truncation of  $S_0$  and  $S_1$  of the layered olivine gabbro by an isotropic, coarse grained phase of olivine-pyroxene gabbro. 54
- Figure 2-14:** The foliation/layering within tectonized olivine gabbro truncated by the multiple intrusion of isotropic, fine grained melanocratic gabbro dikes. Note the abrupt truncation of the  $S_1/S_0$  and contact reactions marked by coarse pyroxene-gabbro margins. 55
- Figure 2-15:** Tectonized olivine gabbro with  $S_0/S_1$  truncated by coarse, isotropic pyroxene gabbro of either the younger or older suite(s). 56
- Figure 2-16:** Intrusion and net veining of trondhjemite into weakly phase layered hypersthene gabbro. 58
- Figure 2-17:** Angular blocks (xenoliths) of vaguely phase layered hypersthene gabbro backveined and brecciated by gabbro and plagiogranite. 59
- Figure 2-18:** Large ( $>3$  cm.) orthopyroxene oikocryst with rounded olivine chadacrysts from the main wehlite intrusion. Note the unstrained optical continuity across the reflecting surface of the oikocryst and the spongy, pitted appearance on weathered surfaces (lower right corner). 60
- Figure 2-19:** Subvertical primary igneous layering within younger suite clinopyroxenite exposed along the highway from Mount Olympus to Prodhromos. 62
- Figure 2-20:** Simplified geological map of the northwestern quadrant of the Troodos plutonic complex showing zones of younger suite intrusion. Legend and symbols as in MAP 1. 63

- Figure 2-21:** Large dike intrusion of coarse to pegmatitic pyroxene-hornblende gabbro (G) into massive dunite (D). Note the intense serpentinization (dark gray) along the contact margins. 64
- Figure 2-22:** Younger suite feldspathic-lherzolite intruding and truncating west dipping layered olivine gabbro near the fault contact with the sheeted dike complex. Symbols: blue = sheeted dikes; red = layered gabbro; orange = intrusive. 67
- Figure 2-23:** Younger suite wehrlite sill intruding concordantly/subconcordantly to the fabric elements in the host layered gabbro. The sill varies in true thickness from 30 to 100 m. Symbols as in Fig. 2.22. 68
- Figure 2-24:** Truncation of layered gabbro by the intrusion of massive, poikilitic and locally banded wehrlite-lherzolite (+ plagioclase) of the main intrusive zone (Zone 1). Symbols: red = layered gabbro; orange-yellow = younger intrusive; blue = trondjemite. 69
- Figure 2-25:** Alignment of elongate and tectonized older suite olivine gabbro xenoliths (OLG) within the younger suite wehrlite intrusion (W) as exposed along Cherry Brook. 70
- Figure 2-26:** Lower hemisphere, equal area projection of 34 poles to the mafic dikes. 75
- Figure 2-27:** Mafic dikes (light green) intruding vari-textured hypersthene gabbro (tan-gray) in roadcut exposure. Note the offshoots of thin dikes from the main dike into the gabbro. The dike is offset by minor faults. 76
- Figure 3-1:** Lower hemisphere, equal area projection of 148 poles to the harzburgite foliation and 5 poles to the dunite foliation. 83
- Figure 3-2:** Lower hemisphere, equal area projection of the poles to the foliation in the layered olivine gabbro. 84
- Figure 3-3:** Lower hemisphere, equal area projection of the poles to the layering/foliation in the layered hypersthene gabbro. 85
- Figure 3-4:** Foliation ( $S_1$ ) in harzburgite defined by the alignment of flattened orthopyroxene grains and aggregates (parallel to the pencil). 87
- Figure 3-5:** Strongly foliated/layered olivine gabbro. The  $S_1$  fabric is defined by the preferred orientation of flattened olivine, pyroxene and plagioclase phases in hand sample. 89
- Figure 3-6:** Tectonized, layered olivine gabbro showing strong alignment of inequant olivine, pyroxene and plagioclase grains parallel to the  $S_0/S_1$ . Note the tapering of layers along strike and possible fold hinges. 90



- Figure 3-7:**  $F_1$  fold hinge of isoclinally folded layered olivine gabbro with axial planar  $S_1$  foliation. 91
- Figure 3-8:** Primary magmatic textures of the layered hypersthene gabbro showing slump folding of the rhythmic layering. 93
- Figure 3-9:** Schematic diagram showing the structurally highest position of the deformation front within the older suite layered gabbro. Note that the position of the front would have been lower in the section prior to intrusion/crystallization of the plutons of the younger suite. Refer to Section 3.4 for discussion. 95
- Figure 3-10:** Typical microstructures of ductilely deformed peridotites: A= Protogranular: no foliation, few kinkbands, undulose extinction; B= Porphyroclastic: kinkbanded and elongate porphyroclasts recrystallized in surrounding neoblasts; C-D= Granoblastic: complete recrystallization into either equant (C) or tabular (D) neoblasts (after Gueguen and Nicolas, 1980). 105
- Figure 3-11:** Deformed orthopyroxene porphyroclast (OPX) in harzburgite exhibiting a sharp kink-band boundary (east-west) and exsolution lamellae of clinopyroxene (CPX). Note the olivine (OL) inclusion in upper right corner of photo. Bar scale = 1 mm. 109
- Figure 3-12:** Equant, granoblastic olivine texture in dunite. Note the recrystallized olivine neoblasts with straight grain margins and triple point junctions. Bar scale = 1 mm. 111
- Figure 3-13:** Equant, granoblastic texture of the recrystallized orthopyroxene (OPX) phase from the Transition Zone. Note the interstitial clinopyroxene (CPX). Bar scale = 1 mm. 112
- Figure 3-14:** Relict laths (porphyroclasts) of orthopyroxene, up to 1.3mm in length, exhibiting weakly undulose extinction and surrounded by a mortar texture of equant orthopyroxene neoblasts. Bar scale = 1 mm. 113
- Figure 3-15:** Orthopyroxene porphyroclast exhibiting development of undulose extinction and distinct equant subgrains (top right corner) in which adjacent subgrain walls (crystal lattice) are offset a few degrees ( $\sim 2^\circ$ ). Bar scale = 1 mm. 114
- Figure 3-16:** Elongate olivine (OL) grain, 10 mm in length with aspect ratios in excess of 14:1, defines the foliation in olivine layered gabbro tectonite (ppl). Olivine = OL, Orthopyroxene = OPX, Clinopyroxene = CPX, Plagioclase = Pl. Bar scale = 1 mm. 117
- Figure 3-17:** The attenuated olivine grain shown in Fig. 3.19 is 118

- composed of elongate subgrains and equant neoblasts with straight grain margins and undulose extinction (cross nicols). Bar scale = 1 mm.
- Figure 3-18:** Equant olivine neoblasts from a section of the olivine layered gabbro exhibiting straight grain boundaries, triple point junctions and undulose extinction. Bar scale = 1 mm. 119
- Figure 3-19:** Recrystallized plagioclase (PL) neoblasts with triple point junctions and straight grain boundaries in an olivine layered gabbro tectonite. Bar scale = 1 mm. 120
- Figure 3-20:** Mesocumulate texture of the layered hypersthene gabbro with alignment of plagioclase (PL) and pyroxene (PX) laths with cleavage and twin traces parallel to the phase layering. Bar scale = 1 mm. 121
- Figure 3-21:** Contact between recrystallized (polygonalized) orthopyroxenite transition zone (lower right corner) and the coarse, weakly undulose to undeformed, isotropic younger suite clinopyroxenite. Note the orthopyroxene neoblasts along grain margins and as inclusions within the younger clinopyroxene grains. Bar scale = 1mm. 130
- Figure 3-22:** Gradational contact between the older transition zone orthopyroxenite and younger suite clinopyroxenite. Note the polygonalized orthopyroxene neoblasts along the margins and enclosed within the undeformed clinopyroxene grains. Bar scale = 1 mm. 131
- Figure 4-1:** Poikilitic wehrlite with large, unstrained orthopyroxene oikocrysts and partially resorbed serpentinized olivine chadacrysts. Bar scale = 1 mm. 138
- Figure 4-2:** Pyroxene grains from the younger suite clinopyroxenite showing a medium-coarse grain size, flat to weakly undulose extinction, equant habit and interlocking grain boundaries. Bar scale = 1 mm. 139
- Figure 4-3:** Extensive subgrain and kink band (KBB) development in large (<4mm) olivine (OL) grains from the feldspathic-wehrlite of ZONE 2. Note the plagioclase (PL) and orthopyroxene (OPX) inclusions within the olivine. Bar scale = 1 mm. 140
- Figure 4-4:** Part of the pyroxene quadrilateral showing analyses of pyroxenes from the the older suite transition zone and younger suite clinopyroxenite and gabbroic intrusives. 144
- Figure 4-5:** Part of the pyroxene quadrilateral showing analyses of pyroxenes from the younger suite ultramafic lithologies. 145
- Figure 4-6:** Part of the pyroxene quadrilateral showing analyses of pyroxenes from the older suite layered olivine and hypersthene gabbros. 146

- Figure 4-7:** Plagioclase (An mol %) mineral analyses for samples from both the older and younger suites. 147
- Figure 4-8:** Na versus Mg\* values of the clinopyroxene phase from both the younger suite intrusives and older suite layered gabbro. Fields A and B are discussed in the text. 149
- Figure 4-9:** Ti versus Mg\* content of the clinopyroxene phase from both the younger suite intrusives and older suite layered gabbro. 150
- Figure 4-10:** Ti versus Cr content of the clinopyroxene phase in the younger suite intrusives and older suite layered gabbros. 151
- Figure 4-11:** Plot of NiO versus Forsterite (Fo) for olivines from the older suite layered olivine gabbro and younger suite ultramafic-mafic cumulates. Symbols as in Fig. 4.8. Early cumulate suite (ECS) and Late cumulate suite (LCS) fields after Benn and Laurent (1987). 152
- Figure 4-12:** Plot of  $\text{Cr}_2\text{O}_3$  versus  $\text{Mg}/(\text{Mg}+\text{Fe}(\text{total}))$  in clinopyroxene from the older suite layered gabbro and younger suite ultramafic-mafic cumulates. Symbols as in Fig. 4.8. Early cumulate suite (ECS) and Late cumulate suite (LCS) fields after Benn and Laurent (1987). 153
- Figure 4-13:** Olivine (Fo) values for the older suite layered olivine gabbro and the younger suite ultramafic intrusives. 154
- Figure 4-14:** Total alkalis versus silica variation diagram for mafic dike (●) and sheeted dike (Δ) samples. Limassol Forest mafic-dike sample is marked as (○). Heavy line is alkalic - tholeiitic division line as defined by MacDonald and Katsura (1964). Dashed line defines the Troodos sheeted dike complex (after Moores and Vine, 1971. Dotted line defines the CY-2A field (from Bednarz *et al.*, 1987). 158
- Figure 4-15:** Bulk rock compositions of the Troodos mafic dikes (●), Limassol Forest mafic dike (○) and sheeted dike (Δ) samples plotted on the AFM diagram. Hawaiian alkaline and tholeiite trends from Malpas (1978). Dashed field delineates Papuan basalts and Oman and Bay of Islands diabase. Dotted field delineates Papuan gabbro. Dot-dash field delineates CY-2A samples (from Bednarz *et al.*, 1987). 159
- Figure 4-16:** Cr versus Y variation diagram (after Pearce, 1975) for the Troodos dikes. Symbols as in Figure 4.12. Fields of magma composition occupied by basalt of the mid-ocean ridge (MORB) and island arc tholeiite (IAT) affinities after Pearce (1980). Solid line delineates field of basalts from the Oman ophiolite (after Alabaster, 1982) while dot-dash line delineates Cy-2A samples (from Bednarz *et al.*, 1987). 161

- Figure 4-17:** Ti versus Cr variation diagram (after Pearce, 1975) for the Troodos dikes. Symbols as in Figure 4.12. Heavy line separates ocean-floor (MORB) from low-potassium tholeiite (LKT) affinities. Dash line delineates the field of the Troodos upper pillow lavas and dotted line represents the field of the Troodos sheeted dikes and lower pillow lavas (after Pearce, 1975). Dot-dash line delineates CY-2A samples (from Bednarz *et al.*, 1987). 162
- Figure 4-18:** Ti versus Zr variation diagram (after Pearce and Cann, 1973) for the Troodos mafic dike samples (●). Symbols as in Figure 4.12. Fields D and B = ocean floor basalts, A and B = island arc basalts, C and B = calc-alkali basalts. Fields of the Troodos upper pillow lavas and lower pillow lavas plus sheeted dikes delineated by dotted and dashed lines, respectively (after Pearce, 1975). Samples from CY-2A delineated by dot-dashed field (from Bednarz *et al.*, 1987). 163
- Figure 4-19:** MgO - FeO\* variation diagram (after Jakes and Gill, 1970) showing the mafic dike (●) and sheeted dike (Δ) samples from the present study in relation to the fields of the Troodos upper pillow lavas (dotted line) and lower pillow lavas (dashed line), Mariana Arc boninite suite (dot - dash line) and IAT trend (after Robinson *et al.*, 1983). The dot<sup>3</sup>-dashed line delineates the field of CY-2A samples (from Bednarz *et al.*, 1987). Averaged ultrabasic (⊠), komatiite (⊞), olivine basalt (⊡) and aphyric basalt (⊢) values from Malpas and Langdon (1984). 165
- Figure 4-20:** MgO - TiO<sub>2</sub> variation diagram of the Troodos mafic and sheeted dike samples. Symbols as in Figure 4.12. The fields of the upper pillow lavas (dotted line) and lower pillow lavas (dashed line) from Robinson *et al.*, 1983. Volcanic suites: A = Galapagos rift (Byerly *et al.*, 1976); B = Mariana back-arc basin (Wood *et al.*, 1980; Hart *et al.*, 1972); C = Tonga arc (Ewart and Bryan, 1972) and D = Mariana arc boninite suite (Meijer, 1980). The dot<sup>3</sup>-dashed field delineates the CY-2A samples (from Bednarz *et al.*, 1987). Dot-dashed field delineates the upper pillow lava suite of Malpas and Langdon (1984). 166
- Figure 4-21:** Plagioclase (An mol%) values over a 20 m section through the layered olivine gabbro. 170
- Figure 4-22:** Olivine (Fo mol%) values over a 20 m section through the layered olivine gabbro. 171
- Figure 4-23:** Olivine (MnO wt%) values over a 20 m section through the layered olivine gabbro. 172



<b>Figure 4-24:</b>	Olivine (NiO wt%) values over a 20 m section through the layered olivine gabbro.	173
<b>Figure 4-25:</b>	Clinopyroxene (Mg* mol%) values over a 20 m section through the layered olivine gabbro.	174
<b>Figure 4-26:</b>	Clinopyroxene (Cr* mol%) values over a 20 m section through the layered olivine gabbro.	175
<b>Figure 4-27:</b>	Clinopyroxene (Na <sub>2</sub> O wt%) values over a 20 m section through the layered olivine gabbro.	176
<b>Figure 4-28:</b>	Clinopyroxene (TiO <sub>2</sub> wt%) values over a 20 m section through the layered olivine gabbro.	177
<b>Figure 4-29:</b>	Clinopyroxene (MnO wt%) values over a 20 m section through the layered olivine gabbro.	178
<b>Figure 4-30:</b>	Orthopyroxene (Mg* mol%) values over a 20 m section through the layered olivine gabbro.	179
<b>Figure 5-1:</b>	Schematic section demonstrating the complex accretionary history of the northwestern Troodos plutonic complex.	189

## List of Tables

<b>Table 3-1:</b>	Classification Scheme of Ductile (Plastic) Deformation Textures in Upper Mantle-Lower Crustal Peridotites.	104
<b>Table 3-2:</b>	Common Textural Features of Cumulus Mineral Phases in Ultramafic-Mafic Rocks (after Jackson, 1961; 1971)	107
<b>Table 3-3:</b>	Shear Flow Stress Related Deformation Feature Developed in the Troodos Layered Gabbro Under Progressive Cooling/Crystallization Conditions.	126
<b>Table 3-4:</b>	Compositions (mol %) of Cumulus/Intercumulus Plagioclase and Plagioclase Inclusions in the Ortho/Clinopyroxene of the Layered Gabbros	128

# **Chapter 1**

## **INTRODUCTION**

### **1.1. A Geographical and Political Perspective**

The Troodos ophiolite complex, site of the field component for this thesis study, occupies the central highland region of the island of Cyprus. This island covers an area of 9,251 sq. km. and is geographically situated along the northeastern margin of the Mediterranean Sea. The closest neighbouring countries to Cyprus are Turkey located 70 km to the north and Syria-Lebanon located approximately 100 km to the east (Figure 1-1).

At the present time, political unrest has resulted in the division of Cyprus into two areas; the northern Turkish occupied region and the southern Greek Cypriot region. The borderland between the two states is presently patrolled by Greek, Turkish and United Nations troops. The Troodos complex is situated entirely within the Greek Cypriot territory.

### **1.2. Regional Geology of Cyprus**

The regional geology of Cyprus is described in terms of the four major east-west trending lithotectonic zones (Figure 1-2).

From north to south, these zones are identified as:

- (1) The Kyrenia (Pentadactylos) Range
- (2) The Mesaoria Plain
- (3) The Troodos Ophiolite Complex, The Limassol

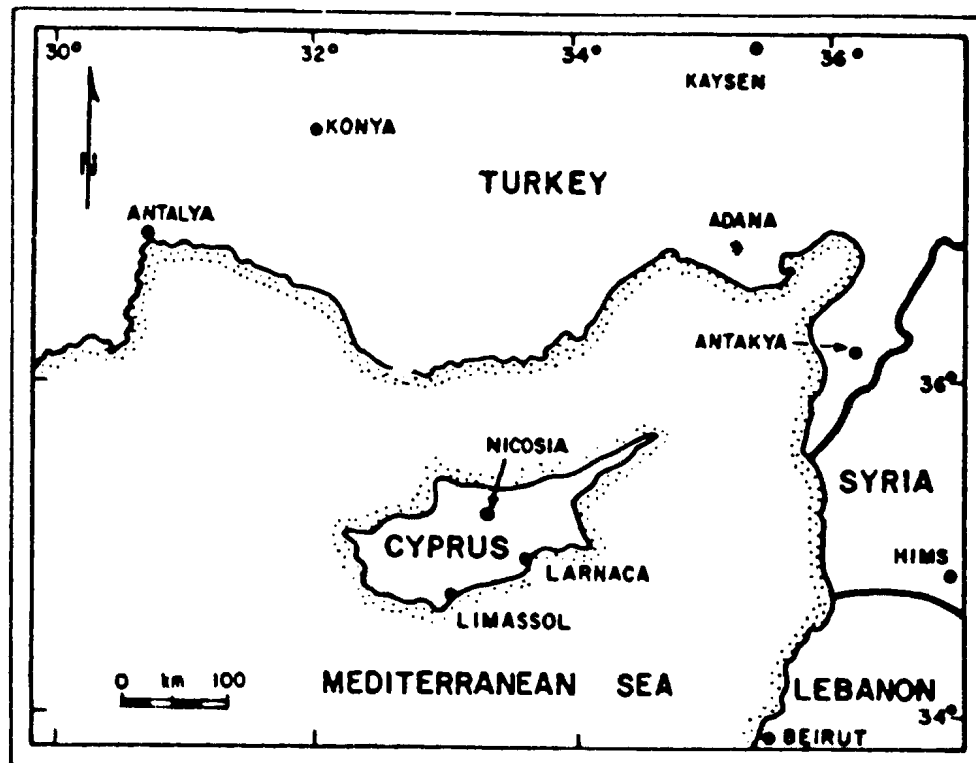


Figure I-1. Location map for the Island of Cyprus situated within the eastern extremity of the Mediterranean Sea .

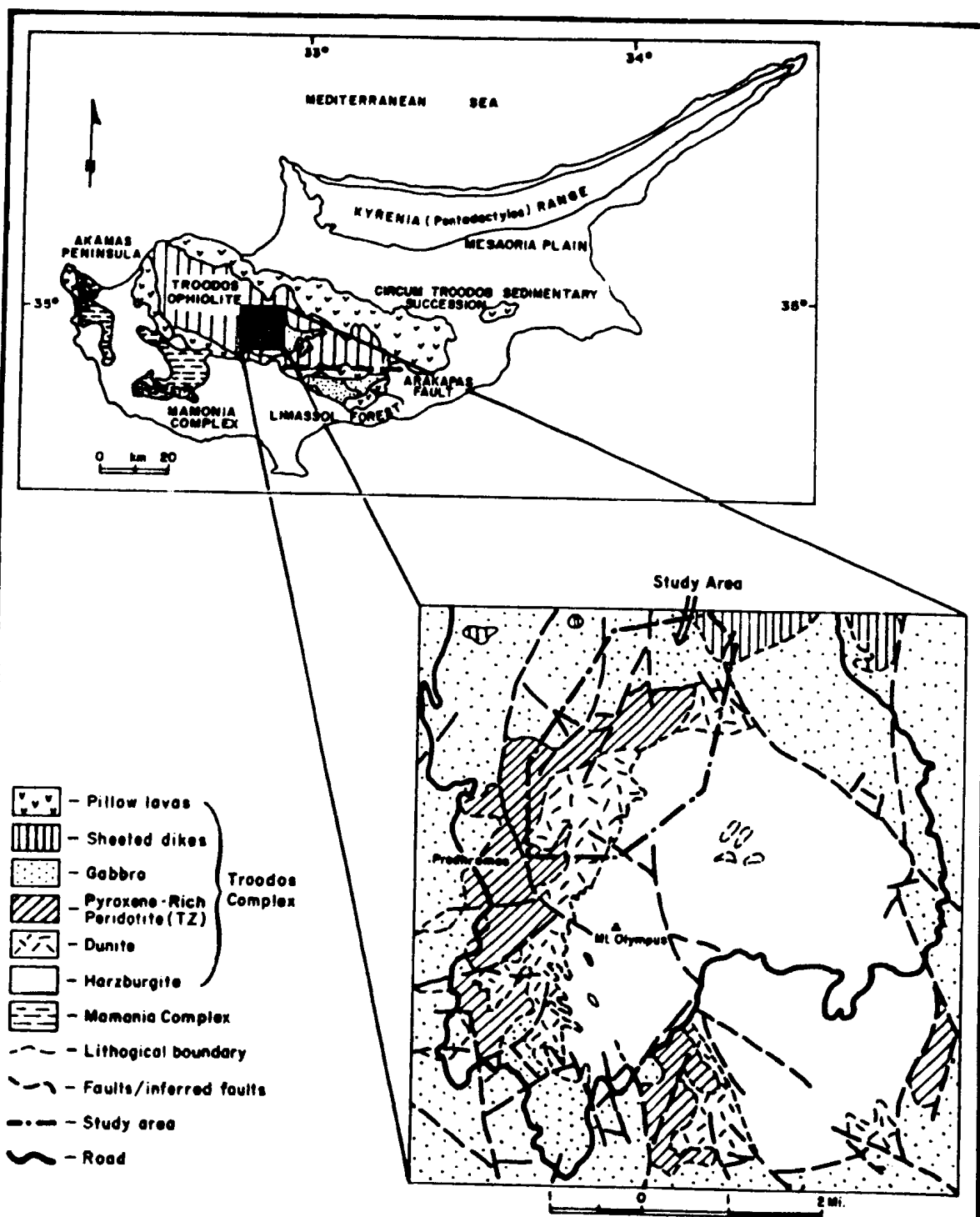


Figure 1-2. Geographical distribution of the four major, east-west trending lithotectonic zones which comprise the island of Cyprus (after Robertson and Woodcock, 1960, Goss, 1967) and geological sketch map of the Troodos massif showing lithological units (after Wilson, 1969) and location of the present study area.

## Forest and The Akamas Peninsula

### (4) The Mamonia Complex

#### 1.2.1. The Kyrenia Range

The mountainous Kyrenia Range rises to an elevation of 1000 m along the northern coastline of Cyprus. The range was first interpreted by Gass (1968) to represent the southernmost expression of the Tauro-Dinaric alpine belt which passes through Greece, Crete and southern Turkey.

The range consists of a series of fault-bounded blocks of Permian to upper Eocene, shallow-water, continental margin sediments with thin slivers of metamorphic rocks. The stratigraphy of the Kyrenia Range is tabulated as follows after Robertson and Woodcock (1980).

FORMATION	LITHOLOGY	AGE
Kalogrea-Ardana	Calcareous, sandy flysch and olistostrome melange	Middle to Upper Eocene
Ayios Nikolaos	Limestones, chert and interstratified volcanics	Palaeocene to Mid-Eocene
Melounda	Pelagic chalks	Maestrichtian
UNCONFORMITY		
Hilarion	Limestone	Jurassic
Sykhari	Dolomitic limestone	Upper Triassic
Dhikomo	Thin bedded marble	Lower-Upper Triassic
UNCONFORMITY		
Kantara	Massive limestone	Permian-Carboniferous

The volcanic suite of the Ayios Nikolaos Formation, occurring interstratified with the Maestrichtian to Palaeocene sediments, consists of two distinct lava types. The lavas of Maestrichtian age exhibit a calc-alkaline trend (Pearce, 1975; Baroz, 1980), while those of Palaeocene age show a characteristic shoshonitic trend (Baroz, 1980). Similar mature island arc, calc-alkaline and shoshonitic lavas occur within the present day Fiji Arc (Robertson, 1977; Baroz, 1980; Robertson and Woodcock, 1980).

Baroz (1980) suggested correlation of the Kyrenia Range island arc volcanic rocks with the similarly aged volcanic-sedimentary flysch (Kannaviou Formation) of island arc-trench origin (Robertson, 1977) which unconformably overlies the Troodos ophiolite. Volcanism within the Kyrenia Range has been attributed to the development of a northward-dipping subduction zone, located south of the range, immediately following obduction of the Troodos massif onto the African plate during Maestrichtian time.

Tectonic disruption of the Kyrenia Range by late Cretaceous to early Tertiary strike-slip faulting (Robertson and Woodcock, 1980), followed by southward thrusting in the Miocene (Baroz *et al.*, 1976), has resulted in the development of four major, steep northward-dipping, lenticular tectonic slices. Following the post-Oligocene development of the Kyrenia Range, the flanks of this allochthonous sequence were overlain by the 3000 m thick, mostly terrigenous Kythrea Flysch of middle Miocene age (Weiler, 1970; Baroz, 1980).

#### **1.2.2. The Mesaoria Plain**

The Mesaoria Plain occupies the central lowland region which separates the the Troodos ophiolite from the Kyrenia Range. The plain is underlain by a more than 4,000 m thick succession of upper Cretaceous to Pleistocene, deep water turbidites, flysch, carbonates and unconsolidated sediments. Towards the north, the upper Cretaceous to Miocene sediments of the Kythrea Flysch are highly deformed and folded, exhibiting a characteristically knobby, rolling topography.

Southward, the relatively undeformed Circum- Troodos Sedimentary Succession outcrops. These two regions are separated by the Ovgos Wrench Fault Zone (Bagnall, 1960).

The base of the Circum-Troodos Sedimentary Succession is delineated by the Campanian to Maestrichtian Perapedhi Formation (Wilson, 1959) which consists of thin, intermittent layers of amber and radiolarian mudstone which unconformably on-lap the extrusive sequence of the Troodos ophiolite. South of the Troodos massif, the Perapedhi Formation is conformably overlain by the Maestrichtian Kannaviou Formation (Lapierre, 1968), noted in the preceding page for its island arc related volcanogenic sediments and correlated with the Ayios Nikolaos formation (Baroz, 1980). Conformably up-section, the Palaeogene Lefkara Formation, consisting of calcareous pelagic sediments, is overlain by lower Miocene reef limestone of the Terra Formation, and middle Miocene chalky marls of the Pakha Formation. These marls are succeeded by a second unit of reef limestone represented by the upper Miocene Koronia Formation. The Koronia Formation limestone is succeeded by marls of the Pliocene Nicosia Formation which is followed by the upper Pliocene to lower Pleistocene biocalcarenes and poorly consolidated sands of the Athalassa Formation.

Erosional debris resulting from intense uplift of the Troodos massif at the beginning of the Pleistocene epoch yielded deposition of the thick, unsorted Conglomerate Formation over the plains bordering the northern margin of the Troodos massif (Wilson, 1959).

### **1.2.3. The Troodos Ophiolite Complex, The Limassol Forest and The Akamas Peninsula**

Ultramafic and mafic igneous (intrusive and extrusive) rocks outcrop within three regions of the island of Cyprus: (1) the Troodos Complex; (2) the Limassol Forest and Arakapas Fault Zone; and (3) the Akamas Peninsula.

#### **(1) The Troodos Ophiolite Complex**



The upper Cretaceous Troodos ophiolite forms an ellipsoidal domal structure which is exposed over an area of 2,300 sq km, rising to a maximum elevation of 1951 m, centered on Mount Olympus (Gass, 1968).

The Troodos complex was reported by Moores and Vine (1971) to be composed of a sequence of ultramafic-mafic plutonic rocks, overlain and intruded by swarms of diabase dikes and extrusive volcanic rocks. Thus, on the basis of the lithological components and stratigraphic succession, the Troodos massif fulfilled the definition of an ophiolite complex that was adopted by members of the Penrose Conference, 1972 (Geotimes, 1973).

Continuing uplift, in excess of 2000 m (Gass and Masson-Smith, 1963), and deep erosion of the Troodos ophiolite has yielded an annular pattern of outcrop exposure with the deepest stratigraphic levels of the ophiolite succession exposed within the highlands of the Troodos Forest area and successively higher stratigraphic levels outcropping at lower elevations around Mount Olympus.

Following the pioneering mapping of the Troodos ophiolite by Wilson (1959), the results of field mapping, petrological, geochemical and geophysical studies by numerous investigators (e.g.: Moores and Vine, 1971; Greenbaum, 1972A,B; Gass and Smewing, 1973; Menzies and Allen, 1974; Kidd and Cann, 1974; Allen, 1975; Robertson, 1975; 1976; Robertson and Woodcock, 1980; Gass, 1980 and Swarbrick, 1980) have yielded a model for generation of the Troodos ophiolite along some type of Late Cretaceous oceanic spreading site. The least equivocal supporting evidence for this setting is the presence of the well-developed sheeted dike complex which represents a large portion of the ophiolite exposure in Cyprus (Wilson, 1959; Kidd and Cann, 1974 and Kidd, 1977).

The plutonic section of the ophiolite incorporates a range of lithologies including harzburgite, minor plagioclase lherzolite, dunite, clinopyroxene-bearing dunite, clinopyroxenite, wehrlite and feldspathic-wehrlite, layered olivine and hypersthene gabbro and "high-level" pyroxene-hornblende gabbro with minor trondhjemite (Moores and Vine, 1971; Allen, 1975).

An irregular and complex, multiple intrusive contact has been reported between the upper gabbro and sheeted dike units (Moore and Vine, 1971). The sheeted dikes grade upwards into the extrusive pillow lava sequences (Wilson, 1959). Early workers divided these extrusives into upper and lower pillow lava suites (Wilson, 1959; Bear, 1960; 1966; Gass, 1958; 1960) while Moore and Vine (1971) suggested that this division into upper and lower pillow lava suites could be made on the basis of chemistry and petrology. Smewing (1975) and Smewing *et al.* (1975) introduced the notion of formation of the lower pillow lavas and sheeted dikes within an axial sequence in a ridge-median valley and generation of the upper lavas within an off-axis volcanic regime. The recent work by Robinson *et al.* (1983) and McHegan and Robinson (1984) has indicated a chemical discontinuity at the 500 m stratigraphic interval between the lower arc-tholeiitic and upper high MgO/low  $\text{TiO}_2$  "boninitic" suites.

Gravity and magnetic surveys suggest that the northern flank of the Troodos ophiolite extends northward beneath the sediments of the Mesaoria Plain and abruptly truncates beneath the Kyrenia Range against the Ovgos Fault (Aubert and Borez, 1974). To the south and west, the Troodos complex has been interpreted by Biju-Duval *et al.* (1976) and Xenophontos and Afrodissis (in prep.) to be in overthrust contact with the Dhiarizos Group and the Mamonia Formation. Contrary to this, reports by Robertson and Woodcock (1980) and Swarbrick (1980) strongly support a model of juxtapositioning of the Troodos complex with its Campanian volcanoclastic cover (Kannaviou Formation) against the Mamonia complex along a series of high-angle faults. These faults are possibly related to large scale, strike-slip movement within an oceanic fault zone domain. Moore *et al.* (1984) suggested that gravity sliding of the Mamonia complex onto the Troodos complex occurred with uplift of the Mamonia during oblique collision of the Troodos spreading segment with a microcontinent.

An in-depth review of previous work on the Troodos ophiolite is presented in Section 1.4.

## (2) The Limassol Forest and the Arakapas Fault Zone

The Limassol Forest complex (Kellaki Massif) is separated from the southeastern margin of the Troodos ophiolite by the Arakapas Fault Zone. Outcropping within the Limassol region is an elevated core of serpentized harzburgite and dunite, syntectonically intruded by mafic to ultramafic intrusions which are in turn intruded by diabase dikes (Murton, 1986). A disrupted envelop of dikes, pillow lavas and sediments surrounds the massif (Simonian and Gass, 1978). The southern margin of the Limassol Forest is bounded by south dipping, deformed, middle Miocene carbonates of the Yerasa fold and fault belt.

The Arakapas Fault Zone defines an east-west trending graben, up to 1.5 km in width and traceable along strike-length for 35 km. Simonian and Gass (1978) interpreted the volcanogenic sediments and blocks of pillow lavas within this graben to represent clastic wedges deposited along the fault scarps.

Simonian and Gass (1978) noted the higher Mg content of the lavas from the Arakapas region relative to the lavas on the northern flank of the Troodos ophiolite. These authors attributed this chemical distinction to differences in the petrogenetic processes occurring within the fault belt. More recently however, Mehegan and Robinson (unpublished data) and Robinson *et al.* (in prep.) have suggested that lavas occurring along the southern flank of the Troodos ophiolite are more primitive than those on the northern flank and that there appears to be no significant chemical difference between the lavas from the Arakapas Fault Zone and those from parts of the Troodos extrusive sequence.

The geological features of the Limassol Forest and Arakapas Fault Zone compare favorably with the topography, magnetic anomaly, composition, sedimentary infill and serpentinite intrusions which are characteristic of present day oceanic fracture zones (Simonian and Gass, 1978; Robinson *et al.*, in prep.). Thus, a number of authors (e.g.: Simonian and Gass, 1978; Bechon and Rocci, 1982 and Robinson *et al.*, in prep.) concluded that the Arakapas Fault and

Limassol Forest area represent different parts of the same fossil transform fault. The western Limassol Forest complex has most recently been interpreted by Murton (1986) to form part of the active domain on a left-lateral leaky transform fault. Simonian and Gass (1978) interpreted the geometry of the sheeted dikes to indicate right-lateral fault offset (left offset of the ridge crest) of the Arakapas fault zone. Alternatively, the work of Varga and Moores (1985) and Moores *et al.* (1984) indicates a left-lateral (sinistral) shear across a right-offset transform for the Arakapas Fault Zone based on the comparison of the pattern of dikes near this fault zone and the structure of modern active ridge/transform intersections.

### **(3) The Akamas Peninsula**

The Akamas region is situated within the westernmost promontory of the Cyprus coastline, located due west of the Troodos ophiolite. Xenophontos and Afrodisis (in prep.) have suggested that the Akamas region may represent a western extension of the Limassol-Arakapas oceanic fracture zone.

Within the Akamas region, quartzitic sandstone, limestone and pelagic sediments of the Jurassic to lower Cretaceous Mamonia Formation occur intercalated with lava flows and pyroclastic rocks and intruded by dioritic or gabbroic sills and dikes of the upper Triassic to Jurassic Dhiarizos Group. Large, dissociated sandstone blocks, up to 500 m long and 40 m thick and belonging to either the Akamas Formation (Gass, 1960; Swarbrick, 1980) or the Pareklishia Formation (Pantazis, 1967), rest conformably on the mudstones of the Mamonia Formation. A mega-boudin origin for these discontinuous blocks was suggested by Lapierre (1975).

#### **1.2.4. The Mamonia Complex**

The Mamonia complex of southwest Cyprus is composed of an imbricated, highly deformed and allochthonous sequence of upper Triassic - lower Jurassic to middle Cretaceous sediments, volcanic rocks, serpentinite, amphibolites and melange (Swarbrick, 1980).

The complex consists of four main units: (1) the middle to upper Triassic Dhiarizos Group; (2) the Triassic to lower Cretaceous Mamonia Formation; (3) the Moni Melange; and (4) the serpentinites and slices of metamorphic rocks.

The Dhiarizos Group (Robertson and Woodcock, 1980; Swarbrick, 1980) or Petra tou Romiou Formation (Lapierre, 1975) incorporates pillow and massive alkaline basalts interbedded with chert, limestone and hemipelagic sediments (Swarbrick, 1980). The Dhiarizos Group is thought to represent a period of either intercontinental (Lapierre and Rocci, 1976) or intraplate oceanic rifting (Lapierre, 1975). Tectonic, intrusive and normal stratigraphic contacts exist between the Dhiarizos Group and the overlying Mamonia Formation. Xenophontos and Afrodisis (in prep.) noted imbricated and overthrust contacts of the Dhiarizos Group and the Mamonia Formation onto the Kannaviou Formation and the Troodos complex.

The Mamonia Formation (Lapierre, 1975) or the Ayios Photios Group (Robertson and Woodcock, 1980; Swarbrick, 1980) records the deposition of continental margin turbidity flows, redeposition of carbonates within a deeper water environment and a late period of sedimentation within coeval deep basin and continental rise conditions (Swarbrick, 1980).

The Moni Melange of Lapierre (1975) or Kathikas Formation of Swarbrick (1980) is composed primarily of rocks from the Mamonia complex and represents an olistostrome melange which originated as a series of submarine debris flows.

The serpentinite sheets, consisting of altered harzburgite and dunite, occur imbricated with both the Dhiarizos Group and Mamonia Formation and in overthrust contact with the Kannaviou Formation and the Troodos ophiolite.

A variety of theories has been proposed regarding the origin of the serpentinites. These include: (1) Troodos ophiolite derived serpentinite intruded into the Mamonia complex (Gass, 1960; Lapierre, 1975); (2) sea-floor derived serpentinite

thrust southward over the Troodos ophiolite and subsequently incorporated with the Mamonia nappes (Robertson and Hudson, 1974); and (3) serpentinite sheets thrust along high-angle, strike-slip faults which juxtaposed Cretaceous oceanic crust (Troodos) against incipient Triassic oceanic crust (Mamonia), (Swarbrick, 1980). Most recently, Robinson *et al.* (in prep.) have suggested an upper Triassic oceanic origin for the serpentinites which are thought to have been extruded and imbricated with the Mamonia Complex during Maastrichtian deformation in response to movement along the westward extension of the Arakapas Fault Zone (Xenophontos and Afrodisis, in prep.).

The origin of the scattered, up to 1 km X 5 km. in size amphibolite slivers is likewise unclear (e.g.: Turner, 1971; 1973; Woodcock and Robertson, 1977; Swarbrick, 1980). Turner (1971) suggested formation of the amphibolitic rocks during contact dynamothermal metamorphism of the Mamonia complex during serpentinite intrusion. Woodcock and Robertson (1977) favoured subduction related metamorphism of the Mamonia complex. Swarbrick (1980) argued that the amphibolites represent metamorphosed Dhiarizos Group equivalents produced during shear heating along major strike-slip fault zones. Spray and Roddick (1981), on the basis of chemistry, mineralogy and  $^{40}\text{Ar}/^{39}\text{Ar}$  geochronology, indicated that these slivers of metamorphic rocks were produced by greenschist to amphibolite facies dynamothermal metamorphism of alkalic and tholeiitic mafic rocks and associated sediments at 83-90 m.y. These authors reported that the field relations suggest this metamorphism occurred within strike-slip fault extensions of the Arakapas transform. Robinson *et al.* (in prep.) interpreted the rocks to be Mamonia Formation equivalents which were metamorphosed in a subduction zone and deformed and emplaced during Maastrichtian time.

Early theories concerning the emplacement of the Mamonia complex as a whole, include both southward-directed thrusting over the Troodos ophiolite and its autochthonous sedimentary cover (Lapierre, 1975; Borez *et al.* 1976), and entrainment of the complex beneath and emplacement with the Troodos

allochthon (Biju-Duval et al.; 1976). Moores et al. (1984) and Robinson et al., (in prep.), suggested that northward subduction during the Cretaceous beneath the Troodos massif resulted in the accumulation of the Mamonia complex as an accretionary melange in the trench subduction zone. Subsequent Maestrichtian trench-microcontinent collision (i.e.: Troodos collision with a microcontinent, possibly the Anatolia complex in southern Turkey) resulted in the cessation of this subduction, uplift of the Mamonia Complex, and gravity sliding northward onto Troodos and its sedimentary cover (Moores et al., 1984).

### **1.3. Regional Tectonic Setting of the Troodos Ophiolite**

The Troodos ophiolite forms a western member to a girdle of ophiolite massifs which extend along the northern margin of the Arabian platform (Ricou, 1971). This zone of ophiolites delineates just one segment of the more than 8,700 km long, east-west trending Tethyan ophiolite belt which extends intermittently from the Alps, through the Hellenides, the Dinarides, the Taurus, the Zagros and Oman Mountains and eastwards into the Himalayan Mountains (Hsu and Bernoulli, 1978; Adamia et al., 1980), (Figure 1-3).

The Alpine-Himalayan mega-suture zone is defined by this linear arrangement of fragmented Tethyan oceanic crust. The zone developed during Cretaceous to early Tertiary collision and subduction of the late Mesozoic Tethyan oceanic plate. Northward movement of the African and Indian plates and coincident eastward movement of Europe due to spreading of the North Atlantic (Bally, 1975; Hsu and Bernoulli, 1978; Bernoulli and Lemoine, 1980) resulted in this collision and the subduction of this late Mesozoic Tethyan oceanic plate.

The Alpine-Himalayan ophiolite belt shows major variations in characteristic features from east to west along its length (Karamata, 1980). The eastern type, with which the Troodos ophiolite is associated, exhibits a more depleted upper mantle represented by harzburgite tectonite, a variably developed pyroxenitic critical zone, abundant plagiogranite and keratophyre, chromite concentrations, a

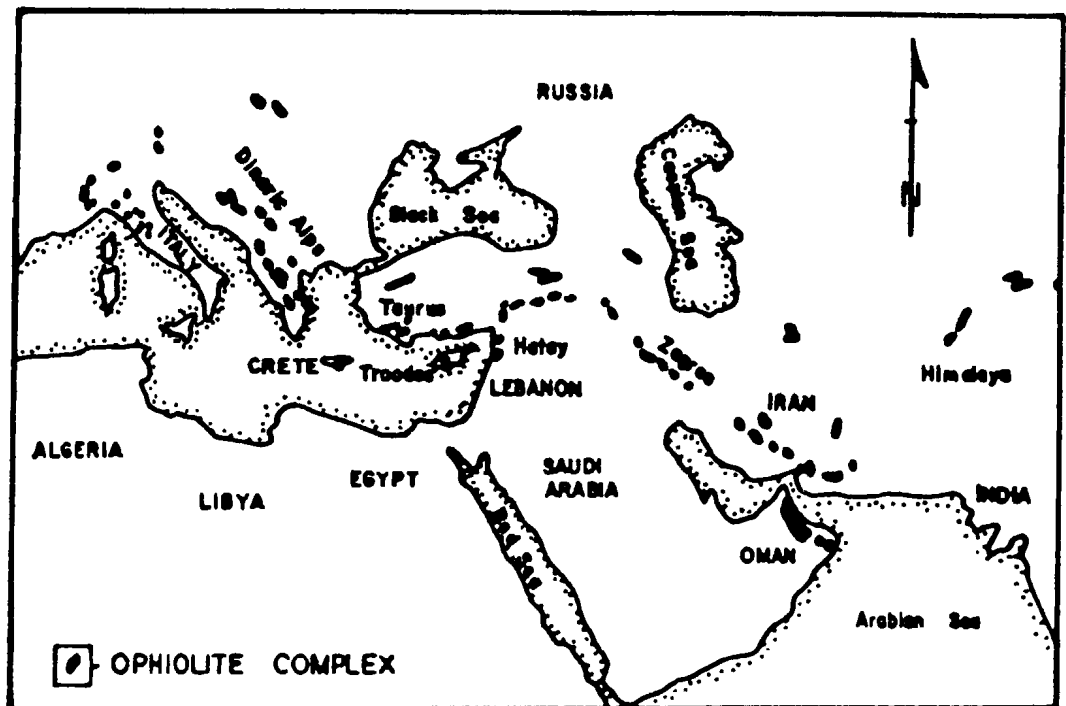


Figure 1-3 . Distribution of Tethyan ophiolite massifs and location of the Troodos ophiolite , Cyprus ( after Searle, 1980 ).



mainly tholeiitic chemistry, well developed sheeted dikes and an association with deep-water pelagic sediments. The western type, on the other hand, typically shows a less depleted lherzolitic upper mantle, a well developed critical zone composed of cumulate plagioclase-bearing lherzolite and harzburgite, massive diabase, infrequent plagiogranite or keratophyre and a terrigenous sedimentary association. A transitional boundary which divides the eastern and western ophiolite types passes through Yugoslavia, Albania and Greece.

According to Karamata (1980), this contrast between the eastern and western ophiolite types may reflect variations in the origin of the oceanic crust along the length of the Tethyan belt in terms of the spreading setting (i.e.: forearc, backarc, marginal sea, oceanic setting), upper mantle source region, heat flow, degree of partial melting and interaction with continental crust. Karamata (1980) reported that in the west, development of the oceanic crust was probably areal oceanization in association with mantle diapirs, low degrees of partial melting or deep-seated melting zones. While, to the east, a mid-oceanic ridge or immature ridge(s) setting associated with microcontinents and island arc development was proposed (Karamata, 1980).

#### **1.4. Review of Previous Work for the Troodos Ophiolite**

The following section is intended to provide an overview of the work done by numerous investigators on the Troodos ophiolite since the late 1950's. A summary of work conducted prior to 1958 is available in Wilson (1959). Extensive summaries are also available in Allen (1975), George (1975) and Gass (1980). The results to date of the ongoing Cyprus Crustal Study Project are included.

##### **1.4.1. Origin and Formational Setting**

An origin for the Troodos lavas by partial melting of a previously depleted mantle source is now widely accepted (e.g.: Peterman et al., 1971; Greenbaum, 1972A; Miyashiro, 1973; Pearce, 1975; 1980; Laurent et al., 1980; Saunders et al.; 1980; Schmincke et al., 1983; Robinson et al., 1983; Malpas and Langdon, 1984).

However, considerable differences in opinion exist concerning the formational setting of the massif with earlier investigators favouring an oceanic setting, while more recent work supports a supra-subduction zone environment.

#### **(1) Oceanic Setting**

Bishopp (1952) was first to recognize that the Troodos igneous body represented a slice of oceanic crust with no underlying sialic crust. Gass (1967, 1968) proposed formation of the massif within an extensional regime on a mid-Tethyan rise based upon both the petrological and geophysical evidence and similarity with the present day mid-oceanic ridges. Moores and Vine (1971) and Gass and Smewing (1973) suggested formation during intracontinental rifting to form a major oceanic basin during late Cretaceous time. Robertson and Woodcock (1980) argued for a narrow rifted oceanic setting while Smewing (1975) and Smewing *et al.* (1975) proposed formation within a ridge median valley for the axial sequence (sheeted dikes and lower pillow lavas) and an off-axis origin for the upper pillow lavas.

#### **(2) Supra-Subduction Zone Environment: Island Arc or Back-Arc Basin Volcanics.**

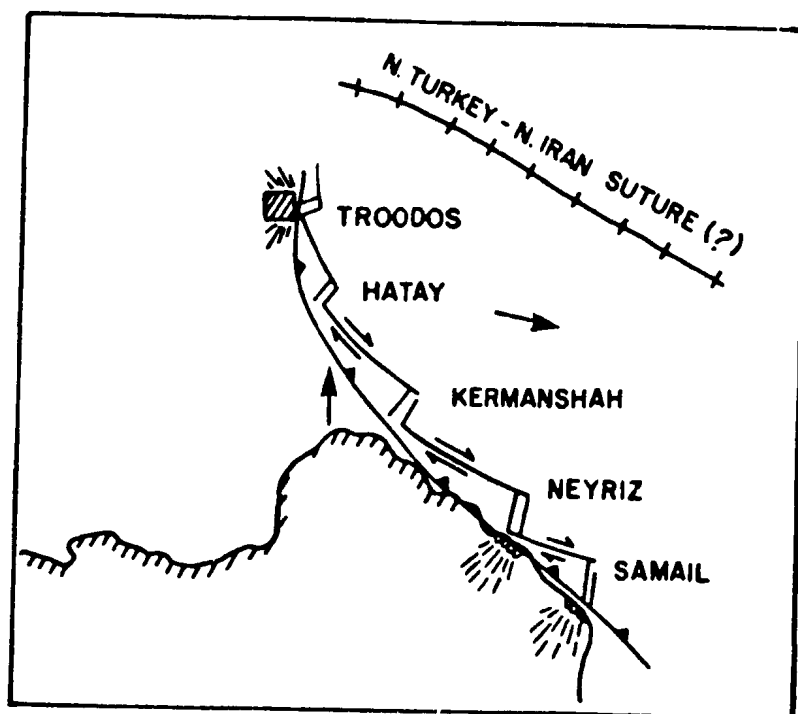
An island arc involvement in the formational setting of the Troodos ophiolite was first suggested by Pearce and Cann (1971, 1973). On the basis of relatively immobile trace elements (e.g.: Ti, Zr, Y, Nb) they proposed an ocean floor setting for the sheeted dike complex and lower pillow lavas and an island arc environment for the upper pillow lavas. Kay and Senechal (1976) concluded on the basis of REE ratios and Zr/Ti values, a mid-ocean ridge, small ocean basin or incipient island arc setting. A formational setting entirely within an island arc environment was proposed by Miyashiro (1973, 1975A,B) based upon a comparison of the major element lava chemistry with those data available from similar present day island-arc environments. Freund *et al.* (1975), Pearce (1975, 1980) and Saunders *et al.* (1980) suggested on the basis of trace element data, a formational setting for the ophiolite within a narrow marginal sea or back arc basin with a subducted oceanic crust signature. Robinson *et al.* (1983) and

Malpas and Langdon (1984) suggested on the basis of lava glass compositions, a formation within a supra-subduction zone environment; probably within an incipient arc or forearc setting. The general absence of volcanoclastic and pyroclastic rocks was noted by Moores (1982) thereby indicating the immature nature of the island arc environment. The isotopic and trace element work of Rautenschlein *et al.* (1985) likewise indicates supra-subduction zone volcanism in the earliest stages of island-arc development.

Moores *et al.* (1984) have recently proposed a recent model for the origin of the Mid-east ophiolites that is based upon the present day situation in the Andaman Sea. The Troodos and other Mid-east ophiolites are viewed as having formed in a series of short spreading segments separated by long transform faults, above a north dipping subduction zone (Figure 1-4). Such a model accounts for the existing evidence of an extensional environment subduction zone involvement and proximity of transform fault and accretionary melange environments.

#### **1.4.2. Emplacement and Tectonic Disruption**

Emplacement of the Troodos ophiolite is still a matter of speculation, conjecture and controversy (Gass, 1980). Gass and Masson-Smith (1963), Gass (1980) and Robertson and Woodcock (1980) suggested an essentially in-situ, uplifted setting for the Troodos massif, overlying northward dipping, tectonically underthrust oceanic or continental crust. Contrary to this, Lapierre (1975), Biju-Duval *et al.* (1976), Bortolotti *et al.* (1976) and Moores *et al.* (1984) support an allochthonous emplacement of the Troodos massif, derived from either a moderate or large distance to the north. Bortolotti *et al.* (1976) likewise stated that the Troodos massif is itself internally thrust, consisting of a pile of allochthonous thrust units with a southward vergence. Contrary to these opinions, no evidence for major thrust repetition of the complex was found by either Robertson and Woodcock (1980) or the present author. Evidence of listric and planar normal faults cutting the sheeted dikes and flattening into a detachment within the upper gabbros was presented by Varga and Moores (1985) and Verosub and Moores (1981). However,



**Figure 1-4:** Schematic model for the formation of the Troodos ophiolite in a short spreading segment above a subduction zone and a collision with a small microcontinent (after Moores et al. 1984).

such faulting and tilting to produce axial valley grabens occurred early in the history of the complex within the spreading ridge domain. Robinson *et al.* (in prep.) noted several thrusts with limited displacement ( $\sim 500$  m) cutting pillow lavas on the southern flank of Troodos. Otherwise, only high-angle, normal faulting has been recognised within the complex, the largest of which has juxtaposed harzburgite against gabbro in a locality to the east of Mt. Olympus (Wilson, 1959).

The present day domal structure of the Troodos ophiolite is attributed to a number of mechanisms which together have yielded more than 2000 m. of uplift centered on Mt. Olympus (Gass, 1980). Wilson (1959), Moores and Vine (1971) and more recently Gass (1980) have suggested that the initial uplift accompanied the  $90^0$  counterclockwise rotation of the massif due to Miocene collision with a microcontinent or the African continental plate. Continued uplift since Miocene time has been related to hydration of the ultramafic rocks and subsequent serpentinite intrusion (Allen, 1975; Gass, 1980). The latter intrusion may have been associated with the liberation of hydrous fluids from an underlying subducted oceanic or continental slab.

#### 1.4.3. The Plutonic Complex

The generalized "stratigraphic" sequence represented in the plutonic complex of the Troodos ophiolite incorporates a mafic (e.g.: gabbro, pyroxenite and minor peridotite) unit which structurally overlies an ultramafic (e.g.: harzburgite) unit (Coleman, 1977). These two major units of the plutonic complex are separated by a transition zone which includes dunite with layered wehrlite, pyroxenite and troctolite (Wilson, 1959; Moores and Vine, 1971).

Origin of the harzburgite tectonite as a depleted mantle residuum following partial melting of plagioclase-lherzolite (Allen, 1975) to yield primary olivine basaltic magmas is supported by the work of Carswell (1968), Moores and Vine (1971), Nicolas and Jackson (1972), Greenbaum (1972a), Menzies and Allen (1974),

Allen (1975) and Kay and Senechal (1976). However, George (1975; 1978), considered a residual mantle versus a high-temperature deformed and recrystallized metacumulate origin to be unequivocal on the basis of structural data. A similar controversy exists in the literature regarding a cumulate versus residual origin for the transition zone (Nicolas and Prinzhofer, 1983). The chromitite, dunite and higher stratigraphic units were interpreted as cumulate in origin by numerous workers (e.g.: Boettcher, 1969; Greenbaum, 1972A; Menzies and Allen, 1974; George, 1975; and Nicolas and Prinzhofer, 1983). In contrast, Moores and Vine (1971); Nicolas and Jackson (1972) and Nicolas and Prinzhofer (1983) classified the dunite as depleted residual mantle resulting from melting out of the orthopyroxene component in the harzburgite. Likewise, the dunite bodies found deep within the harzburgite tectonite were interpreted by Allen (1975) and Gass (1980) to represent olivine +/- chromite which precipitated from trapped rising melts. In contrast, Ringwood (1966) and Moores and Vine (1971) considered these bodies to represent residual material from which the plagioclase, orthopyroxene and clinopyroxene components had been removed during partial melting.

Minor outcrops of plagioclase-lherzolite tectonites within harzburgite were interpreted by Menzies and Allen (1974) to represent relatively undepleted aluminous upper mantle peridotite. Gabbroic pods outcropping within the mantle tectonites were thought to represent batches of melt which crystallized before escaping from their source rock (Gass, 1980).

Cumulus model phase transitions from olivine gabbro to pyroxene, pyroxene-hornblende and hornblende-magnetite gabbro was reported by Allen (1975) within higher stratigraphic levels of the plutonic complex. The presence of plagiogranite bodies were attributed to a process of filter pressing segregation and crystal settling from gabbroic crustal mush in a zone beneath the massive dioritic underplating of the diabase dikes (Allen, 1975).

Greenbaum (1972A) proposed a fractional crystallization sequence of Cr-Ol-Cpx-

Opx-Pl with the last three minerals occurring first as intercumulus and later as cumulus phases. Allen (1975) reported cyclic, cryptic and rhythmic layering in the cumulate sequence commencing with dunite adcumulate. He also suggested a crystallization sequence compatible with that of Greenbaum except for variations in the relative appearance of Cpx., Opx. and Plag. on the solidus. Allen (1975) also demonstrated a tholeiitic fractionation trend with limited Fe enrichment for the plutonic complex, postulating a picritic basalt parental magma low in Ti, Na, K and P.

The complex, irregularly gradational igneous contact between the genetically related (Greenbaum, 1972b) gabbros of the upper plutonic sequence and overlying sheeted dike complex was interpreted to represent a zone of multiple intrusion (Moores and Vine, 1971) during synchronous formation of the two units (Wilson, 1959 ; Allen, 1975).

Two end-member magma chamber models have been proposed for development of the Troodos ophiolite based upon geological field evidence and petrologic data found within the plutonic complex. The first model, proposed by Greenbaum (1972A) and supported by George (1975), involves the accumulation of the broad scale ophiolite stratigraphy by cumulate processes within a single, steady-state magma chamber. Contrary to this, a second model involving multiple magma chambers waxing and waning with time during the cumulate development of the ophiolite has been proposed by Moores and Vine (1971), Allen (1975), Smewing *et al.* (1975), Greenbaum (1977) and Malpas and Langdon (1984). Allen (1975) speculated upon the formation of discrete, linear magma cells, up to 1km sq in size, which were refurbished by magmas of varied compositions beneath a paleo-ridge. Gass (1980) suggested derivation of these melt batches from rising diapirs.

The review by Gass (1980) advocates the multiple magma theory, however, he is quick to point out the lack of documentation of definitive contact relations, pluton margins and overall geometries for these magma chambers. Most recently, Benn and Laurent (1987) have reported two magmatic suites within the plutonic

complex in the Caledonian Falls area, located south of the present author's map area. These author's, however, do not discuss in any detail the contact relations, margins or geometries of the intrusive bodies nor the distribution or patterns of ductile deformation within the plutonic complex. In the following chapters of this thesis, the multiple magma chamber model will be both substantiated and significantly refined by the delineation of spatial and temporal relationships between the various magmatic suites and magma chambers which collectively constitute the Troodos plutonic complex. Also, the findings of Benn and Laurent (1987), regarding the distinction of magmatic suites on the basis of mineral chemistry, will be refuted by the results of the present author's work.

#### **1.4.4. The Volcanic Sequence**

The volcanic sequence incorporates both the sheeted dike complex and the upper and pillow lava sequence of the Troodos ophiolite. The sheeted dike complex varies from 1.2 to 1.4 km. in thickness (Wilson, 1959). It consists of 0.3 to 4.5 m. wide dikes which strike north-south except for a swing to an east-west orientation approaching the Arakapas fault zone. One-way chilling statistics of Kidd (1977) and Kidd and Cann (1974) suggested a spreading center located to the present-day west of the complex. However, ongoing work in the Cyprus Crustal Study Project (e.g.: Baragar and Lambert, 1984) reveals several phases of dike intrusion with no preferred chilling direction.

The dike complex grades upwards to the pillow lava sequences (Wilson, 1959; Gass and Masson-Smith, 1963; Moores and Vine, 1971; Mantis, 1971). Early workers (e.g.: Wilson, 1959; Bear, 1960; 1966; Gass, 1958; 1960; Gass and Smewing, 1973; Smewing, 1975) divided the lavas into two groups: (1) greenish-gray, oversaturated, predominantly aphyric (minor plagioclase and clinopyroxene phenocryst bearing) lower pillow lavas and (2) reddish-brown, undersaturated, olivine and pyroxene-phyric bearing upper pillow lavas with highly picritic zones.

Recent work on lava glass compositions by Robinson et al., (1983) and Mehegan



and Robinson (1984) has suggested two distinct magma suites. The chemical boundary between the two suites is lower in the stratigraphic sequence than the boundary defined earlier by Gass and Smewing (1973). The lower 500 m section of andesite, dacite-rhyolite assemblage exhibits an arc tholeiite chemistry, while the upper 750 m section of picritic basalt-basaltic andesite shows higher MgO and low  $\text{TiO}_2$  suggestive of boninitic affinity (Robinson *et al.*, 1983; Robinson *et al.*, in prep.). A similar chemical signature has been noted from the Bonin Arc (Crawford *et al.*, 1981) and the Mariana Arc (Wood *et al.*, 1980) where a series of high-Mg lavas overlies a less-Mg rich arc tholeiite suite. The ongoing work of others (e.g.: Baragar and Lambert, 1984; Baragar and Gibson, unpub.) has suggested a possibly chemical continuum between these two suites of the Troodos pillow lava sequence. Within the upper pillow lava suite, Malpas and Langdon (1984) have delineated a petrogenetically related suite of ultrabasic lavas, komatiites, olivine basalts and aphyric basalts derived from a highly depleted, primary melt by dominantly olivine fractionation.

#### 1.4.5. Solid State Deformation

Wilson (1959) correlated penetrative deformation features of the harzburgite and dunite with those features observed in alpine-type ultramafic complexes, while Moores and Vine (1971) noted the obscure nature of the contact between harzburgite and dunite due to this penetrative deformation. The steep attitude of planar and linear mesoscopic structures within the harzburgite and lower metacumulates was attributed to a period of ductile deformation (Greenbaum, 1972A), while the attitude of the large scale contact between these units was ascribed to a number of factors, including: (1) late doming of the massif (Greenbaum, 1972A); (2) a primary igneous feature; and (3) tectonic transport of the igneous layering following crystallization of the cumulates (George, 1975).

George (1975) discussed the contemporaneous nature of plastic deformation and infolding of the harzburgite and dunite units, during a temperature interval sufficient for syn- to post-tectonic recovery via recrystallization mechanisms in the

plastically strained grains. Syntectonic recrystallization of the olivine at high temperatures was considered to be the fundamental mechanism of deformation within the harzburgite and dunite. Thus, the strong olivine and weak orthopyroxene petrofabrics, recorded within these units, were attributed to concentration of strain within the olivine phase (George, 1975). The transition from deformed to undeformed cumulates was reportedly gradational over a 500 m interval within clinopyroxene-bearing olivine cumulates; however, some straining of the olivine phase in each of the olivine bearing lithologies, except the gabbros, was reported (George, 1978). George (1975, 1978) interpreted the absence of plastic deformation within the cumulates to signify the presence of an intercumulus liquid which accommodated the strain by a grain boundary sliding mechanism during the ductile deformation. Therefore, ductile deformation during fractional crystallization occurred at deeper levels within the accumulating pile during magmatic deposition (i.e. syntectonic magmatic sedimentation). This plastic deformation ended prior to crystallization of the upper cumulates (George, 1975; 1978). The transition from plastic flow to brittle deformation mechanisms within the plutonic complex (the deformation front) are not discussed at any length by George (1975, 1978).

The major conclusions of George (1975, 1978), particularly those concerning the distribution of high temperature, plastic deformation within the higher cumulate levels of the plutonic complex, are disputed in the following chapters of this thesis.

#### **1.4.6. Metamorphism**

Studies of the metamorphism of the Troodos ophiolite commenced in the early 1970's. Gass and Smewing (1973) presented evidence for a metamorphic discontinuity marking the boundary between the generally fresh upper pillow lavas and the altered lower pillow lavas. A minimal  $150^{\circ}\text{C}/\text{km}$ . thermal gradient was noted, corresponding to an increase in metamorphic grade, from zeolite through greenschist and lower amphibolite facies with depth. Contrary to this, Robinson *et al.* (1983) reported that no significant metamorphic discontinuity

occurs between the upper and lower pillow lavas and that an abundance of fresh glass occurs throughout both units.

Gillis (1983) noted a lack of systematically increasing metamorphic grade with depth in the pillow lava and sheeted dike units. In general, the newly defined upper pillow lava sequence (refer to Subsection 1.4.4), (Robinson *et al.*, 1983) exhibits a weak alteration while the lower lava sequence contains low grade metamorphic assemblages of calcite, secondary silica, smectite, celadonite and zeolites. Isotopic studies in the pillow lava and sheeted dike units showed high water/rock ratios, Cretaceous seawater involvement and significant mass transfer of elements including Na, K, Ca, Fe, Sr, S and base metals (Broughton and Gibson, 1984; Staudigel *et al.*, 1984). An upper greenschist to lower amphibolite facies sub-seafloor metamorphism of the upper plutonic complex involving appreciable chemical alteration was reported by Allen (1975).

#### 1.4.7. Geophysics

Gravity studies by Gass and Masson-Smith (1963) revealed a positive (100-150 mgal.) regional Bouger anomaly located beneath central Cyprus and a negative (-120 mgal.) anomaly to the east of Mount Olympus, which they attributed to a 10 km deep, cylindrical plug of serpentized ultramafic rock. Gass and Masson-Smith (1963) and Gass (1967) suggested the existence of a 11 km thick slab of dense ( $3.3 \text{ gm/cm}^3$ ) material underlain by a 25 km thick slab of less dense ( $2.7 \text{ gm/cm}^3$ ) African continental crust dipping northward beneath Cyprus.

Formation of the Troodos Complex within an east-west spreading axis during "normal" earth polarity was documented by Moores and Vine (1971). The  $90^\circ$  counterclockwise (Shelton and Gass, 1980), mid-Miocene rotation of the Troodos block occurred prior to serpentization during a microcontinent or African plate collision (Moores *et al.*, 1984).

Most recently, seismic refraction profiles between Cyprus and Israel (Makris *et*

al., 1983) indicate that; (1) Cyprus is underlain by 35 km thick continental crust which thickens southward and (2) south of Mount Eratosthenes, a transition in crustal structure indicates a major structural boundary that separates the continental Cyprus-Eratosthenes block to the north from an oceanic region which extends southward to Israel.

### **1.5. Aims and Logistics of the Present Study**

The present study evolved at the initial stage in the remapping of the plutonic complex of the Troodos ophiolite by members of the Cyprus Crustal Study Project. The project represents a joint venture of the International Crustal Research Drilling Group and the Government of Cyprus through the Cyprus Geological Survey Department.

Previous studies of the Troodos plutonic complex (e.g.: Greenbaum, 1972A; Allen, 1975; and George, 1975) have provided valuable information concerning certain aspects of the plutonic complex as outlined in preceding sections of Chapter 1. However, up until 1982, an accurate and detailed lithological and/or structural map for any portion of the complex was not available. Likewise, a number of major controversies are apparent from the literature regarding : (1) magma chamber models; (2) size and shape of the magma chambers; (3) distribution of high temperature deformation; and (4) mineral crystallization sequence(s). Consequently, the intent of the present study was to map in detail an area within the plutonic complex, paying particular attention to the lithological relationships, plutonic geometry and the nature and orientation of structural elements. Such a detailed study would help to further our understanding of the processes of multiple intrusion, the relative age relationships between magmatism and deformation, and the nature and geometry of high temperature plastic deformation associated with crustal accretionary processes operating at deeper levels within the spreading environment.

To this end, a 16 km sq region within the northwestern quadrant of the plutonic

complex was chosen for the study (Figure 1-2). This region incorporates a well exposed cross section through the plutonic complex of the Troodos ophiolite pseudostratigraphy, from harzburgite tectonite to the base of the sheeted dike complex.

The principal objectives of the study were:

1. To systematically map in detail the northwestern quadrant of the plutonic complex in order to:
  - a. delineate the distribution and contact relationships of the various lithologies.
  - b. determine the shape, size and internal geometry of any individual plutons delineated within the complex.
  - c. document the distribution of high temperature solid state deformation throughout the complex via form-surface mapping of all planar and linear fabrics.
  - d. determine the relative age relationships between magmatism and deformation.
  - e. examine the extent of brittle tectonic disruption of the plutonic complex within the study region.
2. To document the characteristic microscopic textures and fabrics of the various lithological units.
3. To determine the petrography and crystallization sequence(s) of the magmatic suite(s).
4. To determine chemical variation and fractionation trends within and between the magmatic suites.
5. To evaluate the major and trace element chemistry of the mafic-dikes which crosscut all other units of the plutonic complex.
6. To further develop a multiple intrusive magma chamber model for the Troodos ophiolite integrating the results of the present study with the data base provided by previous workers.

A total of 4 months was spent mapping an area of 16 km sq, at a scale of 1:5,000, during the 1983 and 1984 summer field seasons. The 1:5,000 scale base map was obtained by photographically enlarging the 1:25,000 Troodos and Hill Resorts topographic map (Department of Lands and Surveys, Nicosia, Cyprus), thereby providing accurate contour, road and stream locations. Areas of particular interest were examined and mapped in closer detail. Access to the field region is very good with numerous roads, footpaths and streams. Exposure is excellent along roadcuts, streams and ridges, although mapping was difficult along the numerous steep, debris covered slopes. Lodging was established in Mitsero Village.

Organization of the thesis is such that the major results of the field component of the study are presented in chapter 2. Chapter 3 presents the mega-, meso- and microscopic structural features of the older suite lithologies. Chapter 4 includes the petrographic descriptions of the younger suite lithologies, mineral chemistry analysis of the younger and older suites and the petrography and geochemistry of the mafic-dikes. In concluding, Chapter 5 will summarize and discuss the results of the study.

It should be noted that the conclusions presented in this thesis are confined to that geology which is exposed within the northwestern quadrant of the plutonic complex. Ongoing studies in other regions of the complex may reveal additional relationships thereby enhancing our progressive understanding of the formation and deformation history of the Troodos plutonic complex.

## Chapter 2

### FIELD RELATIONS

The magmatic and structural features of the geology exposed within the northwestern quadrant of the Troodos ophiolite plutonic complex are described in this chapter. The spatial and temporal relationships between deformation and magmatism are discussed. The lithological units are addressed in terms of their overall macroscopic and mesoscopic outcrop features, spatial distribution and contact relationships. It is recommended that the reader refer to the accompanying 1:7,500 scale geological map and cross-sections of the study area (MAP 1), which are located in the enclosure at the back of the thesis.

#### 2.1. The Northwestern Quadrant of the Plutonic Complex : A Geological Overview

The geological relationships exposed within the northwestern quadrant of the plutonic complex (Lat. 35°00' N; Long. 32°53' E), reveal a complicated history of concomitant magmatic and structural processes related to the construction of oceanic crust within a paleo-spreading regime.

The lithological units of a complete plutonic ophiolite succession, as defined by members of the Penrose Conference, 1972 (Geotimes, 1973), outcrop within the plutonic complex. The "succession" includes residual harzburgite tectonite at the base, massive dunite, chromitite, orthopyroxenite, olivine-pyroxenite, layered olivine and hypersthene gabbros and pyroxene-hornblende gabbros with minor trondhjemitic and diorite in the higher structural levels of the complex. This "succession" of rocks, which outcrops progressively from harzburgite in the south-

southwest to gabbros in the north-northwest (MAP 1) is collectively referred to as the older suite throughout this thesis. Mesoscopic and microscopic features indicative of high temperature, plastic deformation are clearly present not only in the upper mantle and transition zone sections of this older suite (e.g.: George, 1975; 1978; Nicolas and Violette, 1982) but are also heterogeneously developed within the higher crustal "cumulate" levels (i.e.: layered gabbro) of the plutonic complex. Continuity of the structural fabric is maintained from the penetratively deformed harzburgite tectonite through to parts of the inhomogeneously deformed mafic cumulates.

Multiple intrusion and disruption of the older suite by a number of younger suite plutons has been documented on the basis of magmatic and deformational overprinting criteria. Field criteria used to distinguish the older suite units from the younger suite(s) include: (1) xenolith-bearing margins; (2) abrupt truncation of structural and/or magmatic fabrics; (3) contrasting lithologies; and (4) mesoscopic and microscopic deformation and magmatic textures. Mapping of distinct plutonic sequences within the younger suite(s) themselves is likewise possible on the basis of field criteria including: (1) dike swarms and stockworks; (2) xenolith-bearing margins; (3) intrusive contacts which truncate primary magmatic fabrics of earlier plutons; and (4) crosscutting pegmatitic phases intruding host plutons.

The younger intrusive suite(s) incorporates a variety of ultramafic to mafic lithologies consisting of wehrlite, clinopyroxenite, pyroxene +/- hornblende gabbro and mafic dikes. These same cumulate wehrlite and pyroxenite units were incorrectly interpreted by all previous workers (e.g.: Wilson, 1959; Moores and Vine, 1971; Greenbaum, 1972A; Allen, 1975; and George, 1975; 1978) as representing the classic "transition zone" (Geotimes, 1973) or "critical zone" (Irvine and Findlay, 1972) of the Troodos ophiolite succession (Geotimes, 1973).

The main volume of younger suite intrusives outcrops as a continuous, northeast-southwest trending arcuate belt, 4.5 km in length and up to 1 km wide



in plan view, which widens westward along the southern map margin (MAP 1, Fig. 2.20 - ZONE 1). This belt of plutons occupies an area which, in essence, separates the older suite upper mantle, lower metacumulate units (e.g.: harzburgite, dunite) from the older suite layered gabbro cumulates. The geological controls responsible for concentrating the main bulk of these younger suite intrusions along the transitional zone of the older suite will be discussed in Section 2.3.4.

Additional small plugs of younger suite intrusives are exposed farther north. Other mafic to ultramafic plutons have been observed intruding the harzburgite tectonite to the south of the study area (Calon, pers. comm.; Allen, 1975 and Gass, 1980). The latter two authors have, however, interpreted these bodies to represent melt batches which were trapped within the depleted mantle source rock while enroute to an overlying magma chamber.

Isotropic, mesoscopic cumulate textures characterize the generally undeformed nature of the younger suite(s). However, a number of the smaller intrusive plugs and dikes of the younger suite do exhibit a very weakly developed planar fabric in outcrop.

Thus, on the basis of the detailed field observations, incorporating: (1) the geometrical relationships and spatial distribution of units within and between suites; (2) the distribution and style of ductile deformation; and (3) the relative timing of solid-state flow with respect to this magmatism; a working model has been developed for distinguishing both the older and younger magmatic suites as well as multiple plutonism within the younger suite(s). A similar approach has been utilized in establishing relative age relationships in metamorphic terrains [e.g.: Zwart (1958) in the Pyrenees; Johnson (1961, 1963) in Scotland; Rathbone *et al.* (1983) in the Caledonide/Appalachian Orogeny in Scotland; McLelland *et al.* (1987) in the Adirondack Mountains] and complex time-space relationships in accretionary histories of early continental crustal terrains [e.g.: Bridgewater and Collerson (1976) in the early Archean of Labrador; Grant (1978) in the Pan-African domain of northwestern Nigeria].

The detailed, descriptive coverage of the rock types and the geological relationships within the plutonic complex are contained in the following sections of this chapter.

## **2.2. The Older Suite**

The spatial distribution of the lithological units belonging to the older suite matches the annular outcrop pattern for the Troodos ophiolite as described by Wilson (1959). Harzburgite tectonite, the deepest unit, forms the core of the central highlands of the Troodos Forest area giving way to progressively higher structural units at lower elevations to the north and northwest (MAP1).

The nature of the contact between massive dunite, layered transition zone lithologies and the layered gabbro units of the older suite cannot be established in any detail in the field due to the masking effect of the main belt of younger suite intrusives (Map 1). However, the dunite-harzburgite transition noted by previous workers (e.g.: Greenbaum, 1972A; 1977; Allen, 1975 and George, 1975; 1978), is discussed in Subsection 2.2.1.

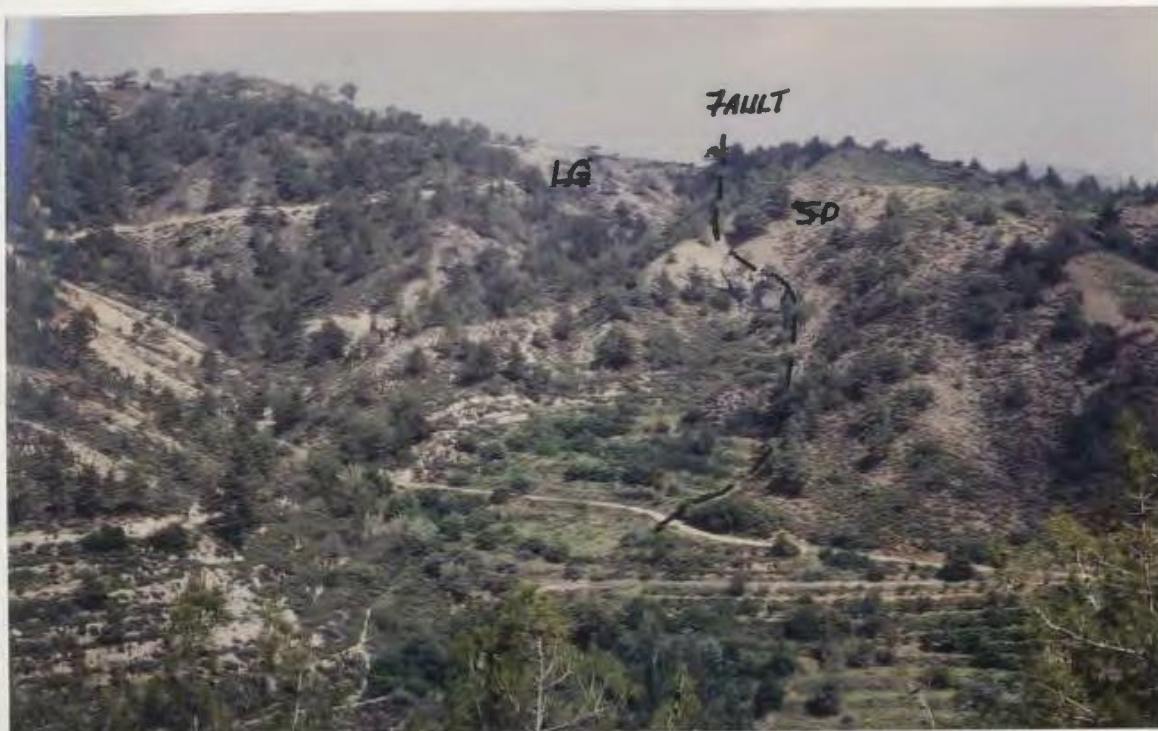
The older suite is distinguished in the field by its characteristically pervasive and penetrative  $S \gg L$  fabric. It is noted that although the older suite gabbros are heterogeneously deformed, the orientation of structural fabrics developed in this unit are consistent with those in the remainder of the penetratively deformed older suite. The foliation is orientated either parallel or slightly oblique to the magmatic accumulation layering and at a high angle to the probable original trend of the major older suite lithological unit contacts. Small scale  $F_1$  isoclinal folds with axial planar fabric were observed in the field and defined by contrasting mineral phases and/or assemblages are rare. The general structural features of the older suite will be briefly presented in this chapter, while discussion of the mega-, meso- and microscopic structural characteristics is reserved for Chapter 3.

It should be noted that although the grouping of all the penetratively deformed lithological units into one older suite is based upon shared structural fabric features, the older suite could in fact be composed of either; (1) progressively fractionated magma batches which were periodically replenished from a deeper seated, evolving magma chamber (auto-intrusive processes) or (2) multiple intrusion from various magma sources. The structural overprinting due to penetrative plastic flow and large scale transposition of lithological boundaries would have ultimately obliterated all criteria for distinguishing such relationships, if they existed. Therefore, for the purpose of this thesis, the older suite includes all of the penetratively deformed ultramafic units (harzburgite, dunite, transition zone orthopyroxenite) and the heterogeneously deformed layered olivine and hypersthene gabbro units exposed within the study area.

A fault controlled contact, exposed in the northeastern part of MAP 1, juxtaposes the layered gabbros of the older suite plutonic complex against the sheeted dike complex. This major,  $45^{\circ}$  east-dipping normal fault exposes west-dipping layered gabbro in the footwall against the  $40^{\circ}$  to  $50^{\circ}$  east-dipping diabase dikes in the hanging wall (Figure 2-1). The sheeted dikes of this region are medium grey to tan-brown and either aphyric or clinopyroxene and plagioclase microphyric. Intense fracturing, shearing and slickenside development in both the gabbroic and diabasic units marks the fault trace in the field. Elsewhere, the nature of the contact between the layered to varitextured gabbros and the sheeted dike complex was not determined as the appropriate outcrops were located beyond the perimeter of the study area.

#### **2.2.1. Upper Mantle-Lower Metacumulate Units**

Harzburgite tectonite, massive dunite and associated chromitiferous bodies form an intricate upper mantle/lower metacumulate section of the older suite sequence. This section of rocks is separated from the structurally higher older suite lithologies by the main zone of younger suite plutons (refer to Section 2.1).



**Figure 2-1:** The  $45^{\circ}$  east-dipping, normal fault contact between west-dipping older suite layered gabbro (LG) and east-dipping sheeted dikes (SD) in the Eso-Galata region.

The upper mantle/lower metacumulate rocks share similar styles of solid-state deformation which has resulted in a complex interleaved contact between these units. Characteristically, a consistent but variably developed,  $N30^{\circ}W$  and steep to vertical fabric can be mapped throughout the entire older suite section (Map 1). This fabric is defined by the preferred dimensional alignment of the orthopyroxene and spinel phases. The general absence of a linear fabric (stretching direction) in the upper mantle-lower metacumulate section is noted, except for those rare occurrences where a weak L fabric is defined by disseminated chromite stringers in the dunite.

Large scale isoclinal folding of the boundary between the harzburgite tectonite and massive dunite during high temperature, solid-state deformation, as suggested by previous workers (e.g.: Moores and Vine, 1971; Greenbaum, 1972A; Allen, 1975 and George, 1975; 1978), is supported by the results of the present author's study. The most important pieces of evidence for this conclusion are: (1) the form-trace of the interdigitated contact between the two lithological units; (2) the presence of a penetrative steep foliation orientated parallel to the boundaries of this interfingered contact; (3) the exposure of lensoidal inliers of dunite (up to 1 km long and .1 km thick) (Gass, 1980) within the harzburgite which are orientated with their long axis parallel/subparallel to the regional foliation ; (4) the presence of schlieren and isoclinally folded chromite layers (Figure 2-2) with an axial planar foliation concordant to the regional structural trend; and (5) the presence of nodular chromite with pull-apart tension cracks orientated normal to the elongation axis of the nodules.

The enveloping surface to the infolded dunite/harzburgite contact trends from N20°E to N40°E in the map region, and is therefore, orientated at a high angle to the regional N30°W foliation (MAP 1). The thickness of this infolded contact varies up to 1 km throughout the map area. Isolated dunite inliers, occurring up to 3.5 km into the harzburgite (Allen, 1975), may represent either extreme attenuation and boudinage along this infolded contact or, more likely, the elongation during ductile deformation of dunite pods inherent to the harzburgite. The penetrative, steep foliation of the harzburgite tectonite and dunite lies parallel to the axial plane of both the large and small scale isoclinal folds with transposition of all original layering and the harzburgite/dunite contact parallel/subparallel with this contact. This folding has thus occurred contemporaneously with the high temperature deformation which generated the S and rare L fabrics at temperatures near the peridotite solidus (1200°C to 1300°C), (Nicolas and Poirier, 1976).

Controversy exists concerning the residual mantle (e.g.: Moores and Vine, 1971;





**Figure 2-2:** Fold hinge of isoclinally folded chromite layer along the harzburgite-dunite boundary near Kokkinorotsos. A strong axial planar  $S_1$  is defined by elongate chromite grains.

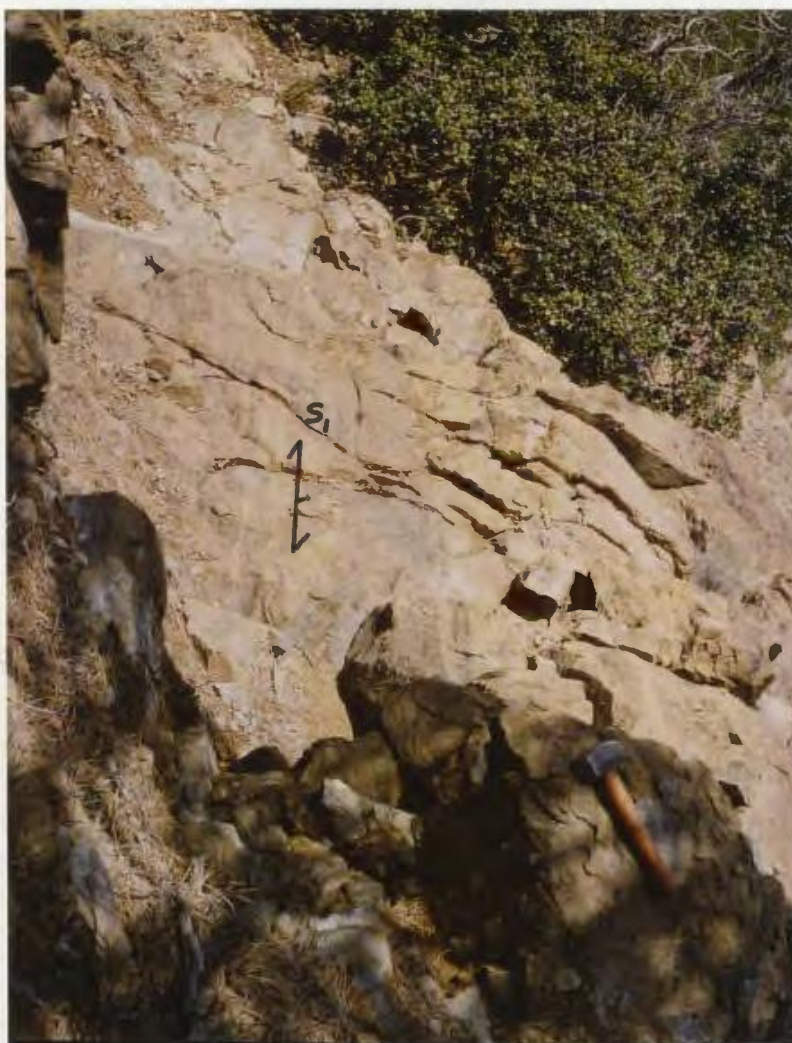
Nicolas and Jackson, 1982; Greenbaum, 1972A; Menzies and Allen, 1974; and Kay and Senechal, 1976) versus cumulate (George, 1975; 1978) origin of the harzburgite tectonite. Likewise, a similar difference in opinion exists for the origin of the dunite +/- chromitite units as representing: (1) depleted residual mantle (Ringwood, 1966; Moores and Vine, 1971; and Nicolas and Jackson, 1982); (2) cumulate (Greenbaum, 1972A; Menzies and Allen, 1974; and George, 1975); or (3) either partial or total derivation by metasomatic transformation of harzburgite (Bowen and Tuttle, 1949; Dungan and Avelallemant, 1977).

#### **2.2.1.1. Harzburgite Tectonite**

The harzburgite appears orange-tan in colour on weathered surfaces and variegated (hobnail texture) with prominent, coarse (5 to 10 mm) brownish-green orthopyroxene grains and aggregates. Weathering penetrates for 1 to 5 cm, with fresh rock surfaces showing black, variably serpentinized olivine and dark green orthopyroxene. The harzburgite exhibits a porphyroclastic to equigranular texture in hand sample with an average modal composition ranging from 70-85% olivine and 15-30% orthopyroxene with trace amounts (~2%) of irregular and spindle shaped spinel and accessory clinopyroxene. Evidence of metamorphic segregation of the olivine and orthopyroxene phases into prominent compositional layering was exposed in two areas. These layers range from 5 mm to 4 cm in thickness (Figure 2-3) and are traceable for up to 4 m along strike, although individual layers are discontinuous over very short distances.

The moderate to strongly developed regional foliation trend within the harzburgite, exhibits a steep to vertical N30°W trend throughout the map area. A swing to a more northerly trend was noted within the northeastern exposures (MAP 1).

Within the harzburgite, numerous lenses, pods and veins of dunite occur in increasing proportions upon approaching the interdigitated harzburgite-dunite contact. These lenses, dikes and sills range from a few centimeters to more than a meter in width, exhibit rare mesoscopic-scale isoclinal folds and trend both



**Figure 2-3:** Compositional layering in harzburgite defined by metamorphic segregation of the olivine and orthopyroxene phases into bands orientated parallel to the regional foliation. Elongate/flattened orthopyroxene grains define the  $S_1$  fabric.

parallel and across the regional  $S_1$  foliation. The lithological contacts are distinct and marked by the abrupt disappearance of the orthopyroxene phase.

Mutually crosscutting dunite veins were observed in a number of localities. Veins of coarse grained orthopyroxene with accessory chromite and rare relict



olivine randomly crosscut the harzburgite and dunite in the map region. Coarse to pegmatitic pyroxene-hornblende gabbro veins, up to 6 cm in width, are sporadically exposed crosscutting the harzburgite and dunite lithologies as well as the later orthopyroxene veins (Figure 2-4). Textures within these gabbroic veins are isotropic except where they exhibit a preferred crystallographic growth of the mineral phases normal to the contact margins.



**Figure 2-4:** Coarse to pegmatitic isotropic pyroxene gabbro vein invading harzburgite near the harzburgite-dunite boundary.

Small scale brittle deformation features with limited displacement were noted within the main body of harzburgite tectonite. One major north-south striking, vertical fault zone occurs within the harzburgite and is exposed along the road section near the lower chromite mine adit (MAP 1). This fault outcrops along strike for more than 500m, varies up to 50 m in width and appears to terminate near the harzburgite-dunite contact. The fault is marked by intense brecciation, with angular to subrounded, centimeter to decimeter sized clasts floating in a magnesite matrix (Figure 2-5). Similar harzburgite breccia with low Mg cement was reported by Bonatti *et al.*, (1974) and referred to as "oficalci" in northern Apennine ophiolites. Major faulting along margins of the harzburgite exposure is discussed in Sections 2.2.1.3 and 2.3.4. In addition, numerous small (1 to 15 cm wide) breccia-shear zones of variable strike orientation occur throughout this region of the harzburgite. The relative senses of movement could not be determined for any of these fault/fracture zones.

#### 2.2.1.2. Chromitite

A detailed study of the origin and distribution of chromitite within the Troodos ophiolite was considered beyond the scope of the present study. The reader is directed to the works of Greenbaum (1972A; 1977), Michaelides (1983), Panayiotou *et al.* (1986) and Malpas and Robinson (1987) for in depth discussions of the Troodos chromite occurrences. For the purposes of this study, only the major structural features and occurrences of the commodity in the present study area will be discussed.

Chromite concentrations within the present study area, as well as elsewhere throughout the lower section of the plutonic complex (Greenbaum, 1977), occur either within dunite near the harzburgite contact or enveloped by dunite inliers hosted by harzburgite. Aggregates of chromite occasionally form elongate stringers orientated parallel to the regional  $S_1$  fabric defined in the harzburgite. In addition, disseminated chromite occurs throughout the older suite harzburgite and dunite, as an accessory phase which exhibits euhedral to subhedral habits and is generally <2 mm in size.





**Figure 2-5:** Angular harzburgite breccia fragments within a magnesite matrix in outcrop exposed along the chromite mine road.

One pod-shaped, massive to nodular type (Greenbaum, 1977) chromite prospect, located to the northeast of Kokkinorotsos (MAP 1), was examined in more detail. This chromite bearing zone is hosted wholly within the dunite along the harzburgite contact. It strikes concordantly with the contact between the two units and lies parallel to the regional tectonite fabric. The nodules are oblate in shape, up to 1cm. in length with aspect ratios (X-Y) in the order of  $<1:5$  and trending parallel to the strike of the pod. The massive chromite nodules have interstitial silicate cores and exhibit smooth contacts with the enclosing dunite (Figure 2-6). Greenbaum (1977) has proposed a magmatic origin for such nodular-type chromite. Modification of the nodules by penetrative solid-state deformation



**Figure 2-6:** Massive to nodular "leopard type" chromite hosted by massive dunite located northeast of Kokkinorotsos.

has yielded a schlieren textured overprinting on the older cumulus features. Isoclinal folding of massive chromite layers was noted in two outcrops (Figure 2-2) with a axial planar foliation concordant to the regional structural trends.

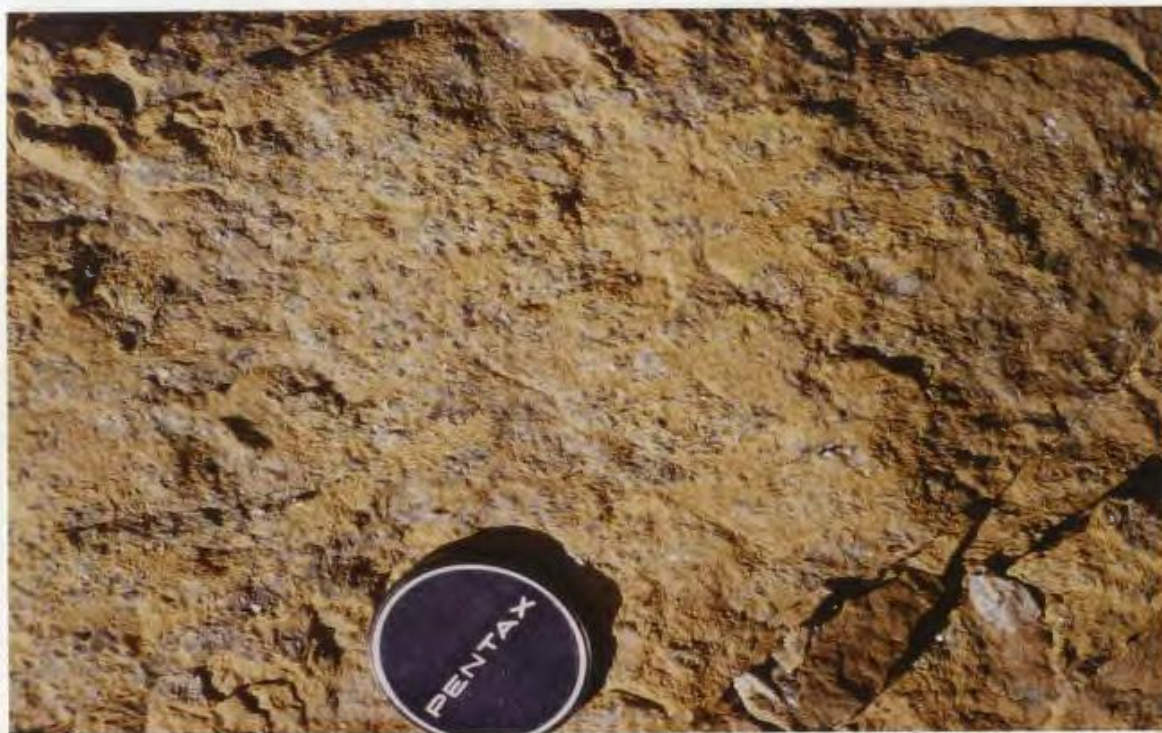
#### **2.2.1.3. Dunite**

The dunite unit is orange to yellow-tan on weathered surfaces and dark green to black on freshly exposed, highly serpentized surfaces. Disseminated (<2%), euhedral chromite contrasts sharply with the olivine phase on weathered surfaces. The main body of dunite is uniform in modal composition and structural style; being devoid of mesoscopic features except for the occasional chromite stringer. These stringers trend parallel to the regional  $S_1$  fabric which is defined in the



harzburgite. Although there is no penetrative foliation visible in the dunite, the infolded character of the harzburgite/dunite contact supports the safe extrapolation of this regional structural fabric for some distance into the dunite.

A gradation from massive dunite to clinopyroxene-bearing dunite was observed in the northeastern and southwestern margin areas of the main dunite body (MAP 1). The pyroxene phase exhibits a disseminated, partially poikilitic texture in hand sample.



**Figure 2-7:** Clinopyroxene oikocrysts enclosing partially resorbed and rounded olivine chadacrysts within undeformed (younger suite) clinopyroxene-dunite.

The clinopyroxene oikocrysts appear undeformed and enclose chadacrysts of olivine (Figure 2-7). The clinopyroxene phase appears cumulate in nature,

however a number of previous workers (e.g.: Niccolas et al., 1980; Secher, 1981; and Nicolas and Prinzhofer, 1983) have argued for a secondary origin of this mineral phase. Their basis of argument rests upon a number of features: (1) the lack of a spatial association with orthopyroxene or spinel; (2) the interstitial habit of the clinopyroxene; (3) augite growth twins; and (4) lack of plastic (crystallographic) deformation. The present author interprets the diffuse and gradational contact with dunite as well as the proximity to the ultramafic plutons to indicate a younger intrusion melt origin by melt impregnation (refer to Subsection 3.7.2) for these clinopyroxene rich patches within the dunite. Such a relationship is in agreement with the multiple intrusive history of the complex as documented during the present study.

The upper boundary of the dunite unit strikes northeast-southwest and is marked by the intrusive margin of the main body of younger plutons. These plutons truncate both the structural fabric of the dunite and harzburgite and the locally developed phase layering near the dunite/harzburgite transition (Map 1).

Crosscutting and randomly orientated veins and dikes of pyroxenite, gabbro and lesser amounts of poikilitic wehrlite intrude near major contact margins as well as deep within the dunite body.

The infolded boundary between the dunite and harzburgite has been discussed in Section 2.2.1. However, along the northeastern margin of the map sheet, dunite and harzburgite are in fault contact with one another for a distance of  $\sim 200$  m (Map 1). This vertical to subvertical, east-west striking normal fault appears to die out towards the west, either within or truncated by a later suite pyroxenite pluton. Eastward, in the stream valley along the eastern map margin (Map 1), the attitude of this fault flattens to a moderate ( $\sim 40\text{-}50^\circ$ ) north dip. Concordance of the regional foliation within both the dunite and harzburgite on either side of the fault indicates minor rigid-body rotation of the adjacent fault blocks. The contact between clinopyroxene-bearing dunite and layered olivine gabbro is also fault controlled in the northeastern part of the map area.

It is not possible to estimate a value for the original thickness of the dunite unit. Extreme infolding and attenuation of the dunite lower boundary with the harzburgite tectonite and truncation of the dunite upper boundary by younger suite intrusives has been discussed. The lack of suitable marker horizons within the essentially monomineralic dunite eliminates any chance of resolving the geometry of the fold repetition within the dunite unit as a whole. In addition, intrusion of the younger suite plutons at different levels within the dunite has likewise yielded a highly variable pseudostratigraphic thickness for the unit as exposed in the field. Within the central map region, only the "lowermost" dunite level is preserved in contact with the harzburgite, while to the southwest and northeast, a much wider zone of dunite remains (MAP 1).

### **2.2.2. The Transition Zone**

Results of the field mapping show that only a few relict blocks of the older suite transition zone are preserved within the northwestern portion of the Troodos plutonic complex. Three separate blocks of layered transition zone orthopyroxenite and olivine-pyroxenite lithologies occur as isolated fragments hosted within younger suite poikilitic wehrlite and pyroxenite plutons (Map 1). The largest block of transition zone lithologies outcrops discontinuously over a 200 m by 100 m area which is best exposed along a 25 m roadcut section on Pine Road (Figure 2-8) (Map 1).

In the field, the light to dark green transition zone is characterized by the well developed layering of the orthopyroxenite and olivine-pyroxenite units. Individual layers range in width from  $< 1$  cm to 10 cm and are traceable along strike for up to 15 m. The attitude of layering within the three separate transition zone blocks shows a consistent north to northwest strike and moderate to steeply west dip. This general attitude is compatible with the orientation of the  $S_1/S_0$  fabric in the structurally lower dunite/harzburgite section (MAP 1). Correspondence of the fabric element in each of the three blocks may suggest little rotation of the segments during a rather passive stopping and assimilation of the older suite





**Figure 2-8:** Layered orthopyroxenite of the older suite transition zone exposed in roadcut along Pine Road.

Transition Zone by the younger suite intrusions (refer to Section 2.3.2). These keels of transition zone rocks (refer to cross-section A-A', Map 1) are all that remains of this section of the older suite sequence as exposed at the present erosional level in the map area. The younger suite plutons have thus obliterated most of the transition zone and its geometrical relationship to the older suite dunite and layered gabbro units.

Contact with the host intrusive lithologies are difficult to determine in the field due to the generally poor exposure. Also, the presence of late, small-scale shearing and/or diffuse assimilated margins have likewise obscured the intrusive nature of the contacts. Nevertheless, close inspection revealed crosscutting



relations with veins of coarse grained, undeformed younger suite clinopyroxenite truncating layering of the transition zone orthopyroxenite (Figure 2-9). Similar relative age relations between the deformed and undeformed units are beautifully preserved on the microscopic level and discussed in Chapter 3, Section 3.9.

### **2.2.3. The Older Suite Gabbros**

The gabbro succession of the older suite, as exposed within the study area, includes layered olivine and hypersthene gabbro and lesser amounts of massive pyroxene and/or hornblende gabbro with minor plagiogranite, dolerite and trondhjemite. These latter, more massive gabbroic units have been collectively referred to as the "high level gabbros" (Allen, 1975) and are thought to represent later differentiates of the magma(s) which during fractional crystallization yielded the plutonic stratigraphy (Wilson, 1959; Moores and Vine, 1971; Allen, 1975). Some ambiguity exists in classifying all of these high level gabbros as strictly older suite in origin (Section 2.2.3.3).

A north-south trending transition boundary between the layered olivine and hypersthene gabbros is marked in the field by the gradual disappearance of the olivine phase (Map 1). Layered olivine gabbro dominates in the northeastern half of the map sheet while mainly hypersthene gabbro outcrops in the west. Within the layered olivine gabbro, the foliation lies parallel/subparallel to layering. A NE strike and moderately S-SW dip is consistent for this layering/foliation. Exposures of the layered hypersthene gabbro show a consistent NE strike and moderate SW dip in the eastern half of the map sheet, whereas the orientation of this layering, and foliation where developed; swings to an E-W strike within western exposures.

A fault controlled, structurally "upper" contact of the layered and massive gabbros with the sheeted dike complex has been previously documented in Section 2.2 (Figure 2.1) and the structural base of the layered olivine gabbro in the eastern map sector may also be fault controlled (Subsection 2.2.1.3). Elsewhere,



**Figure 2-9:** A dike of coarse to pegmatitic, undeformed clinopyroxenite (CPX) of the younger intrusive suite invading and truncating the S<sub>0</sub>/S<sub>1</sub> of the older suite transition zone (TZ) orthopyroxenite.

the base of the layered gabbros is defined by the intrusion of the younger suite plutons (refer to Section 2.1).

### **2.2.3.1. Layered Olivine Gabbro**

The olivine layered gabbro exhibits excellent phase layering as exposed along a number of roadcuts and outcrops; particularly the prime localities west of Ayious Nikolaos and north of the Ezzo Galata River (Map 1). Individual meso, leuco and melanocratic layers range between 5 cm and 50 cm (and in rare localities up to 90 cm) in width and are traceable along strike for upwards of 25 m in the best roadcut exposures (Figure 2-10). Finer scale laminations, between .5 cm and 5 cm in width, are contained within the broader scale layering. The phase layering is defined by alternating mineral assemblages which exhibit a range in modal composition (e.g.:  $Ol_{15-45}$   $CPX_{20-55}$   $OPX_{5-20}$   $PLAG_{10-40}$ ). A strong to weak foliation orientated parallel/subparallel to the layering is defined in outcrop by the preferred orientation of flattened olivine grains (aspect ratios  $<10:1$ ) and plagioclase laths.

A variety of processes has been invoked to explain the development of phase layered (broad and fine scale) differentiated sequences in ultramafic-mafic complexes. These processes include traditional differential crystal settling and accumulation models (e.g.: Bowen, 1915; Wager and Deer, 1939; Hess, 1939; Jackson, 1971) as well as the more recent concepts involving in-situ crystallization (McBirney and Noyes, 1979), magmatic density currents which deposit/redeposit crystals (Irvine, 1980) and double-diffusive convection (McBirney and Noyes, 1979; Irvine, 1980; Wadsworth, 1985). The development of primary structures in the cumulate sequence (e.g. : small scale layering, cross-bedding, graded bedding, slump and load structures) is controlled by physical parameters including gravity, hydraulic properties of the fluid (i.e. magma viscosity) and density currents similar to those which control sedimentary processes (Irvine, 1965; 1967; 1980; Jackson, 1967; 1971; Wadsworth, 1985).

Sedimentary-type structures are best developed within the layered olivine



**Figure 2-10:** Prominent rhythmic phase layering of olivine and minor hypersthene gabbro exposed in roadcut to the north of the Esso Galata River. The  $S_0/S_1$  dips consistently  $35^{\circ}$ - $45^{\circ}$  to the southwest. View structural down-section.

gabbros towards the northeastern map sheet. These structures include: (1) graded layering; (2) slump folds; (3) trough banding; (4) scour and fill; and (5) cross-bedding (Figure 2-11). The latter two structures impart a thickened, thinned and pinched layered appearance to the layering. Such structures are suggestive of formation by the more traditional models of crystal settling and density currents (Wager and Deer, 1939; Jackson, 1971; Irvine, 1980) rather than the more recent models of double-diffusive convection and in situ-crystallization (McBirney and





**Figure 2-11:** Primary flow structures in layered olivine gabbro. Note the well preserved cross laminations and truncation of the phase layering.

Noyes, 1979; Wadsworth, 1985). Allen (1975) attributed the development of crossbedding and scour and fill structures in the layered gabbro to "high energy" magmatic currents within the magma chamber.

The generally discontinuous nature of the layering throughout the unit can in fact be attributed to a combination of factors including: (1) primary sedimentary-type processes as outlined above; (2) additional magmatic features [e.g.: transgressive melts, localized in-situ crystallization in connection with double diffusive convection (Irvine, 1980; Wadsworth, 1985), pegmatitic veining, replacement processes (Irvine, 1980), mush injections (Jackson, 1971)]; and (3) secondary penetrative, plastic deformation (discussed in Chapter 3).

### **2.2.3.2. Layered to Massive Hypersthene Gabbros**

The hypersthene gabbros are varitextured in appearance. They range from fine grained and massive to poorly banded with a wispy, streaky irregularly developed foliation to strongly layered/foliated. The majority of exposures exhibited a combination of the former two textural types.

Phase layering in the gabbros generally ranges from .5 cm to 7 cm in width and is usually discontinuous over a few meters. Primary cumulate structures, similar to those described for the layered olivine gabbros, are variably developed in the hypersthene layered gabbros (Figure 2-12). Phase layering is defined by alternating mineral assemblages exhibiting a range in modal composition.

A weak foliated/lineated fabric, which is variably developed within the strong and wispy layered gabbros, is defined in hand sample by the preferred dimensional orientation of the inequant pyroxene and tabular plagioclase crystals. This alignment may represent either a primary magmatic feature (Schmidt, 1952; Morse, 1969; Jackson, 1971; Wadsworth, 1985) or a secondary deformation induced fabric (Avé Lallement, 1967; Loney *et al.*, 1971; Nicolas *et al.*, 1980; Thayer, 1980; Nicolas and Violette, 1982). This will be discussed in Chapter 3.

### **2.2.3.3. High Level-Massive Gabbros**

High level, more massive gabbro lithologies occur throughout both the layered olivine and hypersthene gabbros. The layered olivine gabbros show gradations to and abrupt truncation by massive, medium coarse to pegmatitic olivine-pyroxene and pyroxene-hornblende gabbros (Figure 2-13, 2-14 and 2-15).

Outcrops of wispy, streaky hypersthene gabbro also grade vertically and laterally along diffuse zones to massive, medium-fine to pegmatitic pyroxene and pyroxene-hornblende gabbro (the so called "high-level" gabbros) interpreted to represent the late differentiates of the layered gabbros (Allen, 1975). The domains in which these textures prevail are marked as stippled areas on Map 1. From the map, it is obvious that the spatial distribution of the main bulk of these



**Figure 2-12:** Primary magmatic flow structures in layered hypersthene gabbro showing well preserved cross laminations and truncation of phase layering.

massive, undeformed gabbros lies within the layered hypersthene gabbro. A genetic link between these zones of massive, isotropic gabbro and the older suite gabbros is favoured on the basis of this spatial association. However, an absolute distinction of the undeformed later differentiates (above the deformation front), (refer to Chapter 3, Section 3.4) of the older suite from diffuse, undeformed gabbroic intrusives of the younger suites is difficult. Late differentiates of the older suite layered gabbros may have solidified above the brittle-ductile transition (the deformation front), (refer to Section 3.4), thus escaping ductile deformation which may have been continuing at structurally deeper levels in the older suite. Alternatively, these anastomosing zones within the post-kinematic gabbro could be





**Figure 2-13:** Vari-textured gabbros of the older suite showing abrupt truncation of  $S_0$  and  $S_1$  of the layered olivine gabbro by an isotropic, coarse grained phase of olivine-pyroxene gabbro.





**Figure 2-14:** The foliation/layering within tectonized olivine gabbro truncated by the multiple intrusion of isotropic, fine grained melanocratic gabbro dikes. Note the abrupt truncation of the  $S_1/S_0$  and contact reactions marked by coarse pyroxene-gabbro margins.



**Figure 2-15:** Tectonized olivine gabbro with  $S_0/S_1$  truncated by coarse, isotropic pyroxene gabbro of either the younger or older suite(s).

fractionated melts of the younger suite intrusives. Thus, subdivision of the undeformed gabbros into time separated suites cannot be achieved within the regions above the ductile deformation front. Discussion of the position of the deformation front which moves with time relative to the magmatic suites is presented in Chapter 3.

Net veining of the massive and faintly banded gabbros by swarms and singular veins of plagiogranite and trondhjemite was observed locally (Figures 2-16 and 2-17). These veins generally range from 1 cm to 6 cm in width and intrude irregularly through the gabbro, showing both diffuse and sharp contacts with the host rocks.

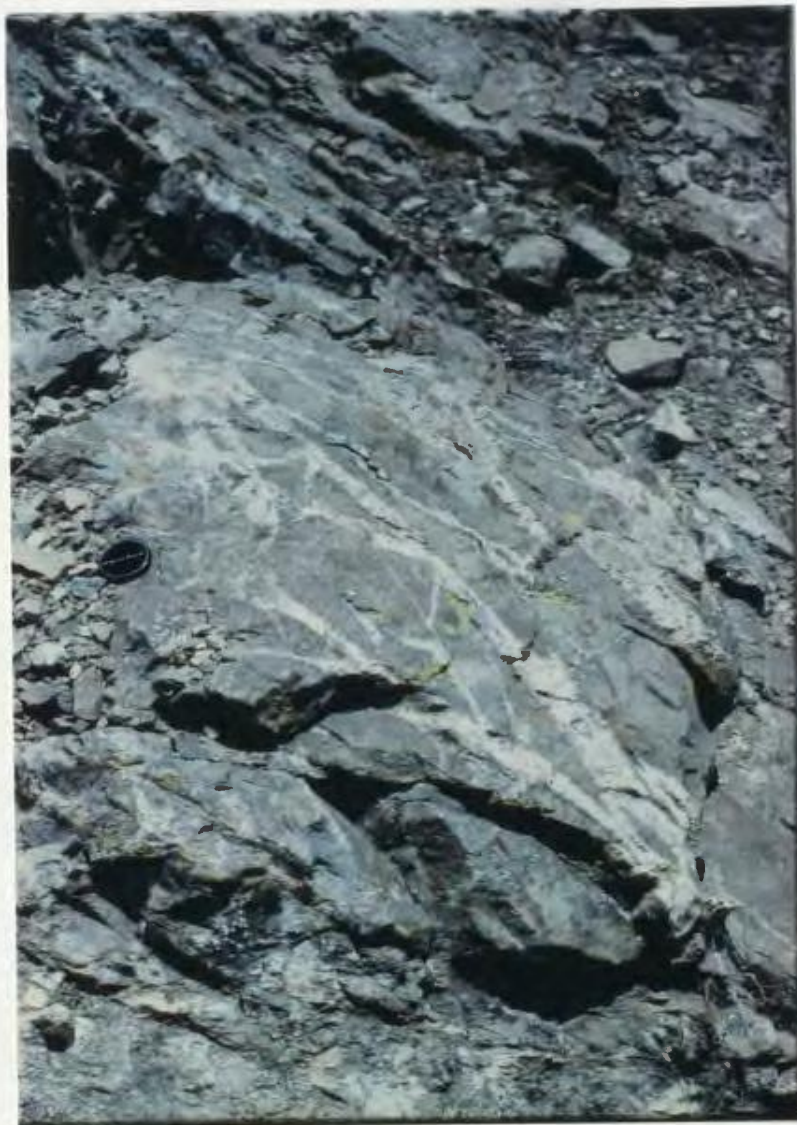
### **2.3. The Younger Intrusive Suite(s)**

The younger suite(s) classification scheme incorporates all of the essentially undeformed, post-kinematic plutons, sills and dikes which characteristically intrude and truncate the layering/foliation fabrics in all lithological units of the older suite. The younger suite(s) is composed of a range of ultramafic to mafic lithologies consisting of wehrlite, feldspathic-wehrlite, lherzolite, feldspathic-lherzolite, websterite, clinopyroxenite, peridotites, pyroxene-hornblende gabbro and mafic dikes. The following sections will discuss : (1) the primary features of the younger suites; (2) the spatial distribution and contact relations with the older suite; (3) the temporal and spatial relations of multiple magmatism (auto-intrusion) within the younger suite lithologies; and (4) the concept of fault controlled intrusion in relation to the deformation front. The mafic dikes of the younger suites will be discussed separately.

#### **2.3.1. Primary Features of the Younger Suites**

The lithological units of the younger suites, excluding the mafic dikes, exhibit well developed primary crystal textures and a highly variable grain size. The wehrlitic and lherzolititic bodies are composed of poikilitic crystal cumulate textures. Weathered surfaces show a pitted, spongy texture due to the presence





**Figure 2-16:** Intrusion and net veining of trondhjemite into weakly phase layered hypersthene gabbro.

of rounded olivine inclusions (chadacrysts) enclosed within the more weathering resistant pyroxene oikocrysts. The oikocrysts generally range from 1 cm to 3 cm in diameter. However, larger orthopyroxene oikocrysts, up to 11 cm in diameter, were observed within the core regions of plutons. Plagioclase oikocrysts, up to 1.5 cm in size, occur within the feldspathic ultramafic units. The undeformed state of the ultramafic units is indicated in the field by the random orientation of crystals and optical continuity across large, well preserved orthopyroxene oikocrysts (Figure 2-18). A weak and heterogeneously developed planar alignment of slightly

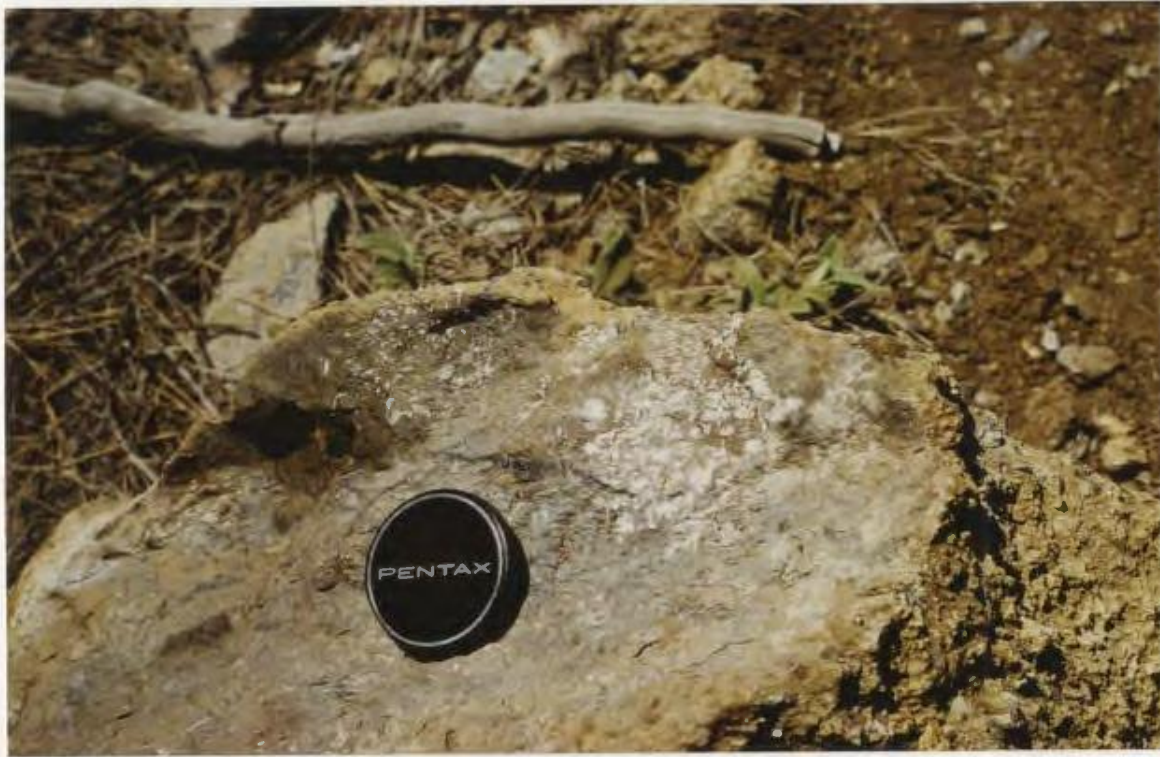


**Figure 2-17:** Angular blocks (xenoliths) of vaguely phase layered hypersthene gabbro backveined and brecciated by gabbro and plagiogranite.

flattened plagioclase oikocrysts was observed within one small outcrop of wehrlite-lherzolite. However, this unit revealed little evidence of crystallographic deformation at the microscopic level (refer to Chapter 4, Subsection 4.1.1).

The pyroxenite and gabbroic units display randomly orientated, primary magmatic (cumulate) crystal textures. Grain sizes are highly variable, ranging from medium-fine ( $< 2$  mm) to pegmatitic ( $> 1$  cm). Pyroxene poikilitic textures were rarely observed within the pyroxenite intrusives. A slight decrease





**Figure 2-18:** Large ( $>3$  cm.) orthopyroxene oikocryst with rounded olivine chadacrysts from the main wehrlite intrusion. Note the unstrained optical continuity across the reflecting surface of the oikocryst and the spongy, pitted appearance on weathered surfaces (lower right corner).

in grain size was noted proximal to pluton margins. Dikes of ultramafic, pyroxenite and gabbroic composition, which intrude along the pluton margins and into the older suite units, commonly exhibit a coarse to pegmatitic grain size.

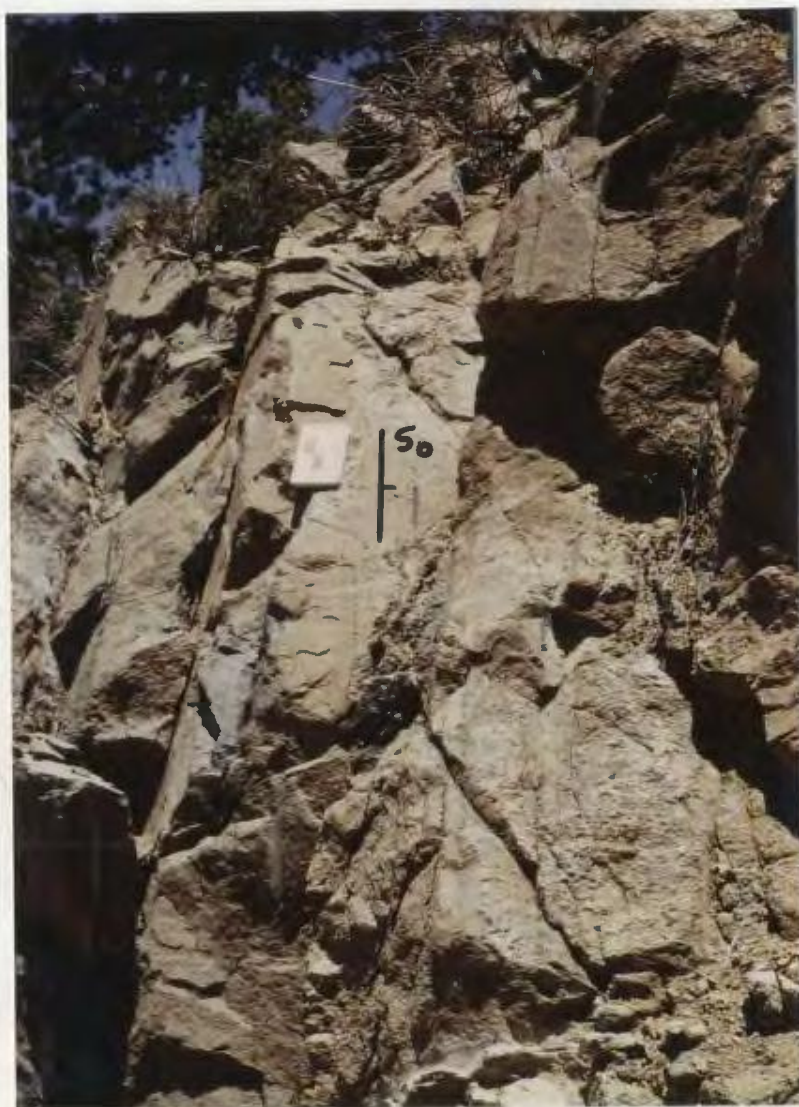
The development of cumulate layering in the younger suite units is rare except within some parts of the central poikilitic wehrlite plutons of the main intrusive belt (Zone 1/Map 1). Within this region, the vertical to subvertical layering is discontinuous and traceable along strike for less than 10 m. Individual layers are

defined by slight changes in grain size and undulating, variably weathered surfaces. These layers range from 1 cm to 12 cm in width and appear to grade both vertically and laterally into massive peridotite. No finer scale layering was observed in any of the plutons. The strike of layering trends both oblique and parallel to the trace of the regional layering/foliation of the older suite (Map 1). Layering within three outcrops of one clinopyroxenite body showed variable orientations. This layering varied from 1 cm to 4 cm in width with a steep to vertical dip (Figure 2-19).

### **2.3.2. Spatial Distribution and Contact Relations Between the Older and Younger Magmatic Suites**

The spatial distribution of the younger suite lithologies illustrates the multiple intrusive history which characterizes the Troodos plutonic complex. These younger suite bodies intrude at various levels within the older suite sequence, from harzburgite through to the layered gabbros (MAP 1).

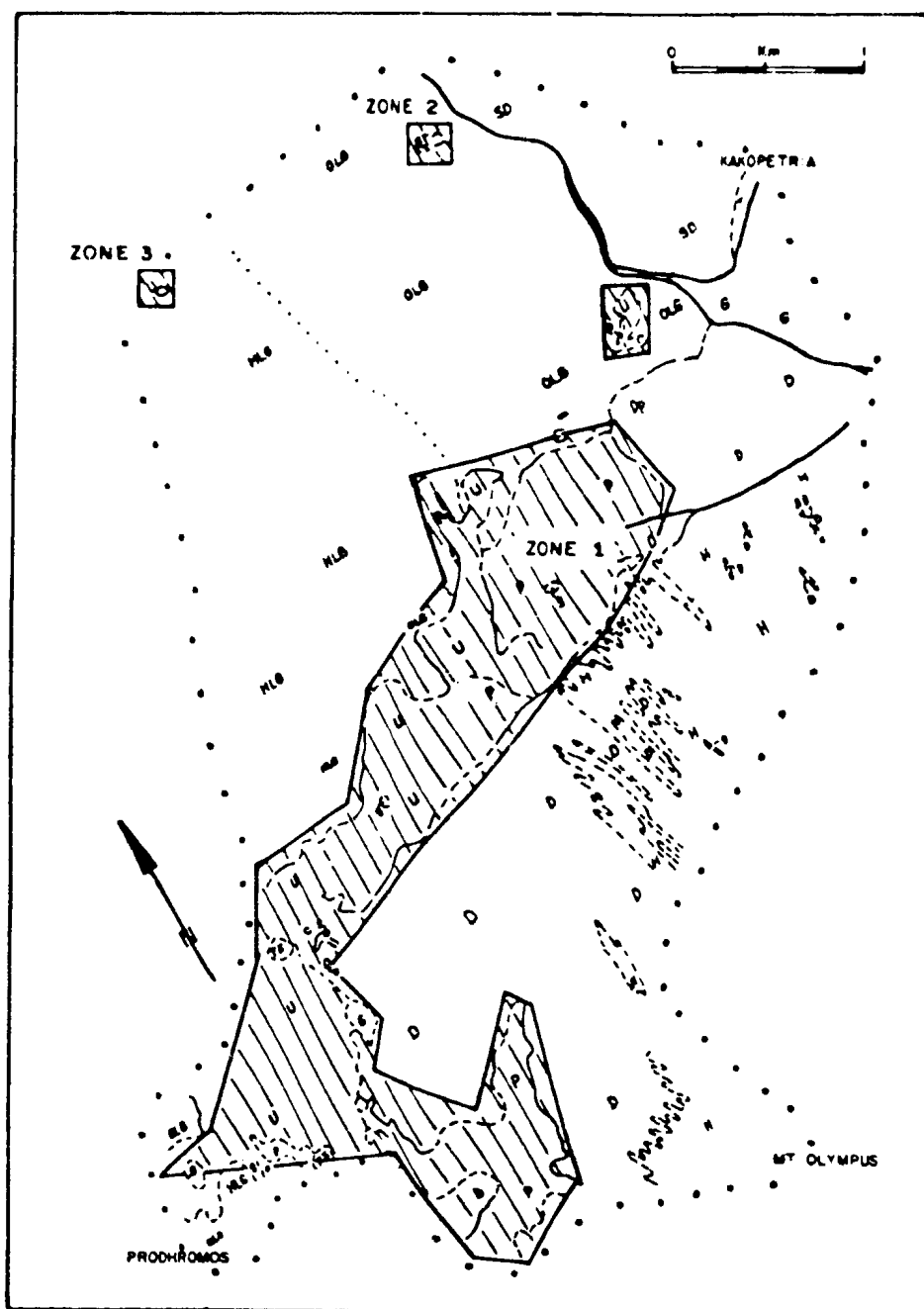
The main volume of younger suite plutons occupies a northeast-southwest striking, up to 1 km. wide region (Zone 1/ Figure 2.20) which separates the dunite from layered gabbro units of the older suite. This intrusive zone widens southward towards the village of Prodhromos (Map 1). Two smaller stocks of younger suite wehrlite, lherzolite and olivine-pyroxene gabbro outcrop at "higher" structural levels within the older suite layered gabbros. These two bodies are located along the northeastern and northwestern map margins (Zone 2 and 3, respectively, Figure 2-20). One small (1 m) plug of cumulate wehrlite was noted intruding dunite along the infolded dunite-harzburgite contact. Similar but much larger bodies of poikilitic feldspathic-wehrlite and lherzolite within harzburgite tectonite were reported by Allen (1975) and George (1978) to be located 1.75 km southeast of Mount Olympus. Large dikes of coarse to pegmatitic isotropic pyroxene-hornblende gabbro were observed to intrude dunite and harzburgite in the southern half of the map sheet (Figure 2.21)



**Figure 2-19:** Subvertical primary igneous layering within younger suite clinopyroxenite exposed along the highway from Mount Olympus to Prodhromos .

The small pods of younger suite intrusives which occur within both the tectonized layered gabbro and harzburgite may or may not be temporally associated with the plutonism of Zone 1. The two intrusive bodies within the layered gabbro, along the northern map margin (Zones 2 and 3), show only weak deformation features (isotropic mesoscopic textures and some kink banding of the olivine on a microscopic level (refer to Chapter 4, Subsection 4.1.1) and intrude and truncate the fabric of the host gabbro. These two pods are, thus, younger





**Figure 2-20:** Simplified geological map of the northwestern quadrant of the Troodos plutonic complex showing zones of younger suite intrusion. Legend and symbols as in MAP 1.



**Figure 2-21:** Large dike intrusion of coarse to pegmatitic pyroxene-hornblende gabbro (G) into massive dunite (D). Note the intense serpentinization (dark gray) along the contact margins.

than the layered gabbro. However, since they are undeformed, they may be part of any post-kinematic intrusive suite. The same holds true for the younger plutons within harzburgite. Thus, all spatially separated plutons which solidified above the deformation front (post-kinematic) could also be temporally separated, having derived their melt from different magma chambers rather than from different melt batches from a common, deeper seated magma chamber.

An argument could be made to support the genetic correlation of these smaller plutons, occurring within the layered gabbro, with the older deformed suite. Such a case would be possible if heterogeneous strain occurred so that some zones of

the suite (i.e.: these ultramafic pods) escaped the penetrative deformation (i.e.: low-strain domains) and/or if hyper-solidus conditions prevailed within such domains so that the strain was magma flow accommodated. It is extremely important to note, however, that this scenario does not hold for the small plutons within the present study area of the Troodos plutonic complex since: (1) the ultramafic magmas would be expected to have solidified before the gabbroic components; and (2) the major boundaries of lower strain domains should exhibit attenuated, lensoidal shapes, aligned parallel with the regional foliation of the surrounding penetratively deformed lithologies. The plutons of zones 2 and 3 within the northwestern quadrant of the Troodos plutonic complex crystallized after the host older suite layered gabbro and the contact relations and structural fabrics observed in the field are not compatible with a low-strain domain geometry.

The lithological make-up of the central belt (Zone 1) shows a major outcrop of clinopyroxenite-websterite with minor pyroxene-gabbro in the northeast while poikilitic wehrlite, feldspathic wehrlite and minor lherzolite, peridotite and pyroxenite occupy the central and southwestern exposures. Pods, dikes and small plutons of pyroxene-hornblende gabbro dominate along the belt, intruding both the younger suite poikilitic wehrlite and older suite dunite (Figure 2.21). The boundaries of this main intrusive zone are marked by the juxtapositioning of contrasting textures and lithologies and the abrupt high-angle truncation of the layering/foliation of the older suite units.

The field relations exposed within three selected areas are illustrated in more detail in Figures 2-22, 2-23 and 2-24 to exemplify the intrusive contact relations between the older and younger suites. These three detailed map areas are marked on Map 1. The abrupt termination of layering/foliation in both the older suite layered olivine gabbro and harzburgite/dunite units by the younger suite ultramafics is clearly illustrated in plan view and cross-section in Figures 2-22 and 2-24. The oblique relationship between the northwest striking and moderate to

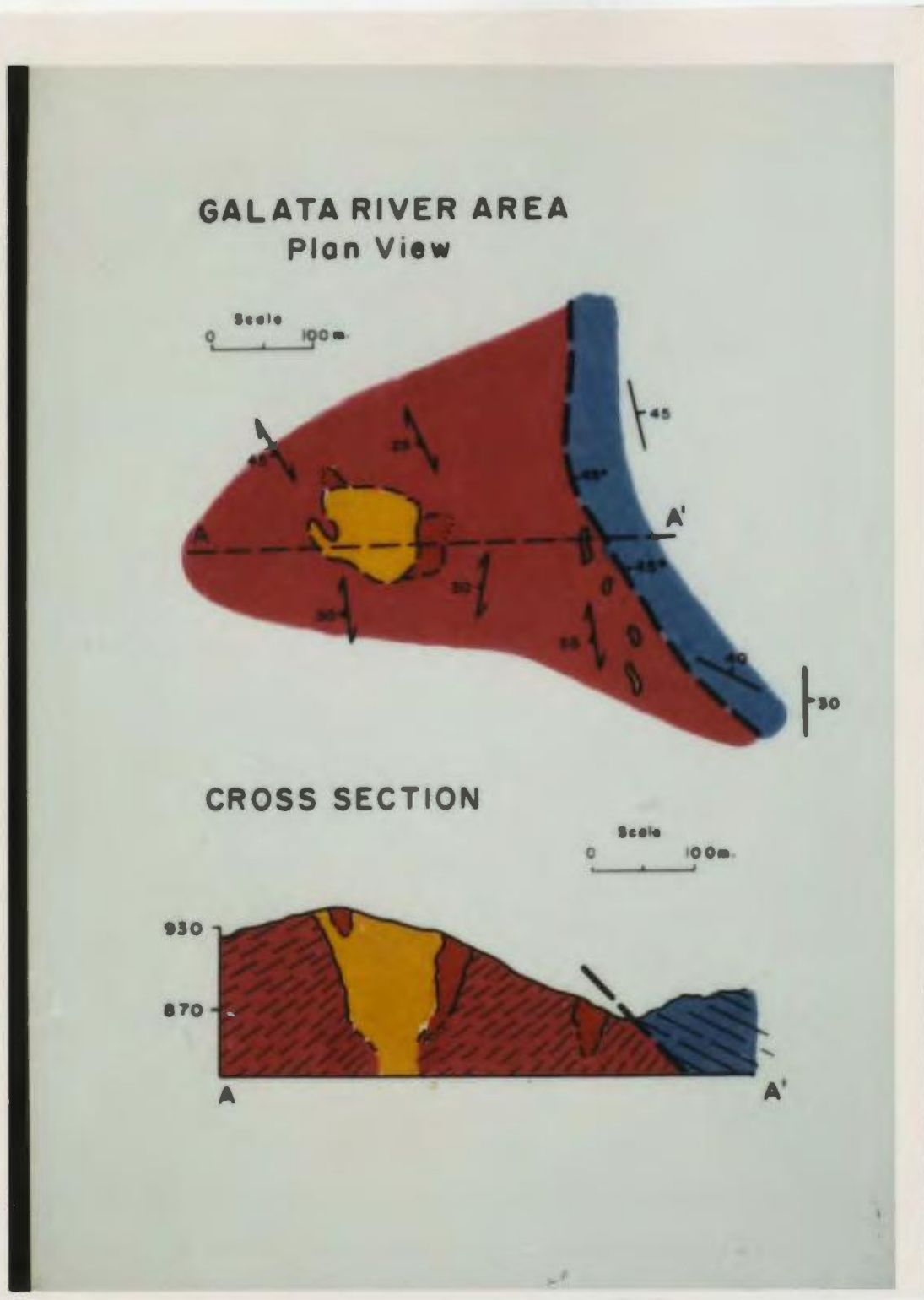
steeply northeast and southwest dipping  $S_0/S_1$  layered gabbro fabric with respect to the north-south striking, vertical primary layering in the younger suite poikilitic wehrlite intrusion is depicted in Figure 2-24. Dike and vein offshoots from the major intrusive bodies into the surrounding country rock are illustrated in Figure 2-24. Large scale concordant intrusion of a poikilitic feldspathic-wehrlite/lherzolite and subordinate clinopyroxenite sill into the older suite layered olivine gabbro host is shown in Figure 2-23. Xenoliths of olivine gabbro within the poikilitic lherzolite are exposed along the lower contact margin of the sill intrusion in Figure 2-23. The xenoliths show a strong parallel alignment of their long axes parallel to the contact base of the sill (Figure 2-25). Xenoliths of intensely serpentinized (100%), medium gray dunite were also noted within poikilitic wehrlite and pyroxenite along the contact margin of the main intrusive belt and older suite dunite (MAP 1).

Cross-section A-A' (Map 1) demonstrates the disruption and probable minor rigid-body rotation of blocks of layered gabbro along the northwestern margin of the main intrusive zone (Zone 1/Map 1). Also, truncation of harzburgite foliation fabric by the younger suite clinopyroxenite body is clearly shown in cross-section B-B' (Map 1).

An abundance of small scale brittle fracturing/faulting was noted along many of the major, younger suite intrusive contacts. However, detailed examination often revealed indisputable evidence for younger suite intrusion into the older suite lithologies based upon xenolith bearing contact margins, truncation of the foliation/layering fabrics and/or crosscutting dikes/veins.

### **2.3.3. Spatial and Temporal Relations of Multiple Intrusion within the Younger Suites**

The spatial and temporal relations within plutons of the younger suites are discussed in the following section. Within the main intrusive belt (Zone 1/Map 1) evidence indicates the presence of multiple intrusive relations indicative of both



**Figure 2-22:** Younger suite feldspathic-lherzolite intruding and truncating west dipping layered olivine gabbro near the fault contact with the sheeted dike complex. Symbols: blue = sheeted dikes; red = layered gabbro; orange = intrusive.



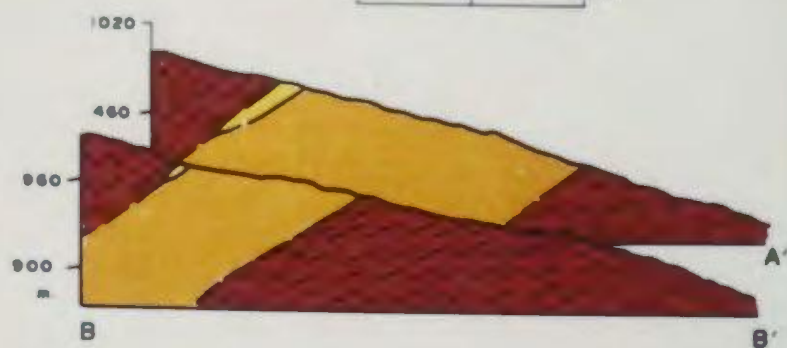
# VIRVIROS AREA Plan View

Scale  
0 100m



## CROSS SECTION

Scale  
0 100m



**Figure 2-23:** Younger suite wehrlite sill intruding concordantly/subconcordantly to the fabric elements in the host layered gabbro. The sill varies in true thickness from 30 to 100 m. Symbols as in Fig. 2.22.

MOUTTI TOU ZOUMI AREA  
Plan View

Scale  
0 100 m



CROSS SECTION

Scale  
0 100 m



**Figure 2-24:** Truncation of layered gabbro by the intrusion of massive, poikilitic and locally banded wehrlite-lherzolite (+ plagioclase) of the main intrusive zone (Zone 1). Symbols: red = layered gabbro; orange-yellow = younger intrusive; blue = trondjemite.



**Figure 2-25:** Alignment of elongate and tectonized older suite olivine gabbro xenoliths (OLG) within the younger suite wehrlite intrusion (W) as exposed along Cherry Brook.

"auto-intrusion" (Gass, 1980) within an undeformed differentiating magma and massive intrusion of this magmatic suite by the gabbroic roof-zone of another deeper-seated magma chamber.

Field criteria indicate a gross compositional differentiation trend, from ultramafic to gabbroic lithologies in Zone 1. The crosscutting, intrusive relations within this belt show poikilitic peridotites intruded by dikes and pods of pyroxenite. Both of these ultramafic lithologies are, in turn, intruded/crosscut by pods, dikes and veins of pyroxene and pyroxene-hornblende gabbro. The marginal zones of the poikilitic peridotite bodies also show an abundance of crosscutting pyroxenite-gabbro dikes/veins which also intrude into the older suite



country rock. The two younger suite stocks (Zones 2 and 3 / Map 1) likewise show marginal pyroxenite, websterite and olivine gabbro phases. Progressive fractionation is also indicated in the field by lithological gradations from pyroxenite to gabbroic compositions marked by an increase in the modal proportion of plagioclase content. Pyroxene fractionation within the younger intrusive suite is also supported by mineral chemistry data in Chapter 4, Subsection 4.2.1.

In essence, a sequence from relatively older to relatively younger plutons corresponds to a progressive differentiation from ultramafic to mafic lithologies for the main bulk of the younger suite magmatism. This differentiation sequence gives support to a case for "auto-intrusive" processes whereby progressively fractionating magmas were being supplied from a larger, deeper-seated, evolving magma chamber. Within these suites, the multiple intrusive relations observed cannot be unambiguously subdivided into time-separated suites and thus may, in fact, be related to one undeformed, continuous suite.

Massive dike swarms of gabbro with minor pyroxenite dikes intrude ultramafic plutons along the southern sector of the main intrusive region (Zone 1/Map 1). These gabbroic dikes and pods are coarse to pegmatitic and intrude throughout both the older suite dunite and younger suite poikilitic peridotites. These intrusive zones are marked by an intense serpentinization of the host lithologies (both older and younger suites). The intrusive relations are clearly illustrated in cross-section A-A' (Map 1). The spatial relations indicate the probable presence of an additional, deeper-seated evolving magma chamber(s), the cupola or roof-section(s) of which is/are represented by these gabbroic dike swarms (Cross-section A-A'/Map 1) stopping into the overlying older and younger suite lithologies.

#### **2.3.4. Fault Controlled Intrusion of the Younger Suite in Relation to the Deformation Front**

Field evidence, along a number of lines, indicates the control of major brittle faulting on the spatial distribution of intrusions of the younger suite(s) plutons along the main belt (Zone 1/Map 1). This evidence includes: (1) the apparent localization of the majority of the intrusions along a somewhat linear northeast-southwest striking zone (MAP 1); (2) an extensional stress regime operating during the younger suite magmatism as indicated by the intrusion of mafic dikes and the permissive nature of intrusion with stoping and assimilation without any indication of large scale rigid-body rotations of the fabric elements in country rocks along the contact margins or in keels within the younger suite plutons (cross-section A-A'/Map 1); and (3) the absence of older suite gabbroic and transitional zone lithologies in contact with dunite along the southeastern margin of the main intrusive zone (Zone 1/Map 1), which may indicate the absence of the older suite gabbroic lithologies and transition zone by fault removal of this section of the older suite prior to the intrusion of the younger suites. Additional evidence for major brittle deformation in this region is also exhibited by the faulting between layered olivine gabbro and clinopyroxene-bearing dunite in the northeastern map area, near the northeastern end of the main intrusive zone (Section 2.2.1.3). Dunite and harzburgite are also in fault contact for a short distance near the northeastern map margin. This vertical, east-west striking fault dies out westward either within or truncated by the clinopyroxenite pluton as mentioned in Section 2.2.1.3. These major brittle structures are most likely normal, moderate to high-angle faults based upon the overall "stratigraphic" drop in progressively northern blocks in cross-sectional view. Such faults can be correlated with axial valley grabens developed early in the accretionary history of the complex during magmatism within the spreading domain. The influence of faults on the intrusion of the smaller ultramafic plutons could not be determined on the basis of field exposure.

Listric normal faults, noted by Varga and Moores (1985) within the sheeted dike

complex, reportedly flatten out upon entering the gabbros. However, the present author's work shows that such graben structures extend deep within the complex, to the paleo upper mantle region and may have acted as major conduits for intrusion/stopping of younger plutons into the older ophiolite sequence. Similar fault controlled intrusion of magmas has been noted by Calon (pers. comm.) to occur within the Troodos plutonic complex, to the south of the present author's study area.

The presence of brittle deformation features within this region of the older suite, having formed either contemporaneously with or prior to intrusion of the younger suite(s) magmas indicates that during this time period the deformation front was situated at a deeper structural level; below the presently exposed lowest level of the younger intrusives within the accreting crust (refer to Chapter 3, Section 3.4 for discussion of the deformation front). Spreading of the crustal segment in response to continued overturn of the upper mantle convection cells beneath the diffuse ridge zone would continue to create an extensional stress field and yield dilational features (i.e.: faulting, fracturing) within this brittle domain. Such faults would have continued to create the least resistant route for magmas to ascend from depth and accumulate in small discrete chambers within the plutonic complex.

The presence of small scale faults, concentrated mainly along the intrusive contacts, and also evident within both the older and younger suites, attests to the continued brittle deformation after crystallization of the younger suite magmas. These brittle features reflect the combined effects of continued spreading, emplacement(?) and uplift of the Troodos massif since the initial time of its accretion as a crustal segment.

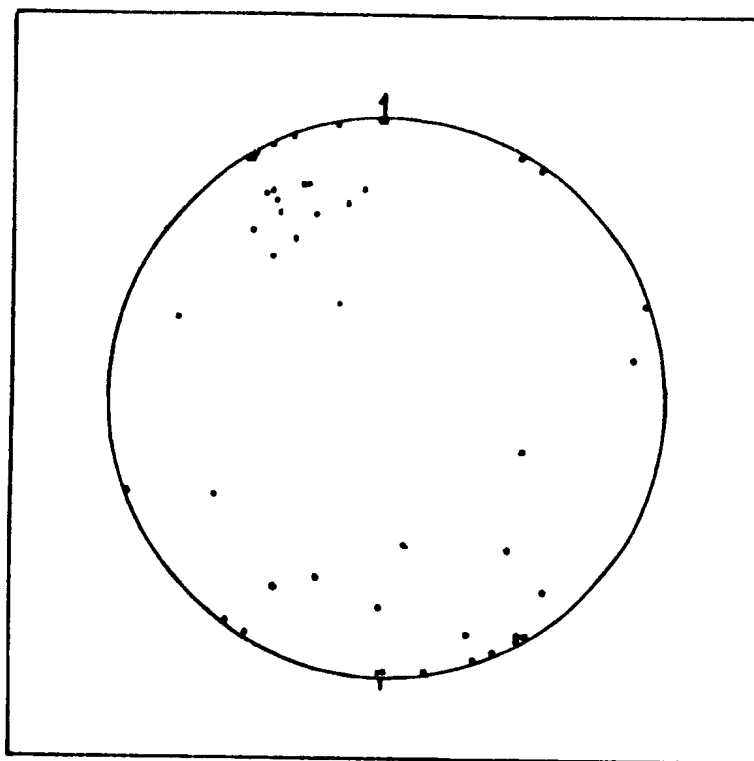
### 2.3.5. The Mafic Dikes

The last stage of magmatism evident within the Troodos plutonic complex is represented by a series of mafic dikes which intrude and crosscut all members of both the older and younger suite plutonic units. The mafic nomenclature for the dikes is based upon their depleted chemistry which will be discussed in Chapter 4. Chemical study of the dikes to determine any variation in their composition is presented in Chapter 4, Section 4.3.

The majority of these dikes intrude the older suite layered olivine and hypersthene gabbros and along the main zone (Zone 1/Map 1) of younger suite wehrlite, pyroxenite and gabbro bodies. The dikes are all post-ductile deformation, that is, they are situated above the deformation front. The dikes intrude as individual entities rather than as spatially associated swarm(s). The equal area projection of the poles to the contact planes of 46 dikes (Figure 2-26) show a weak NE/SW strike and moderate to steep dip.

It is important to note that the majority of dikes are not in a present day vertical orientation or aligned parallel as would be expected if the dikes were intruded into crust which was experiencing a strictly horizontal extensional regime (and excluding rotation tectonics). These dikes, in fact, very likely represent the feeder dike conduits to the structurally overlying upper pillow lavas of the Troodos ophiolite (refer to Chapter 4, Section 4.3 and Chapter 5, Conclusion #18).

The mafic dikes range in width from 4 cm to 1 m and are continuous along strike for up to 4 m in the best outcrop exposures. They are generally fine grained to aphyric although one dike, which intrudes the older suite layered gabbro along Pine Road (Map 1), exhibits euhedral to subhedral plagioclase pseudophenocrysts replaced by an alteration assemblage of actinolite, chlorite, albite and talc. The lath-shaped phenocrysts comprise 40% of the dike by volume and are generally up to 1 cm in length. The dike contacts with host lithologies



**Figure 2-26:** Lower hemisphere, equal area projection of 34 poles to the mafic dikes.

are sharp with rare development of chilled margins which rarely exceed 1 cm. in width. All of the mafic dikes are undeformed except for small scale fracturing/faulting which offsets the dikes in outcrop (Figure 2-27).

#### **2.4. Summary and Discussion**

In summary, the Troodos plutonic complex is composed of a number of spatially and temporally distinct magmatic suites. The older magmatic suite, exhibiting a "type" ophiolite stratigraphy (Geotimes, 1973) and penetrative high temperature ductile deformation, has been intruded, truncated and disrupted by post-kinematic younger suite plutons. The intrusion of sporadically distributed mafic dikes, into both the older and younger suites, marks the last stage of magmatism



**Figure 2-27:** Mafic dikes (light green) intruding vari-textured hypersthene gabbro (tan-gray) in roadcut exposure. Note the offshoots of thin dikes from the main dike into the gabbro. The dike is offset by minor faults.

in this section of the Troodos plutonic complex. A dynamic crustal accretionary history involving multiple intrusion and ductile-brittle deformation is established on the basis of detailed field observations for the Troodos oceanic crustal section.

Previous notions of multiple magmas within the Troodos ophiolite (ie.: Moores and Vine, 1971; Smewing et al., 1975; Allen, 1975; Greenbaum, 1977) involved a

model of discrete, linear multiple magma cells, up to 1 km sq in size and situated in higher stratigraphic levels of the plutonic section (Allen, 1975), which were periodically replenished by melts of various compositions rising as diapirs beneath a paleo-ridge (Gass, 1980). These notions were based upon rather poorly defined physical features including;

- (1) lateral discontinuities in layering (Allen, 1975),
- (2) presence of dikes within the cumulate pile (Moore and Vine, 1971),
- (3) intrusive contacts between gabbro/layered gabbro intruding ultramafics (Allen, 1975) ; (Note, the present author's investigations showed this intrusive relation to, in fact, be the reverse, with ultramafic intruding gabbro),
- (4) cyclic units exhibiting gradational contacts within the cumulate pile (Allen, 1975) ; (Note, one of Allen's cross-sections, which passes through the present author's map area, was interpreted by Allen, (1975) to represent four magma influx cycles when, in fact, this cross-section incorporates both the older and younger intrusive suites, having distinct and sharp intrusive contacts,
- (5) variations in chromite chemistry attributed to separate magma bodies (Greenbaum, 1977).

As such then, the presence of multiple magmas was recognized within the higher levels (i.e.: within the gabbroic units) of the plutonic complex, but previously unrecognized was the existence of spatially and temporally discrete magma chambers which, on the basis of field criteria, clearly occupy the transitional zone of an older magmatic sequence as well as intruding into higher and lower structural levels within the older suite and harzburgite, respectively. Moore and Vine (1971) and Allen (1975) proposed that the intrusive ultramafic pods observed to occur within the layered gabbro (for example zones 2 and 3 within the present authors older suite layered gabbro) represented magma batches that were liberated from the same large, underlying magma chamber which yielded the whole of the Troodos stratiform complex. Thus, their concept of a complete, stratiform ophiolite sequence exhibiting spatially discrete multiple magmas (auto-



intrusive ) at higher stratigraphic levels is not in accordance with the geometries of younger suite intrusions nor their presence throughout the higher and lower structural levels of the Troodos plutonic complex. Likewise, the evidence for a number of large magma source regions (chambers) liberating melt batches into an older, deformed and brittle-faulted suite has not, prior to the present author's work, been recorded to occur within the Troodos plutonic complex.

The transition zone and part of the dunite and layered gabbro units of the older suite have been removed by a combination of large scale faulting and intrusion/assimilation by the main bulk of the younger suite plutons in this northwestern section of the plutonic complex. Thus, the ultramafic cumulates interpreted by previous investigators (e.g: Wilson, 1959; Gass, 1967; Greenbaum, 1972A; Moores and Vine, 1971; Allen, 1975; George, 1975; 1978), to form the transition zone of the ophiolite sequence, in fact, represent intrusions of the younger plutons into the older layered suite. Allen (1975) interpreted wehrlite bodies which were overlying and forming inliers within the harzburgite to represent lower cyclic layers formed synchronously with the dunite, thus explaining the variable thickness of this latter unit. Allen (1975) thought that the high level ultramafic pods within the upper gabbros represented cumulates forming in small cells within an east-west tension zone. Thus, although Allen (1975) regarded the small, high level mafic cumulate bodies as representing discrete magma chambers related to the upper lavas, he still regarded the large scale layered geometry of the plutonic complex to represent cyclic accumulations with gradational contacts forming within a major magma chamber periodically replenished by magma batches. Gass (1980) interpreted the small ultramafic plutons observed within the harzburgite to represent melt batches trapped en-route to an overlying magma chamber.

High temperature, ductile deformation has penetrated all units of the older suite, imparting a consistently steep to subvertical  $S_1$  form trace from harzburgite through to the layered gabbro and major  $S_1$  axial planar infolding of the

harzburgite-dunite boundary. Previous structural studies by George (1975; 1978) in the Troodos plutonic complex reported a 500 m gradation from deformed to undeformed cumulates along the dunite-transition zone contact. He did not recognize the intrusive nature of the undeformed ultramafic-mafic cumulates of the younger suite along this contact with the dunite.

Within the northwestern Troodos plutonic complex, large-scale (axial graben?) brittle fault structures developed within the older suite lithologies following penetrative ductile deformation. These zones of structural weaknesses in the accreting crustal section formed conduits for focusing the main bulk of younger suite intrusions ascending from deeper magma chamber(s). Thus, the younger plutons represent melt pockets intermittently trapped in fault controlled magma chambers which, in turn, led to the development of varying spatial and temporal, multiple intrusive relations on all scales throughout the plutonic complex depending upon the position of the deformation front (refer to Chapter 3, Sections 3.4 and 3.10 for discussion of the deformation front).

No evidence was found in the study area to support the theory proposed by Lapierre (1975) and Bortolotti *et al.*, (1976) for the existence of major thrust planes that structurally repeat sections of the Troodos plutonic complex. These authors interpreted the presence of major thrust planes on the basis of fabric truncation and the abrupt juxtaposition of distinct lithologies (Bortolotti *et al.*, 1976). The fault trace they defined along the western flank of the ophiolite in the present study area in fact represents the trace of the main intrusive belt (Zone 1). There is no evidence for contractional faults (high or low angle) in this section of the plutonic complex, rather, all faults along the northern part of the map are normal, moderate to high angle extensional faults. Also, in the western side of the cross-section of Bortolotti *et al.*, (1976), the inferred thrusts bring "younger" over "older", that is, the lower plutonic complex in the footwall still lies below the "upper" plutonic complex in the hanging wall. This is contrary to the rules of thrusting if the complex is considered to be stratiform, as in their model.

Graben structures mapped within the sheeted dike complex and upper gabbros in the Kakopetria region, by Varga and Moores (1985), can be correlated with the fault structures which control intrusion of the younger suite plutons in the northwestern plutonic complex (MAP 1). The intrusion of these magma bodies along deep graben structures could provide; (1) a magma source for younger multiple dike intrusions along these conduits within higher levels of the ophiolite and (2) a heat source to aid in the convection of sea-water and formation of base and precious metal deposits within the diabase dike and pillow lavas spatially associated with these axial graben structures (Spooner, 1977).

The main zone of younger suite plutonism exhibits crosscutting relationships and fractionation trends (refer to Chapter 4) indicative of auto-intrusion. If similar processes were involved in the development of the older suite, field evidence of that history would have been destroyed during the penetrative, ductile deformation. This main zone of plutons and the older suite dunite have, in turn, both been intruded by the undeformed gabbroic carapace of a deeper seated, evolving magma body (MAP 1, cross-sections A-A' and B-B').

## Chapter 3

# STRUCTURE: MEGA-, MESO- AND MICROSCOPIC FEATURES

### 3.1. Introduction

Chapter 3 documents the megascopic, mesoscopic and microscopic characteristics of the older magmatic suite in the northwestern quadrant of the Troodos plutonic complex. The large scale pattern defined by the foliation trends in the plutonic complex, as well as the mesoscopic and microscopic features indicative of ductile deformation, are documented for the lithological units of the older suite. The textural transition from primary magmatic to solid-state deformation features within the older suite layered gabbros will be presented followed by a discussion of the position of the ductile-brittle transition (deformation front) within the layered gabbros. Difficulties in establishing an accurate fractional crystallization sequence for the older suite gabbros are discussed in light of the effects of multiple intrusion and penetrative deformation during crystallization. A case involving recrystallization via subgrain rotation mechanisms is documented for a series of thin-sections from outcrops of the older suite transition zone. Finally, microscopic scale intrusive relations between the older deformed suite and the younger isotropic suite will be illustrated in thin sections from two outcrops. The salient points of Chapter 3 will be presented in a final summary.

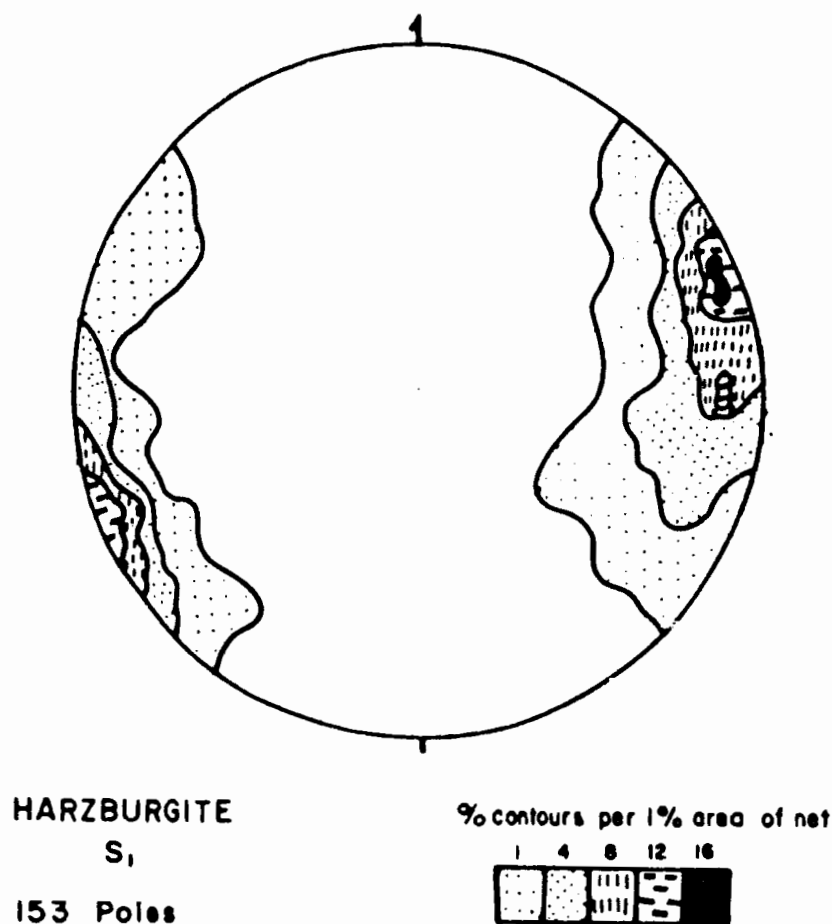
### 3.2. Megascopic Structural Trends

The attitude of the foliation fabric within the harzburgite, dunite, transition zone and layered gabbro units of the older suite has been briefly presented in the field relations of Chapter 2. The high temperature, ductile deformation has variably penetrated all units of the older suite, imparting a consistent NNE-NE striking and vertical to moderately W-SW dipping foliation (Map 1). This foliation trend is axial planar to large scale folds along the infolded harzburgite-dunite boundary (Map 1).

In Figure 3-1, the poles to 153 foliation measurements recorded in the harzburgite are presented. A uniformly NNW-SSE striking ( $\sim 160^0$ ) and steep to vertical dipping foliation is illustrated by the strong point maxima (12% and 16% contour intervals) in Figure 3-1. A secondary 12% contour maximum in the stereonet (Figure 3-1) reflects a gentle swing in the foliation fabric towards a N-S orientation within the northeastern exposures of harzburgite in the map area (MAP 1).

Flattened aggregates of chromite, which form stringers in the dunite, are orientated parallel to the foliation in the harzburgite. The poles to the five foliation measurements from the dunite plot within in the 12% and 16% contour intervals of Figure 3-1. Likewise, the attitude of the layering/foliation in blocks of the transition zone orthopyroxenite is consistent with the NNW-NW strike and steep to subvertical dip of the foliation in the dunite and harzburgite.

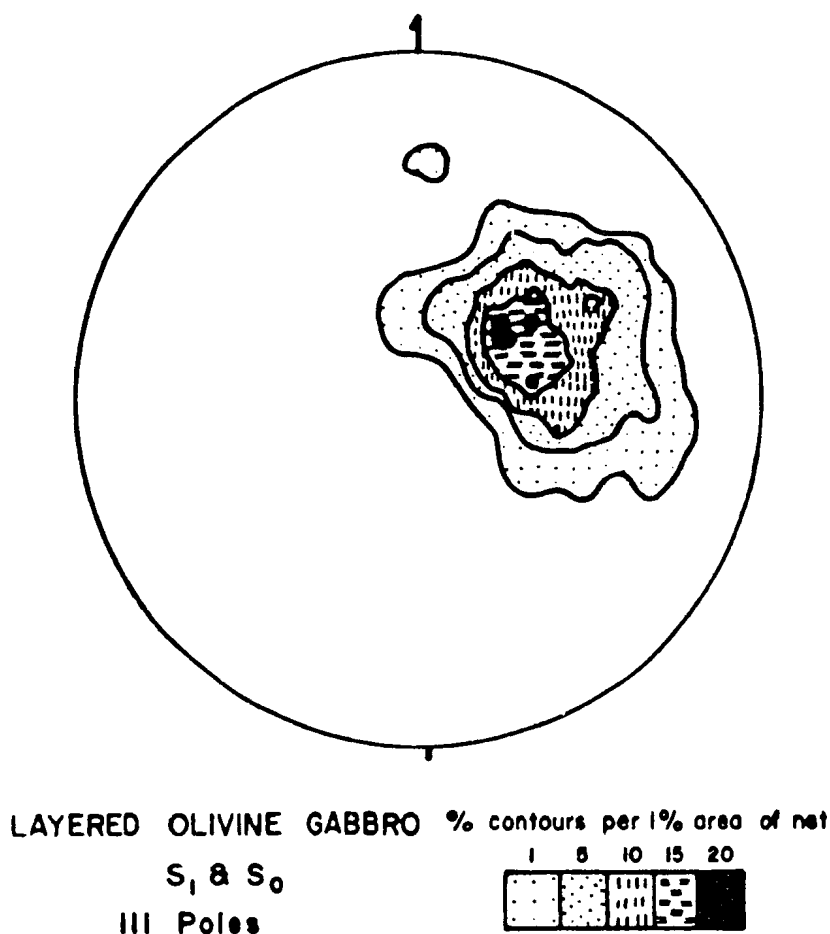
Equal area projection of the poles to the foliation/layering ( $S_1/S_0$ ) planes for the older suite olivine and hypersthene gabbros are presented in Figures 3-2 and 3-3. The layered olivine gabbros show a strong point maxima for 111 measurements (Figure 3-2). This concentration of poles reflects the consistent northwest striking ( $330^0$ ), moderately west-southwest dipping fabric which characterizes the olivine gabbro throughout the northeastern and northwestern map area. The equal area projection of 155 poles for the layered hypersthene gabbro (Figure 3-3) defines a



**Figure 3-1:** Lower hemisphere, equal area projection of 148 poles to the harzburgite foliation and 5 poles to the dunite foliation.

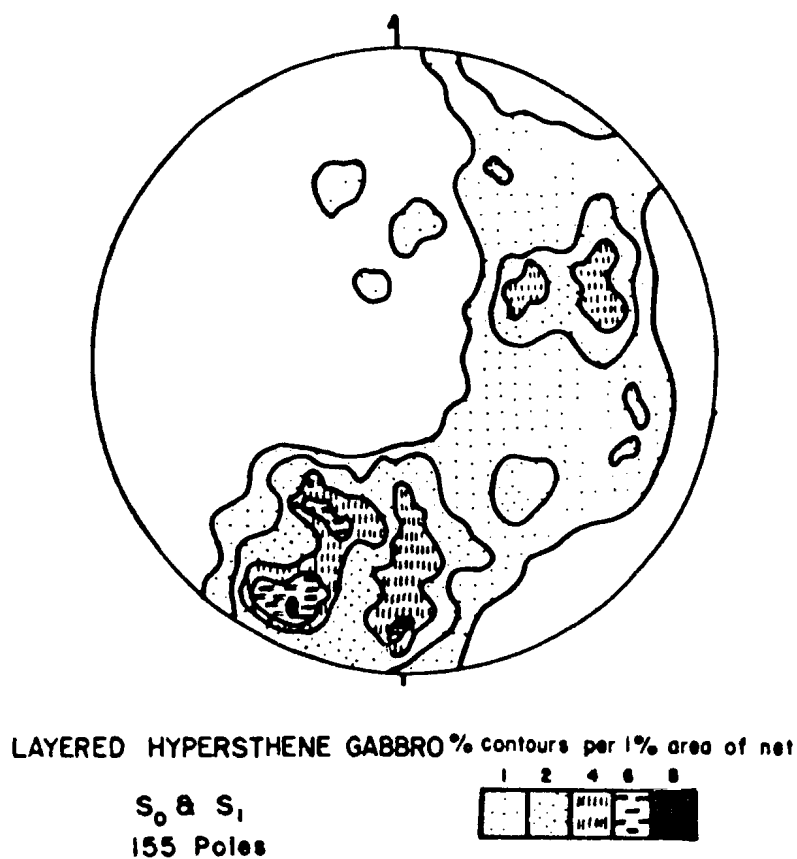
girdle distribution which reflects the gradual swing in the layered/variably foliated fabric from a northwest strike (consistent with that of the olivine layered gabbro) towards an east-west strike which dominates in the western exposures of the layered hypersthene gabbro unit (Figure 3-2 and Map 1). This result of the detailed mapping of the fabric element in the gabbros thus invalidates the conclusion of George (1975, p.60), who stated that extensive brittle faulting and rigid-body rotation of gabbro blocks has resulted in the change of layering (foliation) orientation for this region.





**Figure 3-2:** Lower hemisphere, equal area projection of the poles to the foliation in the layered olivine gabbro.

A comparison of the pole diagrams for the foliation in the harzburgite-dunite units (Figure 3-1) with those of the layered gabbros (Figures 3-2 and 3-3) illustrates a general uniformity of the  $S_1$  form trace in the older suite (Map 1); from harzburgite and dunite (NNW strike and steep dip) through to the layered olivine gabbro and eastern portions of the layered hypersthene gabbro (NW strike and moderate SW dip). The overall geometrical relations of the units thus show a penetrative vertical to subvertical plastic flow induced foliation, large infolding of the harzburgite and dunite units with concomitant small scale parasitic folding in



**Figure 3-3:** Lower hemisphere, equal area projection of the poles to the layering/foliation in the layered hypersthene gabbro.

these units as well as in the layered gabbros and an orientation of the steep foliation fabric at a high angle variance to the enveloping surface of the major lithological boundaries. These geometrical relationships are vitally important in assessing the formational setting of the Troodos ophiolite as is discussed in Chapter 5.

### **3.3. Mesoscopic Structural Features of the Older Suite**

The following section contains descriptions of the mesoscopic-scale field criteria used to distinguish the presence of extensive, high temperature plastic deformation within the lithological units of the older suite.

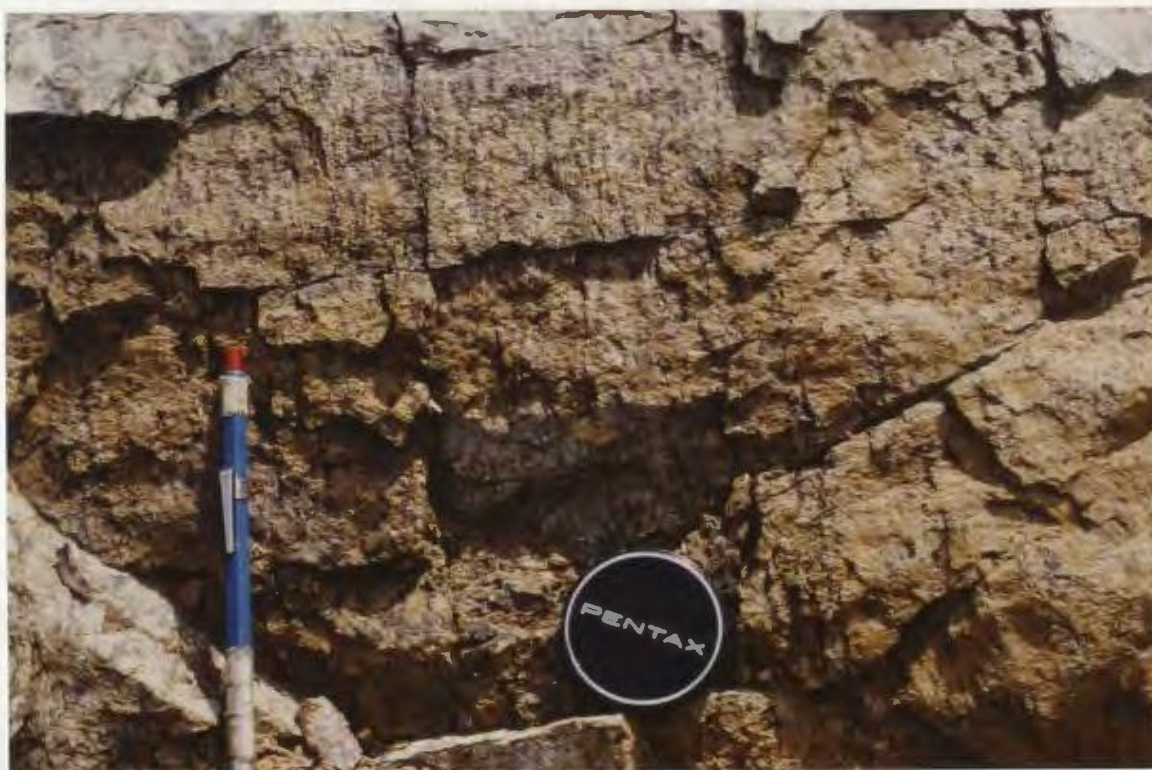
#### **3.3.1. Harzburgite**

The harzburgite foliation fabric is defined in outcrop by the preferred dimensional orientation of the orthopyroxene grains and aggregates (Figure 3-4) and rare chromite stringers.

Four distinct foliation textural styles, defined by the distribution of the orthopyroxene phase, were noted in the harzburgite of the study region. These findings are in agreement with Allen, (1975). The textural styles include: (1) massive to weakly foliated; (2) foliated parallel to a prominent compositional layering; (3) moderate to strong foliation with no apparent compositional layering; and (4) harzburgite exhibiting two mutually crosscutting foliations.

The majority of harzburgite exhibits the strong, single foliation fabric with no associated layering. In the few exposures where layering was observed, the foliation was orientated both parallel to, and in rare cases slightly oblique to the layering.

One small outcrop located near the lower chromite mine adit (along a road section which branches to the east (MAP1)) showed two mutually crosscutting foliations. Relative age relations between the two fabrics could not be determined in either hand sample or thin section. The second, north-south striking foliation may be more typical of the harzburgite fabric to the west of the present study area (refer to George, 1975; 1978). George (1975) noted this north-south orientated fabric and equated it with an  $F_2$  ( $D_2?$ ) event. However, the results of the present study show no evidence for a penetrative  $F_2$  event in this region of the plutonic complex.



**Figure 3-4:** Foliation ( $S_1$ ) in harzburgite defined by the alignment of flattened orthopyroxene grains and aggregates (parallel to the pencil).

A weak linear fabric was noted in a few harzburgite outcrops. The development of a strong  $S \gg L$  in the harzburgite as well as within the other older suite lithologies can be attributed to a flattening, oblate strain path rather than stretched, prolate strain path for the stress field imposed upon this unit during penetrative, high temperature plastic deformation.

The overall apparent lack of clearly defined mesoscopic fold closures within the

harzburgite may be due to either a sparse development of small scale parasitic folds, extreme transposition and/or the extreme difficulty in discerning fold closures due to the overall lack of contrasting phase assemblages in this unit.

### **3.3.2. Dunite and Transition Zone Orthopyroxenite**

Although generally massive, with <2% disseminated, euhedral to subhedral spinel, the dunite does contain a few mesoscopic features that indicate the presence of penetrative, plastic deformation. Rare chromite stringers within the dunite exhibit an alignment parallel to the regional foliation of the harzburgite. Likewise, small lensoidal-shaped dunite pods (<20 cm in length) occur within the harzburgite and exhibit a maximum dimension axis lying concordant to the foliation plane in the surrounding harzburgite. The same relation was described in Chapter 2 with the large-scale infolding of the dunite-harzburgite boundary and lensoidal inliers of dunite within the harzburgite. The schlieren-texture and isoclinal folding of chromite (Figure 2.2) also confirms the penetratively deformed nature of the dunite host.

The orthopyroxenite transition zone shows little evidence of mesoscopic scale plastic deformation. Neither minor fold closures nor mineral elongation or flattening were apparent in the transition zone outcrops to indicate the presence of a penetrative foliation. However, the recrystallized, equant nature of the pyroxene phase will be documented on the microscopic level in Section 3.7.2.

### **3.3.3. High Temperature Deformation Features of the Layered Gabbros**

The following subsection will describe the main field criteria used to distinguish the presence of extensive high temperature plastic deformation within the layered olivine gabbro of the Troodos plutonic complex. Evidence to support the positioning of the high temperature deformation front well into the structurally higher layered gabbro section of the older suite is exposed on the mesoscopic scale in the study area. This deformation front marks the transition from dominantly ductile to brittle deformation mechanisms and is discussed at length in Subsection 3.3.4.



The best developed solid-state flow fabrics are exposed within the well layered olivine gabbros along the southeastern part of the map sheet and near the contact between olivine gabbro and clinopyroxene-bearing dunite (Map 1). In this region, a strongly developed  $S \gg L$  fabric is defined by the preferred dimensional orientation of flattened (X-Y aspect ratios on the order of 1:10) olivine crystals (Figure 3-5).



**Figure 3-5:** Strongly foliated/layered olivine gabbro. The  $S_1$  fabric is defined by the preferred orientation of flattened olivine, pyroxene and plagioclase phases in hand sample.

Associated pyroxene and plagioclase phases likewise exhibit a pronounced planar mineral alignment orientated parallel with foliation defined by olivine as exposed in hand sample (Figure 3-6). This distinct planar secondary fabric lies both parallel and slightly oblique to the phase layering. Hinge zones of isoclinally folded ( $F_1$ ) layered olivine gabbro, with well developed axial planar fabrics lying



parallel to the regional foliation, were occasionally observed in outcrop (Figure 3-7). However, more ambiguous fold structures have been observed within tectonized, layered olivine gabbro (Figure 3-6).



**Figure 3-6:** Tectonized, layered olivine gabbro showing strong alignment of inequant olivine, pyroxene and plagioclase grains parallel to the  $S_0/S_1$ . Note the tapering of layers along strike and possible fold hinges.

Within the strongly ductilely deformed layered olivine gabbro, progressive rotation of the phase layering into the regional  $S_1$  plane may have yielded the overall parallel/subparallel attitude of the  $S_0/S_1$  fabric elements in this unit (refer to Subsection 3.6.3.3). This process of progressive reorientation of the pre-existing planar elements into parallelism with new structural planes (i.e.: foliation) is termed "transposition" (Nicolas and Poirier, 1976) and occurs during penetrative



**Figure 3-7:**  $F_1$  fold hinge of isoclinally folded layered olivine gabbro with axial planar  $S_1$  foliation.

solid-state deformation. Similar concordant relations between the foliation and metamorphic banding were observed within the harzburgite (refer to Subsection 2.2.1.1). The largest angle between the phase layering and axial planar foliation is observed in the hinge zones of  $F_1$  major and minor folds.

Within the less deformed layered olivine gabbro, a weak to moderately developed foliation is evident, defined by the alignment of phase assemblages both

parallel and slightly oblique to the layering. The fact that primary layering within the weakly deformed gabbro is generally orientated parallel to the regional penetrative foliation suggests an original concordance between these two planar elements. Regions (domains) with weaker foliation fabrics and apparently lower strain also preserve more of the sedimentary-type structures previously described in Section 2.2.3.1. These include fold structures possibly related to slumping in the accumulating crystal pile rather than isoclinal folding during plastic deformation.

The preservation of some cumulate structures during pervasive solid-state flow deformation was noted as early as 1965 by Raleigh. Thus, the layered gabbro units of the Troodos plutonic complex may exhibit both primary cumulate and secondary tectonite features. These complexities are the result of the heterogeneous nature of the distribution of ductile deformation through time and space in the plutonic complex as discussed in both Section 3.3.4 and the summary of Chapter 3.

A streaky foliated/lineated fabric, defined by the preferred orientation of the pyroxene and plagioclase phases, is heterogeneously developed throughout the layered, wispy and more massive hypersthene gabbros. This fabric element lies both parallel and slightly oblique to the layering. A primary igneous versus secondary deformational origin of this fabric is discussed in Section 3.6. Ambiguous fold closures exposed within the layered hypersthene gabbro are probably related to either slump folding within the accumulating pile, or folding of layering within the melt/crystal mush mixture (hyper-solidus) during deformation shear stress conditions (Figure 3-8) rather than formation during solid-state deformation.





**Figure 3-8:** Primary magmatic textures of the layered hypersthene gabbro showing slump folding of the rhythmic layering.

### **3.4. Position of the Ductile-Brittle Transition within the Layered Gabbros**

Within the upper mantle and plutonic sections of the ophiolite, two mechanisms of rock deformation, ductile and brittle, were operative in response to the stresses imposed upon the accreting crustal section during spreading. The occurrence of either mechanism is dependent upon the rheological behavior of the rocks in response to physical conditions during this period of deformation. The physical variables that determined the style of deformation include : (1) strain rate(s); (2) lithostatic and fluid pressures; (3) dissipation of strain energy as heat during flow; and (4) release of heat of crystallization during freezing of melts following the various periods of magmatism.

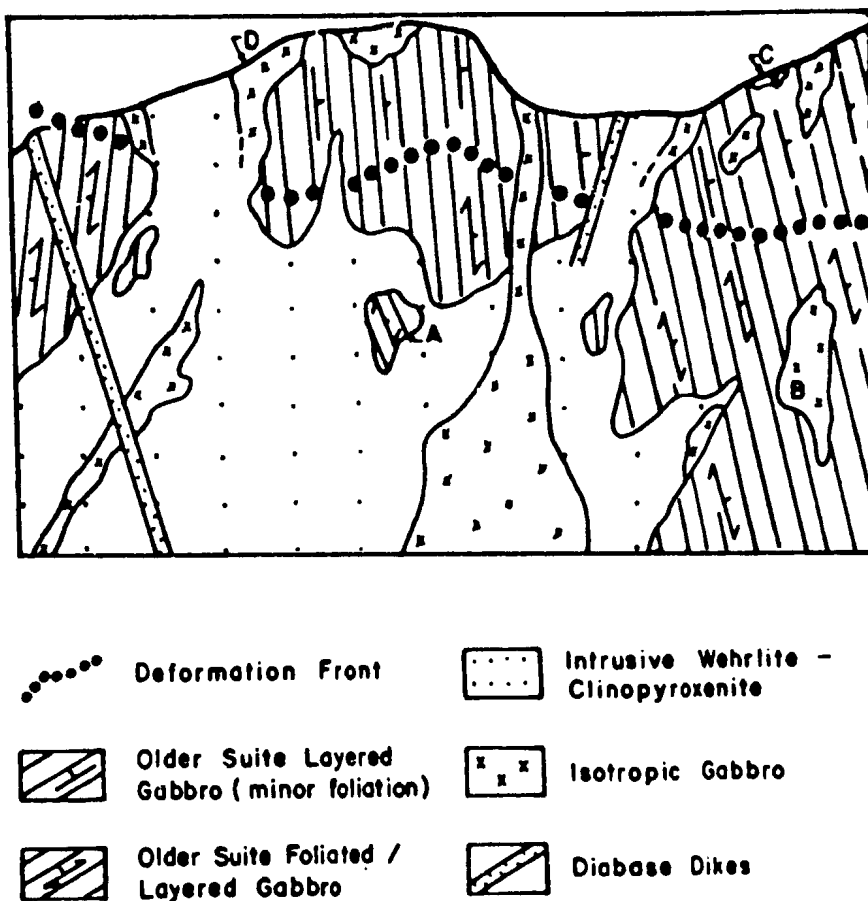
In general, the brittle deformation features, such as normal faults and dilational

faults/fractures, develop during conditions of relatively low temperature-high stress and are accompanied by the release of accumulated strain energy. Ductile deformation, in the form of crystallographic flow processes (Nicolas and Poirier, 1976), occurs during high temperature (homologous temperature =  $T/T_m > .8$ ) and relatively low stress conditions and results in the development of penetrative lineated and/or foliated fabrics, transposition of pre-existing fabric elements, annealed fabrics, large scale and parasitic folds and ductile shear zones (refer to Section 3.3). Crystallographic or plastic flow can occur during both subsolidus and hyper-solidus conditions (Thayer, 1980).

In the study area, the structurally highest position of the transition from predominantly ductile to brittle deformation mechanisms, referred to as the deformation front, is situated in the upper portions of the plutonic complex, within the older suite layered gabbros (Figure 3-9). This zone delineates the transition from dominantly plastic flow to brittle displacement mechanisms and is marked by the gradual change over from primary cumulate textures and extensional faulting/fracturing to secondary, low grade penetrative tectonite fabrics in the layered gabbros (Figure 3-9, Table 3.3).

The position of the deformation front in the Troodos plutonic complex differs from that of other ophiolites. For example, within the Bay of Islands ophiolite, Newfoundland, the ductile-brittle transition is situated within the upper gabbros, along the base of the sheeted dikes (Rosencrantz, 1983; Calon and Malpas, 1985; Dunsworth *et al.*, 1986), whereas in the Oman ophiolite, the deformation front reportedly lies within the ultramafic cumulates (Pallister and Hopson, 1981).

In general within an accreting crustal section, the position of the ductile-brittle transition will change with time depending upon thermal conditions at the accreting center. The periodic influx of major heat sources due to multiple magmatism contemporaneous with deformation in the plutonic complex will result in fluctuations of the ridge isotherms which in turn will bear directly upon the spatial distribution of plastic flow in the complex. Also, the development and



**Figure 3-9:** Schematic diagram showing the structurally highest position of the deformation front within the older suite layered gabbro. Note that the position of the front would have been lower in the section prior to intrusion/crystallization of the plutons of the younger suite. Refer to Section 3.4 for discussion.



distribution of ductile flow fabrics will be heterogeneous within the plastic strain field due to strain partitioning and to variations in the other parameters noted above.

As a result, complex spatial and temporal relations will exist between the magmatic crystallization of the younger intrusive suite and the heterogeneous metamorphic recrystallization as a result of plastic flow in the older foliated suites. These complexities characterize the "higher" crustal levels of the Troodos plutonic complex. As the deformation front moved through time in the accreting crust and strain related plastic flow was heterogeneously developed within the ductile field, some sections of the layered gabbros were plastically deformed while others sections completely escaped ductile deformation. These undeformed sections either existed outside of the ductile field or acted as essentially rigid-bodies within the region of plastic flow (strain partitioning). The deformation history of the accreting cumulate plutons was largely dependent upon their position with respect to the deformation front. During progressive time intervals, the most recently accreted cumulates (i.e. intrusive plutons) may enter the field of ductile deformation depending upon their position relative to the spatial distribution of this front. Such situations have been documented by Dunsworth et al., (1986) for the Bay of Islands ophiolite, Newfoundland, where syn- to postkinematic younger suite intrusives exhibit a range in texture from isotropic, undeformed to penetratively deformed fabrics depending upon their spatial and temporal position relative to the deformation front during the accretionary history of the Bay of Islands plutonic complex.

An approximate "uppermost" position of the deformation front located in the older suite gabbros is schematically represented in Figure 3-9. The position of the deformation front would have been lower in this section prior to the emplacement and recrystallization of the younger suite intrusions along planes of structural weakness (e.g.: faults developed within a brittle domain) and crystallized above the field of ductile deformation (deformation front) in the brittle domain. The

transitional boundary between ductile to brittle deformation is, in fact, a rather vague feature due to the gradational and heterogeneous distribution of crystallographic flow within the lower grade, plastically flowing regions of the layered gabbros. Below the deformation front, the lithologies of the older, deformed suite (Figure 3-9, A ) can be distinguished on the basis of deformation features from those of the younger, isotropic suite (Figure 3-9, B ). The only exception to this are the rare cases where low strain domains within the deformed layered/foliated gabbro preserve small zones of isotropic gabbro. Above the deformation front, the massive, isotropic gabbro of the older suite (Figure 3-9, C ) cannot be distinguished in the field from the visually identical gabbro of the younger suite (Figure 3-9, D ) except for its spatial association with the younger suite wehrlite-clinopyroxenite (e.g.: gabbroic margins of plutons) is visible in the field.

### **3.5. Microfabrics and Mechanisms of High-Temperature, Ductile Deformation within Ultramafic-Mafic Rocks under Upper-Mantle/Lower Crustal Conditions : An Overview.**

#### **3.5.1. Introduction**

The following section summarizes the main principles concerning the mechanisms of plastic flow during simple shear (Nicolas et al., 1973) under upper-mantle/lower crustal conditions. Included in the summary are: (1) how minerals flow (deform) in solid state by crystallographic defects; (2) how large degrees of accumulated strain are attained through strain softening mechanisms during ductile deformation to yield steady-state flow; and (3) the characteristic textures and features (microfabrics) of intracrystalline flow in the principle mineral components of ultramafic-mafic rocks. This review has been included in Chapter 3 in order to familiarize the reader with the main principles of ductile deformation and its application to the plastically deformed lithologies within the Troodos plutonic complex. For a more complete survey of the literature, the reader is referred to extensive reviews on the subject of ductile deformation under upper

mantle conditions by Nicolas and Poirier (1976), Carter (1976), Christie and Ardell (1976), Tullis (1979) and Gueguen and Nicolas (1980).

### 3.5.2. Ductile Deformation Theory

The overprinting effect of penetrative strain, related to solid-state deformation, on the primary igneous (cumulate) textures in the upper mantle/lower crustal sections of ophiolitic complexes has been recognized by numerous workers (i.e.: Raleigh, 1965; Ave'Lallement, 1967; Den Tex, 1969; Nicolas, 1969; Loney *et al.*, 1971). The recent recognition of tectonite fabrics within the gabbroic units of the Bay of Islands ophiolite plutonic complex, western Newfoundland, by Thayer (1980), Moll (1981), Calon and Malpas (1985), Neyens (1986), Dunsworth *et al.* (1986) and Dunsworth (1988, in prep.) and within the Zambales complex, by Thayer, (1980), led the latter author to conclude that the effects of penetrative, hypersolidus to subsolidus deformation within the structurally higher sections of ophiolites had been to a large extent overlooked.

The mechanisms of tectonic deformation which result in the movement of the lithosphere over the underlying asthenosphere operating under a range of upper mantle-lower crustal conditions including: (1) moderate to high temperatures (subsolidus-hypersolidus, homologous temperature =  $T/T_m > .5$ , Carter, 1976); (2) variable pressures depending upon depth; (3) varying strain rates from  $10^{-10}$  to  $10^{-15} \text{ sec}^{-1}$  (geological strain rate for mantle flow is regarded as  $10^{-14} \text{ sec}^{-1}$ ); and (4) stresses of 100-1000 bars (Nicolas and Poirier, 1976; Christie and Ardell, 1976).

Ductile, intracrystalline, solid-state deformation is the principle mechanism of upper mantle-lower crustal flow at moderate to high temperatures (homologous temperature  $T/T_m > .5$ ). As a direct result of applied stress, strain induced crystal defects will develop within minerals in the form of line dislocations (edge or screw types) and point defects. Each line dislocation moves through the crystal along a crystallographic slip plane to yield a small, incremental strain displacement in the crystal lattice (Nicolas and Poirier, 1976). Point defects migrate through the

crystal at higher temperatures ( $T/T_m > .6$ ) (Christie and Ardell, 1976). During low temperature deformation conditions, the movement of line dislocations is restricted to particular slip planes (conservative motion of dislocations). In order to continue to increase the strain within the crystal(s) of a deforming rock, more applied stress is required as the dislocation densities increase and begin to pile up, becoming pinned along grain boundaries, stuck at other dislocations and/or atomic impurities. This increase in the dislocation density of the crystal lattice results in the work-hardened (cold working) of the crystal (deforming medium), (Nicolas and Poirier, 1976) such that the continued increase of strain will eventually exceed the plastic limit of the material and result in brittle failure (brittle deformation).

In order to attain the large degrees of finite strain observed to occur within naturally deforming, ductile environments, syntectonic recovery mechanisms must operate, reducing the internal stored strain energy of the system (crystal or rock) before brittle failure occurs. A condition of steady-state deformation is achieved when the recovery rate (dynamic recovery and recrystallization, White, 1976) balances the strain hardening rate (White, 1976). At higher temperatures ( $T/T_m > .5$  ; Kerrich and Allison, 1978), dislocation movement combined with point defects can lead to dislocation climb whereby the dislocations can move to another slip plane within a crystal structure (Nicolas and Poirier, 1976) and screw dislocations can cross-slip (a situation of non-conservative motion of dislocations; White, 1976).

These climb and cross-slip dislocation movements yield intracrystalline recovery (strain softening) by allowing for the rearrangement of dislocations into low angle ( $< 1^\circ$ ) subgrain boundaries, dislocation networks and the attraction and annihilation of dislocations with like Burgers vectors and opposite signs of climb (Christie and Ardell, 1976). The end result of this process is the development of strain free regions within crystals. Thermodynamic forces drive this annealing process in order to lower the stored strain energy of the system, thus allowing for

continued intracrystalline deformation via non-conservative dislocation movement such that work hardening does not occur. When the syntectonic recovery processes do not keep pace with the increase in dislocation densities, then the process of dynamic recrystallization will occur (White, 1976).

Recrystallization reduces stored strain energy by forming new strain free grains via two distinct processes; (1) by the nucleation of small, strain free grains in crystallographic regions of high stored strain energy (ie.: high misorientations of stable grain boundaries, deformation bands etc.) and the subsequent migration of the new, high angle grain boundary, thermodynamically driven by the differences in the stored strain energy, to consume the deformed matrix (Tullis, 1979; Poirier and Nicolas, 1975; Nicolas and Poirier, 1976; Christie and Ardell, 1976; Etheridge and Kirby, 1977); and (2) by the progressive rotation (misorientation, up to  $15^{\circ}$ ) of adjacent subgrains with increasing strain (accumulation of dislocations) after which these subgrains can be considered as independent grains (Nicolas, 1975; Nicolas and Poirier, 1976; White, 1976; 1977; Etheridge and Kirby, 1977; Tullis, 1979; Christie and Ardell, 1976). Poirier and Nicolas (1975) have noted that a similarity in the size of subgrains and neoblasts is suggestive of recrystallization by subgrain rotation (SGR) while indented grain boundaries are suggestive of grain boundary migration (GBM) leading to bulge-nucleation (Ave' Lallement, 1985). The newly formed grains will in turn deform by dislocation creep as cumulative strain increases, and will subsequently recrystallize again in cyclic fashion to produce a condition of steady-state flow. Poirier and Nicolas (1975) reported higher stress conditions operating during bulge-nucleation recrystallization and lower stresses during recrystallization by progressive rotation mechanisms. The presence of pore fluids enhances ductility by promoting mobility and multiplication of slip dislocations and therefore lowering the temperature required for the non-conservative motion of dislocations to yield recovery and recrystallization mechanisms (Carter, 1976). Tullis (1979) has reported that the presence of aqueous fluids may either hinder recrystallization by promoting recovery mechanisms or assist recrystallization.

Thus, two principle creep or flow mechanisms operate in mantle peridotites; (1) dynamic recovery by intragranular flow (dislocation glide, dislocation creep; Nicolas *et al.*, 1971); and (2) dynamic recrystallization (Ave' Lallement and Carter, 1970).

Grain growth of dynamically recrystallized grains (neoblasts) is inhibited if there is a rapid increase in the dislocation density of the new grains (White, 1976). It has been suggested by a number of authors (ie: White, 1976; Post, 1973; Mercier, 1976), that grain size may be used as a piezometer for determining stress conditions operative during dynamic recrystallization (ie: grain size as a function of stress).

Dislocation creep (intracrystalline flow) has been found to be replaced by Cobble-creep mechanisms (grain boundary diffusion of point defects to change grain shape) when grain size is significantly reduced (ie:  $<100\mu\text{m}$  for quartz; White, 1976). Nabarro-Herring creep mechanisms (the volume diffusion of point defects) can also occur but plays a minimal role in upper mantle-lower crustal flow conditions (Ashby, 1972; Nicolas and Poirier, 1976). It should be noted that strongly deformed rocks, submitted to prolonged, post-tectonic annealing will yield equant, equigranular mosaic textures (static recrystallization). This finite texture will obliterate all older deformed grains (porphyroclasts) and yield the migration of grain margins into  $120^\circ$  triple point junctions (lowest stored strain energy state thermodynamically favoured in nature).

### **3.5.3. Microfabrics of the Principal Mineral Phases within Plastically Deformed Ultramafic-Mafic Rocks**

The microscopic features indicative of intracrystalline strain within minerals as a result of solid-state deformation include:

- (1) grain elongation (the preferred dimensional orientation of crystals which leads to the development of foliation and/or lineation fabrics)



- (2) undulatory extinction (early stages of recovery)
- (3) deformation bands and lamellae (essentially elongate subgrain walls of dislocation tangles)
- (4) kinkband boundaries (organized walls of dislocations which offset the crystal lattice along adjacent regions)
- (5) subgrains, both equant and elongate (tabular) with  $>1^\circ$  of lattice misorientation between adjacent grains and containing a mosaic of smaller, less misorientated ( $<1^\circ$ ) subgrains (dynamic recovery)
- (6) recrystallization (mosaic textures with triple point junctions of  $120^\circ$ )

Olivine deforms primarily by dislocation creep (slip, climb and cross-slip) in mantle conditions while rare cases of Cobble-creep (superplasticity) have been reported by Boullier and Gueguen, (1975). Dynamic recrystallization by both bulge nucleation and subgrain rotation mechanisms as well as static recrystallization in olivine has been reported by Nicolas and Gueguen, (1980).

Experimental studies on clinopyroxene deformation have been reported by Avé Lallement, (1978); Kirby and Etheridge, (1980) and Etheridge and Kirby, (1980). At low temperatures, dislocation slip is limited to parallel  $\langle 001 \rangle$  while at higher temperatures, multiple slip, recovery and recrystallization by both mechanisms (bulge nucleation and subgrain rotation) occur in clinopyroxene. Subgrain rotation was reported to occur only after extensive strain and subgrain development in the clinopyroxene grains (Kirby and Etheridge, 1980).

Orthopyroxene deforms at lower temperatures by a shear induced ortho-enstatite to clino-enstatite transition (Coe and Kirby, 1975). At higher temperatures (lower strain rates) orthopyroxene exhibits recovery features and recrystallization by both mechanisms (Etheridge and Kirby, 1980).

Spinel deform by dislocation climb at higher temperatures ( $T > .6T_m$ ) and crystal strength increases as grains approach chemical stoichiometry.

Optical features of crystallographic deformation documented for plagioclase phase (single and polycrystalline) include : (1) mechanical twinning by simple shear along particular crystal planes (rather than dislocation movement), (Borg and Heard, 1969; 1970; Marshall and Wilson, 1976; Marshall and McLaren, 1977); (2) deformation lamellae (slip on 010), (White, 1975; Seifert and Verploeg, 1977; Borg and Heard, 1970); (3) kinkbands (Marshall and McLaren, 1977); (4) undulose extinction and subgrain development and; (5) recrystallization by both bulge nucleation and subgrain rotation mechanisms to yield mortar textures with triple point junctions (White, 1975; Vernon, 1975; Marshall et al., 1976; Shelly, 1977; 1979) and core/mantle structures (White, 1975).

A classification scheme, summarizing the main optical features of upper mantle peridotite deformation, is presented in Table 3-1 and Figure 3-10, after Mercier and Nicolas, (1975) and Gueguen and Nicolas, (1980). This nomenclature will be used extensively in the following chapter to document the microscopic ductile deformation features within the rock units of the Troodos plutonic complex.

### **3.6. Microscopic Textural Features and Terminology of the Cumulate Mafic-Ultramafic Rocks**

The following section is included to familiarize the reader with the microscopic features of primary cumulate rocks and to provide a comparison with the microfabrics of the deformed older suite lithologies. The petrographic description of the undeformed, younger suite cumulates is presented in Chapter 4.

The terminology to be used for describing the primary igneous textures of the younger suite(s) is based upon the nomenclature devised by Wager et al., (1960) and Jackson, (1961; 1971). The framework mineral phase(s) of the cumulate rock are referred to as the cumulus grains while the intercumulus (or post-cumulus)

**Table 3-1:** Classification Scheme of Ductile (Plastic) Deformation Textures in Upper Mantle-Lower Crustal Peridotites.

Proto-granular	Oldest texture, least deformed, low strain. no crystal elongation, no preferred dimensional orientation, few kinkband boundaries and minor recrystallized neoblasts along grain margins. Olivine grain boundaries are curvilinear, spinel blebs in orthopyroxene. Grain size of opx. and ol. averages 2-7 mm; cpx. and sp. <2mm.
Porphyro-clastic	Moderate to strongly deformed, elongate and strained xenomorphic olivine and pyroxene porphyroclasts and polygonal neoblasts, holly-leaf shaped spinel grains flattened parallel to porphyroclasts ( $S_1$ ) and elongate parallel to the lineation.
Grano-blastic (equant, tabular)	Completely recrystallized, relict porphyroclasts, equant polygonal mosaic (foam) structure and tabular neoblasts, grain size generally < 1 mm (up to 10 mm), straight grain margins, converging triple point junctions ( $120^0$ ), cpx. and spinel scattered within and along grain margins concentrating at triple point junctions. Coarser textures indicative of high temperature and moderate stress deformation in upper parts of the mantle peridotites (Nicolas <u>et al.</u> , 1980).

NOTE : Primary protogranular to primary porphyroclastic to primary equigranular textures may be recycled to secondary proto-granular, porphyroclastic and equigranular textures (Mercier and Nicolas, 1975). The principal optical distinction between primary and secondary cycles is the presence of relict spinel inclusions within the secondary porphyroclasts.



**Figure 3-10:** Typical microstructures of ductilely deformed peridotites: A= Protogranular: no foliation, few kinkbands, undulose extinction; B= Porphyroclastic: kinkbanded and elongate porphyroclasts recrystallized in surrounding neoblasts; C-D= Granoblastic: complete recrystallization into either equant (C) or tabular (D) neoblasts (after Gueguen and Nicolas, 1980).

phase(s) are those which crystallized interstitial to the framework cumulus phases. The relationship between the cumulus and the intercumulus materials has led to three major textural groupings for cumulate rocks : (1) orthocumulates, in which the intercumulus phase encloses original cumulus grains; (2) adcumulates, in which post-cumulus overgrowth (enlargement) of the cumulus phase(s) occurs by the crystallization of melt with the same composition; and (3) mesocumulates, which are intermediate between the ortho- and adcumulate textures, with some overgrowth of material on the cumulus grains but also some pore mineral crystallization as in the orthocumulate types. Post-cumulus minerals that differ in composition from those of the cumulate phase(s) may react and partially absorb the older phase(s). Crystallization of intercumulus liquid, with a different mineral composition than the cumulate phase(s), results in few nucleation sites and poikilitic textures (heteradcumulates).

Cumulus crystals typically display apposition fabrics in which equant crystals will exhibit no preferred shape orientation, tabular crystals are orientated such that their short axis lie normal to layering and elongate crystals are positioned with their long axes in the layering plane (Jackson, 1961; 1971; Wager *et al.*, 1960). The orientation of elongate cumulate crystals may form either a random girdle distribution in the layering plane (Jackson, 1961) or a preferred linear alignment developed in response to magmatic flow (Morse, 1969). It is important that such features are distinguished from secondary, plastic deformation induced crystal elongation and alignment, particularly within the layered gabbro as will be discussed in this chapter. It has been noted by Raleigh (1965) and Thayer (1980) that some cumulate structures may survive penetrative solid-state flow. This depends upon the total accumulated strain, rheological behaviour of the various cumulus phases and strain heterogeneity within the deforming unit. Preservation of cumulus textures during pervasive serpentinization was also noted by Jackson (1971) with oikocryst and enclosed chadacryst phases being pseudomorphed by different serpentine polymorphs, yet still preserving the primary textural features. Similar features will be documented for the younger suite in Chapter 4.

The textural terminology is purely descriptive, and not intended to imply any of the various formational processes which have been proposed over the years by numerous authors (e.g.: Jackson, 1961; 1971; Irvine, 1965; 1980; McBirney and Noyes, 1979; Wadsworth, 1985) to explain the development of cumulate sequences by gravity accumulation, magmatic density currents, in-situ crystallization or double-diffusive convection processes.

A summary of the main features for the common cumulus mineral phases in ultramafic-mafic rocks is presented in Table 3-2 after Jackson, 1961; 1971.

**Table 3-2:** Common Textural Features of Cumulus Mineral Phases in Ultramafic-Mafic Rocks (after Jackson, 1961; 1971)

PHASE	SIZE RANGE	HABIT
Olivine	.4-50 mm (1-4 mm)	Equidimensional, euhedral, prismatic crystals slightly flattened on (010).
Orthopyroxene	.5-20 mm (1-4 mm)	Euhedral, stubby crystals, slightly flattened on (100) or (010), rare broad prisms or elongate in C-axis.
Clino- pyroxene	.5-20 mm (1-4 mm)	Euhedral, more often flattened and elongate than opx.
Feldspar	1-3 mm	Euhedral, tabular.
Spinel	.02-5 mm (.1-.4 mm)	Rare crystals up to 5 mm and nodules up to 30 mm, euhedral octahedral.

### 3.7. Microfabrics of the Tectonized Older Suite Lithologies



### 3.7.1. Upper Mantle - Lower Crustal Peridotite Tectonites

The effects of a penetrative, high temperature ductile deformation signature upon the harzburgite and dunite lithologies of the plutonic complex has been demonstrated in Sections 2.2, 3.2 and 3.3 on the basis of field evidence, including; (1) the isoclinally infolded boundary of these two units and (2) the mesoscopic scale features and structurally concordant foliation development in both lithologies. The optical evidence of plastic strain, recovery and recrystallization mechanisms operating within the harzburgite and dunite units is documented on microscopic level in the following section.

The harzburgite tectonite exhibits a generally coarse porphyroclastic to occasionally granoblastic equant texture. Modal mineral abundances exhibit: olivine (70-85%), orthopyroxene (15-30%) and spinel (<2%). Olivine occurs primarily as coarse (<1 mm) equant neoblasts with straight grain boundaries, triple point junctions ( $120^0$ ) and some internal straining and kinking of the neoblasts. Relict, large (1.5-3.5 mm) xenomorphic olivine porphyroclasts show some elongation (aspect ratios <3:1), sharp multiple kinkband boundary development with elongate subgrains orientated at a high angle to foliation. Orthopyroxene occurs as granoblastic, equant, polygonalized neoblasts (<1 mm) and xenomorphic porphyroclasts, up to 2 mm in size with subgrain walls, exsolution clinopyroxene lamelle along the [100] cleavage trace and sharp kinkband boundaries. (Figure 3-11).

The recrystallized orthopyroxene grains often show straight grain boundaries and triple point junctions. The spinel phase is dark red-brown (ppl) and opaque (cross nicols), <.5 mm in size with an irregular (xenomorphic) to relict holly-leaf texture with serpentinized olivine inclusions. A weak  $S_1$  fabric is defined by the alignment of attenuated and broken spinel fragments. The spinel phase occurs spatially associated with both the olivine and orthopyroxene phases, along the orthopyroxene grain boundaries and inter/intrastitital to the olivine. Mercier and Nicolas, (1975) documented a strain dependent spinel textural relationship in



\_\_\_\_\_

**Figure 3-11:** Deformed orthopyroxene porphyroblast (OPX) in harzburgite exhibiting a sharp kink band boundary (east-west) and exsolution lamellae of clinopyroxene (CPX). Note the olivine (OL) inclusion in upper right corner of photo. Bar scale = 1 mm.

which silicates co-existing with holly-leaf shaped spinel is characteristic of the porphyroclastic stage of deformation. This spinel texture (holly-leaf, wormy) is associated with mantle spinel rather than cumulate spinels (Nicolas *et al.*, 1980). Talkington and Malpas (1980) noted temporal relations between microtexture and spinel form. They reported that the spinel in least deformed rocks forms droplets and vermicules exsolved in orthopyroxene and interstitial grains to silicate phases. With increased deformation, spinels exhibit "holly-leaf" textures and form porphyroclasts with recrystallized trails and exsolved droplets along the kink band boundaries of pyroxene as well as xenoblastic spinels in granoblastic samples.

The massive dunite exhibits a dominantly equant, granoblastic texture with some olivine porphyroblast preservation. The recrystallized neoblasts (<1.2 mm) form a well developed foam structure with straight grain boundaries, triple point

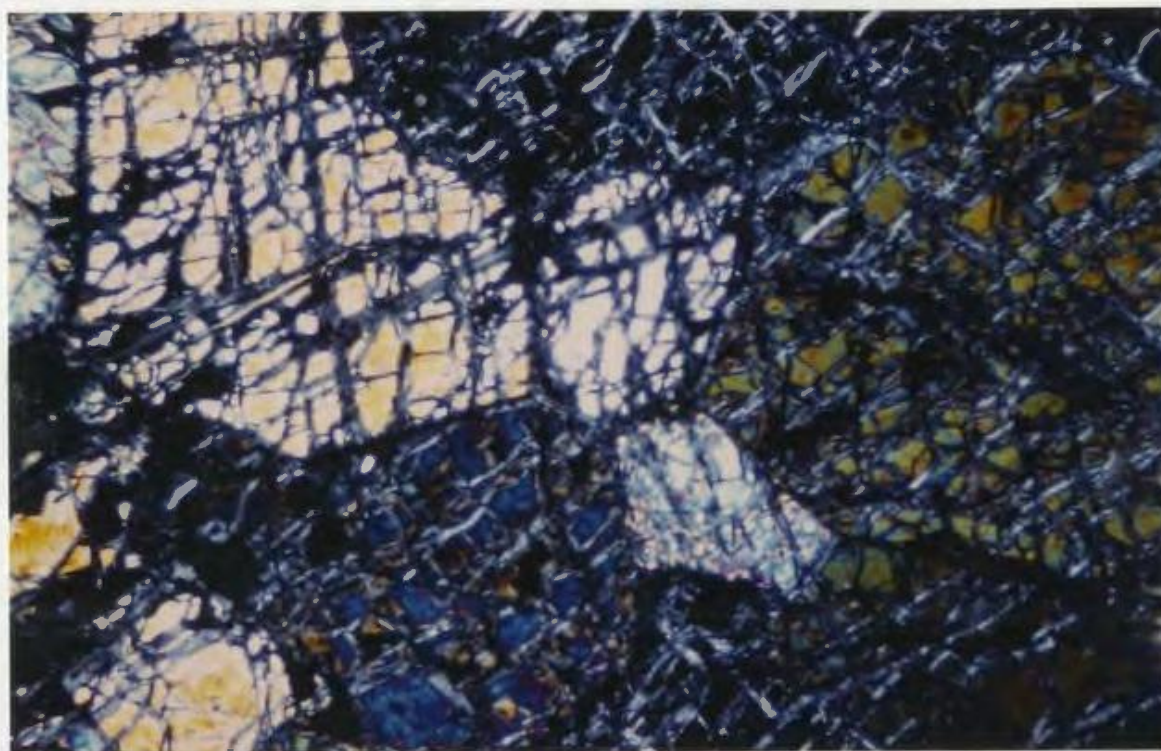
junctions and some internal subgrain wall development (Figure 3-12). The olivine porphyroclasts (<20% of the rock) range up to 6 mm (rarely up to 9 mm) in size, are slightly elongate (aspect ratios <3:1) with intense, sharp kinkband boundary development. Strained neoblasts mantle core porphyroclasts (White, 1976). Spinel occurs as small (<.3 mm), 2-5%, opaque to dark red-brown, disseminated, euhedral to anhedral grains interstitial to the olivine and accessory clinopyroxene and intrastitial to the olivine porphyroclasts. Similar spinel features were correlated with deformed cumulate ultramafics rather than mantle peridotites by Nicolas *et al.*, (1980). The accessory clinopyroxene (<1%) occurs as small (<.3 mm), irregular grains interstitial to olivine and internally strained. This type of clinopyroxene features has likewise been correlated with a cumulate ultramafic source rather than a mantle peridotite origin (Nicolas *et al.*, 1980).

### **3.7.2. Transition Zone Peridotites : A Case for Recrystallization via Subgrain Rotation Mechanism**

In this section, the rocks of the older suite orthopyroxenite transition zone exhibit a strongly recrystallized texture (Figure 3-13) defined by orthopyroxene grains (85-95%) with lesser amounts of olivine (<10%) and accessory clinopyroxene (<1%). The orthopyroxene phase consists of dominantly recrystallized neoblasts (.4-.8 mm) with straight grain boundaries, internal straining (undulose extinction and subgrain walls) and triple point junctions which form an equant granoblastic or mortar (foam) texture (Figure 3-13). Larger relict laths of orthopyroxene (up to 1.3 mm in length) comprise up to 20% of the orthopyroxene phase and exhibit a preferred dimensional orientation parallel to the layering/foliation. These larger, porphyroclastic orthopyroxene crystals show variable degrees of internal (intracrystalline) strain as indicated by their undulose extinction, rare sharp kinkband boundaries and abundant, equant subgrain wall development (Figure 3-15).

A case in support of recrystallization via a progressive subgrain rotation mechanism for the older suite transition zone is indicated by the deformation

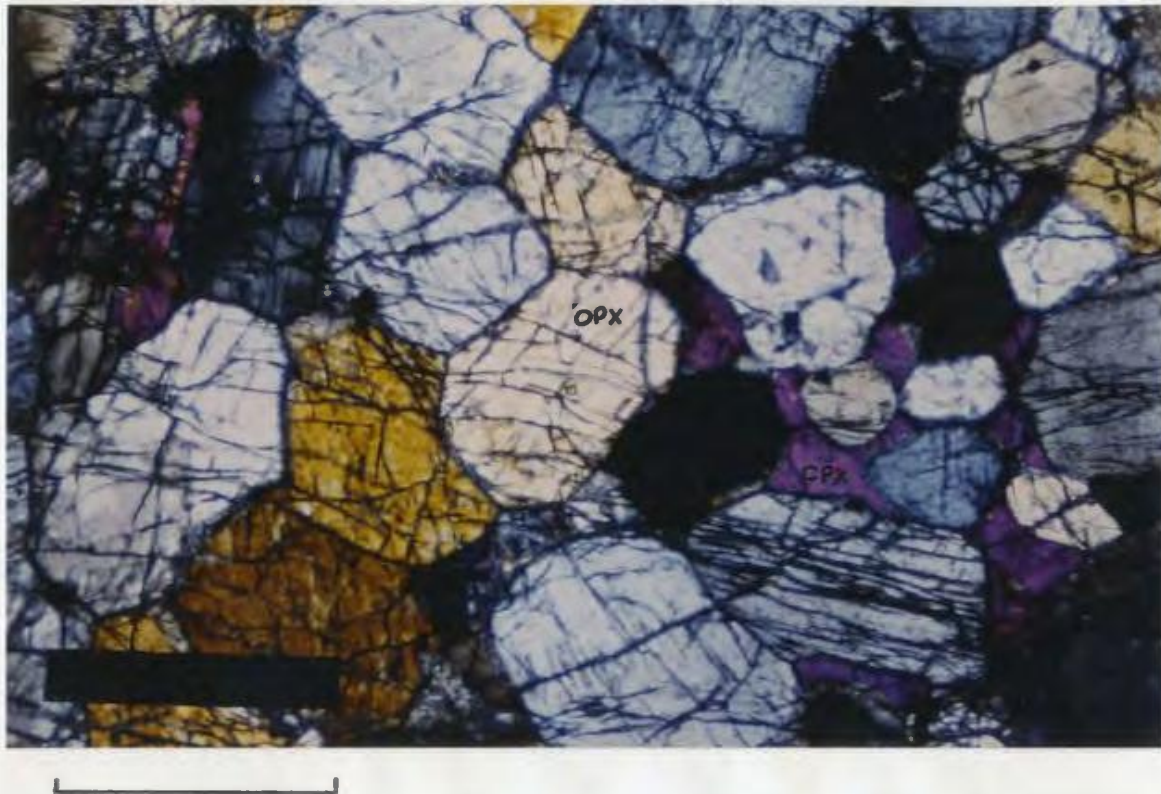




**Figure 3-12:** Equant, granoblastic olivine texture in dunite. Note the recrystallized olivine neoblasts with straight grain margins and triple point junctions. Bar scale = 1 mm.

features of the orthopyroxene phase. Various stages of increased intracrystalline strain are evident within the orthopyroxene laths (porphyroclasts) as documented by a sequence of photographs (refer to Figures 3-14, 3-15 and 3-13) from transition zone outcrop exposed along Pine Road. Weakly undulose orthopyroxene grains (porphyroclasts) surrounded by a mortar texture of equant orthopyroxene neoblasts are shown in Figure 3-14. An increase in the intracrystalline strain state of the orthopyroxene grains (porphyroclasts) is indicated in Figure 3-15 by the development of distinct subgrain walls (dislocation walls) with small ( $<2^{\circ}$ ) offsets in their crystal orientation (extinction angle between adjacent subgrains) on opposite sides of the central dislocation (subgrain) wall. Ultimately, a

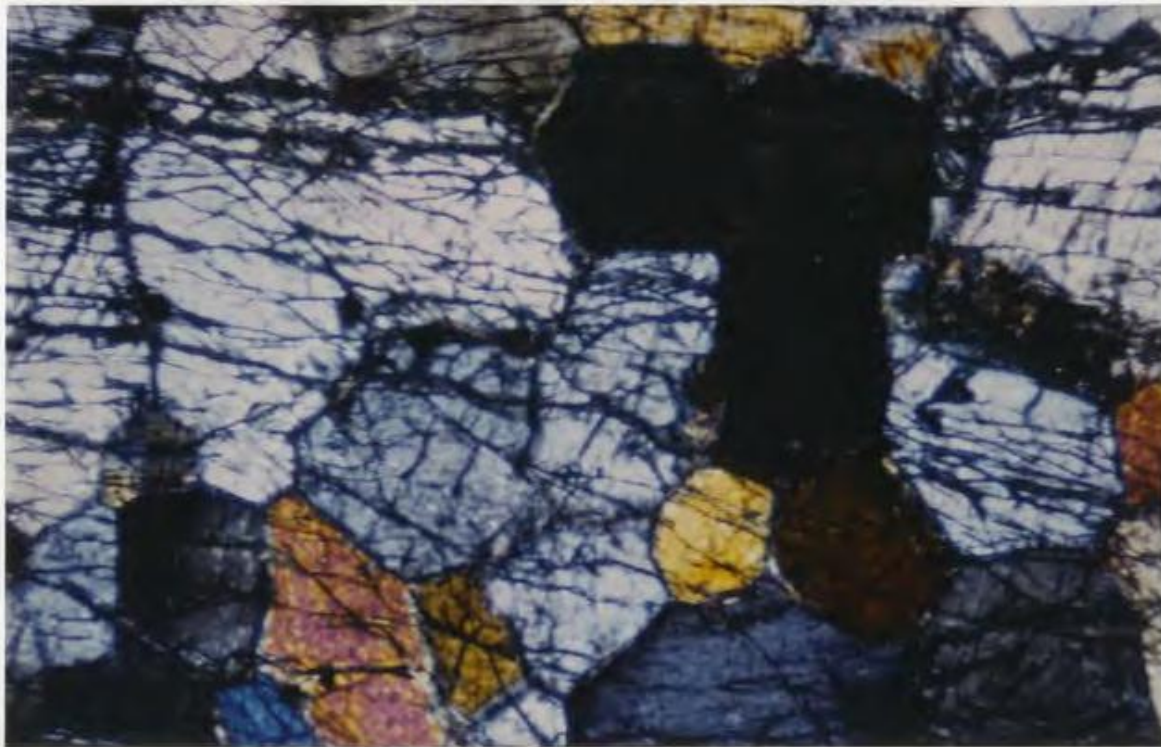




**Figure 3-13:** Equant, granoblastic texture of the recrystallized orthopyroxene (OPX) phase from the Transition Zone. Note the interstitial clinopyroxene (CPX). Bar scale = 1 mm.

progressively larger offset angle between adjacent subgrains has been attained in parts of the thin section such that these subgrains begin to appear as distinct grains (neoblasts) which are the same size as the surrounding equant recrystallized grains and share the same straight grain margins with well developed triple point junctions (Figure 3-13). The similarity in the size of the subgrains and recrystallized neoblasts suggests that progressive subgrain rotation was the operating mechanism responsible for the recrystallization rather than bulge-nucleation. Similar progressive rotation and misorientation of adjacent subgrains with increasing intracrystalline strain (accumulation of dislocations) to yield independent grains ( $>10^0$  offset) has been reported for a variety of minerals (e.g.:by White, 1975; 1976; Nicolas, 1975; Nicolas and Poirier, 1976; Christie and Ardell, 1976; Carter, 1976; Etheridge and Kirby, 1977; Tullis, 1979). It is of interest to note that the mineral chemistry of the variably strained orthopyroxene porphyroclasts (  $\text{Mg}(\text{mol}\%)=91.37$  and  $\text{Fe}(\text{mol}\%)=5.06$  for an average of 14





**Figure 3-14:** Relict laths (porphyroclasts) of orthopyroxene, up to 1.3mm in length, exhibiting weakly undulose extinction and surrounded by a mortar texture of equant orthopyroxene neoblasts. Bar scale = 1 mm.

analysis) is the same as that of the recrystallized orthopyroxene neoblasts (Mg(mol%)=91.54 and Fe(mol%)=5.07 for an average of 5 analysis ); (refer to Appendix B-3 for the complete mineral analysis).

The actual mechanism of rotation is believed to be driven by the accumulation and reorganization of dislocations into subgrain walls in the deforming crystal lattice such that with progressive deformation, the misorientation of the crystal lattice increases across the subgrain boundaries, ultimately yielding two unique crystals or neoblasts (syntectonic recrystallization).

The olivine phase within the older suite orthopyroxenite unit is unusual in that it occurs as large (up to 1.5 mm), equant to slightly elongate (aspect ratios <3:1) grains with irregular grain margins, occurring interstitial to the orthopyroxene as well as enclosing orthopyroxene neoblasts. These olivine grains exhibit both





**Figure 3-15:** Orthopyroxene porphyroblast exhibiting development of undulose extinction and distinct equant subgrains (top right corner) in which adjacent subgrain walls (crystal lattice) are offset a few degrees ( $\sim 2^\circ$ ). Bar scale = 1 mm.

uniform extinction (unstrained) and minor development of kinkband boundaries in other grains. An indigenous origin for the olivine in the orthopyroxenite appears unlikely as the olivine appears relatively undeformed in comparison to the surrounding recrystallized orthopyroxene. Rheologically, the olivine will more easily deform via intracrystalline strain and recovery mechanisms, than the orthopyroxene phase under typical upper mantle-lower crustal conditions (Nicolas and Poirier, 1976); (and as is observed in the olivine phase from harzburgite, dunite and layered olivine gabbro units in the Troodos plutonic complex).

A later, post orthopyroxene recrystallization stage origin for the olivine is supported by the inclusion of strained orthopyroxene neoblasts within the relatively undeformed olivine phase. The most feasible explanation for the origin of this olivine phase is by impregnation of a melt phase originating from the younger suite clinopyroxenite-wehrlite pluton which has intruded near the outcrop

from which these samples of the the older suite orthopyroxenite were taken (see Section 3.7). The older suite transition zone occurs as isolated keels which are completely enclosed and "floating" within the younger plutons (as described in Chapter 2). Thus, a younger melt infiltration is a reasonable explanation for the origin of the olivine phase. Magmatic "infiltration metasomatism", a process by which melt initially trapped within an accumulating crystal framework is capable of substantial upward migration, has been discussed by Irvine (1978, 1979) and Wadsworth (1985). This process is not applicable to the origin of the olivine phase occurring within these thin sections of the older suite transition zone since: (1) there is no evidence of chemical disequilibrium (i.e.: zoning) within and between the orthopyroxene and olivine phases; and (2) the solid-state deformation of the orthopyroxene to yield an equigranular texture had to occur prior to the infiltration and crystallization of the undeformed olivine phase. Therefore, the spatial association with the younger suite wehrlite-clinopyroxenite intrusion lends overwhelming support to a younger suite melt origin for the olivine phase that occurs within these samples of the older suite transition zone.

The mineral chemistry from the olivine phase in both the younger suite clinopyroxenite intrusive and the intruded older suite transition zone also supports a younger suite magmatic origin for the olivine phase. The Fo(mol %) values of the olivine grains from the younger suite clinopyroxenite (Fo=90.36 for an average of 11 analysis) are equivalent to the Fo values of the olivine phase (Fo=90.39 for an average of 8 analysis) present within the transition zone orthopyroxenite (refer to Appendix B-3 for the complete mineral analysis).

Accessory clinopyroxene (<1%), present within the older transition zone, occurs as small (<.3 mm), irregular grains situated interstitial to, and sometimes partially enclosing the orthopyroxene neoblasts (Figure 3-13). The clinopyroxene grains exhibit only minor internal straining (undulose extinction). A younger magmatic suite origin for these clinopyroxene grains which occur within the older suite transition zone orthopyroxenite, is also supported by the mineral chemistry

of the clinopyroxene phase. The clinopyroxene  $Mg^*$  values from the clinopyroxenite intrusive ( $Mg^*=91.08$  to  $93.08$  for 12 analysis) are similar to the  $Mg^*$  value of  $93.40$  for the clinopyroxene phase occurring interstitial to the transition zone orthopyroxene (refer to Appendix B-C and C-2 for complete mineral analysis).

### **3.8. Layered Mafic Cumulates/Metacumulates**

#### **3.8.1. Layered Olivine Gabbro**

Documentation of the occurrence of high temperature, plastic deformation within the layered olivine gabbros of the Troodos plutonic complex is based primarily upon the deformation and recovery features exhibited by the olivine phase of the gabbro as well as supporting evidence of strain-induced features within the accompanying pyroxene and plagioclase phases.

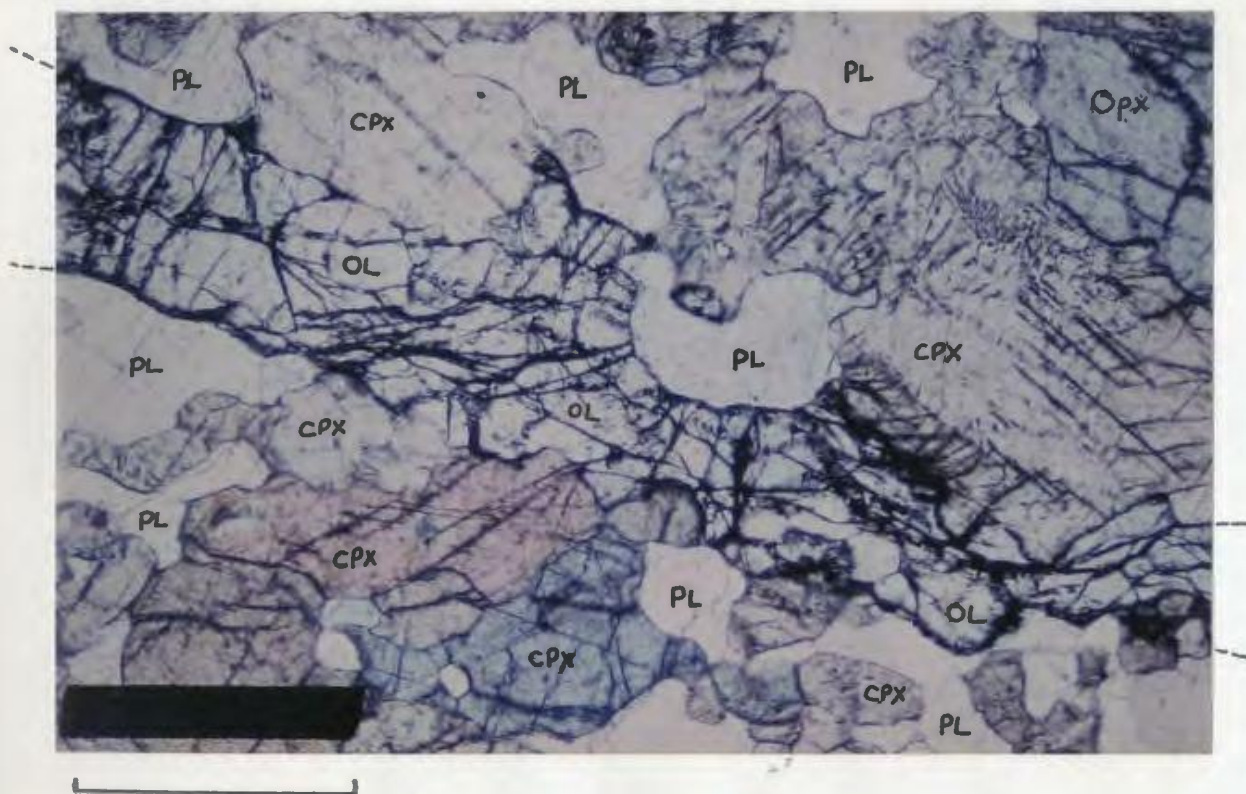
The layered olivine gabbros exhibit variable modal compositions, ranging from olivine (5-25%), orthopyroxene (5-15%), clinopyroxene (30-40%) and plagioclase (40-55%). Some clinopyroxene rich layers grade up to ~80% clinopyroxene; to the near exclusion of the orthopyroxene or plagioclase phases. The prevailing mesocumulate to orthocumulate igneous textures are modified to varying degrees by the high temperature ductile deformation.

A moderately to strongly developed preferred dimensional orientation of the flattened olivine grains and pyroxene and plagioclase laths (cleavage and twinning) parallel/subparallel to the phase layering is evident in thin sections cut perpendicular to the foliation/layering. Weak to isotropic textures were noted in sections cut parallel to the foliation, thereby supporting the field observations of an  $S \gg L$  fabric within the layered gabbro.

The most intensely ductile deformed gabbros show excellent examples of stretched, flattened olivine grains (up to 10 mm in length) with aspect ratios in excess of 14:1 which define the foliation and occur aligned parallel/subparallel to



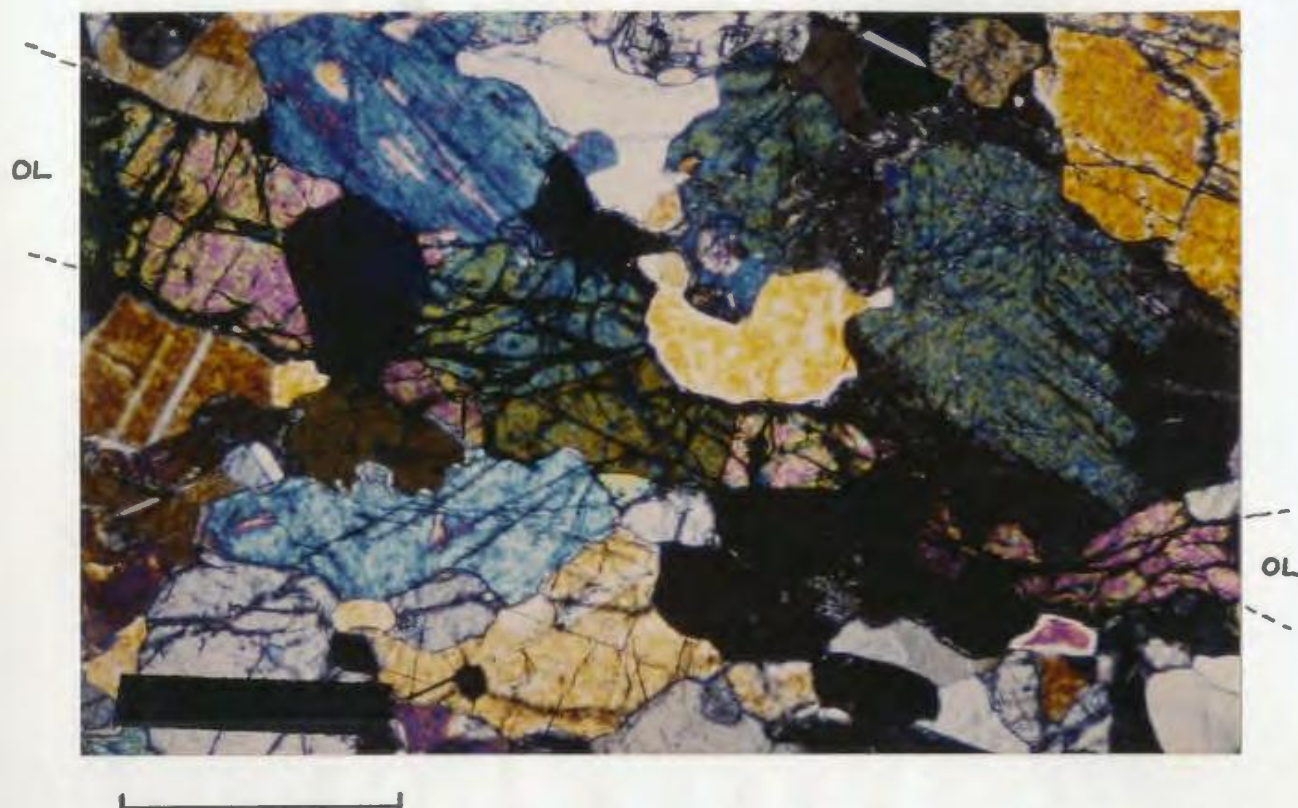
the layering plane (Figure 3-16). These attenuated olivine grains comprise both polygonal subgrains (Figure 3-17) and neoblasts as well as elongate subgrains defined by kinkband boundaries which are orientated at a high angle to the foliation (grain elongation). The equant olivine subgrains and distinct neoblasts exhibit straight grain boundaries, triple point junctions (Figure 3-18) and undulose extinction (Figure 3-17). They range in size from .2 to .8 mm (averaging .3-.6 mm). Small, (<.2 mm) rounded, strained plagioclase inclusions sometimes occur interstitial to subgrains, near and at triple point junctions. The olivine phase within least deformed samples shows a weak foliation, equant to slightly elongate grains <3 mm in size (aspect ratios <3:1) and minor intercrystalline strain as indicated by the presence of few kinkbands and minor elongation.



**Figure 3-16:** Elongate olivine (OL) grain, 10 mm in length with aspect ratios in excess of 14:1, defines the foliation in olivine layered gabbro tectonite (ppl). Olivine = OL, Orthopyroxene = OPX, Clinopyroxene = CPX, Plagioclase = PL. Bar scale = 1 mm.

The pyroxene and plagioclase phases of the layered olivine gabbro show some

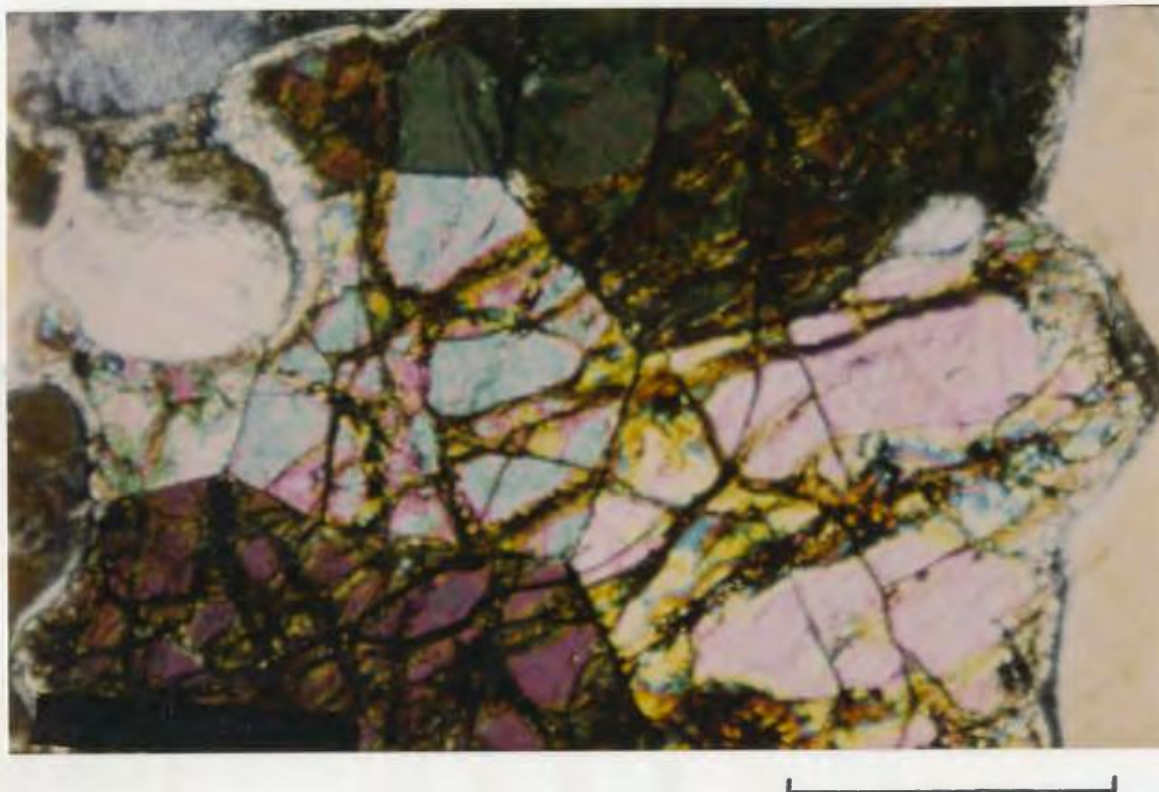




**Figure 3-17:** The attenuated olivine grain shown in Fig. 3.19 is composed of elongate subgrains and equant neoblasts with straight grain margins and undulose extinction (cross nicols). Bar scale = 1 mm.

degree of intercrystalline strain with variable development of undulose extinction. Both the pyroxene and plagioclase phases occur as inequant laths and smaller, equant grains. A preferred dimensional alignment of these inequant laths may be due to either; (1) ductile flow alignment, (2) a primary magmatic alignment as has been documented by Jackson (1961; 1971) and Wager *et al.* (1960) or a combination of both factors. Thus, additional features indicative of intracrystalline strain (i.e.: subgrains, neoblasts) become important in documenting the effects of plastic deformation within these mineral phases.

The clinopyroxene phase occurs both as laths, 1-2 mm in length (rarely up to 3 mm) with a euhedral to subhedral grain habit and as smaller (.5-1 mm) more equant grains with a subhedral to anhedral (xenomorphic) habit and curvilinear grain boundaries. These small clinopyroxene grains occur interstitially to the plagioclase laths and rarely exhibit triple point junctions. The clinopyroxene



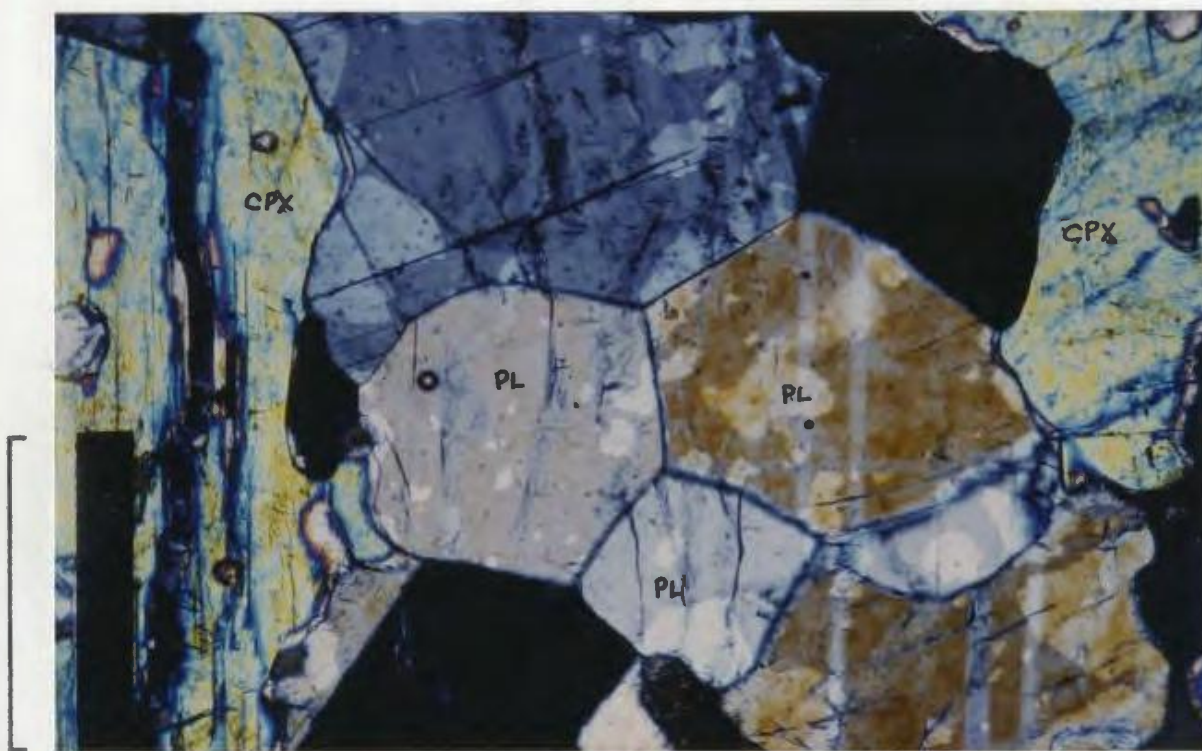
**Figure 3-18:** Equant olivine neoblasts from a section of the olivine layered gabbro exhibiting straight grain boundaries, triple point junctions and undulose extinction. Bar scale = 1 mm.

grains show a generally uniform to weakly undulose extinction. Clinopyroxene rich layers are generally coarse grained ( $<2.5$  mm) with ragged, interlocking grain boundaries, uniform extinction and rarely orthopyroxene oikocrysts (weakly undulose) containing rounded clinopyroxene chadacrysts ( $<.4$  mm).

The orthopyroxene phase occurs both as laths up to 2.5 mm in length and occasionally, as postcumulus (adcumulate) oikocrysts ( $<3$  mm) with olivine, clinopyroxene and plagioclase inclusions. Both the ortho- and clinopyroxene phases show minor evidence of intracrystalline lattice strain (ie.: undulose extinction) and also a small degree of recrystallization as suggested by localized, small zones of equant,  $<.3$  mm pyroxene grains with straight grain margins and triple point junctions.



Plagioclase occurs dominantly as euhedral laths, generally  $< 2.5$  mm in size with abundant deformation lamellae, growth twins and minor kink bands. Small, variably strained polygonalized plagioclase grains (neoblasts) with triple point junctions exhibit straight grain boundaries (Figure 3-19), whereas other small grains show irregular to curvilinear margins and variable degrees of undulose extinction. Small ( $< .3$  mm), rounded plagioclase grains occur as inclusions within the olivine and both pyroxene phases. The plagioclase rich layers show the strongest alignment of crystal laths and exhibit variable degrees of intracrystalline strain (ie.: deformation lamellae, kink bands and minor occurrences of neoblasts).



**Figure 3-19:** Recrystallized plagioclase (PL)neoblasts with triple point junctions and straight grain boundaries in an olivine layered gabbro tectonite. Bar scale = 1 mm.

Thus, within the layered olivine gabbro, the olivine phase shows the strongest tectonite fabrics with an abundance of intracrystalline recovery and recrystallization features. The accompanying plagioclase and clinopyroxene phases give supporting evidence for the presence of penetrative ductile flow on the basis of their localized recrystallization and intracrystalline strain features.

### 3.8.2. Layered Hypersthene Gabbro

The layered hypersthene gabbros show a dominantly mesocumulate texture (Figure 3-20). The overall modal composition ranges are orthopyroxene (5-20%), clinopyroxene (30-45%) and plagioclase (45-60%). Thin sections cut normal to the foliation/layering in handsample show a moderate to strongly developed preferred alignment of the plagioclase and pyroxene laths with cleavage and twin traces lying parallel to the layering (Figure 3-20).



**Figure 3-20:** Mesocumulate texture of the layered hypersthene gabbro with alignment of plagioclase (PL) and pyroxene (PX) laths with cleavage and twin traces parallel to the phase layering. Bar scale = 1 mm.

The orthopyroxene and clinopyroxene phases occur as euhedral shaped cumulate laths, ranging from 0.5 to 3 mm and rarely up to 7 mm in length. Both phases exhibit weakly undulose but generally uniform extinction and minor



recrystallization in some thin sections. These recrystallized neoblasts occur as equant grains with weakly undulose to uniform extinction. They are generally 0.2 to 0.8 mm in size and show straight to curvilinear grain margins, variably developed triple point junctions and occur interstitially to the larger pyroxene laths.

The plagioclase phase of the layered hypersthene gabbro occurs as both cumulus textured laths ranging from 0.5 to 2.5 mm in size, and as more irregular, xenomorphic intercumulus grains interstitial to the pyroxene and plagioclase laths (Figure 3-20). The plagioclase grains show variable development of strain induced deformation bands and weak development of diffuse subgrain walls. Small, equant, variable strained grains with triple point junctions are locally developed interstitial (along grain boundaries) to larger, lath shaped grains.

Overall, the plagioclase phase exhibits the most conclusive evidence of intracrystalline strain within the hypersthene gabbro. This strain is characterized by the deformation bands, undulose extinction and localized patches of recrystallized plagioclase neoblasts.

### **3.8.3. Tectonized versus Undeformed Layered Gabbro**

It becomes obvious from the examination of the gabbros in thin section that the subtle transition from strictly undeformed cumulate textured gabbros to strongly tectonized gabbro is gradational and very difficult to determine at a microscopic level, particularly within the layered hypersthene gabbro. The simple presence of a preferred dimensional orientation of inequant mineral phases cannot be unambiguously interpreted as a primary magmatic feature versus a plastic flow induced texture. Thus, other criteria indicative of intracrystalline flow (refer to Section 3.4) are required to establish a solid-state deformation history for the rocks, particularly if total strain is low and plastic deformation is heterogeneously developed within the units.

The well developed olivine tectonite fabrics, described from hand sample (Section 3.3.3) and thin sections (Section 3.6.3.1) of the layered olivine gabbros, verify the presence of solid-state flow within parts of this unit. Likewise, the accompanying plagioclase and pyroxene phases exhibit some degree of undulose extinction, development of deformation bands and minor recrystallization, all supporting the presence of solid-state flow within the layered gabbros. Thin sections of the layered olivine gabbro outcrops with the least apparent alignment of inequant grains in hand sample, exhibited relatively equant grains with a weak to moderately deformed (kinkbanded and subgrained) olivine phase. These thin sections are difficult to distinguish from the mildly deformed younger suite olivine gabbros on a strictly petrographic basis without the appropriate field relationships.

The variations noted in the development of deformation fabrics within different outcrops of the layered gabbros support the concept of a heterogeneous distribution of strain within these units. This contrast in development of strain induced microscopic features within the olivine versus pyroxene and plagioclase phases of the gabbros is a direct reflection of the differences in the rheological behavior of the various deforming mediums. That is, olivine deforms (ie. via dislocation creep, recovery and recrystallization) more easily under upper mantle-lower crustal conditions than do other phases. This feature is due primarily to the large number of slip planes (pencil glide) operable in olivine versus only 1,2 or 3 dominant slip planes within the pyroxene and plagioclase phases and the lower critical resolved shear stress required for slip in the crystal lattice of the olivine versus the pyroxene and plagioclase phases (Nicolas and Poirier, 1976).

The layered hypersthene gabbros present an even more ambiguous situation for distinguishing the presence of weak to moderate plastic deformation textures. In the absence of olivine, the intracrystalline features indicative of strain must be determined by the more subtle features of undulose extinction, deformation lamellae and minor recrystallization as evident within the pyroxene and

plagioclase phases. The least deformed samples exhibit dominantly primary igneous textures (i.e.: interlocking grain boundaries, cumulate textures).

Thus, the transition from strongly tectonized gabbro to the moderate to weakly deformed and undeformed rocks within which primary cumulus textures are preserved, occurs at various stratigraphic levels within the layered gabbro units (Figure 3-9). The thin-sections from a number of diffuse patches of the isotropic gabbro (pyroxene + hornblende), which outcrop within the layered hypersthene gabbro, showed typical primary igneous textures with cumulus, intercumulus phases and no or only minor evidence of intracrystalline straining of the crystal phases.

One of the most striking features of this heterogeneous distribution of solid-state plastic flow within the gabbroic section of the Troodos plutonic complex, is the parallel/subparallel orientation of phase layering and foliation fabrics within the deformed gabbro and the concordance of this foliation fabric with the phase layering of relatively undeformed gabbro (solid-state flow versus igneous laminations), (refer to Subsections 3.6.3.1 and 3.6.3.2). The orientation of the  $S_1$  fabric in the layered gabbro is concordant with the  $S_1$  fabric of the harzburgite and dunite (Section 3.2). Also, the enveloping surface of the major lithological boundaries appears to be at a high angle to this foliation (Subsection 2.2.1). Planar features are incrementally transposed into parallelism with the X-Y plane (foliation) of a shear zone during progressive simple shear deformation. Thus, the present parallel/subparallel attitude of the  $S_1/S_0$  in the variably deformed gabbros may indicate either; (1) the complete transposition of the gabbro layering into the foliation plane, or (2) an original parallel/subparallel relationship between the foliation and the primary phase layering. The first argument is unlikely since the overall trends of the phase layering within undeformed gabbro are conformable with the regional foliation trends. The second, and more likely argument is supported by the sparsity of parasitic, isoclinal folds which are characteristically associated with the mechanism of transposition.

An original parallel/subparallel relation between the layering and foliation in the gabbro leads to an interesting speculation on the influence of shear stress (flow) on the development and orientation of primary magmatic phase layering within a magma body during crystal mush conditions and accompanying development of ductile deformation features in the gabbro under subsolidus-hypersolidus conditions (refer to Table 3-3). The attitude of fine scale layering, development of primary igneous features (i.e.: cross bedding, slump folds) as well as primary crystal alignments in a flowing, partially solidified magma (crystal mush) may be controlled (to some extent) by the orientation of the stress regime operating during magma flow and crystallization (by which ever means or combination of ways the crystallization occurs; e.g.: insitu, double diffusive convection etc.). Within a magma undergoing shear stress conditions (flow), inequant crystals may develop a preferred orientation during flow while strain is accommodated by the liquid phase. Progressive cooling and crystallization of the magma during continued lower crustal stress conditions (i.e.: flow within an uprising diapir or convection-flow overturn away from an upwelling and spreading zone) would ultimately lead to the development of intracrystalline strain features, that is, ductile deformation (subsolidus plastic flow), within the mineral phases of the fractionating body as the ratio of crystals to melt increases such that the strain is no longer melt accommodated along grain margins.

Such a scenario is applicable to the layered gabbro of the Troodos plutonic complex where: (1) the concordance of layering/foliation and layering in the relatively undeformed gabbro occurs; (2) the presence of "sedimentary-type" primary textures are indicative of magma-crystal mush flow (these are presently regarded as magma current structures; Jackson, 1961; 1971; Irvine, 1980); (3) the planar alignment of inequant grains occurs in relatively undeformed gabbro; and (4) heterogeneous and transitional development of plastically deformed features are present with variable preservation of primary igneous textures. The generally planar fabric development and the overall lack of any linear alignment of crystals within either the undeformed or the more strongly tectonized gabbros, as well as,



DEFORMATION FEATURES

		COOLING/CRYSTALLIZATION	
		- LIQUID -	- SOLID - (intracrystalline strain)
		(fluid accommodated strain)	
DEFORMATION FEATURES	Mesoscopic	None <ul style="list-style-type: none"> <li>- broad and fine-scale phase layering</li> <li>- streaky-wispy layering</li> <li>- cross-lamination</li> <li>- graded layering</li> <li>- trough banding</li> <li>- scour and fill</li> <li>- slump folds</li> <li>- preferred dimensional orientation of inequant pyroxene and plagioclase phases parallel/subparallel to layering and forming a random girdle to vaguely linear distribution</li> </ul>	<ul style="list-style-type: none"> <li>- weak to strong foliation parallel/subparallel to layering</li> <li>- mesoscopic <math>F_1</math> folds with axial planar foliation (<math>S_1</math>)</li> <li>- preferred dimensional orientation of elongate/flattened olivine defining the foliation</li> <li>- preferred dimensional orientation of inequant pyroxene and plagioclase parallel the foliation/layering</li> </ul>
	Microscopic	None <ul style="list-style-type: none"> <li>- undulose extinction within olivine</li> </ul>	<ul style="list-style-type: none"> <li>- Intracrystalline strain and recovery features: undulose extinction, grain elongation, deformation bands and lamellae, kink-band boundaries, subgrains, recrystallised neoblasts with triple point junctions and straight grain boundaries.</li> <li>- Porphyroclastic texture</li> </ul>

TABLE 3.3. Shear (flow) stress related deformation features developed in the Troodos layered gabbro under progressive cooling/crystallization conditions.

within the harzburgite and dunite at lower structural levels, suggests a dominance of planar shear over simple shear conditions during the development and solid-state deformation of the layered gabbro units.

#### **3.8.4. Fractional Crystallization Sequence for the Layered Gabbros**

The dominant fractional crystallization sequence indicated by the mineral assemblages of the least deformed layered olivine and hypersthene gabbro is OL-CPX-OPX-PL. Allen (1975) and Greenbaum (1972A; 1977) reported the same general sequence (ie.: CR-OL-CPX-OPX-PL-MT-QTZ) with various intermediate assemblages of OL-CPX-PL, OL-CPX-OPX and OL-OPX-CPX (Allen, 1975) for the Troodos stratigraphic complex. Greenbaum (1972A), envisioned a simple case of gravity-aided crystal fractionation with few repeated cycles, slow cooling and a minor influence of current convection on the crystallization process(s). Variation in the crystallization sequence between opx-cpx was observed in this study where rare oikocrysts of CPX form post-cumulus overgrowths that contain inclusions of OPX, PL and infrequently OL. The common occurrence of small (<1 mm) plagioclase inclusions within the olivine and pyroxene phases as well as forming the dominant intercumulus phase may be related to: (1) a continuum of plagioclase solidus conditions throughout the history of crystallization, a feature not reported by Allen (1975), Greenbaum (1977) or George (1975; 1978); or (2) flotation of less dense plagioclase grains from a portion of a crystallizing melt which was incorporated (+/- resorbed) into another portion of the same magma or new magma batch (along the same lines as the plagioclase flotation problem discussed by Irvine, 1980). The occurrence of these plagioclase inclusions within relatively undeformed samples eliminates a simple explanation of plagioclase incorporation during recrystallized grain growth of the other phases. A comparison of inclusion versus intercumulus plagioclase mineral compositions in a number of samples (Table 3-4) showed no significant chemical zonation within individual grains nor compositional variations between the two modes of plagioclase occurrence.

**Table 3-4:** Compositions (mol %) of Cumulus/Intercumulus Plagioclase and Plagioclase Inclusions in the Ortho/Clinopyroxene of the Layered Gabbros

SAMPLE	CUMULUS GRAIN(AN)	INCLUSION(AN)	
		IN OPX	IN CPX
152	94.22		95.
209	87.62		91.10
265	95.49	95.18	
402	95.12, 94.01		94.73

(Refer to Appendix B-1 and B-2 for complete mineral analysis)

The sequence of crystal fractionation, as interpreted from the relationship expressed by cumulus and intercumulate primary textures of the mineral phases, can be affected by a number of post-crystallization factors including: (1) penetrative ductile deformation and recrystallization; (2) primary magmatic flow yielding crystal migration; (3) xenocryst inclusion from other melts, particularly near contacts; and (4) metamorphic overgrowths of phases. The latter factor would be of minor consequence in the layered gabbro of the study area. However, the penetrative deformation yielding grain elongation and recrystallization can completely obliterate crystallization textural relations between cumulate, intercumulate and overgrowth relationships. Also, recrystallization and subsequent grain growth can lead to the inclusion of other smaller grains by these secondary processes, thereby yielding invalid crystal sequences. The possible influences of crystal migration (due to slumping, density currents and magmatic convection) on the relationship between mineral phases has not been detected in outcrop or in thin section. Nevertheless, a significant influence on the apparent crystallization sequence of a magma would be the likely result.

### **3.9. Microscopic Evidence of Multiple Intrusion within the Troodos Plutonic Complex**

Multiple intrusive relationships between the deformed older suite lithologies and undeformed younger suite plutons are documented on a microscopic scale for samples from two regions of the Troodos plutonic complex.

The syn- to post-tectonic (above the deformation front) intrusion of relatively undeformed isotropic textured clinopyroxenite and wehrlite of the younger suite(s) into the recrystallized, older suite transition zone orthopyroxenite is documented at the microscopic level in a series of thin sections from the older suite transition zone as exposed along the Pine Road (Map 1). The same intrusive relationship has been shown in outcrop (Figure 2.9) and briefly discussed in Subsection 3.6.2.

The younger suite intrusive consists of clinopyroxenite (90-98%) with olivine (2-10%) and minor orthopyroxene (<1%). The clinopyroxene phase occurs as coarse (up to 3 mm), equant, uniform to weakly undulose cumulus grains with ragged, interlocking grain boundaries. The olivine phase occurs as equant grains, <1 mm in size with uniform to weakly undulose extinction and rare kinkbanded boundaries. These olivine grains occur interstitial to the clinopyroxene phase and as small (<.5 mm) rounded grains within clinopyroxene. Graphic overgrowths of clinopyroxene into the orthopyroxene grains (<1.2 mm) occur as well as rounded inclusions of clinopyroxenite within orthopyroxenite. The interlocking grain boundaries, coarse undeformed grains and general absence of recovery features illustrate the undeformed, primary igneous texture for the cliopyroxenite, with only minor secondary alteration. Description of the recrystallized orthopyroxenite transition zone has been presented in Subsection 3.6.2.

The intrusive contact between the coarse, undeformed clinopyroxenite of the younger pluton and the recrystallized orthopyroxene mortar texture of the older suite transition zone, as shown in the field relations (Figure 2.9), is demonstrated on the microscopic level in Figure 3-21. A more gradational transition between

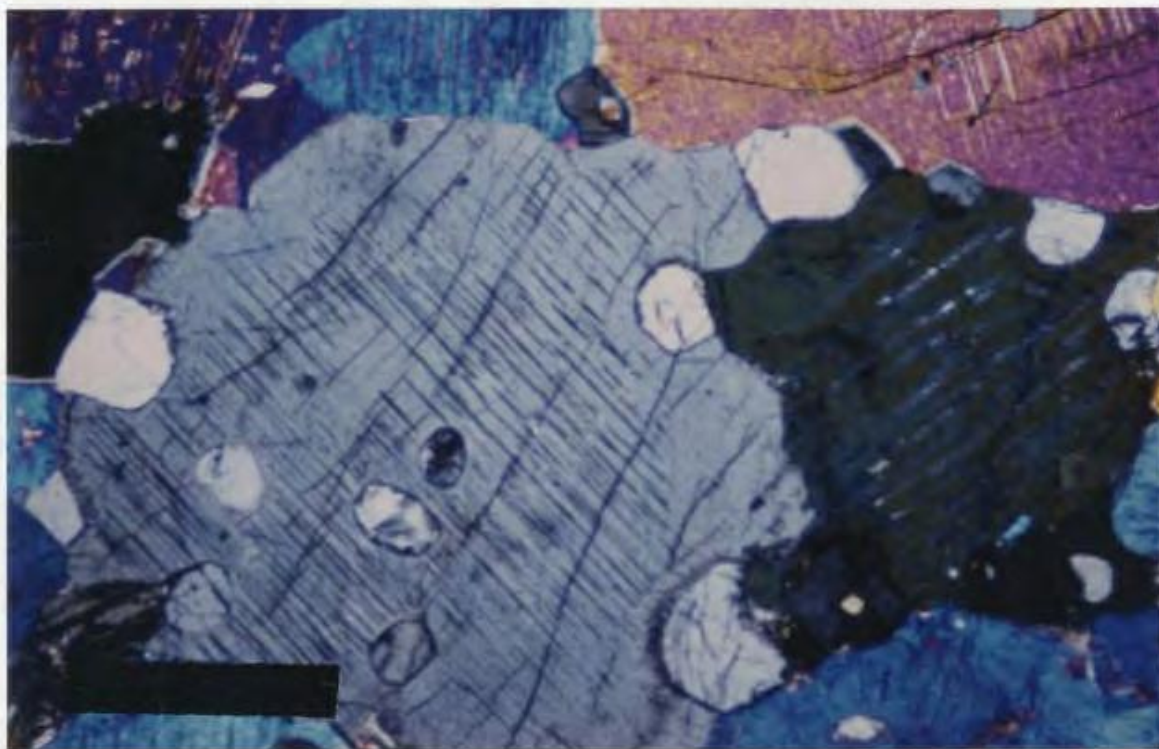
these two units is evident in Figure 3-22. This latter photograph shows the polygonalized neoblasts of the recrystallized orthopyroxene (older suite) occurring along the margins and enclosed within the undeformed clinopyroxene and olivine phases of the younger intrusive.



**Figure 3-21:** Contact between recrystallized (polygonalized) orthopyroxenite transition zone (lower right corner) and the coarse, weakly undulose to undeformed, isotropic younger suite clinopyroxenite. Note the orthopyroxene neoblasts along grain margins and as inclusions within the younger clinopyroxene grains. Bar scale = 1mm.

Syntectonic intrusion of massive, granoblastic dunite by wehrlite-clinopyroxenite veins and disseminations (now weakly deformed protogranular texture) occurs along the southern end of the Chromite Mine Road (Fig. 1/ Map 1). This intrusive relation is also well exposed in thin section. The older suite recrystallized dunite contains polygonalized olivine neoblasts (<1 mm) with straight grain boundaries,





**Figure 3-22:** Gradational contact between the older transition zone orthopyroxenite and younger suite clinopyroxenite. Note the polygonalized orthopyroxene neoblasts along the margins and enclosed within the undeformed clinopyroxene grains. Bar scale = 1 mm.

triple point junctions and rare porphyroclasts ( $<2$  mm) which contain intense kink banding. This older dunite mortar texture is truncated by coarse grained ( $<3$  mm), weakly strained wehrlite-clinopyroxenite. The olivine grains in this younger intrusive unit comprise up to 30% of the rock and exhibit irregular and curvilinear grain margins, undulose extinction, some kink band boundary development in coarser grains ( $<3$  mm) and rare neoblasts. Subhedral laths of clinopyroxene ( $<60\%$ ), up to 3 mm in size, show interlocking grain margins and intergrowth with orthopyroxene, weakly undulose extinction and rarely forming inclusions within orthopyroxene. The orthopyroxene phase ( $<10\%$  ;  $<2$  mm) exhibits irregular, interlocking grain margins with rare poikilitic textures



containing olivine inclusions and rarely clinopyroxene inclusions. Small ( $<1$  mm), red spinel grains ( $<1\%$ ) show a subhedral habit and occur inter/interstitial to both olivine and orthopyroxene.

Thus, the post-kinematic (above the deformation front) intrusion of undeformed, isotropic, younger suite clinopyroxenite-wehrlite plutons into the plastically deformed and recrystallized older suite dunite and transition zone lithologies of the Troodos plutonic complex is clearly documented for both the mesoscopic and microscopic scales.

### **3.10. Summary**

The megascopic, mesoscopic and microscopic scale structural features of the older suite lithological units document the presence of a penetrative, high-temperature ductile deformation within the harzburgite, dunite and transition zone orthopyroxenite. A heterogeneously developed plastic deformation is evident within the layered gabbros. This ductile deformation imparts a consistent, steep to subvertical  $S_1$  form-trace, from harzburgite through to the layered gabbro. The foliation lies parallel to the axial plane of parasitic minor folds ( $F_1$ ) and axial planar to the large scale infolding of the harzburgite-dunite boundary. As mentioned in Chapter 2, the previous studies by George (1975; 1978) in the Troodos plutonic complex reported a 500 m gradation from deformed to undeformed cumulates along the dunite-transition zone contact. George (1975; 1978) did not recognize the intrusive nature of the undeformed ultramafic-mafic cumulates along this contact with the dunite.

An equant, granoblastic to porphyroclastic ductile deformation texture prevails throughout the harzburgite, dunite and transition zone lithologies of the older suite. This same deformation is heterogeneously developed within the layered gabbros, such that regions of low strain preserve the primary ortho- to mesocumulate igneous textures while higher strain regions exhibit a preferred dimensional orientation of elongate grains and recrystallized and subgrain shaped

microstructures. George (1975; 1978) reported a distinct absence of crystallographic strain within the layered gabbro, even within the olivine phase. The present author's work clearly documents the excellent tectonite fabrics, with elongate olivine (aspect ratios  $<14:1$ ) being documented from hand sample and thin-sections of the layered olivine gabbro. This deformation clearly occurs above George's transition to undeformed lithologies in the Troodos plutonic complex. The differences in the degree of crystalline deformation within each mineral phase of a given rock type is dependent on the rheological behaviour of the various mineral phases.

Evidence of recrystallization via progressive subgrain rotation mechanism is suggested by the textural relations evident in thin-sections of the older suite transition zone orthopyroxenite.

The multiple intrusive nature of the Troodos plutonic complex, which is documented on the basis of field relations in Chapter 2, is also documented at the microscopic level from two regions of the plutonic complex (Section 3.7.2). The penetratively deformed and recrystallized dunite and transition zone units of the older suite show microscopic scale intrusive relations with the younger suite, isotropic, undeformed clinopyroxenite-wehrlite. Many other examples of this relation can be found elsewhere in the plutonic complex.

The transition from dominantly ductile to brittle deformation mechanisms, referred to as the deformation front, occurs at various structural-stratigraphic levels within the layered gabbros of the Troodos plutonic complex. This position, in fact, represents the structurally highest level which underwent ductile deformation processes in the history of the complex. Through time, with progressive cooling (hypothetically assuming constant strain rate, stress, pressure and rheological conditions), the relative position of this front would have lowered in the sequence and units which had previously experience plastic flow would have developed brittle failure features in response to continued axial stresses. Likewise, the periodic intrusion of plutons would supply a major influx of heat to raise the temperature isograds, hence, raising the position of the deformation front.

The development of ductile deformation and associated transposition of contact margins within the younger plutons intruded above the deformation front could then occur following crystallization, if the position of the ductile-brittle transition were to rise above the pluton level due to the influx of melt generated heat and if spreading-related shear stress conditions were still operating on this portion of the crustal section. A similar scenario has been documented by Dunsworth *et al.* (1986) within the Lewis Hills massif of the Bay of Islands ophiolite, western Newfoundland. Conversely, the development of brittle, tensile fault structures in the crustal section occurring above the deformation front, at any particular spatial position in time, would allow for fault-controlled intrusion of magma bodies along these structurally weak zones. Fault-controlled intrusion of the younger suite has been discussed in Subsection 2.2.4. Thus, it becomes clear that an interdependent relationship occurs between the spatial and temporal position of the deformation front, periodic influx of magma bodies and the development of ductile versus brittle deformation features within structurally active oceanic crustal sections.

The progressive structural transposition of primary planar and linear elements during penetrative ductile deformation into parallelism/subparallelism with the regional foliation trends has direct application to the geometry of layering within the plutonic complex. The geometrical patterns of fine scale layering and major lithological boundaries cannot be regarded as representing a paleo-horizontal nor the original geometry of the bounding surfaces along which crystal accumulation has occurred within the magma chamber; clearly in contradiction to the conclusions of George, (1975; p.59), Casey and Karson, (1981) and Greenbaum, (1972A). Also, the concordancy between fine-scale cumulate layering within undeformed gabbro and the foliation/layering within deformed gabbro suggests an original parallelism between this primary igneous layering and the foliation plane. Such a relation may indicate some degree of control of the orientation of principal shear stresses within a flowing magma on the development and orientation of fine-scale primary layering and the evolution of ductile deformation features under

hypersolidus-subsolidus conditions (refer to Table 3.3). Thus, the effects of penetrative deformation must be accounted for when attempting to reconstruct magma conduits and magma chamber profiles within a dynamic spreading regime.

The fractional crystallization sequences of the older suite layered gabbro consist of (OL-CPX-OPX-PLAG+/-SP, HBL, QTZ). Variations occur in the relative order of the pyroxene phases. The relative order of crystallization of the pyroxenes may have been affected by : (1) penetrative ductile deformation and recrystallization; (2) primary magmatic flow yielding crystal mixing and migration; (3) xenocryst inclusions from other magmas; and (4) metamorphic overgrowths. The problem of plagioclase inclusions within the olivine, ortho- and clinopyroxene phases of the older suite layered olivine gabbro may indicate a long history of plagioclase crystallization contemporaneous with the other phases. However, the inclusion of the plagioclase phase within olivine during ductile deformation and recrystallization of the olivine phase in the layered gabbro may also occur. Primary magmatic conditions such as plagioclase flotation due to the lower density of the plagioclase relative to the other mafic mineral phases may have led to the incorporation of plagioclase grains floating in the melt, possible forming nucleation centers for the surrounding host phases.

## Chapter 4

# PETROGRAPHY AND CHEMISTRY

The petrographic description of the undeformed, primary cumulate textures of the younger suite intrusives are presented in Chapter 4, followed by a geochemical examination of the younger and older suites to determine fractionation trends and to delineate any chemical criteria which can be used to distinguish between these suites. The mafic-dikes are examined in terms of their petrography and major and trace chemistry. Mineral chemistry from a 20 m. section of the layered olivine gabbro is discussed at the end of the chapter. The terminology to be used in describing the primary igneous textures of the younger suite intrusives is based upon the nomenclature of Wager et al. (1960) and Jackson (1961, 1971) as reviewed in Section 3.6.

### 4.1. Petrography of the Younger Suite Intrusives

The petrographic description and crystallization sequence of the younger suite(s) is presented in the following section. The younger suite plutons incorporate a range of ultramafic and mafic lithologies.

#### 4.1.1. The Ultramafic Cumulates

The younger suite ultramafic plutons consist of wehrlite, feldspathic-wehrlite, lherzolite, feldspathic-lherzolite, clinopyroxenite and websterite compositions. Serpentinization of the olivine phase varies from moderate to intense (<98%). A weak to strong actinolite alteration occurs within the pyroxene phases (uralitization).

The bulk of the ultramafic intrusives that occur within Zone 1 (refer to Figure 2.20) are composed primarily of wehrlite and clinopyroxenite with lesser amounts of lherzolite, feldspathic-lherzolite and websterite. The mineral proportions vary widely as exemplified by olivine (35-90%), orthopyroxene (<1-40%), clinopyroxene (<1-90%), plagioclase (0-8%) and spinel (<1%).

The most striking feature of the Zone 1 wehrlitic to lherzolitic rocks is the common occurrence of poikilitic, heterocumulate textures and the generally undeformed nature of the mineral phases, including olivine. The ortho- to mesocumulate textures which occur along the margins of the intrusive bodies have interlocking framework (cumulate) and intercumulus phases. Oikocrysts of orthopyroxene ( $En = 91.55-92.08$ ) range up to 5 cm in size (generally 3 cm) with uniform to weakly undulose extinction and enclose partially resorbed, rounded olivine chadacrysts (generally <1 mm,  $Fo = 85.80-87.64$ ), (Figure 4-1). Complete mineral analysis are available in Appendix C-1. These olivine inclusions as well as the rounded to slightly inequant (cumulate) olivine grains (<1.5 mm) exhibit uniform to weakly extinction with subgrains and kink bands and no preferred dimensional orientation. Rare orthopyroxene oikocrysts with rounded to subhedral clinopyroxene inclusions were observed within the undeformed lherzolite zones. The clinopyroxene phase (<1 mm) occurs primarily as an interstitial phase to olivine and also as small (<2.5 mm) oikocrysts that enclose rounded olivine chadacrysts (<.8 mm). The plagioclase phase, when present, occurs primarily as small, undeformed interstitial grains and also as small (<.4 mm) inclusions within the olivine, ortho- and clinopyroxene phases. Accessory spinel (<1%) occurs as small (<.5 mm), euhedral to subhedral, dark red-brown, infrequently mottled grains which are situated either along the grain boundaries of the olivine and orthopyroxene phases or interstitial to the clinopyroxene and olivine.

The pyroxenite units of the main intrusive belt (Zone 1) are composed primarily of clinopyroxenite with lesser amounts of websterite. Modal abundances vary with



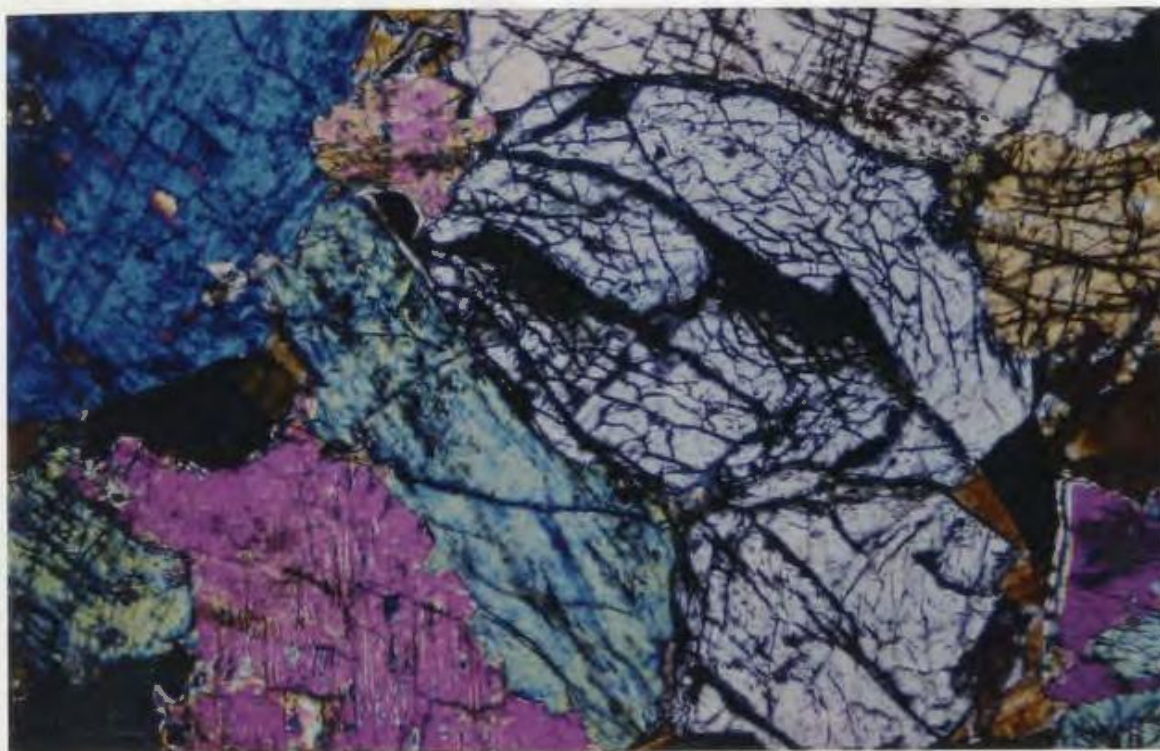


**Figure 4-1:** Poikilitic wehrlite with large, unstrained orthopyroxene oikocrysts and partially resorbed serpentinized olivine chadacrysts. Bar scale = 1 mm.

clinopyroxene (60-95%), orthopyroxene (5-40%) and plagioclase (<2%). The clino- and orthopyroxene grains are <3 mm in size (generally .5-1.5 mm), with uniform to weakly undulose extinction, are equant in shape and exhibit interlocking grain boundaries and orthocumulate textures (Figure 4-2). The orthopyroxene occurs both as a cumulate phase composed of euhedral to subhedral laths and as an interstitial phase to the clinopyroxene. Rare oikocrysts of orthopyroxene (<4 mm), with exsolution lamelle and uniform to weakly undulose extinction, enclose rounded clinopyroxene chadacrysts (.3-1 mm). Two samples showed small (<.4 mm) inclusions of orthopyroxene within the clinopyroxene grains. Accessory plagioclase (<1%) occurs as an interstitial phase to the pyroxenes and exhibits a slightly undulose extinction and twinning.

The younger suite intrusive pods in the NE (ZONE 2) and NW (ZONE 3) map area (Figure 2.20) show a range in lithologies, from feldspathic-lherzolite to olivine norite, depending on the relative abundances of the olivine, pyroxene and



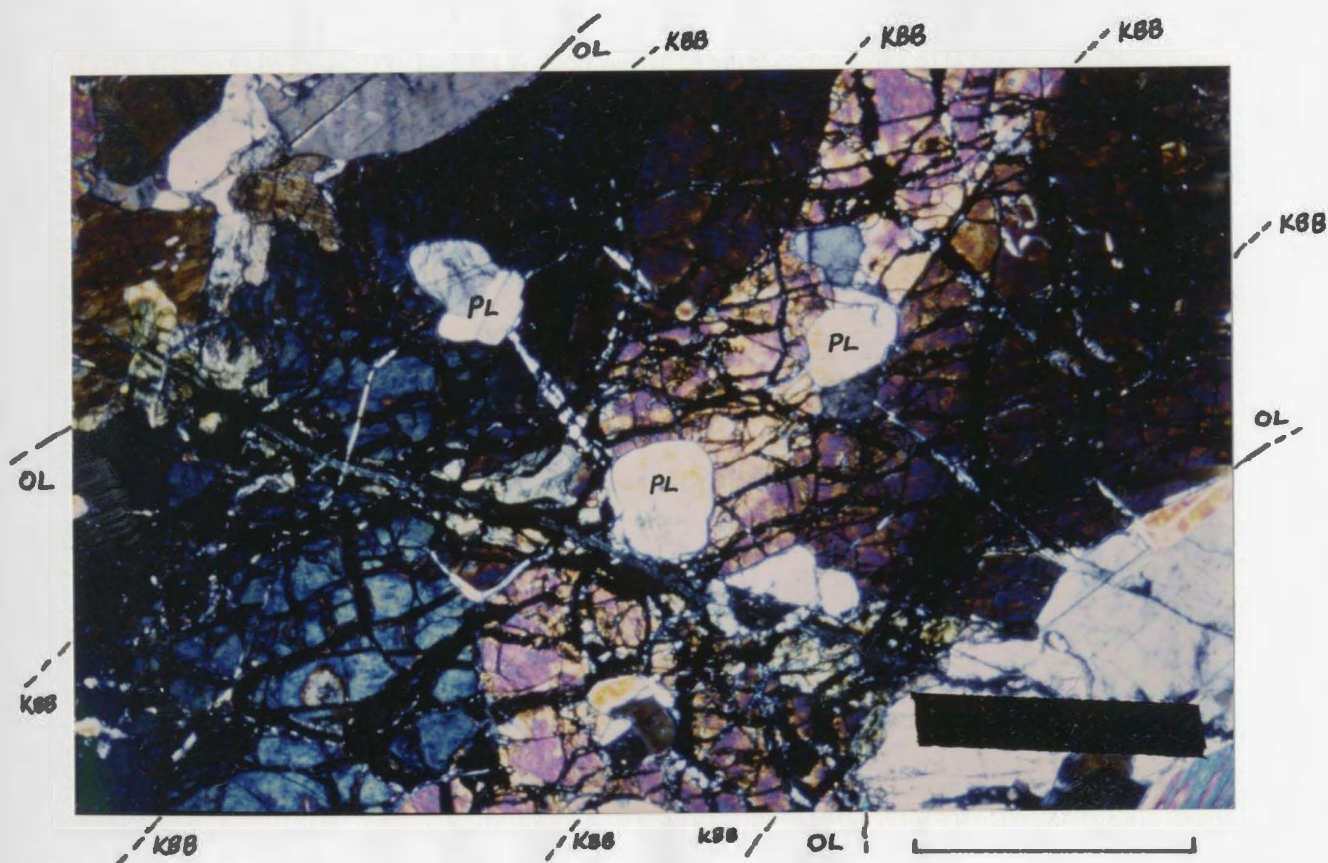


**Figure 4-2:** Pyroxene grains from the younger suite clinopyroxenite showing a medium-coarse grain size, flat to weakly undulose extinction, equant habit and interlocking grain boundaries. Bar scale = 1 mm.

plagioclase phases. Within the NW pod, an undeformed feldspathic-lherzolite body outcrops that exhibits an interlocking ortho- to mesocumulate texture. The olivine cumulate phase (50-60%) ranges from .5 to 3 mm in size (generally 1-2 mm) and exhibits irregular, interlocking grain boundaries, equant and uniform to weakly undulose extinction with minor kinkbands. Clinopyroxene (10-15%) occurs as <2 mm sized grains and orthopyroxene (15-20%) forms intercumulus grains with an occasional oikocryst development. The orthopyroxene oikocrysts are <3 mm in size and enclose olivine, plagioclase and clinopyroxene grains. Both pyroxene phases show a uniform to weakly undulose extinction. Plagioclase (<10%) forms both small (<1 mm) intercumulus grains with weakly undulose to uniform extinction and small inclusions within both the orthopyroxene and clinopyroxene phases. Anhedral accessory opaque (<1%, <.3 mm) occurs spatially associated with the olivine.



The NE pod (Zone 2, Figure 2.20) consists of a more differentiated feldspathic-wehrlite to olivine norite composition. The clinopyroxene (20-30%), orthopyroxene (15-20%) and plagioclase (10-30%) phases show equant, ortho- to mesocumulate textures with interlocking grain boundaries, uniform to weakly undulose extinction and interstitial orthopyroxene and plagioclase phases. The olivine phase (20-35%) exhibits microscopic features indicative of some degree of plastic deformation. The olivine grains exhibit extensive development of subgrains and kink bands (Figure 4-3). The olivine are  $<4$  mm in size and in places contain small ( $<.25$  mm) plagioclase and rare orthopyroxene inclusions (Figure 4-3). The pyroxene phases are generally  $<2$  mm in size. Rare orthopyroxene oikocrysts contain inclusions of clinopyroxene and plagioclase. The plagioclase occurs mainly as an interstitial phase (grain size  $<1$  mm) while euhedral to subhedral cumulate laths ranging up to 2 mm in size.



**Figure 4-3:** Extensive subgrain and kink band (KBB) development in large ( $<4$ mm) olivine (OL) grains from the feldspathic-wehrlite of ZONE 2. Note the plagioclase (PL) and orthopyroxene (OPX) inclusions within the olivine. Bar scale = 1 mm.

The intrusive sill of wehrlite, located just north of the main zone of plutonism (Zone 1, Figure 2.20), also contains some evidence of ductile deformation within the olivine phase. All samples taken from this sill are intensely altered but a few samples still preserve slightly elongate olivine porphyroclasts (aspect ratios  $<3:1$ ) with internal kink banding and subgrain development. The clinopyroxene and minor orthopyroxene ( $<5\%$ ) cumulus grains are equant in habit with interlocking grain boundaries. Both pyroxene phases show a weakly undulose extinction.

#### 4.1.2. The Mafic Cumulates

The pyroxene-hornblende gabbro of the younger suite intrusives is isotropic in appearance with an ortho- to mesocumulate texture. Interlocking cumulate grains dominate (70-85%) and plagioclase represents the predominant interstitial phase. The plagioclase (45-85%), pyroxene (orthopyroxene and clinopyroxene =  $<35\%$ ) and hornblende ( $<10\%$ ) phases showed uniform to weakly undulose extinction. The grain size averages 1-4 mm while plagioclase laths, up to 7 mm in size, are present within the coarser grained portions of the gabbro. Interstitial quartz ( $<1\%$ ) occurs in one sample and exhibits a recrystallized neoblast substructure (neoblasts = .2-.4 mm). One of the coarser grained samples (#193) exhibits a strong compositional zonation of the plagioclase laths (i.e.: Core - anorthite = An - 94.12 / Rim - labradorite = An - 66.46). The same sample also shows zonation of the primary hornblende with Ca poor and Fe-Mg rich rim compositions relative to the core composition (i.e.: Core - Ca[11.68], Mg[15.01], Fe [15.13] / Rim - Ca[1.73], Mg[18.94], Fe[20.57] (wt% oxide)). Refer to Appendix C-3 for the complete mineral analysis. The primary amphibole appears as an interstitial phase that encloses both the plagioclase and pyroxene cumulus grains. An abundance of fibrous actinolite alteration ( $<60\%$ ) of the pyroxene and hornblende was noted in all samples of the gabbro.

### **4.1.3. Fractional Crystallization Sequence of the Younger Suite Intrusives**

The overall fractional crystallization scheme of the ultramafic to mafic younger suite intrusives, as indicated by the primary igneous cumulate textures, shows a sequence of (+/-SP)-OL-CPX-OPX-PLAG-HBL-QTZ. This scheme duplicates that observed for the older suite layered gabbros (refer to Subsection 3.6.3.4).

Small but important variations on this sequence of crystallization indicate an overlapping in the timing of crystallization of different mineral phases. Concurrent crystallization of the ortho- and clinopyroxene phases occurs within the gabbroic bodies as indicated by the cumulus grain textures and small inclusions of clinopyroxene in orthopyroxene grains and vice-versa. Small plagioclase inclusions occur within the olivine, ortho- and clinopyroxene cumulate grains of the ultramafic lithologies and within the ortho- and clinopyroxene and hornblende phases of the mafic intrusives. Analyses of the plagioclase chadacrysts ( $An = 97.56$ ) within the clinopyroxene grains of sample #257 shows that they are of the same composition as the intercumulus plagioclases ( $An = 97.15$ ) in the sample. Refer to Appendix C-3 for complete analysis.

### **4.2. Mineral Chemistry**

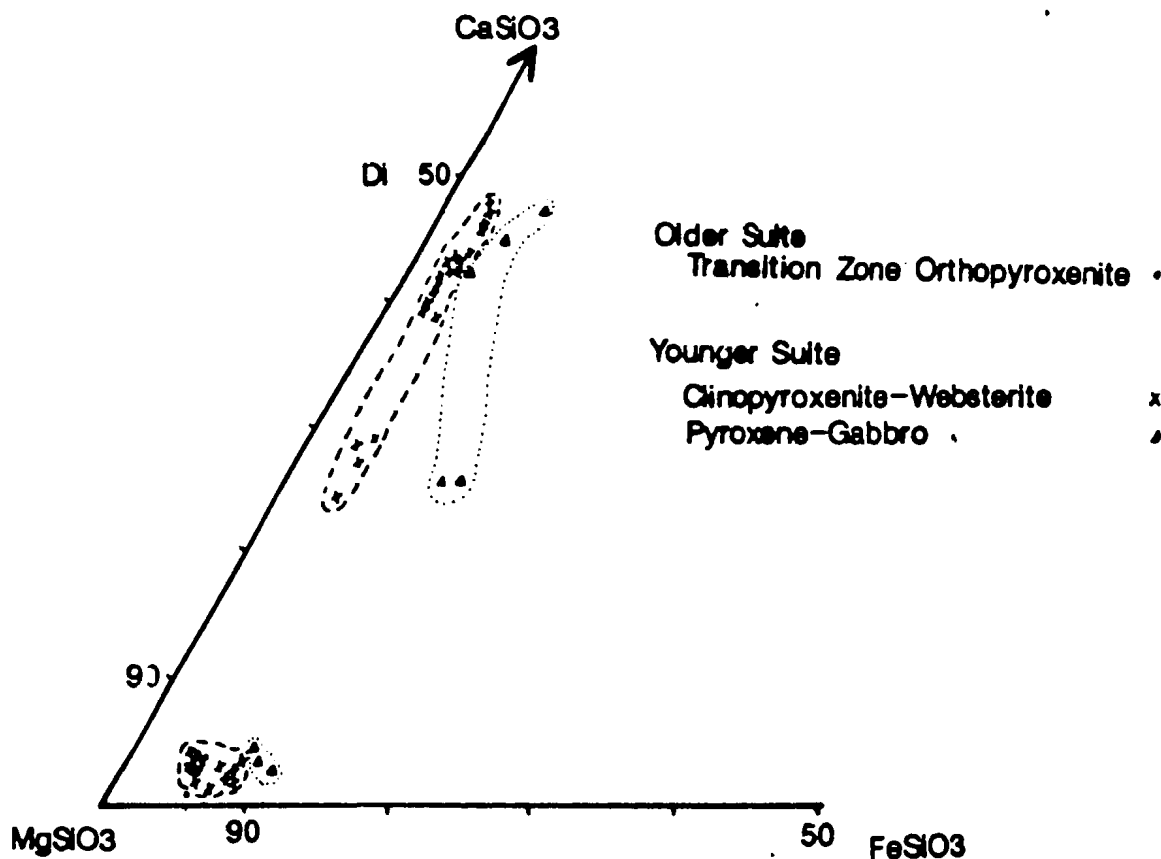
The mineral chemistry of various lithologies is examined in the following section. Evidence of fractionation trends within the younger and older suites is presented, followed by an attempt to delineate any chemical differences for distinguishing between the igneous suites. Complete microprobe analyses are available in Appendices B and C. None of the minerals shows any significant difference in mineral chemistry from grain to grain in the same sample. Likewise, no chemical zonation was detected within individual grains except for normal core-rim zonation in the plagioclase and hornblende grains of the coarse grained younger suite gabbro. Sample locations are presented in MAP 1.

#### 4.2.1. Fractionation Trends within the Younger Suite Plutons

Analyses of the clinopyroxene and orthopyroxene phases from the younger suite clinopyroxenite-websterite and pyroxene gabbro units are plotted in Figure 4-4. Orthopyroxenes from both the pyroxenite and gabbro lithologies are enstatites compatible with the range of orthopyroxene values in alpine peridotites (Himmelberg and Coleman, 1968). The clinopyroxene analyses fall within the diopside to endiopside (low Ca-Cpx) field. A fractionation trend from pyroxenite to gabbro is evident within the younger suite. Both the clinopyroxene and orthopyroxene phases show an increase in Fe content within the more differentiated gabbro unit. The composition of the plagioclase in the clinopyroxenite-websterite ( $An = 91.57-96.69$ ) and gabbro ( $An = 55.35-97.94$ ) lithologies (refer to Figure 4-7) likewise shows the same fractionation trend which is marked by the Na-enriched rim compositions of the plagioclase within coarse grained gabbro versus the more Ca-rich plagioclase from the feldspathic-pyroxenites.

A general fractionation trend is also observed for different structural levels of intrusion of the younger suite(s). The orthopyroxene and clinopyroxene compositions of the younger suite ultramafic cumulates are plotted in Figure 4-5. Both pyroxene phases plot within the appropriate enstatite and diopside-endiopside fields. A trend towards increased fractionation is marked by the increased Fe content of the pyroxene phases within the structurally higher ultramafic pods of Zones 2 and 3 relative to the main zone of intrusion (Zone 1) which is situated at a lower structural level in the Troodos plutonic complex. The same trend in fractionation is evident from analysis of the olivine component in the younger suite ultramafics (refer to Figure 4-13) where lower Fo ( $=Mg/Mg+Fe$ ) values were observed to correspond to samples from the structurally higher NE and NW intrusive pods relative to Zone 1. Refer to Appendix C.1.1 for complete mineral analyses.

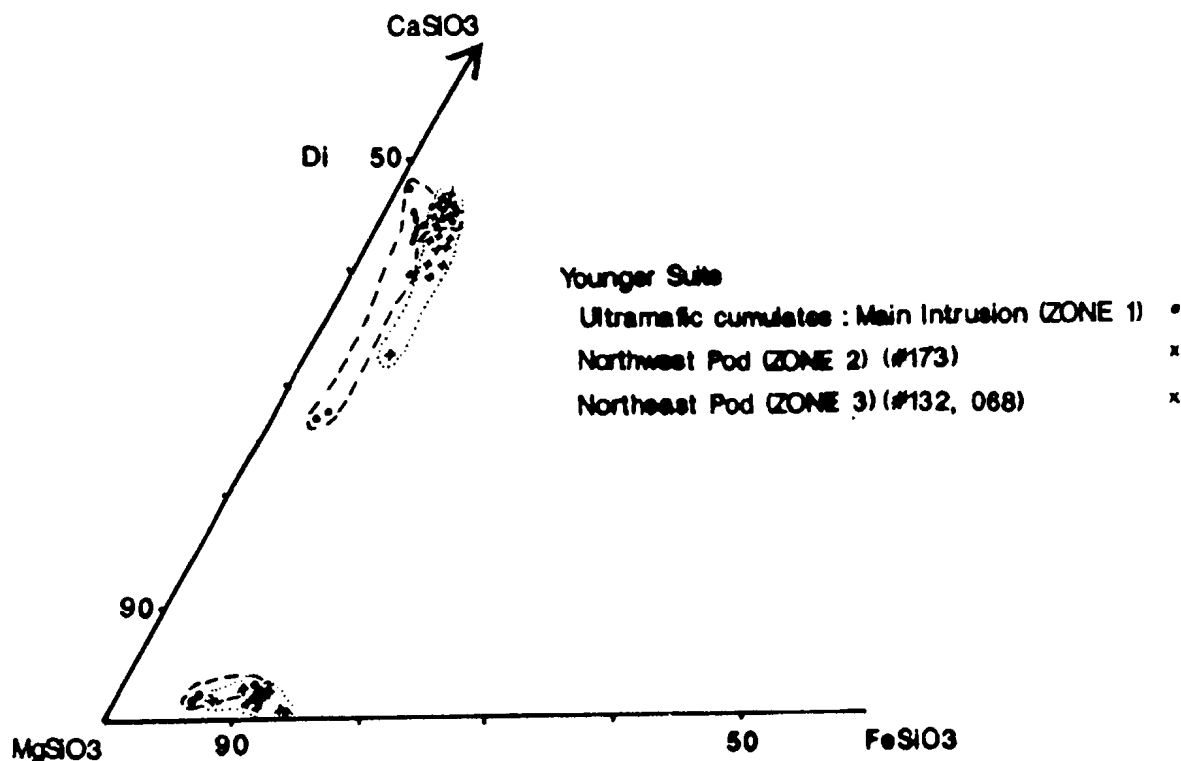




**Figure 4-4:** Part of the pyroxene quadrilateral showing analyses of pyroxenes from the older suite transition zone and younger suite clinopyroxenite and gabbroic intrusives.

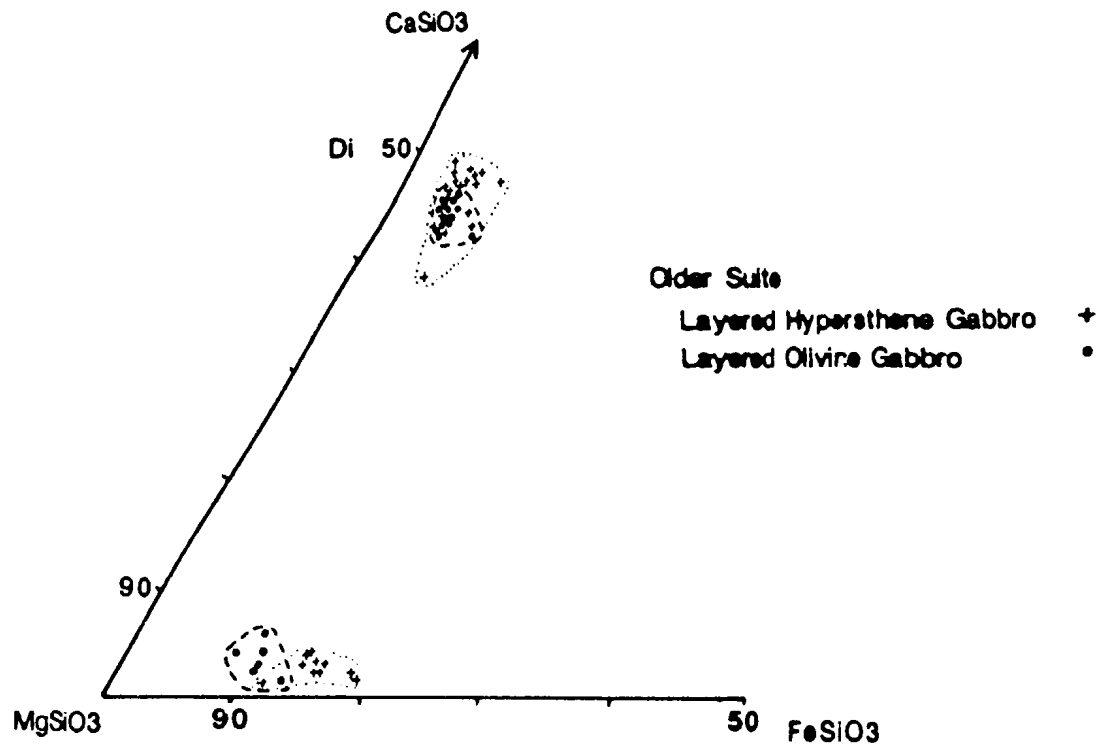
#### 4.2.2. Fractionation Trends within the Older Suite Gabbro

Representative analyses of the clinopyroxene and orthopyroxene components of the older suite layered olivine and hypersthene gabbro are plotted in Figure 4-6. The orthopyroxene phase plots within the enstatite field while the clinopyroxene plots as diopside. The clinopyroxene values from both the olivine and hypersthene gabbro are overlapping, however the orthopyroxene phase shows a smooth fractionation trend that indicates an increased degree of differentiation from the layered olivine gabbro to the layered hypersthene gabbro.



**Figure 4-5:** Part of the pyroxene quadrilateral showing analyses of pyroxenes from the younger suite ultramafic lithologies.

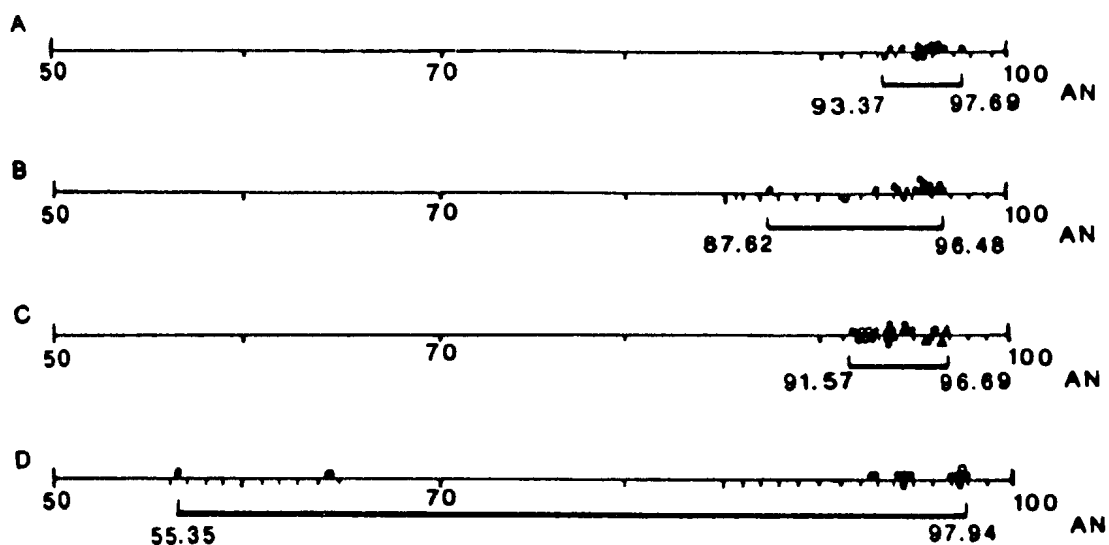
Comparison of the orthopyroxene compositions from both the layered gabbros and the older suite transition zone (Figures 4-4 and 4-6) shows a progressive differentiation trend for the older suite, from the transition zone orthopyroxenite to the olivine then hypersthene layered gabbros. The same trend towards advanced differentiation within the layered gabbros is evident from the composition of the plagioclase phase (Figure 4-7). The anorthitic ( $An = 93.37-97.69$ ) composition of the plagioclase from the layered olivine gabbros gives way to a more Na-enriched bytownite-anorthite ( $An = 87.62-96.48$ ) composition within the older suite layered hypersthene gabbro.



**Figure 4-6:** Part of the pyroxene quadrilateral showing analyses of pyroxenes from the older suite layered olivine and hypersthene gabbros.

#### 4.2.3. Geochemical Comparison of the Older and Younger Suites

The chemical criteria used to try and distinguish between the younger and older suite are presented in the following subsection. Figure 4-8 is a plot of the Na versus  $Mg^*$  ( $Mg^* = Mg \times 100 / (Mg + Fe)$ ) values of the clinopyroxene phase from both the younger and older suites. The overall trend shows higher Na/ $Mg^*$  ratio for the older suite layered gabbro relative to the younger suite intrusives. However, abundant overlapping of the suites occurs with the younger suite cumulates of Zones 2 and 3 (+) and younger suite pyroxene-hornblende gabbro (0) falling within the broad field of the older suite layered gabbros (•) as indicated by



Plagioclase (AN mol %) compositions for A-Layered Olivine Gabbro (older suite) B-Layered Hypersthene Gabbro (older suite) C-Feldspathic Wehrlite-Lherzolite-Pyroxenite (younger suite) D-Pyroxene-Hornblende Gabbro (younger suite)

NOTE: Open circles represent analyses of plagioclase inclusions within pyroxene cumulus phases. Triangles represent plagioclase analysis from clinopyroxenite.

**Figure 4-7:** Plagioclase (An mol %) mineral analyses for samples from both the older and younger suites.

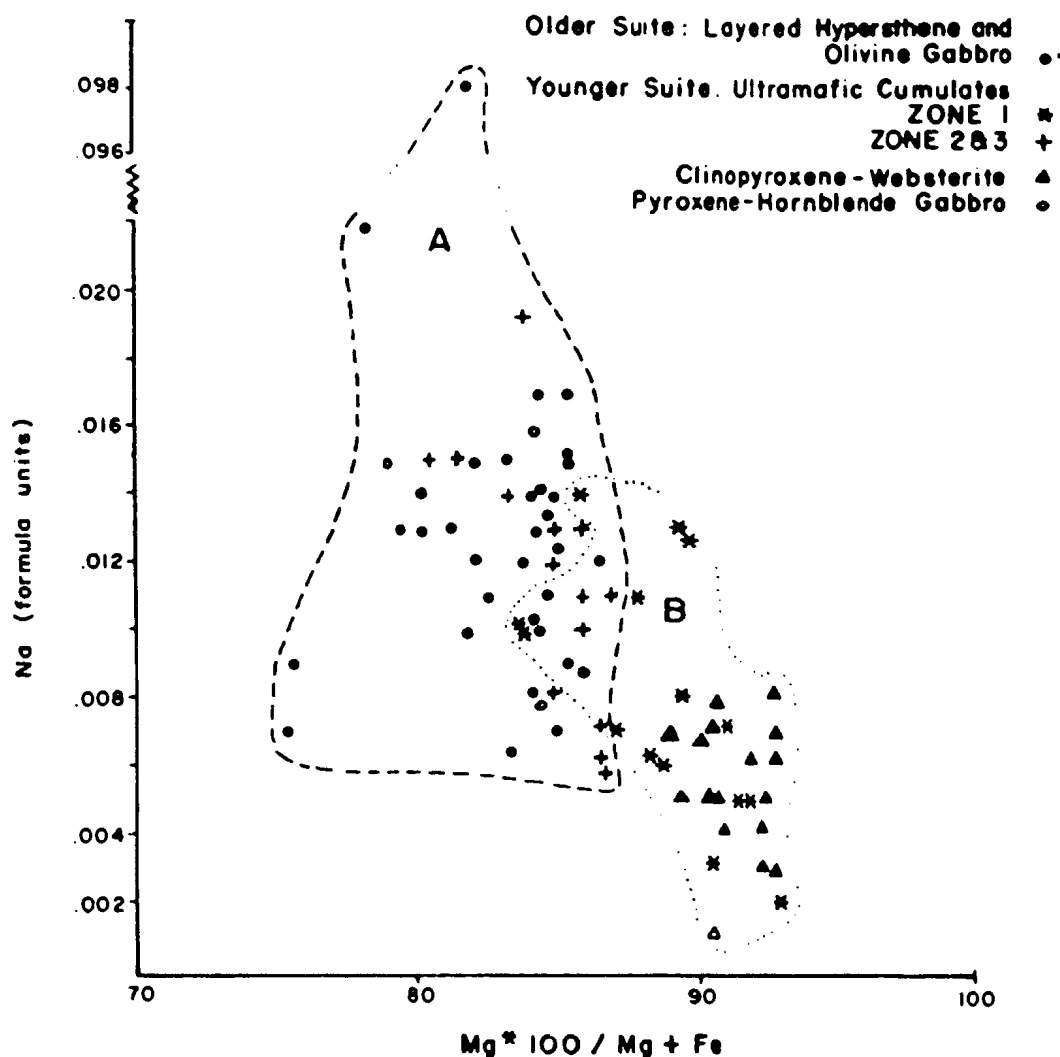
field A in Figure 4-8. The ultramafic cumulates (\*) and clinopyroxenite-websterite (▲) of the younger suite Zone 1 (outlined by field B, Figure 4-8) exhibit distinctly lower Na/Mg\* values than those of the more differentiated gabbroic units of both the older and younger suites. Therefore, although a broad distinction can be made between the suites, the lithologies with equivalent degrees of fractionation (i.e.: younger suite gabbro and older suite layered gabbro) cannot be separated on the basis of the Na/Mg\* ratios.

The Ti versus Mg\* content of the clinopyroxene phase in the older and younger suites is plotted in Figure 4-9. In general, Figure 4-9 exhibits a high Ti/Mg\* value for the older suite layered gabbros (●), (field A) and, conversely, a lower Ti/Mg\* ratio for the younger suite. However, as observed in Figure 4-8, the younger suite gabbro (○) and the younger suite cumulates of Zones 2 and 3 (+) fall within the same "A" field as the older suite layered gabbro (●) while the ultramafic cumulates (\*) and clinopyroxene-websterite (▲) of ZONE 1 (as outlined by field B, Fig. 4-9) shows lower Ti/Mg\* values. Therefore, as observed in the previous Figure 4-8, lithologies with similar degrees of fractionation but from different magmatic suites cannot be distinguished on the basis of their major and trace element chemistry.

The Ti versus Cr content of clinopyroxene from the older and younger suites is plotted in (Figure 4-10). The high Ti/Cr values of the older suite layered gabbros (●) is outlined by field "A". Field "B" shows the overlap between the younger suite pyroxene-hornblende gabbro (○) and ZONES 2 and 3 (+) and the older suite layered gabbro (●). Field "C" delineates the distinctly higher Cr, lower Ti (<Ti/Cr) composition of the younger suite wehlite, lherzolite and clinopyroxenite lithologies (\*,▲) from Zone 1. Once again, the lithologies from different suites but of similar degrees of fractionation cannot be separated into the different magmatic suites.

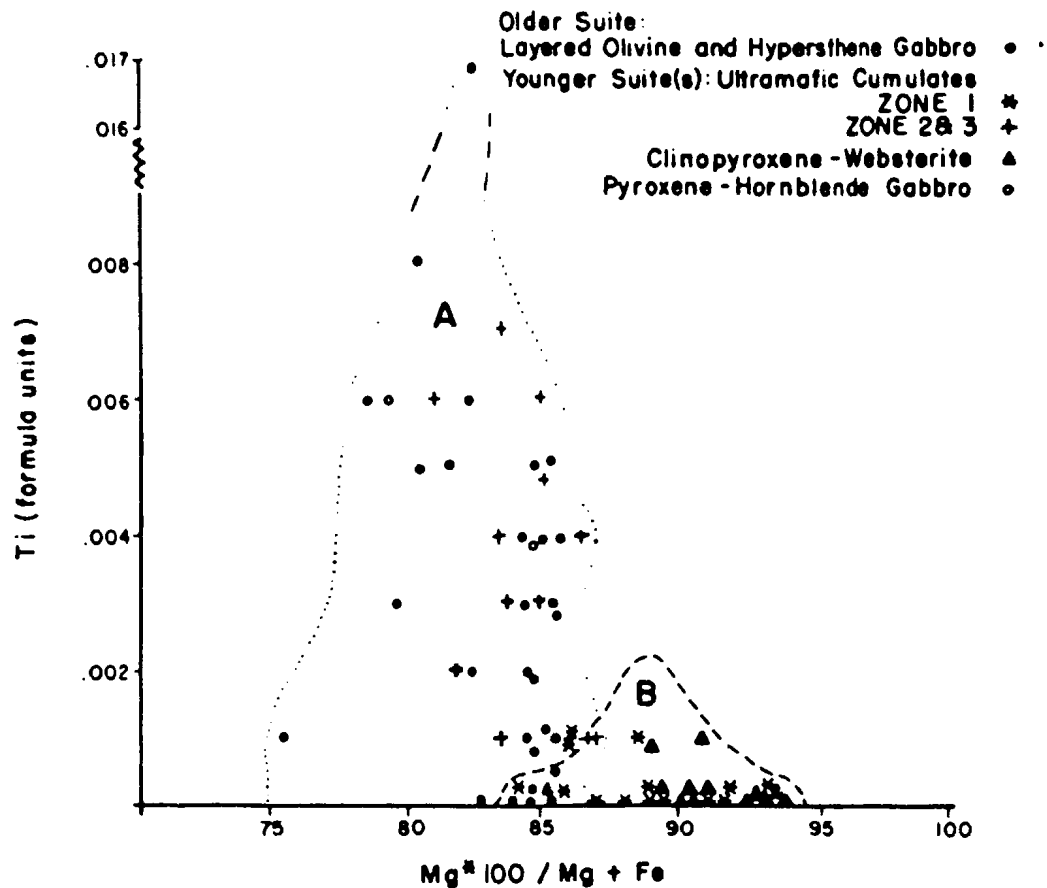
In Figure 4-11 and Figure 4-12, the NiO (wt %) versus Forsterite (Fo) of olivine and the Cr<sub>2</sub>O<sub>3</sub> (wt %) versus Mg\* of clinopyroxene are plotted, respectively, for the older and younger suites.





**Figure 4-8:** Na versus Mg\* values of the clinopyroxene phase from both the younger suite intrusives and older suite layered gabbro. Fields A and B are discussed in the text.

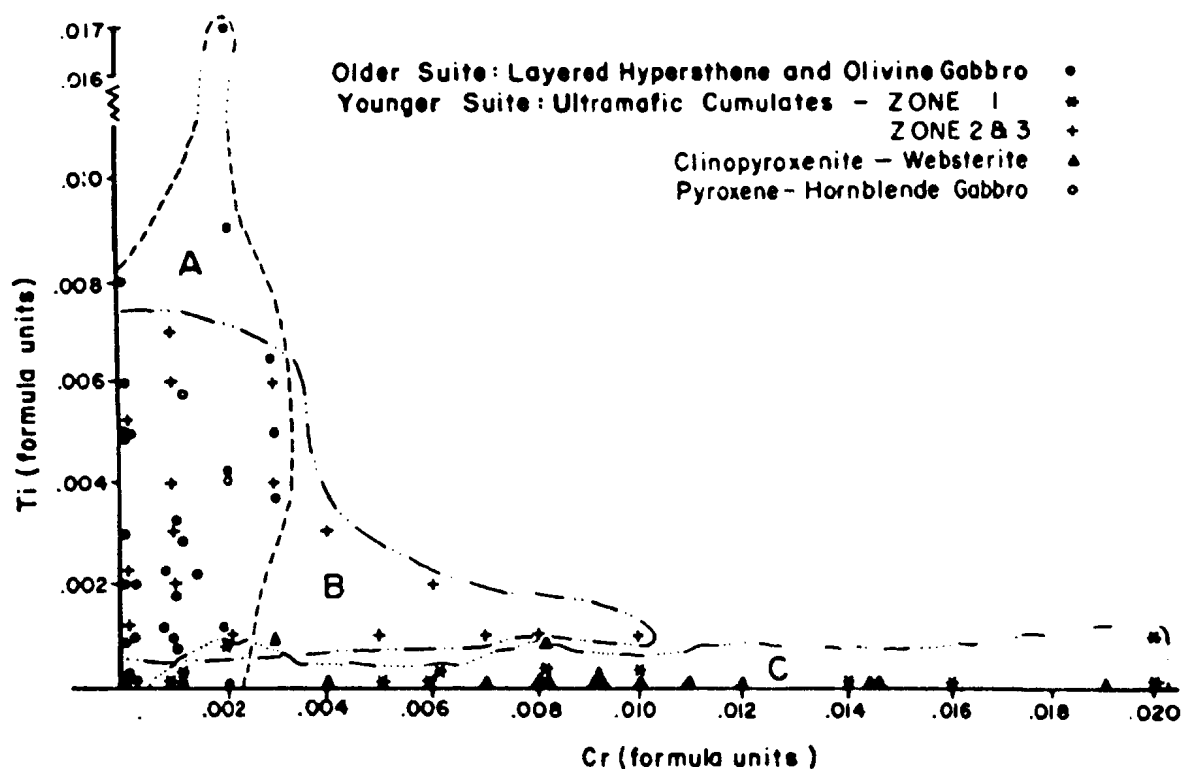
Both Figures 4-11 and 4-12 show the same overlap for lithologies from different suites as observed in Figures 4.8, 4.9 and 4.10. Benn and Laurent (1987) have reported the presence of an early cumulate suite (ECS) and late cumulate suite (LCS) in the Caledonian Falls region, south of the present author's map area. The mineral chemistry fields for the ECS and LCS, as plotted by Benn and Laurent (1987), are included in Figures 4-11 and 4-12. These authors reported that on the



**Figure 4-9:** Ti versus  $Mg^*$  content of the clinopyroxene phase from both the younger suite intrusives and older suite layered gabbro.

basis of mineral chemistry for rocks at similar stages of fractionation, the rocks of the ECS can be distinguished from rocks of the LCS. They reported that the olivines of the LCS are enriched in Ni relative to olivines from the ECS and that clinopyroxene of the LCS are enriched in Cr relative to clinopyroxene of the ECS.

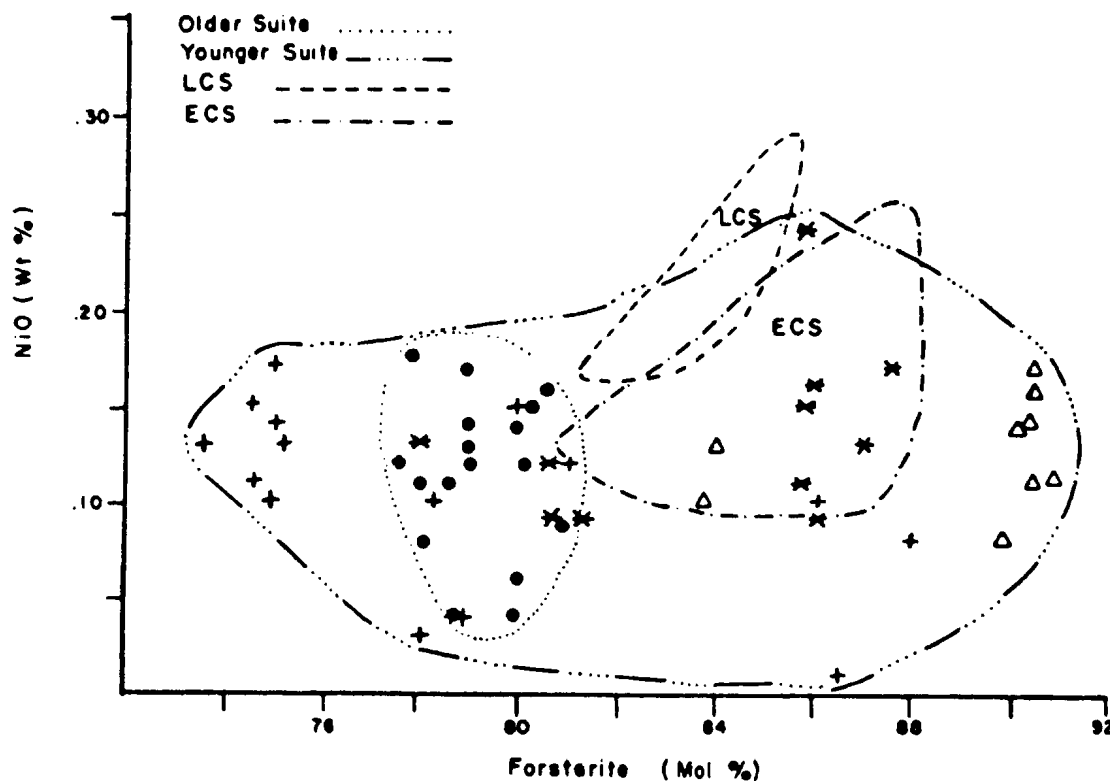
The results of the present author's work contradict the conclusions of Benn and Laurent (1987). Figure 4-11 shows the older suite layered gabbros (●) from this study define a field that plots along the fractionation trend of both the older (ECS) and younger (LCS) suites of Benn and Laurent (1987). Also, the older suite layered gabbros (●) of this study, as well as the older (ECS) and younger (LCS)



**Figure 4-10:** Ti versus Cr content of the clinopyroxene phase in the younger suite intrusives and older suite layered gabbros.

suites of Benn and Laurent (1987), fall within the large field defined by the younger intrusive suite samples of the present study. It can be seen in Figure 4-12 that the same result occurs within the fields of the older suite layered gabbro (●) in the present study, which together with the ECS and LCS of Benn and Laurent (1987) plots within the field of the present studies younger intrusive suite.

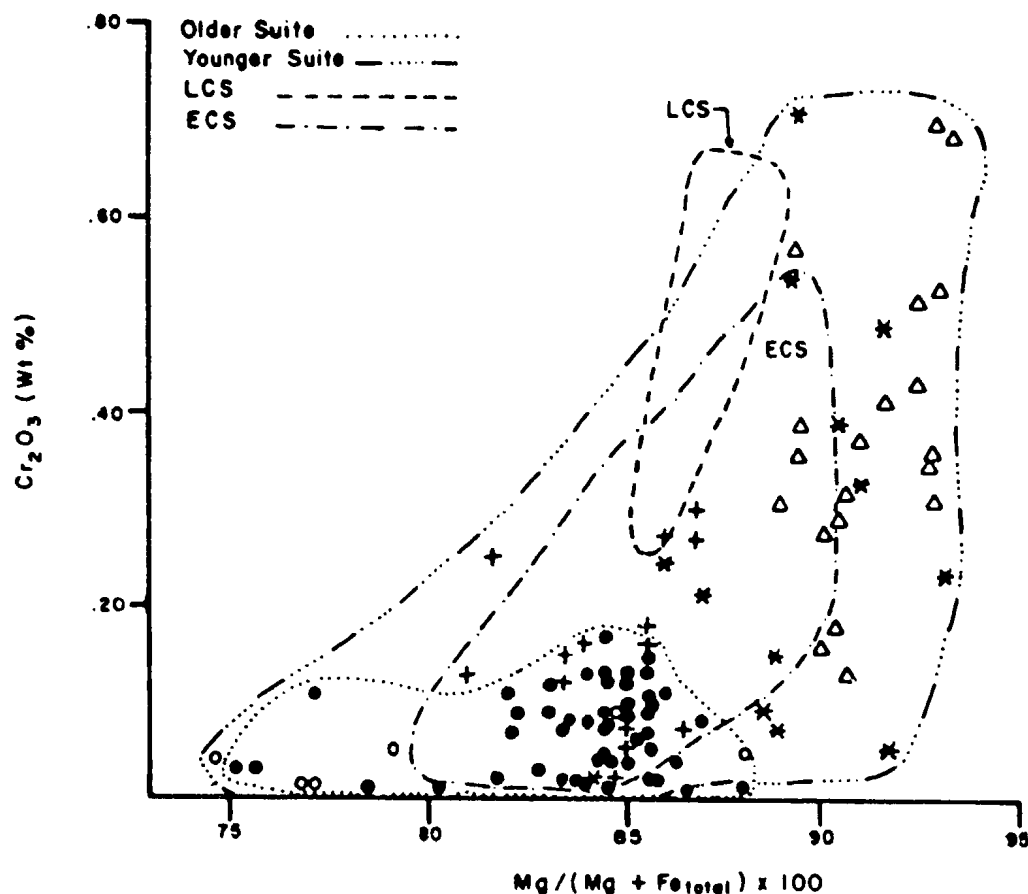
The same absence of distinct mineral chemistry for the younger and older suites



**Figure 4-11:** Plot of NiO versus Forsterite (Fo) for olivines from the older suite layered olivine gabbro and younger suite ultramafic-mafic cumulates. Symbols as in Fig. 4.8. Early cumulate suite (ECS) and Late cumulate suite (LCS) fields after Benn and Laurent (1987).

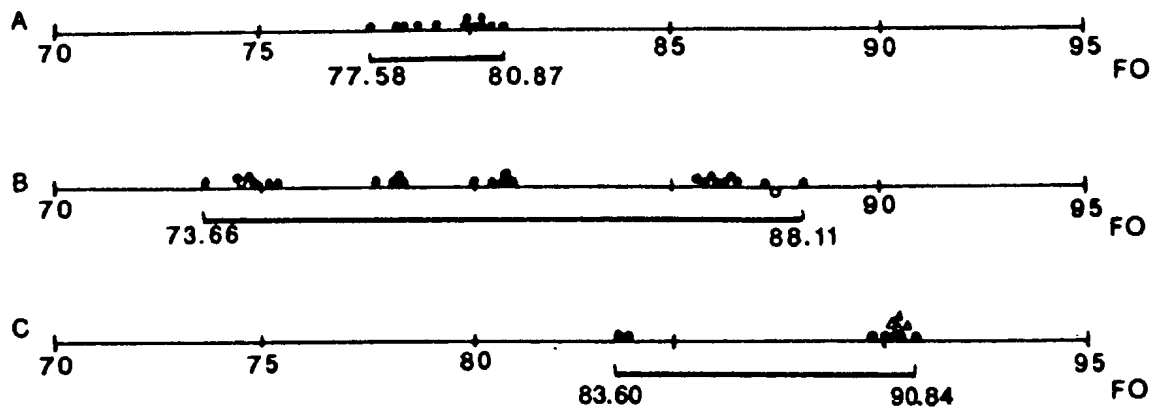
is also shown by the plagioclase compositions. In Figure 4.7, the range in anorthite values ( $An = 87.62-97.69$ ) of the older suite layered gabbro encompasses the anorthite range ( $An = 91.57-96.69$ ) of the younger suite feldspathic wehrlite-lherzolite-pyroxenite and core analyses of zoned plagioclase from the younger suite gabbro.

The olivine composition of the older suite layered gabbro and younger ultramafic-mafic lithologies is presented in Figure 4-13. The younger suite



**Figure 4-12:** Plot of  $\text{Cr}_2\text{O}_3$  versus  $\text{Mg}/(\text{Mg}+\text{Fe}(\text{total}))$  in clinopyroxene from the older suite layered gabbro and younger suite ultramafic-mafic cumulates. Symbols as in Fig. 4.8. Early cumulate suite (ECS) and Late cumulate suite (LCS) fields after Benn and Laurent (1987).

lithologies exhibit a wide olivine compositional range ( $\text{Fo} = 73.66\text{--}90.84$ ) whereas the olivine values from the older suite layered gabbro are more Fe-rich with a restricted range of ( $\text{Fo} = 77.58\text{--}80.87$ ). The  $\text{Fo}$  values of the layered gabbro fall within the  $\text{Fo}$  range of the younger suite but the more Mg-rich (more basic) nature of the younger suite olivine, particularly from the clinopyroxenite, may serve as a criterion for separating the magmatic suites in the absence of convincing field relations.



Olivine (Fo mol %) compositions for A.-Layered Olivine Gabbro (older suite) B.-Wehrlite-Lherzolite-Olivine Gabbro (younger suite) C.-Clinopyroxenite-Websterite (younger suite).

NOTE: Open circles represent analyses of olivine inclusions within pyroxen or plagioclase cumulus phases. Triangles designate olivine cumulus grains of younger suite melt origin within orthopyroxenite of the older suite transition zone (refer to Section 3.7).

**Figure 4-13:** Olivine (Fo) values for the older suite layered olivine gabbro and the younger suite ultramafic intrusives.



#### 4.2.4. Summary and Discussion

In summary, the younger and older magmatic suites, which outcrop within the northwestern quadrant of the Troodos plutonic complex, cannot be distinguished from each other on the basis of their mineral chemistry. The  $\text{Na/Mg}^*$ ,  $\text{Ti/Mg}^*$ ,  $\text{Ti/Cr}$  and  $\text{Cr}_2\text{O}_3/\text{Mg}^*$  ratios of the clinopyroxene and  $\text{NiO}$  versus  $\text{Fo}$  (mol %) of olivine from the younger and older suites show that lithologies of equivalent fractionation level plot within the same fields. The plagioclase and olivine mineral chemistries exhibit the same absence of chemical distinction between the magmatic suites although the younger suite ultramafic unit contains a more Mg-rich olivine than the older suite layered olivine gabbro. This Mg-rich olivine content of the younger suite ultramafic units combined with the anomalously high Cr and low Ti values of these rocks may be useful in distinguishing the ultramafic components of the various suites when the relationships are not exposed in outcrop. The distinction of suites on the basis of limited mineral chemistry, as presented by Benn and Laurent (1987), is not supported by the results of the present author's work.

Fractionation trends are evident in both the younger and older suites. A pyroxenite to gabbro differentiation can be documented within the younger suite as well as an overall fractionation trend towards structurally higher levels of intrusion of the younger suite plutons. A progressive differentiation trend from transition zone orthopyroxenite to the layered gabbro is evident within the older suite. It is interesting to note that the compositions of the orthopyroxene porphyroclasts and recrystallized neoblasts from the younger suite transition zone are equivalent. Such a feature may indicate that the chemical composition of the orthopyroxene phase is not altered by high-temperature plastic deformation and recrystallization or that an equilibrium event may have homogenized the chemical compositions of the orthopyroxene neoblasts and porphyroclasts (i.e.: no evidence of reaction rims or zoning).

### **4.3. Petrography and Geochemistry of the Mafic Dikes**

The field relations of the mafic dikes have been discussed in Chapter 2, Section 2.4.5. In thin section, the mafic dikes are aphyric to porphyritic and comprised of a quench textured groundmass composed of  $< .5$  mm, acicular plagioclase laths and remnants of a green pleochroic amphibole. Microprobe analysis of the amphibole (hornblende) phase is available in Appendix D.

The relative proportions of plagioclase to amphibole varies as a penetrative greenschist grade metamorphism has partially (40-98%) altered the groundmass to a fibrous assemblage of actinolite and chlorite. The one porphyritic mafic dike sample (#1510) consists of a completely altered groundmass of actinolite and minor chlorite which encloses pseudomorphs after the porphyritic phase(s). These altered blebs range up to 2 mm in size and are filled with a low temperature alteration assemblage consisting of talc rims surrounding core regions of talc, actinolite and chlorite with possible remnants of a primary(?) amphibole and/or pyroxene. The opaque phase ( $< 2\%$ ) consists of  $\sim .25$  mm, euhedral to subhedral grains spatially associated with both the groundmass and the alteration filled blebs.

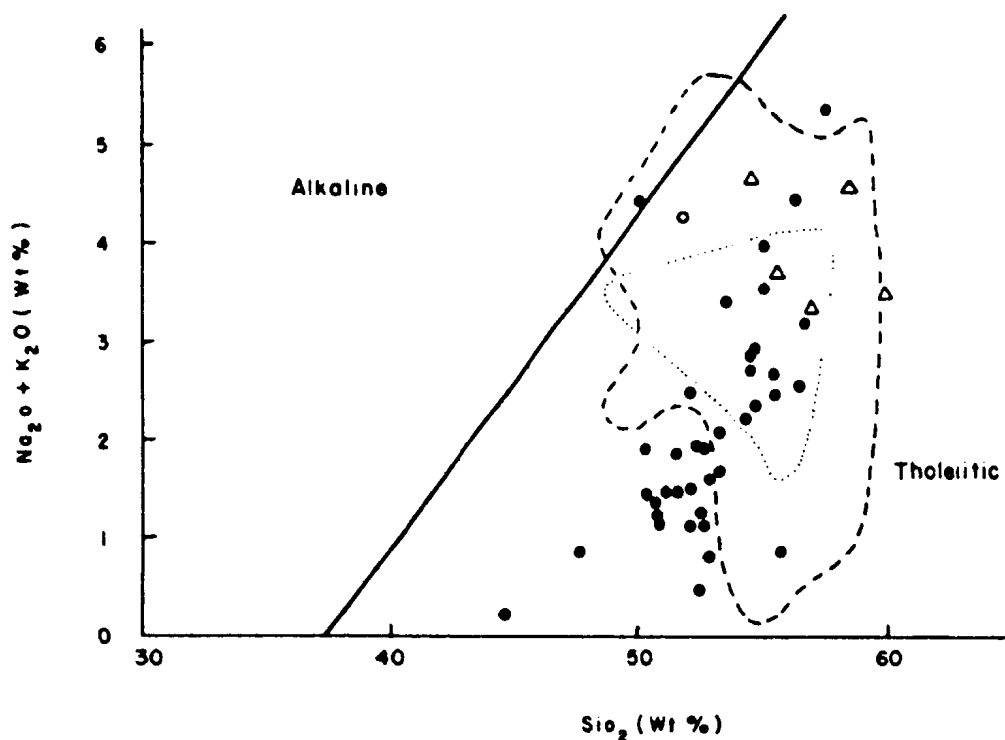
The major and trace element analyses of 40 mafic dike samples are available in Appendix E. Five additional analyses are included for samples of the sheeted dike complex which outcrops in fault contact with the plutonic complex in the northeastern map area (MAP 1). The prime objective in analysing the dikes was to characterize their chemistry and to compare these results with the chemistry of the Troodos sheeted dike complex and pillow lavas as documented by earlier workers (i.e.: Moores and Vine, 1971; Pearce, 1975; Robinson *et al.*, 1983; Malpas and Langdon, 1984). In 1982, the Cyprus Crustal Study Project drilled CY-2A which intersected upper pillow lavas in the first 70 m of the hole and extended through the lower pillow lavas to a depth of 689 m (Robinson and Malpas, 1987). The chemical analyses of 11 representative samples of massive basalt, basalt dikes and pillow lavas from the CY-2A drill core are included for comparison with the

mafic dikes. These samples were chosen at  $\sim 70$  m intervals along the length of the drill core (depths: 4.40m, 72.55m, 141.85m, 218.00m, 282.10m, 346.50m, 434.78m, 502.65m, 576.20m, 625.30m, 667.70m). The complete chemical analyses of these samples are available in Bednarz *et al.* (1987). Mafic dike sample #4501 was collected from a mafic dike which intrudes a poikilitic wehrlite pluton hosted by harzburgite in the Limassol Forest region. The Limassol Forest massif outcrops to the south of the Troodos ophiolite massif. This sample was included in the analysis so as to compare its chemistry to the mafic dikes which intrude similar lithologies in the Troodos massif.

In Figure 4-14 the total alkalis versus silica values are plotted for the mafic dike samples. From Figure 4-14, the majority (95%) of the mafic dikes fall within the tholeiitic field. Two of the samples (#4503 and #4501-Limassol Forest) lie along the transition to the alkaline field. This trend toward an alkalic affinity is probably related to a metasomatic increase in the relatively mobile alkaline elements and/or loss of silica during low-grade metamorphism of the dikes. The tholeiitic fields outlined by samples from the Troodos sheeted dikes (Moore and Vine, 1971) and the dike-pillow lava samples from CY-2A (Bednarz *et al.*, 1987) are included in Figure 4-14. The mafic dikes clearly plot within the fields of Moores and Vine (1971) and CY-2A as well as towards a more basic (lower Si and higher Na+K) composition. Likewise, the five sheeted dike samples collected from the study area all plot within and/or close to the fields of Moores and Vine (1971) and CY-2A.

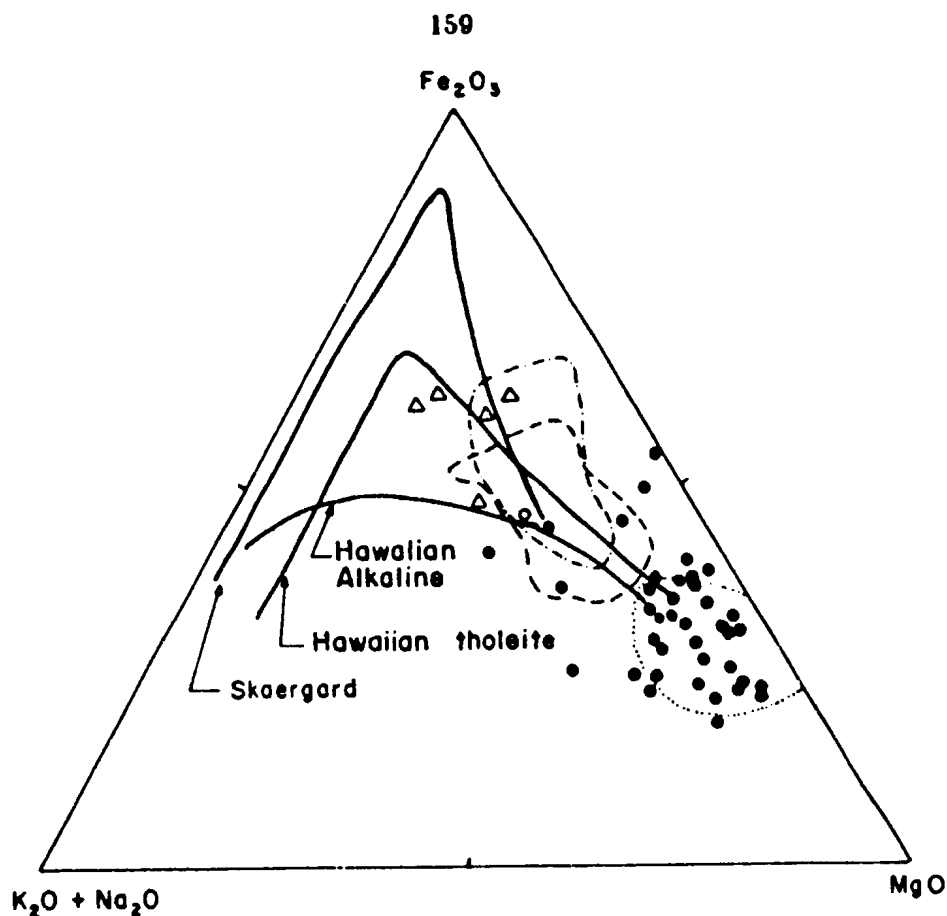
The mafic dikes of the Troodos plutonic complex are plotted on the AFM diagram in Figure 4-15. The samples from CY-2A as well as the standard Hawaiian tholeiitic and alkalic differentiation trends and the fields for gabbro, diabase and pillow basalt from other well documented ophiolites (i.e. : Oman, Papuan and Bay of Islands) are included for comparison to the Troodos mafic dike compositional field.

The trend defined by the mafic dikes in Figure 4-15 follows the standard Fe-



**Figure 4-14:** Total alkalis versus silica variation diagram for mafic dike (●) and sheeted dike (Δ) samples. Limassol Forest mafic dike sample is marked as (○). Heavy line is alkalic - tholeiitic division line as defined by MacDonald and Katsura (1964). Dashed line defines the Troodos sheeted dike complex (after Moores and Vine, 1971). Dotted line defines the CY-2A field (from Bednarz *et al.*, 1987).

enrichment trend and suggests a chemical continuum between the mafic dike samples and the five samples collected from the sheeted dike complex in the study area. Similarly, the CY-2A field includes the more fractionated sheeted dike samples. The majority of the mafic dikes plot towards the Mg-rich compositional field which indicates their primitive chemistry in comparison to the Troodos sheeted dikes and the field outlined for the diabase samples from the Oman and Bay of Islands ophiolites (Norman and Strong, 1975; Malpas, 1978). The variation in the alkali content of the dikes may be the result of the penetrative alteration noted within thin sections of the samples. The Limassol Forest sample (#4501) plots close to the most differentiated Troodos mafic dike samples.



**Figure 4-15:** Bulk rock compositions of the Troodos mafic dikes (●), Limassol Forest mafic dike (○) and sheeted dike (△) samples plotted on the AFM diagram. Hawaiian alkaline and tholeiite trends from Malpas (1978). Dashed field delineates Papuan basalts and Oman and Bay of Islands diabase. Dotted field delineates Papuan gabbro. Dot-dash field delineates CY-2A samples (from Bednarz *et al.*, 1987).

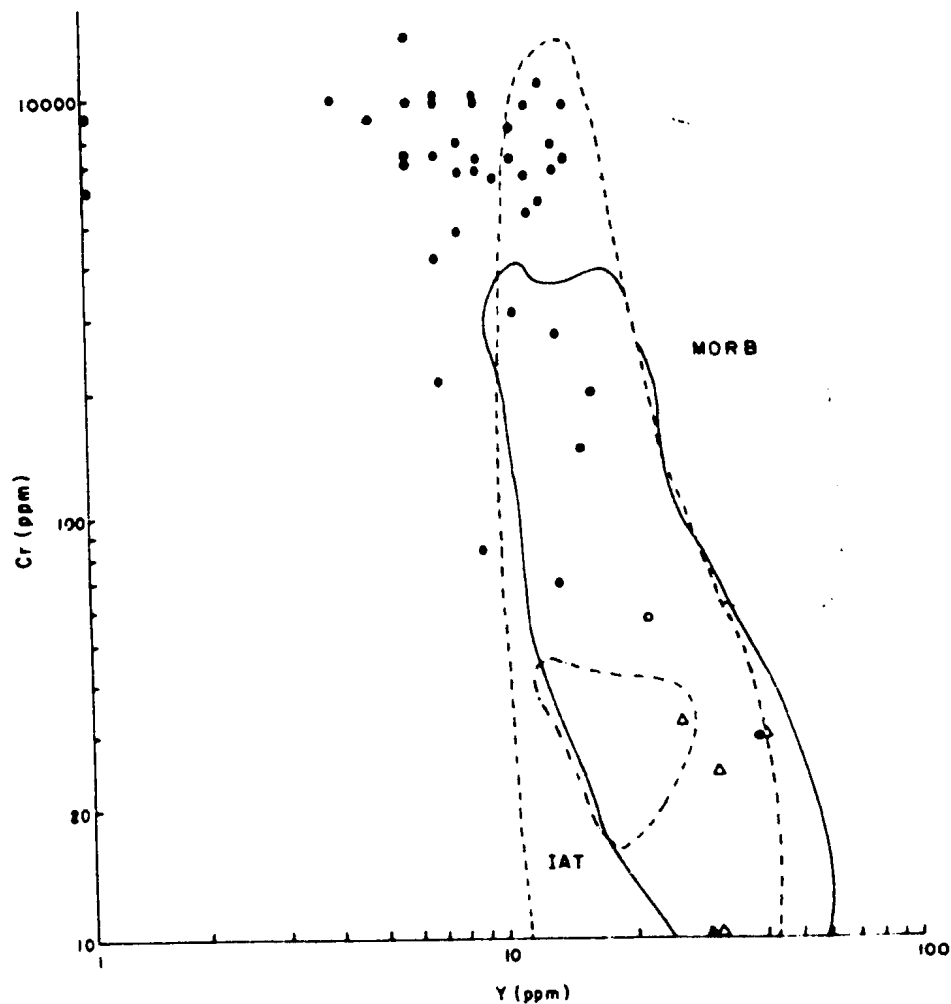
The relatively immobile trace elements (i.e. : Ti, Cr, Zr, Sr and Nb) have been used by Pearce and Cann (1971, 1973), Pearce (1975) and Bloxam and Lewis (1972) to distinguish tholeiitic basalts of ocean-floor (MORB) from island-arc (IAT/LKT) affinity. These elements are believed to be relatively insensitive to secondary processes such as low to greenschist grade metamorphism (Cann, 1970; Pearce and Cann, 1971).

In Figure 4-16 the Cr versus Y content of the Troodos dikes is presented. The fields of mid-oceanic ridge (MORB) and island-arc tholeiite (IAT) basalts are from Pearce (1980) and the CY-2A field is from the data of Bednarz *et al.* (1987). The field defined by the pillow lavas, flows and diabase of the Oman ophiolite is reported by Alabaster *et al.* (1982). All of the Troodos mafic dikes and the five sheeted dike samples exhibit an island-arc affinity, falling either within the island-arc tholeiite field or towards a more primitive magma composition. The less primitive Troodos sheeted dike samples and seven of the mafic dikes (including #1501) also plot within the island-arc field of the Oman pillow and diabase samples.

The same island-arc (low potassium tholeiite) affinity of the Troodos mafic dikes is seen in the Ti versus Cr variation diagram of Pearce (1975), (Figure 4-17). The fields of magma compositions occupied by the Troodos upper pillow lavas and the lower pillow lavas and sheeted dikes were defined by Pearce (1975), based upon data from Pearce and Cann (1973). All of the dike samples fall within the island-arc, low potassium tholeiite (LKT) field. The samples from CY-2A and the sheeted dikes in the present study area plot within the range of the lower pillow lavas. Most of the mafic dike samples lie either within or towards a more primitive ( $>Cr$ ,  $<Ti$ ) composition than the Troodos upper pillow lava (UPL) field. The fields of magma compositions occupied by the Troodos upper pillow lavas and the lower pillow lavas and sheeted dikes were defined by Pearce (1975), based upon data from Pearce and Cann (1973).

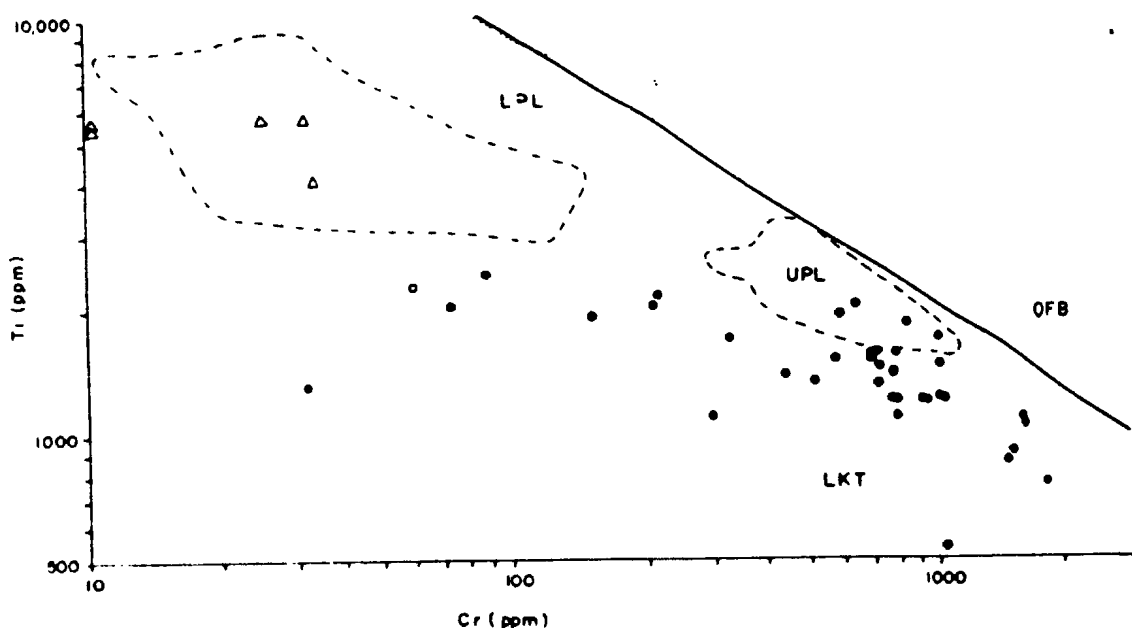
The Ti versus Zr variation diagram of Pearce and Cann (1973), (Figure 4-18) shows the same correlation between the Troodos mafic dikes and the field defined by Pearce (1975) for the Troodos upper pillow lavas. Both types of dikes exhibit the same LKT affinity although the mafic dikes again show a more primitive ( $<Ti$ ,  $<Zr$ ) composition. Pearce (1975) suggested that the upper pillow lavas most resemble the primitive basalt of island-arcs with melts being derived from refractory mantle. The even more primitive composition of the Troodos mafic





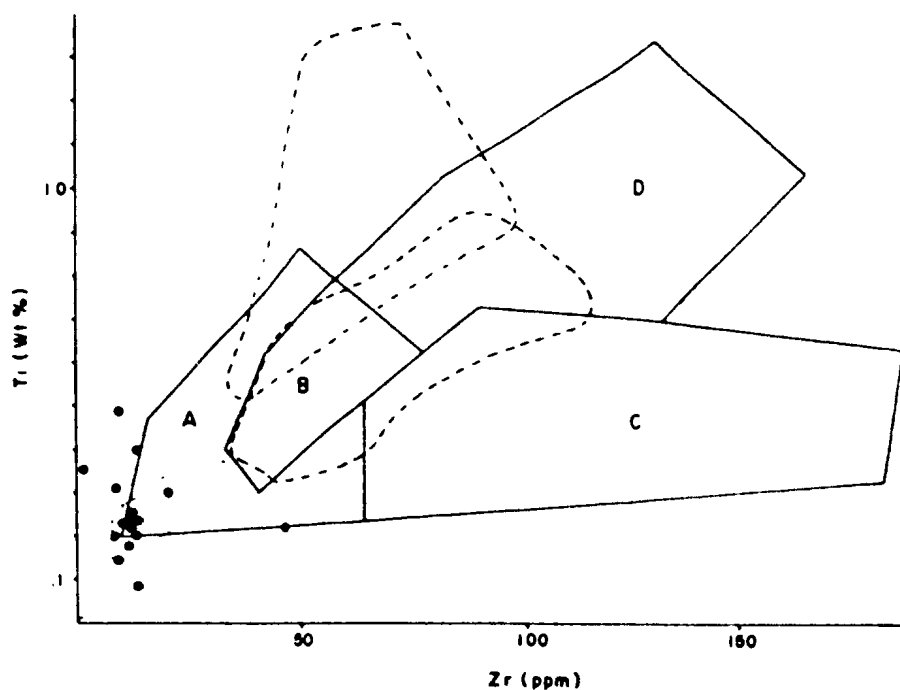
**Figure 4-16:** Cr versus Y variation diagram (after Pearce, 1975) for the Troodos dikes. Symbols as in Figure 4.12. Fields of magma composition occupied by basalt of the mid-ocean ridge (MORB) and island arc tholeiite (IAT) affinities after Pearce (1980). Solid line delineates field of basalts from the Oman ophiolite (after Alabaster, 1982) while dot-dash line delineates CY-2A samples (from Bednarz *et al.*, 1987).

dikes indicates a derivation from a residual mantle source already highly depleted in the incompatible elements (i.e. : Ti, Zr, Cr, etc.). The CY-2A samples from Bednarz *et al.* (1987) define a field that is compatible with the lower pillow lavas of Pearce (1975).



**Figure 4-17:** Ti versus Cr variation diagram (after Pearce, 1975) for the Troodos dikes. Symbols as in Figure 4.12. Heavy line separates ocean-floor (MORB) from low-potassium tholeiite (LKT) affinities. Dash line delineates the field of the Troodos upper pillow lavas and dotted line represents the field of the Troodos sheeted dikes and lower pillow lavas (after Pearce, 1975). Dot-dash line delineates CY-2A samples (from Bednarz *et al.*, 1987).

In Figure 4-19 the MgO - FeO\* variation diagram (after Jakes and Gill, 1970) shows the mafic and sheeted dike samples of the present study in relation to the fields of the upper and lower pillow lavas as defined by Robinson *et al.* (1983) and the field of the CY-2A samples. The Mariana arc boninite field and the island-arc tholeiite trend are taken from Robinson *et al.* (1983). The work of Robinson *et al.* (1983) has shown a correlation between the Troodos lower pillow lavas and evolved arc-tholeiites (Figure 4-19) and the Troodos upper pillow lavas and a boninitic suite (Figure 4-19). The Troodos basaltic rocks are less mafic than the typical boninite and represent liquids from which olivine and clinopyroxene have been removed (Robinson *et al.*, 1983). The CY-2A samples span the field of both



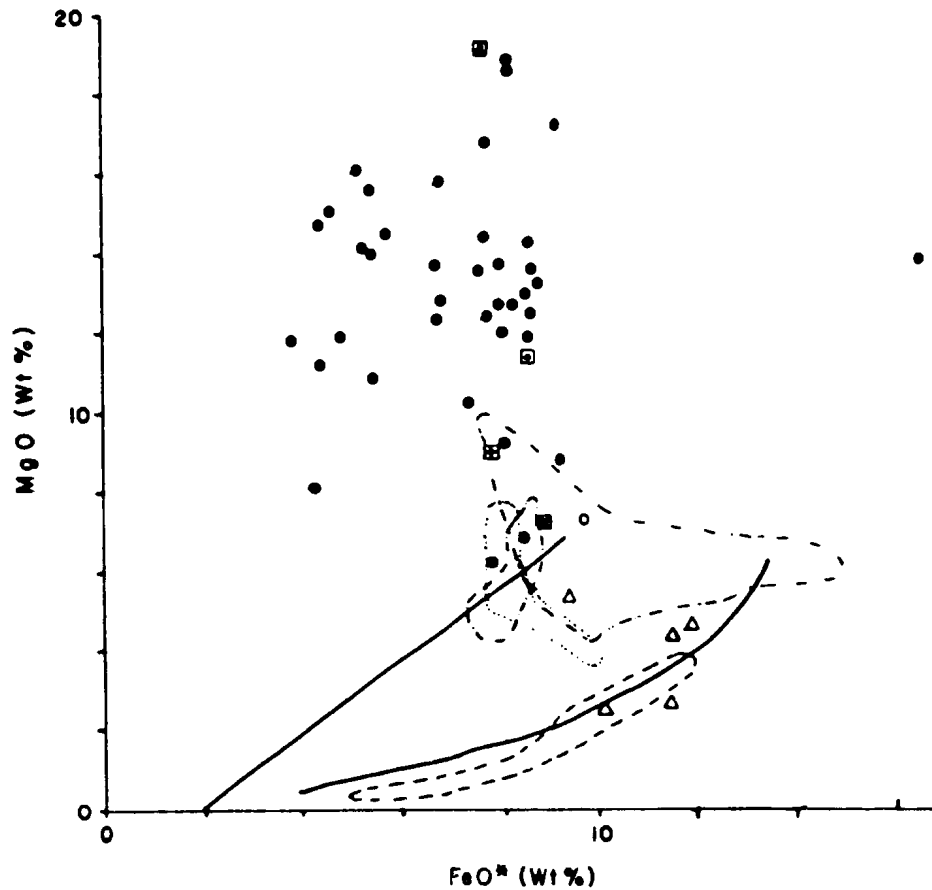
**Figure 4-18:** Ti versus Zr variation diagram (after Pearce and Cann, 1973) for the Troodos mafic dike samples (●). Symbols as in Figure 4.12. Fields D and B = ocean floor basalts, A and B = island arc basalts, C and B = calc-alkali basalts. Fields of the Troodos upper pillow lavas and lower pillow lavas plus sheeted dikes delineated by dotted and dashed lines, respectively (after Pearce, 1975). Samples from CY-2A delineated by dot-dashed field (from Bednarz *et al.*, 1987).

the upper and lower pillow lavas. Malpas and Langdon (1984) reported averaged ultrabasic rock, komatiite, olivine basalt and aphyric basalt compositions from the upper pillow lava suite. These compositions are plotted on Figure 4-19. Malpas and Langdon (1984) concluded that these rocks of the upper pillow lava suite were derived from a highly depleted melt (a melt equivalent in composition to basaltic komatiites) by mainly olivine fractionation. Differentiation within high-level magma chambers, involving ~25% olivine fractionation, would result in the range of magmas observed in the field (Malpas and Langdon, 1984). A liquid with boninitic affinities (~19% MgO) was proposed by Malpas and Langdon (1984) to approach the primary melt composition for the upper pillow lava suite. The

mafic dike samples from the plutonic complex exhibit a primitive, high-Mg boninitic affinity. Two of the mafic dike samples plot within the upper pillow lava field of Robinson *et al.* (1983) and close to the aphyric basalt composition of Malpas and Langdon (1984). However, the majority of the mafic dikes show more depleted, strongly Mg-enriched parental melt compositions and plot along the same fractionation trend as defined by Malpas and Langdon (1984) for the olivine ultrabasic-komatiite-basaltic rocks of the upper pillow lava suite. It is clear from Figure 4-19, that on the basis of major element chemistry, the mafic dikes of the plutonic complex represent chemical equivalents of the most primitive melt compositions of the structurally overlying upper pillow lava suite. It is interesting to note that the mafic dike samples of the present study span the compositional gap between the komatiite and ultrabasic rock samples of Malpas and Langdon (1984).

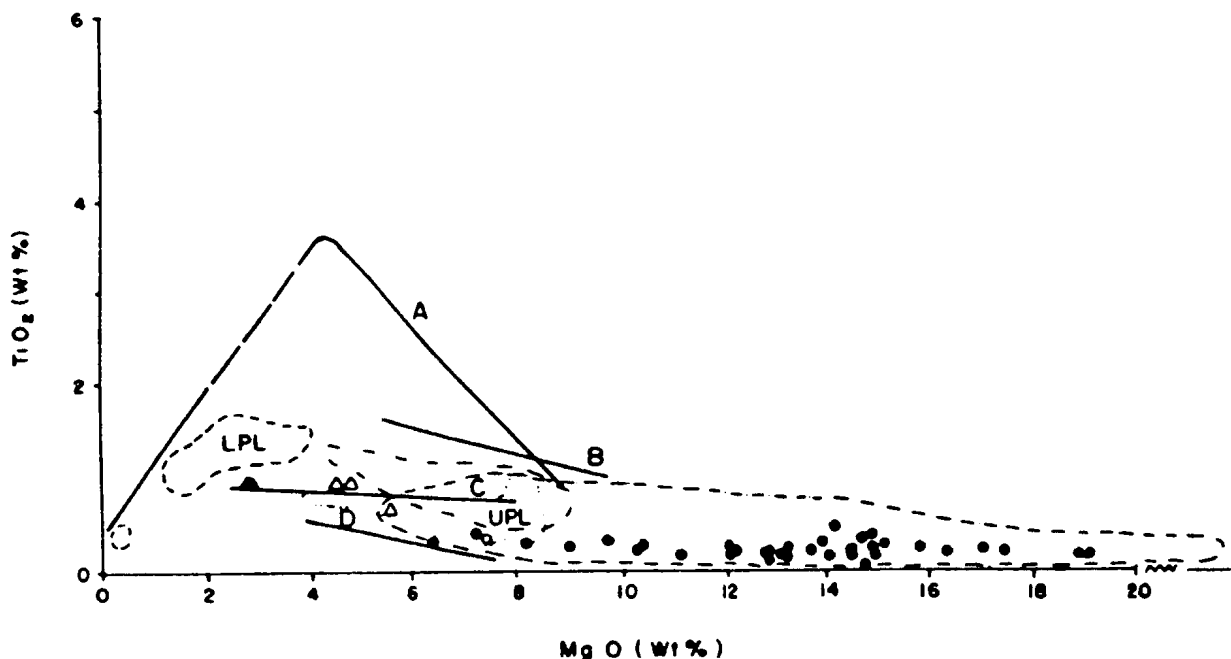
Figure 4-20 shows the low  $\text{TiO}_2$ , MgO-rich composition of the upper pillow lavas (Robinson *et al.* (1983) and their affinity to the field of the Mariana arc boninite suite. The CY-2A samples plot as upper pillow lavas with a trend towards the lower pillow lava composition. The sheeted dike samples from the present study area lie within the transition from upper to lower pillow lavas (Figure 4-20). The mafic dikes of the present study area show the same strong correlation with the upper pillow lavas of Robinson *et al.* (1983), the arc boninite suite of Meijer (1980) and the primitive melt compositions of the aphyric basalt to ultrabasic rocks of the upper pillow lava suite as defined by Malpas and Langdon (1984). The anomalously MgO enriched and  $\text{TiO}_2$  depleted chemistry of the mafic dikes indicates an extremely primitive parental melt composition and derivation from a residual mantle source which has undergone considerable partial melting and depletion during previous magma extraction(s).

In Figure 4-20, a continuous trend is evident from the upper pillow lava arc tholeiites to the more primitive upper pillow lavas through to the extremely primitive mafic dike composition. Such a trend may indicate successive



**Figure 4-19:** MgO - FeO\* variation diagram (after Jakes and Gill, 1970) showing the mafic dike (●) and sheeted dike (Δ) samples from the present study in relation to the fields of the Troodos upper pillow lavas (dotted line) and lower pillow lavas (dashed line), Mariana Arc boninite suite (dot-dash line) and IAT trend (after Robinson *et al.*, 1983). The dot<sup>3</sup>-dashed line delineates the field of CY-2A samples (from Bednarz *et al.*, 1987). Averaged ultrabasic (⊠), komatiite (⊡), olivine basalt (⊞) and aphyric basalt (⊞•) values from Malpas and Langdon (1984).

derivation of progressively depleted melt compositions during multistage partial melting of the same mantle source. Each incremental melting event would yield a progressively more primitive melt composition. Additional REE and isotope data are required to further model the source region of the mafic dikes and to establish their genetic relationship to the structurally overlying sheeted dike complex and pillow lava suite(s).



**Figure 4-20:** MgO -  $\text{TiO}_2$  variation diagram of the Troodos mafic and sheeted dike samples. Symbols as in Figure 4.12. The fields of the upper pillow lavas (dotted line) and lower pillow lavas (dashed line) from Robinson *et al.*, 1983. Volcanic suites: A = Galapagos rift (Byerly *et al.*, 1976); B = Mariana back-arc basin (Wood *et al.*, 1980; Hart *et al.*, 1972); C = Tonga arc (Ewart and Bryan, 1972) and D = Mariana arc boninite suite (Meijer, 1980). The dot<sup>3</sup>-dashed field delineates the CY-2A samples (from Bednarz *et al.*, 1987). Dot-dashed field delineates the upper pillow lava suite of Malpas and Langdon (1984).



In summary, the Troodos mafic dikes exhibit a typical tholeiitic affinity on both the AFM and  $\text{Na}_2\text{O} + \text{K}_2\text{O}$  versus  $\text{SiO}_2$  diagrams. The Cr versus Y, Ti versus Cr and Ti versus Zr variation diagrams show an island-arc tholeiitic melt composition for the mafic dikes. When compared to the Troodos upper and lower pillow lavas in the  $\text{TiO}_2$  - MgO diagram, the sheeted dike samples from the study area plot along the transition between the upper and lower pillow lavas while the mafic dikes exhibit a more primitive parental melt composition equivalent to the primitive compositions defined by Malpas and Langdon (1984) for the ultrabasic to aphyric basalt compositions of their upper pillow lava suite. The anomalously Mg-rich and Ti depleted chemistry of the mafic dikes indicates an extremely primitive parental melt composition derived from a residual mantle source which had undergone previous partial melting and magma extraction events. On the basis of the compatibility of the major and trace element chemistry from the mafic dikes and that of the upper pillow lava suite (Malpas and Langdon, 1984), the mafic dikes of the plutonic complex are interpreted to represent the feeder dikes to the structurally overlying upper pillow lavas. Additional REE and isotope chemistry is required to further define the genetic correlation between the basaltic units and to model the source region of these primitive melt(s).

#### **4.4. Mineral Chemistry of a Section through the Layered Olivine Gabbro**

A geochemical study of a small section through the layered olivine gabbro was undertaken as an initial step in the investigation of phase chemistry variations in the older suite gabbros of the Troodos plutonic complex. A section of the layered olivine gabbro, which outcrops in a roadcut located just north of the Esso Galata River ( *MAP 1* ), was sampled in detail over a 20 m section which was orientated normal to the attitude of the multiple rhythmic layering. The layered olivine gabbro in this section dips consistently  $35^\circ$ - $45^\circ$  to  $215^\circ$ - $225^\circ$ . A total of 35 orientated samples were collected at a 50 to 100 cm spacing. An increase in the sample number (from 4560 to 4596) corresponds to a structurally lower position in the section.

The layered gabbro which outcrops in the sampled section exhibits a strong rhythmic phase layering with individual layers extending continuously along strike for up to 25 m. The fractional crystallization sequence of OL-CPX-OPX-PLAG, as documented for the layered gabbro in Chapter 3, is also present throughout this section of the layered olivine gabbro. Plagioclase occurs as both a cumulate and intercumulus phase while the clinopyroxene represents a dominant cumulus phase. Plagioclase also appears as xenocrysts within olivine (where present) and clin- and orthopyroxene whereas clinopyroxene inclusions were observed within orthopyroxene and plagioclase. The olivine occurs as a cumulate and intercumulate phase in a few samples. Orthopyroxene occurs as a cumulate and intercumulate phase whereas rare inclusions of orthopyroxene within clinopyroxene may indicate local reversals in the order of crystallization. The primary ortho- to mesocumulate textures of the layered olivine gabbro are variably overprinted by subsolidus deformation in this sample section. Detailed description and discussion of various aspects of the layered gabbro has been presented in Sections 2.2.3 and 3.6.3.

Microprobe analyses were conducted on the least deformed cumulate phases. Checks for element zonation within the mineral phases were made in a number of samples (Appendix A-5). At least 4 analysis / mineral phase / thin section were completed for the study unless otherwise noted in Appendix A1 to A4. No significant chemical zonation, either normal or reverse, was found to occur within any of the mineral phases. The listing of the microprobe analyses (in Wt.% oxide) is presented in Appendices A1-A4 for each mineral phase (305 analyses in total).

The primary conclusion to be drawn from the microprobe analyses of the various mineral phases, is a distinct absence of cryptic layering over the 20 m section of the layered gabbro, even though a well developed phase layering occurs in this section. The plagioclase phase chemistry exhibits a constant anorthite composition (Figure 4-21) with a limited range in An (mol %) values from 93.70

to 97.35 (one anomalous core in sample #4595 yielded an  $An = 98.10$ ). This net change in the Ca-Na content of the plagioclase phase of different samples ( $\Delta An = 4.35$ ) barely exceeds the maximum compositional spread of An values within individual samples (i.e. :  $\Delta An = 3$  for # 4590,  $\Delta An = 2.86$  for # 4578; refer to Figure 4-21 and Appendix A.3). The calcium rich anorthitic composition of the plagioclase may suggest that the magma(s), from which this section of the layered gabbro was derived, had undergone minimal fractionation prior to the development of this cumulate section. The consistent chemical composition also suggests an absence of multiple magma influx (i.e. : magma replenishment) during the development of this 20 m section.

The olivine phase also exhibits a restricted chemical range with Mg-rich (forsterite) compositions ( $Fo = 77.93-80.90$ ) throughout the sampled section (Figure 4-22). The range in Fo values between samples ( $\Delta Fo = 2.97$ ; refer to Figure 4-22 and Appendix A.4) is again very close to the maximum spread in Fo values within individual samples (i.e. :  $\Delta Fo = 2.24$  in sample #4575). The Mg-rich content of the olivine phase also indicates the undifferentiated nature of the magma prior to crystallizing this section of gabbro. The compositional ranges of the olivine and plagioclase phases are compatible with fractionation at a temperature range of  $\sim 1500-1600$  C for 1 ATM. (Cox *et al.*, 1979). The MnO(wt.%) and NiO(wt.%) content of the olivine phase (Figure 4-23 and Figure 4-24, respectively) likewise show no significant variation within and between samples. The variations in these oxide abundances are within the .1% detection limit of analysis.

The  $Mg^* = Mg \times 100 / (Mg + Fe)$  (mol.%) value of the clinopyroxene phase throughout the 20 m section exhibits no systematic variation (Figure 4-25). A maximum spread in the  $Mg^*$  value between samples, from 82.31 to 86.89 ( $\Delta Mg^* = 4.58$ ), is only slightly greater than the change in  $Mg^*$  content exhibited within individual samples ( $\Delta Mg^* = 2.88$  for 4571), excluding samples #4590 and #4596. From Figure 4-25, it is apparent that one rim analysis from each of

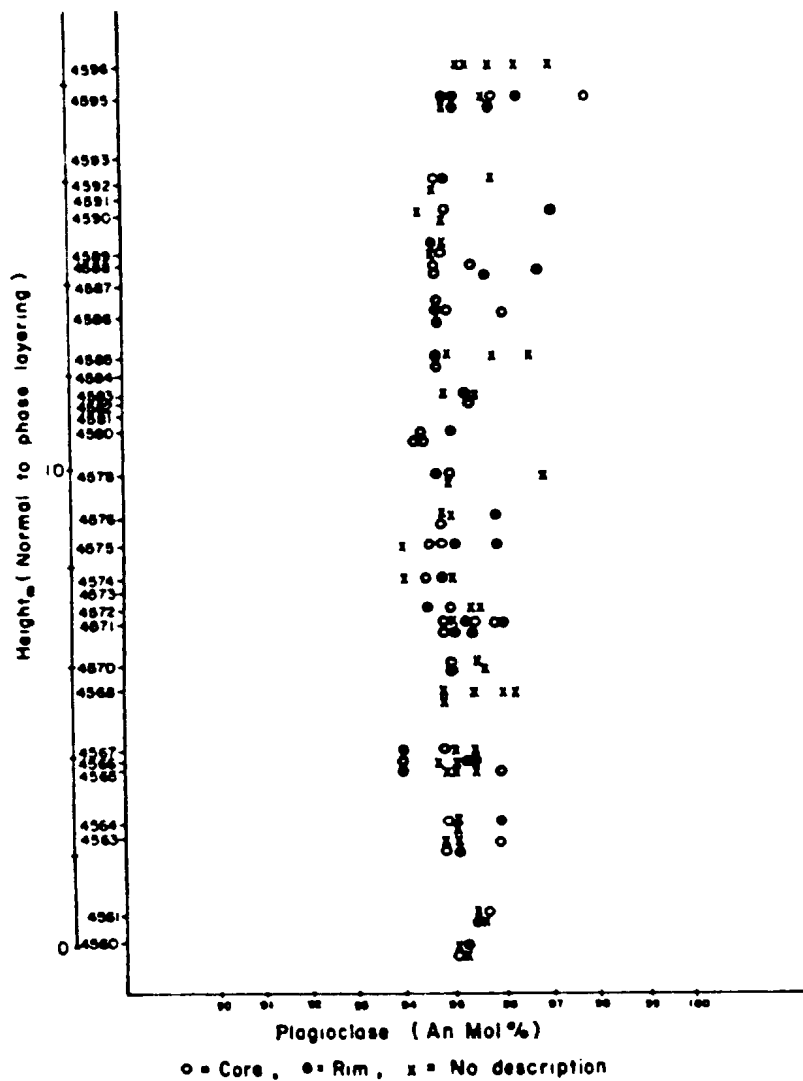
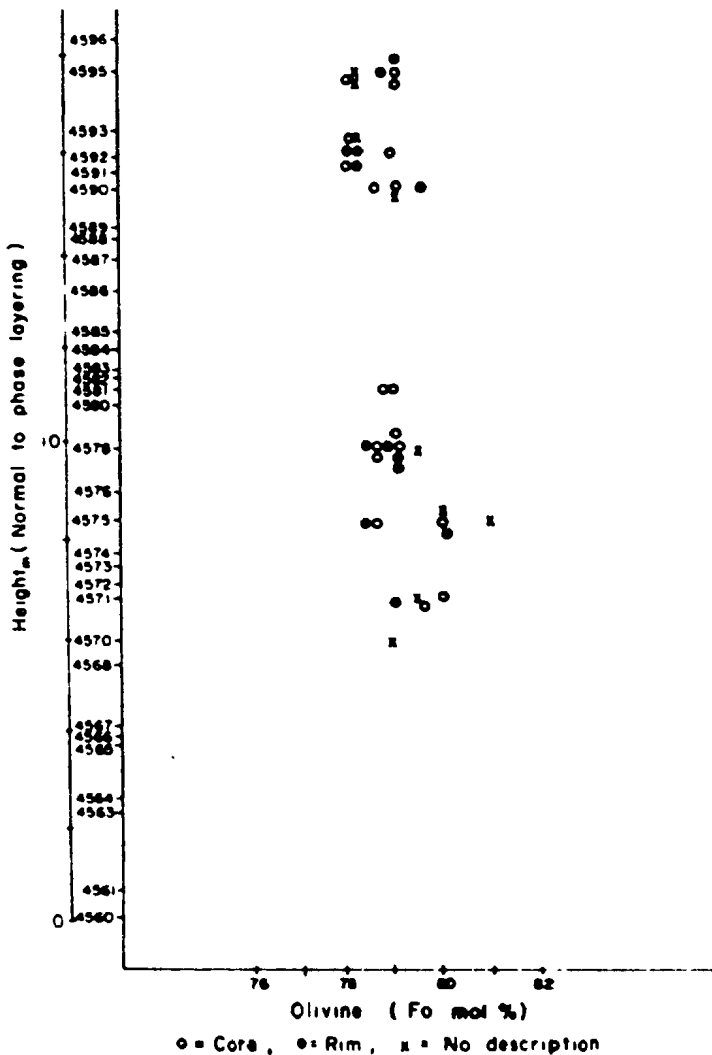


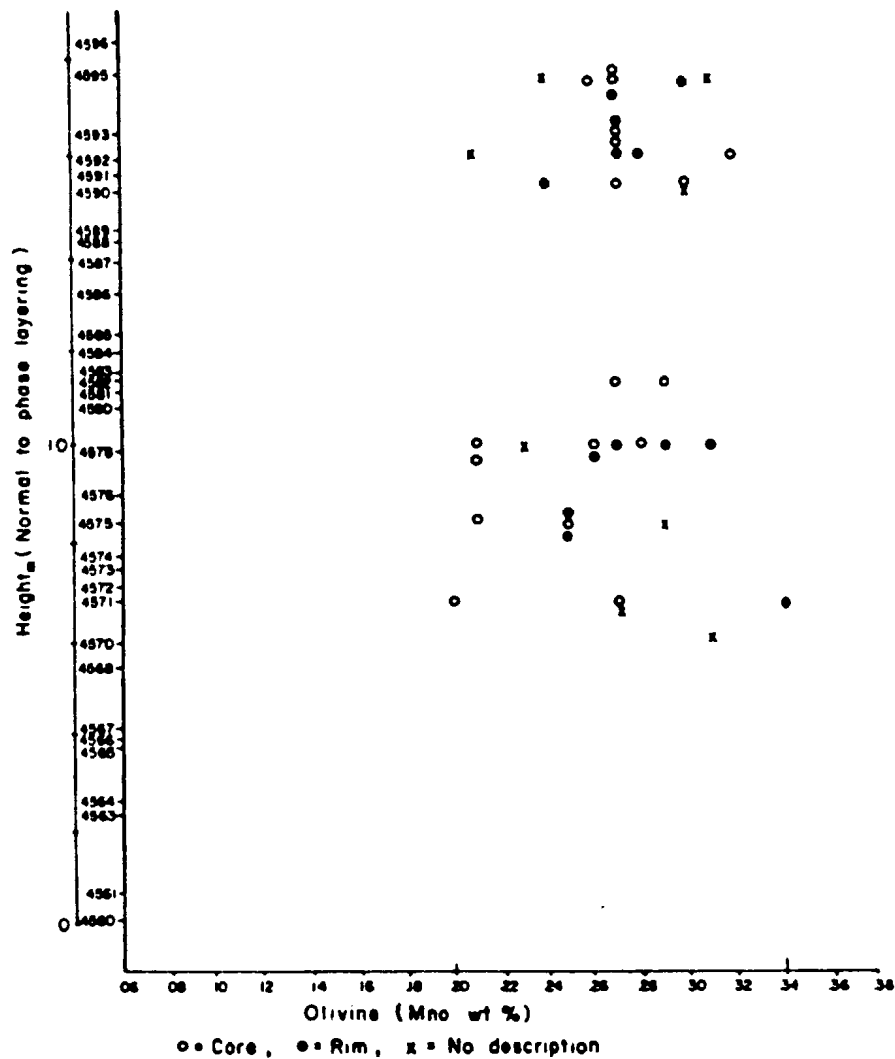
Figure 4-21: Plagioclase (An mol%) values over a 20 m section through the layered olivine gabbro.

samples #4590 and #4596 gave anomalously high  $Mg^*$  numbers (88.5 and 88.28, respectively). This is due to the correspondingly lower Fe content of the rim analysis (#4590=Fe 3.91 and #4596=Fe 3.95) versus the matching core analysis (#4590=Fe 5.54 and #4596=Fe 5.37). This type of reverse zonation is not observed elsewhere in the layered gabbro samples. The  $Cr^*=Cr \times 100 / (Cr + Fe^*)$  (mol.%) value, a sensitive indicator of fractionation in clinopyroxene, likewise shows no significant variation between or within samples



**Figure 4-22:** Olivine (Fo mol%) values over a 20 m section through the layered olivine gabbro.

(Figure 4-26). The maximum  $\Delta\text{Cr}^*$  value between samples equals  $\text{Cr}^*=3$  whereas the  $\Delta\text{Cr}^*$  within individual samples equals  $\text{Cr}^*=2.2$ . Three samples (#4590, #4591 and #4592) show a few analyses with anomalously higher  $\text{Cr}^*$  values, however, the bulk of the analyses for these samples fall within the range exhibited throughout the remainder of the section. Thus, the increased  $\text{Cr}^*$  content in the clinopyroxene phase of these three samples reflects an inhomogeneous Cr content within individual samples rather than a significant variation in magma

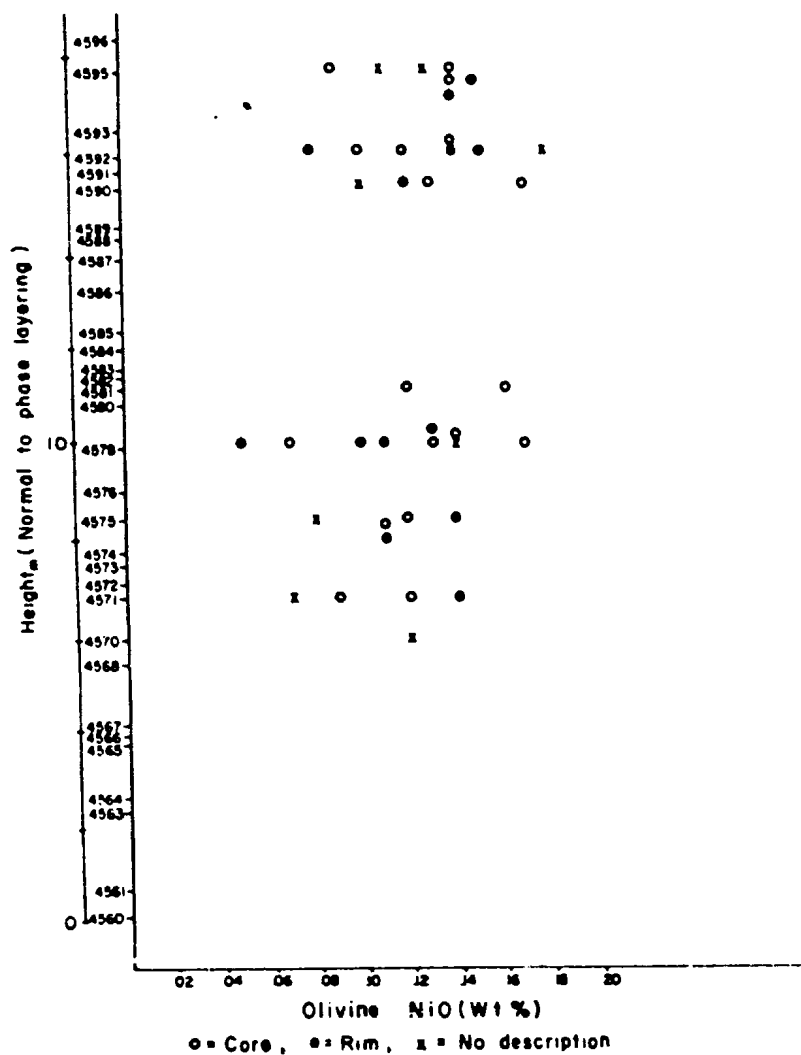


**Figure 4-23:** Olivine (MnO wt%) values over a 20 m section through the layered olivine gabbro.

composition. The minor oxides,  $\text{Na}_2\text{O}$ (wt.%),  $\text{TiO}_2$ (wt.%) and  $\text{MnO}$ (wt.%), (Figure 4-27, Figure 4-28 and Figure 4-29) also exhibit insignificant variation within and between samples, with all elemental ranges falling within a  $\pm 0.1\%$  detection limit.

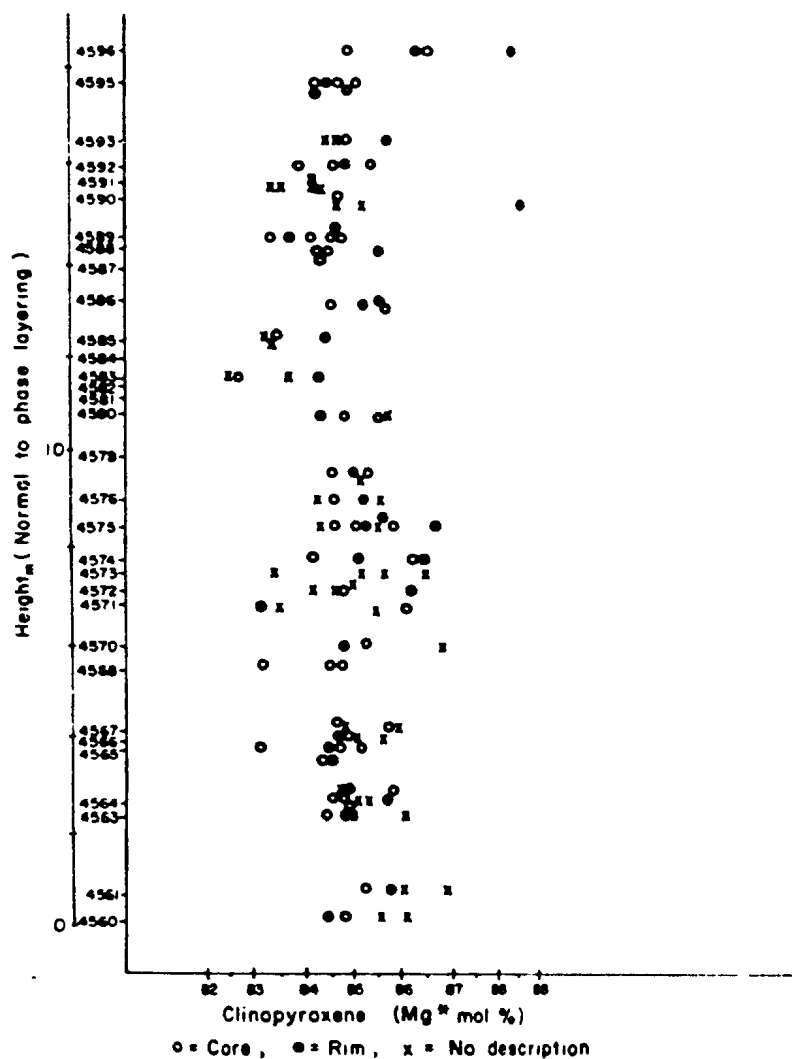
The orthopyroxene phase exhibits the same consistent mineral chemistry for both the major oxides (i.e. :  $\text{Mg}^*$ , Figure 4-30) and trace oxides.





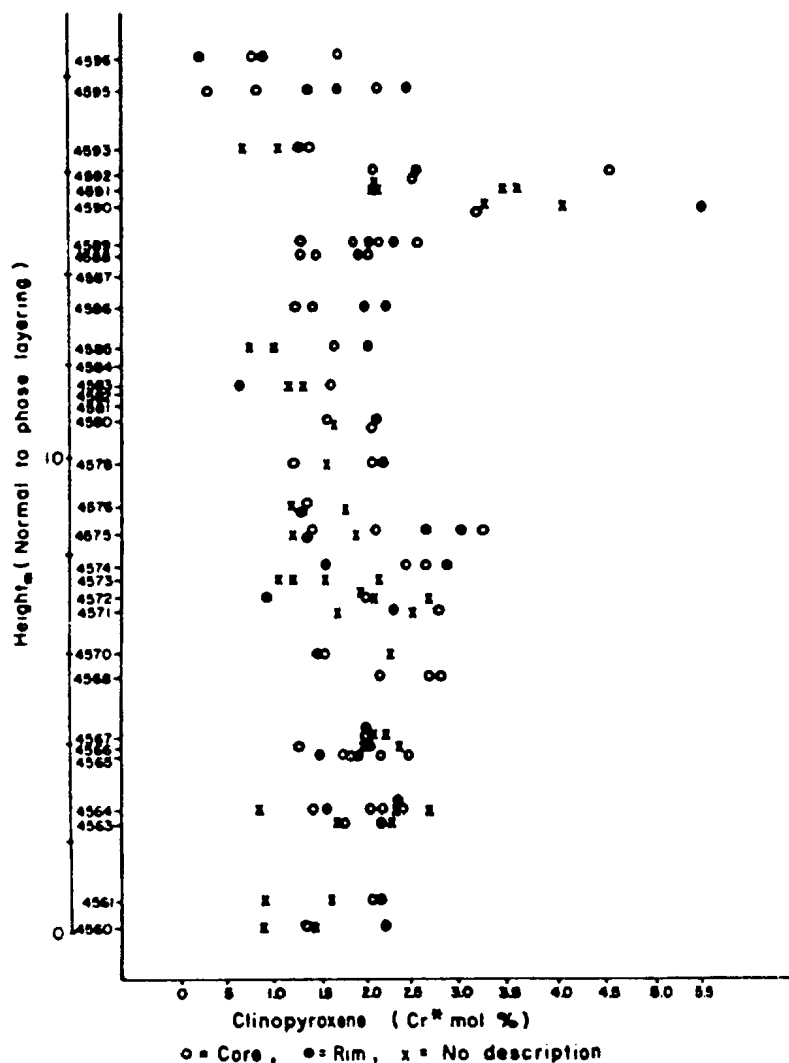
**Figure 4-24:** Olivine (NiO wt%) values over a 20 m section through the layered olivine gabbro.

In conclusion, a distinct absence of chemical zonation exists within the various mineral phases of the layered gabbro section. Point traverse analyses across representative cumulus phases in a number of samples (refer to Appendix A-5) show no significant elemental (major or trace) variation across the grains and low homogeneity indexes (HI=.97 to 5.33).



**Figure 4-25:** Clinopyroxene (Mg\* mol%) values over a 20 m section through the layered olivine gabbro.

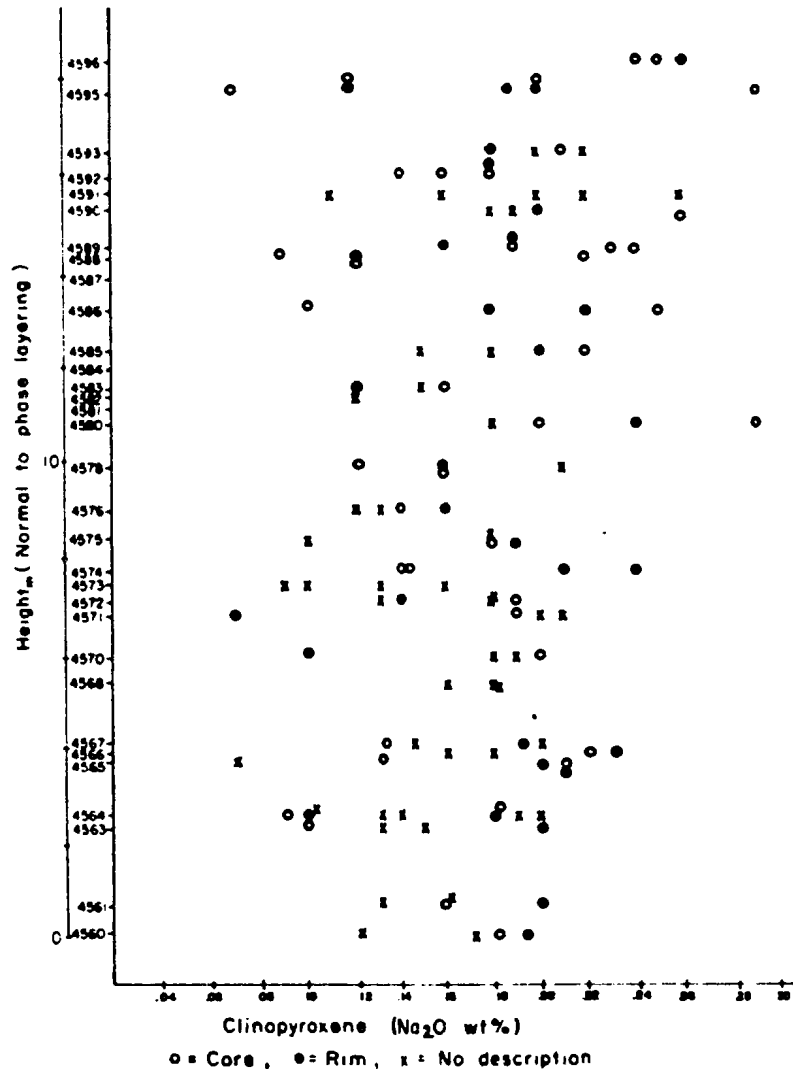
Core and rim analyses were conducted for each mineral phase per slide, where possible, as is represented in the analyses descriptions in Appendix A1 to A5. Calcium-rich rim analysis are noted for one plagioclase grain in samples #4588 and #4590. However, this minor reverse zonation ( $\Delta An = 1.5$  rim-core) is not observed for other grains from the same samples. Core and rim olivine analysis show no significant zonation with a maximum change in the Fo value between



**Figure 4-26:** Clinopyroxene (Cr\* mol%) values over a 20 m section through the layered olivine gabbro.

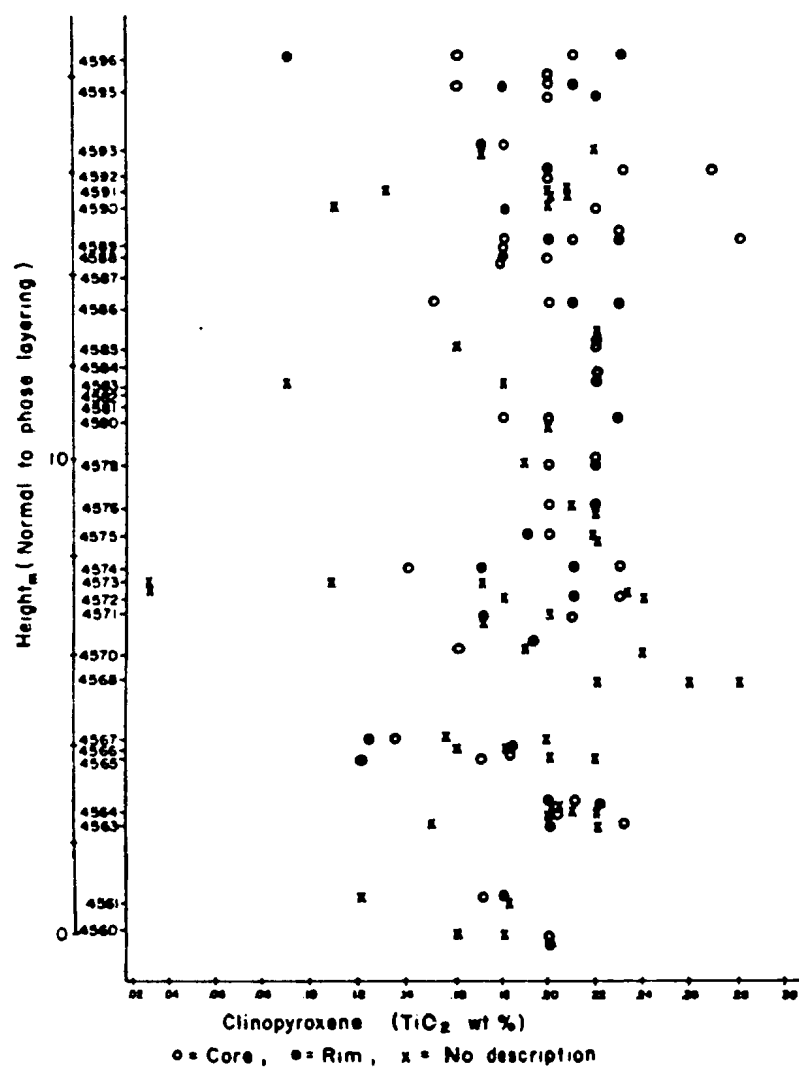
core and rim = .37. Reverse zonation of the Mg:Fe content is noted for one clinopyroxene grain in each of samples #4590 and #4596, however, the main bulk of clinopyroxene analyses show no significant chemical zonation in all samples.

In conclusion, phase chemistry variation is not detected at a fine scale (50-100 cm spacing) over the 20 m section through the rhythmically layered olivine gabbro. Chemical fractionation trends may, however, be present on a broader



**Figure 4-27:** Clinopyroxene (Na<sub>2</sub>O wt%) values over a 20 m section through the layered olivine gabbro.

scale within the Troodos plutonic gabbro section. Hence, future investigations of this type should initially incorporate a wider sample spacing to delineate any major variation trends. As a cautionary note, the field relationships delineating between older and younger suites must first be completed before any apparent chemical trends could be correlated to magmatic fractionation processes within the gabbroic suite rather than multiple magma batches or multiple intrusion of distinct magma sources.



**Figure 4-28:** Clinopyroxene (TiO<sub>2</sub> wt%) values over a 20 m section through the layered olivine gabbro.

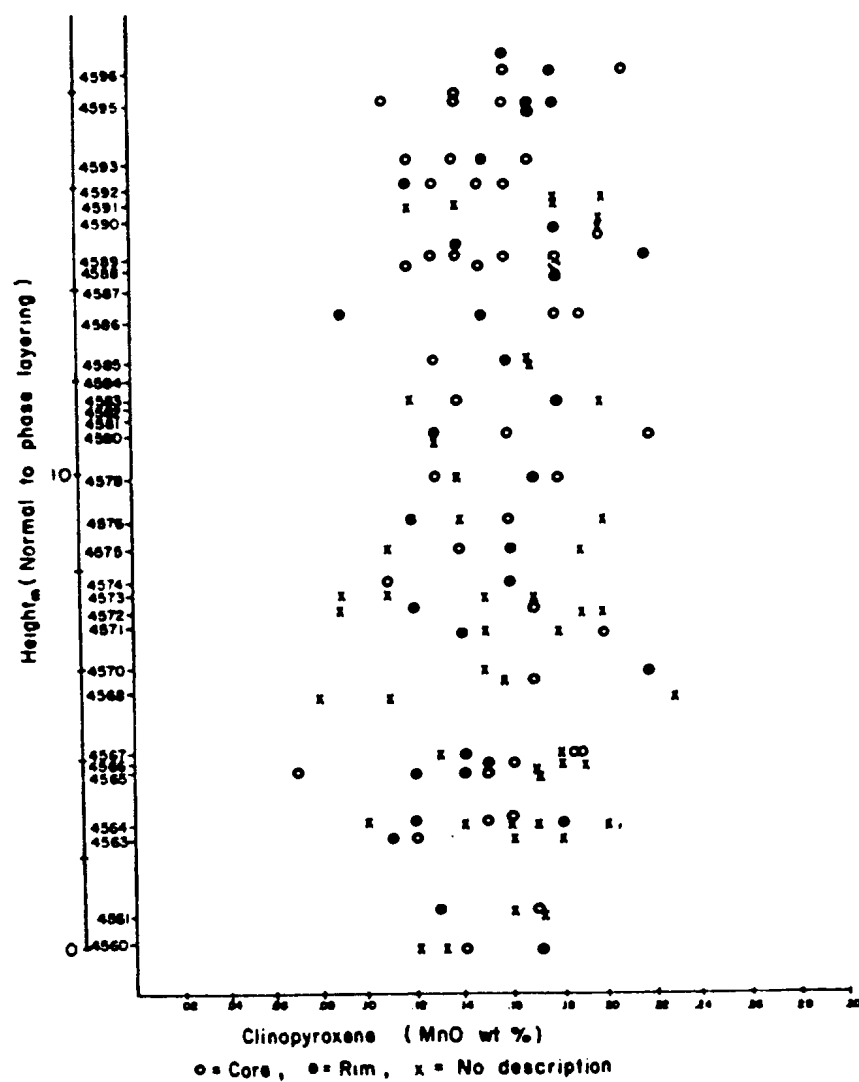
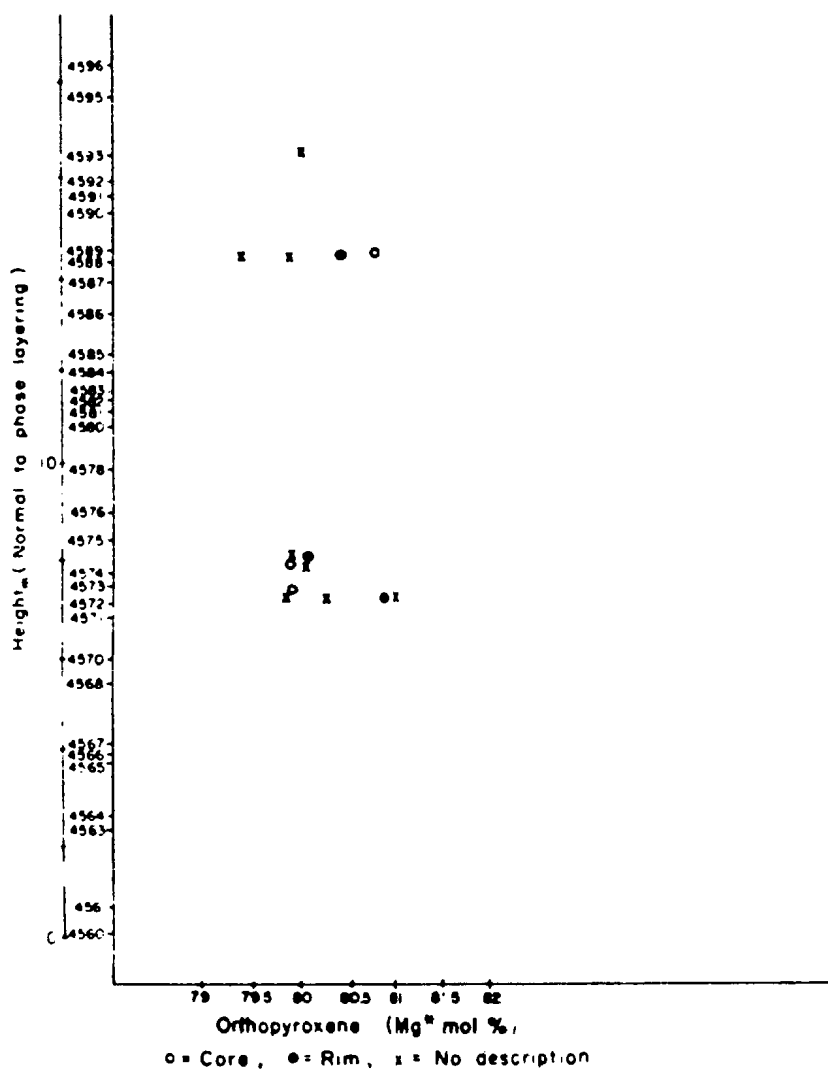


Figure 4-29: Clinopyroxene (MnO wt%) values over a 20 m section through the layered olivine gabbro.





**Figure 4-30:** Orthopyroxene (Mg\* mol%) values over a 20 m section through the layered olivine gabbro.

## Chapter 5

# SUMMARY OF CONCLUSIONS

Throughout this thesis, at the end of each chapter or major section, the overall conclusions of the field relations, structural relations and chemical characteristics have been summarized, discussed and/or compared to the results of previous workers. Therefore, in this final chapter, these conclusions will be presented in point form to allow the reader easy access of the main results of the work.

Writing of the thesis has been approached from the field relationships, which provide a major component of the work, followed by the structural and geochemical aspects that lend support to the conclusions from the field observations. Likewise, the review of the results of the work will follow the same progression from field aspects through to the supporting structural and chemical criteria. In ending, a schematic representation of the geology of the Troodos plutonic complex is presented with a discussion on the present setting of the complex.

On the basis of the investigations carried out within the northwestern quadrant of the Troodos plutonic complex, the following conclusions have evolved:

1. The Troodos plutonic complex is composed of spatially and temporally distinct magmatic suites, the older of which exhibits a "type" ophiolite stratigraphy (Geotimes, 1973) and a penetrative, high-temperature ductile deformation fabric. The lithological units of the older suite are intruded and truncated/disrupted by a series of post-kinematic plutons which together constitute the younger suite(s). The last stage of magmatism within this section

of the Troodos plutonic complex is marked by the intrusion of mafic dikes into both the younger and older suites.

2. The younger suite plutons, pods, sills and dikes are composed of ultramafic-mafic lithologies (i.e.: wehrlite, feldspathic-wehrlite, lherzolite, feldspathic-lherzolite, clinopyroxenite, websterite, and pyroxene-hornblende gabbro). These intrusive bodies are characteristically undeformed and isotropic, exhibiting primary cumulus textures (i.e.: poikilitic, heteradcumulate, ortho- to mesocumulate) with only minor kink banding and undulose extinction in the olivines and pyroxenes in a few outcrops.

3. High-temperature plastic deformation is penetratively developed within the harzburgite, dunite and transition zone and heterogeneously developed within the layered gabbro of the older suite. The deformation is documented on the mega, meso and microscopic level. The consistent, steep to subvertical foliation is coaxial with both the large-scale infolding of the harzburgite-dunite boundary and parasitic minor folds. The position of the transition from ductile deformed metacumulates to undeformed cumulates was previously reported by George (1975, 1978) to occur across a 500 m wide gradation from dunite to transition zone lithologies. The present mapping, however, clearly shows that the contact between these two units is of an abrupt intrusive nature and marks the sharp change from older suite dunite to younger suite isotropic wehrlite intrusives. George (1975, 1978) reported that the change to undeformed cumulates occurred within the transition zone. Within this transition zone, the strain was thought to have been accommodated by an interstitial melt and that a distinct absence of crystalline strain was reported by George (1975; 1978) to occur even within the olivine phase of the layered gabbro. The results of the present study clearly contradict the previous author's conclusions. Sections of the layered olivine gabbro are strongly tectonized (aspect ratios  $<14:1$ ) and the dunite and wehrlite share an intrusive contact with deformation occurring within the older dunite prior to the intrusion of the younger suite wehrlite pluton.

4. The highest position of the deformation front, representing the transition from ductile to brittle deformation mechanisms within the ophiolite, occurs at various structural levels within the layered gabbro section of the Troodos plutonic complex. In general, the position of the deformation front changes with time depending upon fluctuations in the temperature gradients, pressure and strain rates during the history of crustal accretion. That is, domains that have undergone ductile deformation will yield to brittle failure mechanisms during continued stress conditions as progressive cooling results in the lowering of the deformation front. Likewise, periodic magma intrusions will supply a heat influx to raise temperature gradients in the accreting crustal section and thereby raising the position of the deformation front. Ductile deformation and associated transposition of contact margins could occur following crystallization of these intrusive plutons if the position of the deformation front were to rise due to heat influx and rise in the temperature gradients during continued spreading-related shear stress conditions. A similar scenario has been documented by the author within the Lewis Hills massif of the Bay of Islands ophiolite, Newfoundland (Dunsworth *et al.*, 1986; Dunsworth, in prep.).

5. A multiple magmatic history for the Troodos plutonic complex is marked by the presence of spatially and temporally discrete magma chambers which intrude, and for the most part, occupy the former position of the older suite transition zone as well as intruding into both the underlying dunite and harzburgite and the structurally overlying layered gabbros. These intrusive relations are also documented on the microscopic scale in thin sections from two regions of the plutonic complex where deformed and recrystallized dunite and transition zone lithologies are intruded by undeformed clinopyroxenite-wehrlite.

6. The majority of the older suite transition zone and portions of the dunite and layered gabbro have been removed by a combination of large scale faulting during accretion of this section of the oceanic crust and by intrusion/assimilation of the younger suite intrusives. The main bulk of younger suite plutonism has focused

along large (axial graben?) fault structures that developed within the older suite following a lowering of the deformation front (i.e.: cessation of plastic deformation in this section of the plutonic complex). Thus, the younger suite represents variably fault-controlled magma chambers of various sizes that exhibit varying spatial and temporal relations relative to the position of the deformation front. These large scale fault structures in the plutonic complex, which may be situated in any spatial position above the deformation front through time, would allow for fault-controlled intrusion of magma bodies along these zones of structural weakness. Therefore, an inter-relationship exists between the position of the deformation front, periodic influx of magmas and development of ductile versus brittle deformation features within structurally active crustal accretion regimes. These large-scale faults appear to correlate well with the graben structures mapped by Varga and Moores (1985) within the sheeted dike complex and upper gabbros near Kakopetria. No evidence of contractional faults or thrust repetition was identified in the northwestern quadrant of the plutonic complex (MAP 1); contrary to the report by Bortolotti *et al.* (1976).

7. The ultramafic cumulates, interpreted by previous workers (i.e.: Wilson, 1959; Glass, 1967; Greenbaum, 1972A; Moores and Vine, 1971; Allen, 1975 and George, 1975; 1978) to represent the transition or critical zone of the ophiolite sequence, in fact represent the main zone along which concentration of the younger suite intrusions occurred. Likewise, the previous concepts of Allen (1975) regarding the large scale geometry of the plutonic complex are incorrect. Allen (1975) modelled the geometry of the Troodos plutonic complex on the basis of cycles of crystal accumulation with gradational contacts within a major magma chamber that was periodically replenished by magma batches. Allen's cycles were based upon mineral chemistry sections that passed through both the older and younger magmatic suites in the present study area. Allen did not recognize the magmatic relations between older and younger suites in this region of the Troodos plutonic complex nor did he realize the spatial relations and geometry of the main zone of plutonism (ZONE 1). Allen (1975) did, however, recognize the small

ultramafic plutons in the layered gabbros (ZONES 2 and 3) which he equated with small magma chambers which intrude at high levels into an otherwise "typical" ophiolite stratigraphy (Geotimes, 1973).

8. The main zone (ZONE 1) of younger suite plutonism within the northwestern Troodos plutonic complex exhibits crosscutting relations and fractionation trends indicative of multiple intrusion within this main zone of younger intrusives. The ZONE 1 intrusives and the host older suite dunite (+/- layered gabbro) were, in turn, intruded by an undeformed gabbroic carapace of an even deeper-seated evolving magma chamber (refer to Map 1, cross-sections A-A' and B-B').

9. An equant granoblastic to porphyroclastic microfabric prevails in the harzburgite, dunite and transition zone lithologies. Higher strain domains in the layered gabbro exhibit preferred dimensional orientations of elongate grains, recrystallization and subgrain development whereas in the lower strain to undeformed domains, the primary ortho- to mesocumulate igneous textures dominate. Recrystallization via subgrain rotation mechanism is suggested by the microfabric features of the older suite transition zone orthopyroxenite.

10. Transposition of planar and rare linear igneous features during ductile deformation into orientations parallel/subparallel to the regional foliation has direct consequences on the geometry of fine and large scale layering and lithological contacts within the plutonic complex. This conclusion contrasts with the results of George (1975, p. 59), Casey and Karson (1981) and Greenbaum (1972A). The geometrical patterns of the layering and major lithological boundaries within penetratively ductile deformed sections of the plutonic complex cannot be used to model paleo-horizontal surfaces nor the original geometry of bounding surfaces of magma chambers (i.e.: walls, roofs, floors) along which crystals accumulated. Instead, the present day orientations of these features represent a structurally transposed and variably modified geometry controlled by the orientation of the stress fields within the plastically flowing accreting crustal section.



11. The concordancy between fine-scale cumulate layering in the undeformed gabbro and the layering/foliation in tectonized gabbro may suggest an original parallelism between the igneous layering and foliation plane and may indicate some degree of control of the original orientation of principle shear stresses in a flowing magma on the development and orientation of fine-scale primary layering and the evolution of ductile deformation features under hypersolidus-subsolidus conditions. Thus, effects of penetrative deformation must be accounted for when attempting to reconstruct the profile of magma conduits and overlying magma chambers in a dynamic spreading regime.

12. The fractional crystallization sequence of the older suite layered gabbro is : Olivine->Clinopyroxene->Orthopyroxene->Plagioclase +/- Hornblende (+/- Quartz). This sequence may be affected by (a) penetrative ductile deformation and recrystallization, (b) primary magmatic flow yielding crystal mixing and migration, (c) xenocryst inclusion from other melts and (d) metamorphic overgrowths. The presence of plagioclase inclusions in the olivine and pyroxene phases of the layered gabbro may indicate a long history of plagioclase crystallization contemporaneous with the other phases and may be indicative of higher pressure fractionation (Elthon *et al.*, 1982). However, plagioclase inclusions also occur in olivine during recrystallization. Likewise, plagioclase flotation may lead to the incorporation of plagioclase grains floating in a melt and possibly forming nucleation centers for other mineral phases.

13. The younger suite ultramafic-mafic lithologies exhibit the same fractional crystallization sequence as the older suite layered gabbros and textural features suggesting simultaneous crystallization of the clino- and orthopyroxene phases in the younger suite isotropic gabbro.

14. Electron microprobe analyses of the mineral phases from both the older and younger suites show little change in composition from grain to grain for each phase and no chemical zonation within individual grains except for normal core-rim zonation in the plagioclase and hornblende grains of the coarse grained, younger suite pyroxene-hornblende gabbro.

15. Fractionation trends are evident within the mineral chemistry of both the older and younger suites. Fe-enrichment occurs within the pyroxene compositions of the younger suite clinopyroxenite-websterite to pyroxene-hornblende gabbro. Likewise, a general fractionation trend occurs towards structurally higher levels of the younger suite intrusion as marked by Fe-enrichment of the pyroxene and olivine compositions in the ZONE 2 and 3 pods relative to the ZONE 1 plutons. A progressive differentiation trend in the older suite is evident, on the basis of the orthopyroxene and plagioclase compositions, for the transition zone orthopyroxenite to layered gabbro as well as within the layered gabbro from olivine to hypersthene gabbro. The clinopyroxene and olivine compositions exhibit overlapping mineral compositions within the older suite gabbros.

16. The younger and older suites cannot be distinguished from each other on the basis of their respective mineral chemistry. The  $\text{Na/Mg}^*$ ,  $\text{Ti/Mg}^*$ ,  $\text{Ti/Cr}$  and  $\text{Cr}_2\text{O}_3/\text{Mg}^*$  ratios of the clinopyroxene phase and  $\text{NiO}$  versus  $\text{Fe}(\text{mol } \%)$  of olivine in both suites show that lithologies of equivalent fractionation levels plot within the same range for the various chemical parameters. However, the distinctly higher Cr and lower Ti content of the younger suite ultramafic from ZONE 1 is noted. These results clearly contradict the conclusions of Benn and Laurent (1987) who reported a mineral chemistry distinction between early cumulate and late cumulate suites in the Troodos plutonic complex. The plagioclase and olivine mineral chemistry show the same absence of a chemical distinction between the suites although a more Mg-rich olivine composition of the younger suite ultramafic rocks relative to that of the older suite layered olivine gabbro is noted. Thus, the anomalously high Cr, low Ti content and Mg-rich olivine contents of the younger suite ultramafic rocks may be of help for distinguishing between the ultramafic component of the suites when the relations are not exposed in outcrop.

17. The mineral chemistry through a 20 m section of the rhythmically layered older suite olivine gabbro shows no significant chemical zonation within the grains

of each phase and an absence of cryptic chemical variation with consistent plagioclase (An), olivine (Fo), clinopyroxene ( $\text{Mg}^*$ ,  $\text{Cr}^*$ ,  $\text{Na}_2\text{O}$ ,  $\text{TiO}_2$ ,  $\text{MgO}$ ) and orthopyroxene ( $\text{Mg}^*$ ) compositions. It is noted that chemical trends may, however, exist on a broader scale within the plutonic complex.

18. Major and trace element study of the mafic dikes revealed the following chemical characteristics: (a) a typical tholeiitic affinity of the dikes on AFM and alkali versus silica plots; (b) an island-arc tholeiitic melt composition on the basis of Cr versus Y, Ti versus Cr and Ti versus Zr variation diagrams; (c) the Ti versus Mg diagram shows that the sheeted dike samples from the study area plot along a transition from upper to lower pillow lavas (Robinson *et al.*, 1983); and (d) the  $\text{MgO}$  versus  $\text{FeO}$  and  $\text{TiO}_2$  versus  $\text{Mg}$  diagrams show that the mafic-dike samples of the plutonic complex plot along a Mg-rich, Ti-depleted, primitive composition trend that directly correlates with the composition of the rocks from the upper pillow lava suite (as reported by Malpas and Langdon, 1984). This anomalous Mg-rich and Ti depleted chemistry of the mafic dikes indicates an extremely primitive parental melt composition derived from a residual mantle source that had undergone previous partial melting and melt extraction event(s). The mafic dikes are interpreted to represent the feeder dike conduits to the structurally overlying upper pillow lavas of similar depleted chemistry. Additional REE and isotopic data are required to model the source region of these depleted dyke suite(s).

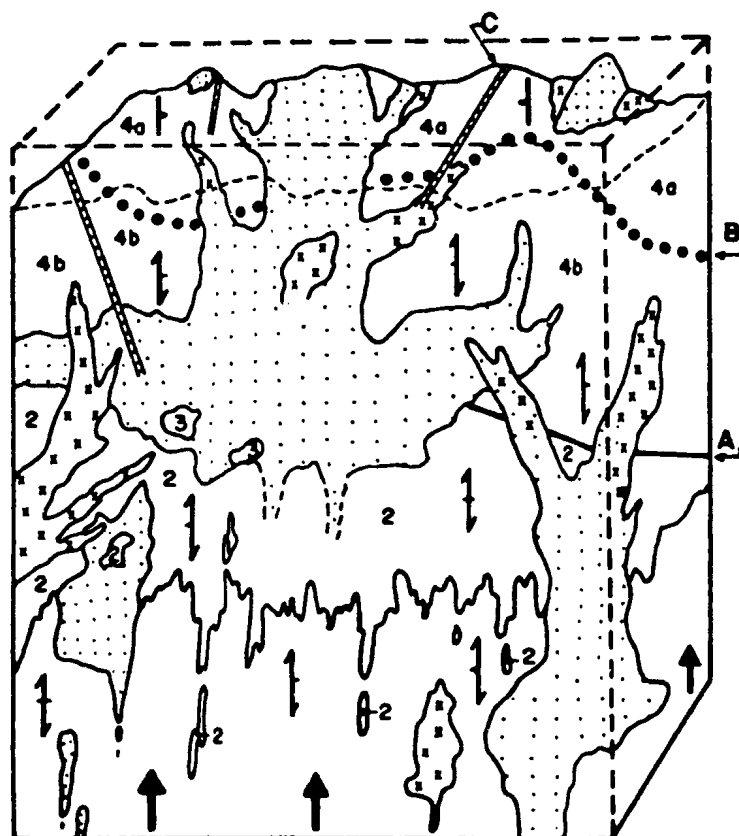
19. Within the NW Troodos plutonic complex, the geometrical relation between: (1) the lower crustal-upper mantle flow induced penetrative  $S_1$  foliation; (2) the infolding along the paleo-Moho (dunite-harzburgite contact) in which the axial surface of the meso- and megascopic folds lies parallel to the  $S_1$  foliation; and (3) the orientation of the enveloping surface of the major petrological boundary at a high angle to the foliation suggests that this section of the upper mantle/lower crust may represent a diapirically-flowing asthenospheric segment of an oceanic (or marginal sea) spreading regime. A direct analogy can be drawn with the

Acoje-type diapirically-spreading asthenosphere model proposed by Nicolas and Violette (1982). These authors also suggested correlation of the Cyprus ophiolite with the Acoje-type setting, however, they reported a post-flow  $D_2$  event within the Troodos massif which resulted in variation of structural fabrics over short distances and large-scale  $F_2$  folds, the axis of which were reported to not lie parallel to the penetrative  $S_1$  fabric. The present author's work shows no evidence of a  $D_2$  folding event within the present study area. The effect of later uplifting of the harzburgite core of the Troodos plutonic complex would only be to render more shallow the few (three in total) south plunging lineations to their present plunges with no effect on the overall geometrical configuration of the planar structural elements in the plutonic complex of the NW quadrant of the Troodos ophiolite.

In conclusion, on the basis of field relations, deformation features and geochemistry, a dynamic crustal accretionary history of multiple intrusion and ductile-brittle deformation is established for the Troodos plutonic complex. A schematic representation of the younger and older magmatic suites, multiple intrusive relations between the various post-kinematic plutons, distribution of high-temperature ductile deformation within this section of the plutonic complex (highest position of the deformation front) and geometry of foliation, layering and major lithological contacts is presented in Figure 5-1. The main features to emphasize in this schematic section through the plutonic complex (Figure 5-1) are:

(1) Magma entering the lower crustal domain (above a diapirically- flowing asthenospheric upper mantle) has cooled/crystallized/ deformed under the influence of upper mantle-lower crustal flow- related stress conditions.

(2) A penetrative  $S_1$  fabric develops in response to the upper mantle-lower crustal flow in an orientation concordant from the harzburgite through dunite, transition zone orthopyroxenite and into the layered gabbro (older suite), (Figure 5.1). This  $S_1$  fabric lies parallel to the axial planes along the infolded harzburgite-dunite boundary (Figure 5.1). Evidence of probable infolding of the dunite,



Older Suite:

- 1 Depleted mantle tectonite  
( harzburgite)
- 2 Dunite
- 3 Transition Zone Orthopyroxenite
- 4a Layered gabbro (minor foliation)
- 4b Foliated / layered gabbro

Younger undeformed intrusives:

- Wehrlite and Clinopyroxenite
- Pyroxene Gabbro
- Mafic Dykes
- Deformation front
- Mantle flow line

5/10/89

Figure 5-1: Schematic section demonstrating the complex accretionary history of the northwestern Troodos plutonic complex.

transition zone and layered gabbro is thought to have been obliterated (at least within the present study area) by later intrusions and large-scale faulting ( A , Figure 5.1). Also, note that any intrusive relations which may have existed within the older suite would have been obliterated by the penetrative plastic deformation with transposition of contact margins towards the regional structural trends.

(3) The deformation front, marking the gradual transition from dominantly ductile to brittle deformation mechanisms, occurs within the layered gabbro ( B , Figure 5.1) and marks the highest level of ductile deformation within the plutonic complex.

(4) Above the deformation front (the highest level of ductile deformation), the orientation of developing igneous layering/laminations is controlled (to some extent) by the orientation of the principal stresses in the flowing magma (stress related to upper mantle-lower crustal flow), thus resulting in the parallelism between planar fabrics (primary and secondary) above and below the deformation front. For further discussion refer to Chapter 3, Section 3.8.3 and Chapter 5, Conclusion #11. The relation between the orientation of accreting planes (e.g.: layering) within cooling/crystallizing lithologies and flow-related stress has not previously been reported within any existing models for the Troodos plutonic complex.

(5) With continued cooling (and possible uplifting of the crustal section), the resultant lowering of the deformation front allowed for the development of brittle deformation structures (e.g.: large-scale faults - grabens?) at deeper levels (e.g.: within the transition zone, dunite and harzburgite), ( Figure 5.1, A ) which may have provided zones of structural weakness to act as conduits for intrusion/emplacement of the younger plutons (above the now lowered deformation front).

(6) The younger suite(s) plutons, of various shapes and sizes, intruded/ascended through all levels of the deformed older suite and crystallized as isotropic bodies within the brittle deformation domain (i.e.: above the deformation front,

essentially post-kinematic). The intrusive contacts between the plutons and the older suite are marked by truncated layering/foliation, xenoliths and abrupt lithological contrasts. Below the deformation front, the suites can be separated in time due to the penetrative deformation of the older suite. However, above the deformation front, it is not always possible to distinguish between the younger and older suite lithologies. This is particularly true for the older suite isotropic gabbro zones within the layered gabbro and zones of younger intrusive isotropic gabbro intruding the older suite layered gabbro (refer to Chapter 3, Section 3.4 for further discussion).

(7) Multiple intrusion within/between the younger plutons occurs with large bodies of isotropic gabbro intruding/truncating the wehrlite-clinopyroxenite-minor gabbro plutons (refer to Figure 5.1). These gabbroic intrusions may be feeding from deeper-seated evolving magma chambers (plutons), (refer to Map 1, Cross-section A-A').

(8) The highly depleted mafic dikes (Figure 5.1, C ) "feed" from the intrusive plutons to the sheeted dike complex and act as conduits to the overlying upper pillow lava suite (refer to Chapter 4, Section 4.3 and Chapter 5, Conclusion #18).

(9) Note: The Troodos ophiolite appears to represent a section of oceanic crust "caught" within the diapirically-flowing domain prior to lateral spreading. This is based upon the correlation with the Acoje-type setting (Nicolas and Violette, 1982) and the fact that no evidence exists to suggest reorientation of existing structural fabrics or overprinting by secondary structural fabrics in the older suite. Such features would be expected to occur in crustal sections that experienced lateral spreading. The essentially post-kinematic intrusions within the brittle domain could have occurred at any time; being related to magma influxes within a diffuse spreading regime, intruding at some distance from the initial formation of the older suite lithologies (i.e.: off-axis) or above a subduction zone. Additional geochemical and structural studies are required to unravel the answers to these questions.



## REFERENCES

- Adamia, S., Bergougnan, H., Fourquin, C., Haghipour, A., Lordkipanidze, M., Ozgul, N., Ricou, L., and Zakariadze, G.  
 1980: The Alpine Middle East between the Aegean and the Oman traverses, In: Geology of the Alpine chains born of the Tethys, Editors: Aubouin, J., Debelman, J. and Latreille, M., Memoire de B.R.G.M., No. 115, p. 122-136.
- Alabaster, T., Pearce, J.A. and Malpas, J.  
 1982: The volcanic stratigraphy and petrogenesis of the Oman ophiolite complex, Contribution to Mineralogy and Petrology, V. 81, p. 168-183.
- Allen, C.R.  
 1975: The petrology of a portion of the Troodos plutonic complex, Cyprus, Unpub. Ph.D. Thesis, Cambridge University, England, 161 p.
- Ashby, M.F.  
 1972: A first report on deformation - mechanism maps, Acta. Met. 20, p. 887-897.
- Avé Lallement, H.G.  
 1985: Subgrain rotation and dynamic recrystallization of olivine, upper mantle diapirism and extension of the Basin-and-Range province, Tectonophysics, #119, p. 89-117.
- Avé Lallement, H.G.  
 1978: Experimental deformation of diopside and websterite, Tectonophysics, #46, p. 1-27.
- Avé Lallement, H.G.  
 1976: Structure of the Canyon Mountain (Oregon) ophiolite complex and its implications for sea-floor spreading, Geological Society of America Special Paper, #173, p. 49.
- Avé Lallement, H.G. and Carter, N.L.  
 1970: Syntectonic recrystallization of olivine and modes of flow in the upper mantle, Geological Society America Bulletin, V. 81, p. 2203-2220.
- Avé Lallement, H.G.  
 1967: Structural and petrofabric analysis of an "Alpine-type" peridotite: the lherzolite of the French Pyrenees, Leidse Geol. Meded., V. 42, p. 1-57.
- Aubert, M. and Baroz, F.  
 1974: Structure profonde de la chaîne du Pentadaktylos et de la Mésaoria (Chypre), Rev. Inst. Fr. Pet. Paris., V. 29, p. 361-373.

- Bagnell, P.S.  
1960: The geology and mineral resources of the Pano Lefkara-Larnaca area, Cyprus Geological Survey Department, Memoir #5, p. 116.
- Bally, A.W.  
1975: A geodynamic scenario for hydrocarbon occurrences, Proceedings Ninth World Petroleum Congress #2, p. 33-44.
- Baragar, W.R.A. and Lambert, M.B.  
1984: Sheeted dyke complex, Troodos ophiolite, Geological Association of Canada, Mineralogical Association of Canada Program with Abstracts, V. 9, p. 44.
- Baroz, F.  
1980: Volcanism and continent-island arc collision in the Pentadaktylos Range, Cyprus, In: Panayiotou, A., (ed.), Ophiolites: International Ophiolite Symposium, Cyprus, 1979, Proceedings, p. 73-85.
- Baroz, F., Desmet, A., and Lapierre, H.  
1976: Les traits dominants de la geologie de Chypre, Société Géologique de France Bulletin, V. 18, p. 429-437.
- Bear, L.M.  
1960: The Geology and mineral resources of the Akaki-Lythrodonda area Cyprus, Geological Survey Department, Memoir, #3, p. 122.  
1966: The Evolution and petrogenesis of the Troodos complex, Annual Report of the Geological Survey Department, Cyprus, #3, p. 26-37.
- Bechon, F. and Rocci, G.  
1982: C.R. Acad. Sc. Paris, t. 214, serie II, p. 999-1002.
- Benn, K. and Laurent, R.  
1987: Intrusive suite documented in the Troodos ophiolite plutonic complex, Cyprus, Geology, V.15, p. 821-824.
- Bernoulli, D. and Lemoine, M.  
1980: Birth and early evolution of the Tethys: the overall situation, In: Geology of the Alpine chains born of the Tethys, Editors: Aubouin, J., Delemas, J., and Latreille, M. Memoire de B.R.G.M., #115, p. 168-179.
- Biju-Duval, B., Lapierre, H. and Letouzey, J.  
1976: Is the Troodos massif (Cyprus) allochthonous?, Bull. Soc. Geol. Fr., V. 18, p. 1347-1356.

- Bishopp, D.W.  
 1952: Some new features of the geology of Cyprus, 19th International Geological Congress, #17, p. 13-18.
- Bloxam, T.W. and Lewis, A.D.  
 1972: Ti, Zr and Cr in some British pillow lavas and their petrogenetic affinities, *Nature, Physical Science*, V. 237, p. 134.
- Boettcher, W.  
 1969: Zur Entstehung des Magmatischen Troodos - Komplexes (Zypern). *Neves Jahr. Mineral. Abh.*, #110, p. 159-187.
- Bonatti, E., Emiliani, C., Ferrara, G., Honnorez, J. and Rydell, H.  
 1974: Ultramafic-carbonate breccias from the equatorial Mid-Atlantic Ridge, *Marine Geology*, #16, p. 83-102.
- Borg, I.Y. and Heard, H.C.  
 1970: Experimental deformation of plagioclase, *In: Experimental and Natural Rock Deformation*, Ed.: P. Paulitsch, Springer-Verlog, Berlin, Germany, p. 375-403.
- Borg, I.Y. and Heard, H.C.  
 1969: Mechanical twinning and slip in experimentally deformed plagioclases, *Contributions Mineralogy and Petrology*, V. 23, p. 128-135.
- Bortolotti, V., Lapierre, H. and Piccardo, G.B.  
 1976: Tectonics of the Troodos massif (Cyprus): preliminary results, *Tectonophysics*, V. 35, #4, T1-T5.
- Boullier, A.M. and Gueguen, Y.  
 1975: SP-Mylonites: Origin of some mylonites by superplastic flow, *Contributions Mineralogy and Petrology*, V. 50, p. 93-104.
- Bowen, N.L.  
 1915: Crystallization differentiation in silicate liquids, *American Journal of Science 4th Series*, #39, p. 175-191.
- Bowen, N.L. and Tuttle, O.F.  
 1949: The system  $MgO-SiO_2-H_2O$ , *Bulletin of the Geological Society of America*, #60, P. 439-460.
- Bridgewater, D. and Collerson, K.D.  
 1976: The major petrological and geochemical characters of the 3,600 m.y. Uivak Gneisses from Labrador, *Contribution to Mineralogy and Petrology*, V.54, p. 43-56.

- Broughton, D.W. and Gibson, I.L.  
1984:  $C^{13}$  and  $O^{18}$  compositions of secondary calcites from a 267m cored section through the Troodos ophiolite lava succession Geological Association of Canada, Mineralogical Association of Canada, Program with Abstracts, V. 9, p. 48.
- Byerly, G.R., Melson, W.G. and Vogt, P.R.  
1976: Rhyodacites, andesites, ferrobasalts and ocean tholeiites from the Galapagos spreading center, Earth and Planetary Science Letters, V. 30, p. 215-221.
- Calon, T.J., Malpas, J.G., and Neyens, M.  
1985: Role of deformation in the evolution of the plutonic complex, Bay of Islands ophiolite, Newfoundland, Geological Association of Canada. Mineralogical Association of Canada, Program with Abstracts, V. 10, p. A8.
- Calon, T.J.  
1984: Patterns of high-temperature, plastic deformation in the plutonic sections of ophiolites, Geological Association of Canada, Mineralogical Association of Canada, Programs with Abstracts, V. 9, p. 50.
- Cann, J.R.  
1970: New model for the structure of the ocean crust, Nature, V. 226, p. 928.
- Casey, J.F. and Karson, J.A.  
1981: Magma chamber profiles from the Bay of Islands ophiolite complex: Implication for crustal level magma chambers at oceanic ridges, Nature, V. 292, p. 295-301.
- Carswell, D.A.  
1968: Picritic magma-residual dunite relationships in garnet peridotite at Kaskaret near Tafjord, South Norway, Contributions to Mineralogy and Petrology, #19, p. 97-124.
- Carter, N.  
1976: Steady state flow of rocks, Reviews of Geophysics and Space Physics, #14, p. 301-353.
- Christie, J.M. and Ardell, A.J.  
1976: Deformation structures in minerals from electron microscopy. In: Mineralogy Ed. H.R. Wenk, Springer - Verlag, Berlin, Heidelberg, Germany.

- Coe, R.S. and Kirby, S.H.  
 1975: The orthoenstatite to clinoenstatite transformation of shearing and reversion by annealing: mechanism and potential applications, *Contributions Mineralogy and Petrology*, V. 52, p. 29-55.
- Coleman, R.G.  
 1977: *Ophiolites*, Springer, Heidelberg, New York, p 229.
- Cox, K.G., Bell, J.D., and Pankhurst, R.J.  
 1979: The interpretation of igneous rocks, Allen and Unwin, London, p. 450.
- Crawford, A.J., Beccaluva, L. and Serri, G.  
 1981: Tectono-magmatic evolution of the West Philippine-Mariana region and the origin of boninites, *Earth and Planetary Science Letters*, #54, p. 346-356.
- Den Tex, E.  
 1969: Origin of ultramafic rocks, their tectonic setting and history, *Tectonophysics*, #7, p. 457-458.
- Dungan, M.A. and Ave Lallemant, H.B.  
 1977: Formation of small dunite bodies by metasomatic transformation of harzburgite in the Canyon Mountain ophiolite: Northeast Oregon, *In: Magma Genesis*, Dick, H.J.B. (Ed.), *Bulletin of the Oregon Department Geology and Mineralogy, Indiana*, #96, p. 109-128.
- Dunsworth, S.M.  
 1989: Geology of the Central Lewis Hills Massif: A history of synkinematic, multiple intrusive oceanic crustal accretion for the Bay of Islands ophiolite, Newfoundland, (in prep).
- Dunsworth, S., Calon, T., and Malpas, J.  
 1986: Structural and magmatic controls on the internal geometry of the plutonic complex and its chromite occurrences in the Bay of Islands ophiolite, Newfoundland, *Geological Survey of Canada, Current Research Paper* 86-1A, p. 471-482.
- Elthon, D., Casey, J.F. and Komar, S.  
 1984: Cryptic mineral chemistry variations in a detailed traverse through the cumulate ultramafic rocks of the North Arm Mountain massif of the Bay of Islands ophiolite, Newfoundland, *In: Ophiolite and Oceanic Lithosphere*, ed.: I.G. Gass, S.J. Lippard and A.W. Shelton, *Geological Society of London, Special Publication* # 13, p. 83-97.

- Etheridge, M.A. and Kirby, S.H.  
 1980: Experimental deformation of rock forming pyroxenes: recrystallization mechanism and preferred orientation development, Tectonophysics.
- Etheridge, M.A. and Kirby, S.H.  
 1977: Experimental deformation of rock-forming pyroxenes: recrystallization mechanisms and preferred orientation development, Transactions American Geophysics Union, V. 58, p. 513.
- Ewart, A. and Bryan, W.B.  
 1972: Petrography and geochemistry of the igneous rocks from Eua, Tongan Islands, Geological Society of America Bulletin, V. 83, p. 3281-3298.
- Freund, R., Goldberg, M., Weissbrod, T., Drunckman, Y. and Derin, B.,  
 1975: The Triassic-Jurassic structure of Israel and its relation to the origin of the eastern Mediterranean ophiolites, Bulletin of Geological Survey of Israel, #65, p. 1-26.
- Gass, I.G.  
 1980: The Troodos massif: Its role in the unravelling of the ophiolite problem and its significance in the understanding of constructive plate margin processes; In: Panayiotou, A. (ed.), ophiolites: International Ophiolite Symposium, Cyprus, 1979, Proceedings, p. 23-35.
- Gass, I.G. and Smewing, J.D.  
 1973: Intrusion and metamorphism at constructive margins: Evidence from the Troodos massif, Cyprus, Nature 242 p. 26-29.
- Gass, I.G.  
 1968: Is the Troodos massif of Cyprus a fragment of Mesozoic ocean floor? Nature 220, p. 39-42.
- Gass, I.G.  
 1967: The ultrabasic volcanic assemblage of the Troodos massif, Cyprus In: Ultramafic and Related Rocks. Ed. R.J. Wyllie, New York, Wiley, p. 121-134.
- Gass, I.G., and Masson-Smith, D.  
 1963: The geology and gravity anomalies of the Troodos massif, Cyprus, Phil. Trans. Roy. Soc. London, Series A, 255, p. 417-467.

- Gass, I.G.  
1960: The geology and mineral resources of the Dhali area, Cyprus Geological Survey Memoir, #4, p. 116.
- Gass, I.G.  
1958: Ultrabasic pillow lavas from Cyprus, *Geology Magazine*, 95, p. 241-251.
- George, R.P.  
1978: Structure and petrology of the Olympus ultramafic complex in the Troodos ophiolite, Cyprus, *Geological Society of America Bulletin*, V. 89, p. 845-865.
- George, R.P.  
1975: The internal structure of the Troodos ultramafic complex, Cyprus, Ph.D. unpub. New York State University, p. 223.
- Gillis, K.M.  
1983: Low temperature alteration of the extrusive sequence, Troodos ophiolite, Cyprus, *Geological Association of Canada, Mineralogical Association of Canada, Program with Abstracts*, V. 8, p. A27.
- Grant, N.K.  
1978: Structural distinction between a metasedimentary cover and an underlying basement in the 600 m.y. old Pan-African domain of Northwestern Nigeria, West Africa, *Geological Society of America Bulletin*, V.89, p. 50-58.
- Greenbaum, D.  
1977: The chromitiferous rocks of the Troodos ophiolite complex, Cyprus, *Economic Geology*, V. 72, p. 1175-1194.
- Greenbaum, D.  
1972a: The geology and evolution of the Troodos plutonic complex and associated deposits, Cyprus, Unpub. Ph.D. Thesis, University of Leeds, p. 143.
- Greenbaum, D.  
1972b: Magnetic processes at ocean ridges and evidence from the Troodos massif, Cyprus, *Nature Physical Science*, V. 238, p. 18-21.
- Gueguen, Y. and Nicholas, A.  
1980: Deformation of mantle rocks, *Annual Review of Earth and Planetary Science*, #8, p. 119-144.



## Geotimes

- 1973: Penrose Field Conference Participants on Ophiolites, Sept. 14-24, 1972, Geotimes V. 17, #12, p. 24-25.

Hart, S.R., Glassley, W.E. and Karig, D.E.

- 1972: Basalts and sea floor spreading behind the Mariana island arc, Earth and Planetary Science Letters, V. 15, p. 12-18.

Hess, H.H.

- 1939: Extreme fractional crystallization of a basaltic magma: the Stillwater Igneous Complex, Transactions American Geophysical Union, #3, p. 430-432.

Himmelberg, G.R. and Coleman, R.G.

- 1968: Chemistry of primary minerals and rocks from the Red Mountain - Del Puerto Ultramafic Mass, California, United States Geological Survey Professional Paper 600-C, p. C18-C26.

Hsu, K.J. and Bernoulli, D.

- 1978: Genesis of the Tethys and the Mediterranean; In: Initial Reports Deep Sea Drilling Project, Ed.: Hsu, K.J., Montadert, L. et al. 42, Washington, US Government Print Off., p. 943-949.

Irvine, T.N.

- 1980: Magmatic density currents and cumulus processes, American Journal of Sciences, V. 280-A, p. 1-58.

Irvine, T.N.

- 1979: Rocks whose compositions are determined by crystal accumulation and sorting, In: Evolution of the Igneous Rocks- 50th Anniversary Perspectives, ed.: H.S. Yoder, Princeton, New Jersey, Princeton University Press., p. 588.

Irvine, T.N.

- 1978: Infiltration metasomatism, adcumulus growth, and secondary differentiation in the Muskox intrusion, Carnegie Institute of Washington Year Book #77, p. 743-751.

Irvine, T.N. and Findlay, T.C.

- 1972: The ancient ocean lithosphere, E. Irving (Ed.), Earth Physics Branch, Energy, Mines and Resources, Ottawa, V. 42(3), p. 97-128.

Irvine, T.N.

- 1967: The Duke Island ultramafic complex, southeastern Alaska. In: Ultramafic and Related Rocks, P.J. Wyllie, (Ed.), New York, John Wiley p. 84-96.

- Irvine, T.N.  
 1965: Sedimentary structures in igneous extrusions with particular reference to the Duke Island ultramafic complex, In: Primary sedimentary structures and their hydrodynamic interpretation, Middleton, G.V., (Ed.), Society Economic Paleontologists Mineralogists, Special Publication #12, p. 220-232.
- Jackson, E.D.  
 1971: The origin of the ultramafic rocks by cumulus processes, Fortschr. Miner. 48, 1, p. 128-174.
- Jackson, E.D.  
 1967: Ultramafic cumulates in the Stillwater, Great Dyke and Bushveld intrusions. In: Ultramafic and related rocks, P.J. Wyllie, ed. New York, John Wiley and Sons. p. 20-38.
- Jackson, E.D.  
 1961: Primary textures and mineral associations in the ultramafic zone of the Stillwater Complex, Montana, United States Geological Survey Professional Paper, #358, p. 1-106.
- Jakes, P. and Gill, J.  
 1970: Rare earth elements and the island arc tholeiitic series, Earth and Planetary Science Letters, V. 9, p. 17-18.
- Johnson, M.R.W.  
 1961: Polymetamorphism in movement zones in the Caledonian thrust belt of north-west Scotland, Journal of Geology, V.69, p. 417-432.  
 1963: Some time relations of movement and metamorphism in the Scottish Highlands, Geologie en Mijnbouw, V.42, p. 121-147.
- Karamata, S.  
 1980: Tethyan ophiolites: A short review and the main problems, In: Panayiotou, A. (ed.), Ophiolites, International Ophiolite Symposium, Cyprus, 1979, Proceedings, p. 257-260.
- Kay, R.W. and Senechal, R.G.  
 1976: The rare earth geochemistry of the Troodos ophiolite complex, Journal of Geophysical Research, #81, p. 964-970.
- Kerrich, R. and Allison, I.  
 1978: Flow mechanisms in rocks: microscopic and mesoscopic structures and their relation to physical conditions of deformation in the crust, Geosciences Canada, V. 5, #3, p. 109-118.

- Kidd, R.G.W.  
 1977: A model for the process of formation of the upper oceanic crust, *Geophysical Journal of the Royal Astrological Society*, V. 50, p. 149-183.
- Kidd, R.G.W. and Cann, J.R.  
 1974: Chilling statistics indicate an ocean-floor spreading origin for the Troodos complex, Cyprus, *Earth and Planetary Science Letters*, V. 19, p. 290-300.
- Kirby, S.H. and Etheridge, M.A.  
 1980: Experimental deformation of rock forming pyroxenes: ductile strengths and mechanisms of flow, *Tectonophysics*.
- Lapierre, H. and Rocci, G.  
 1976: Le volcanisme du sud-ouest de Chyre et le probleme de l'ouverture des region Tethysiennes au Trias., *Tectonophysics*, 30, p. 299-313.
- Lapierre, H.  
 1975: Les formations sedimentaire et eruptive des nappes de Mamonia et leurs relations avec le Massif de Troodos (Chyre occidentale), *Societe geologique France Memoir*, #123, p. 132.
- Lapierre, H.  
 1968: Decouverte d'une serie volcano-sedimentaire problemement d'age Crétacé supérieur au S-W de l'île de Chypre, *C.R. Acad. Sci., D.*, #266, p. 1817-1820.
- Laurent, R., Delaloye, M., Vuagnat, M., and Wagner, J.J.  
 1980: Composition of parental basaltic magma in ophiolite, *In: Ophiolites, Proceedings of International Ophiolite Symposium, Cyprus*, p. 172-181.
- Loney, R.A., Himmelburg, G.R., and Coleman, R.G.  
 1971: Structure and petrology of the alpine-type peridotite at Burro Mountain, California, USA, *Journal of Petrology*, V. 12, p. 245-309.
- MacDonald, G.A. and Katsura, T.  
 1964: Chemical Composition of Hawaiian lavas, *Journal of Petrology*, V. 5, p. 82-133.
- Makris, J., Ben Abraham, Z., Behle, A., Ginzburg, A., Giese, P., Steinmetz, L., Whitmarsh, R.B. and Eleftheriou, S.  
 1983: Seismic refraction profiles between Cyprus and Israel and their interpretation, *Geophysical Journal Royal Astronomical Society*, V.75, p. 575-591.

- Malpas, J. and Robinson, P.T.  
 1987: Chromite mineralization in the Troodos ophiolite, Cyprus, *In: Evolution of Chromium Ore Fields*, ed.: C.W. Stone, Van Nostrand - Reinhold Publishers, p. 220-227.
- Malpas, J. and Langdon, G.S.  
 1984: Petrology of the upper pillow lava suite, Troodos ophiolite, Cyprus, *In: Ophiolites and Oceanic Lithosphere*, Ed. by I.G. Gass, S.J. Lippard, and A.W. Shelton, Blackwell Scientific Publications London, p. 155-167.
- Malpas, J., Castaneda, G. and Palagonas, U.  
 1984: Investigations of the geochemistry of some Cyprus lavas from holes CY-1 and CY-2a of the Cyprus Drilling Project, *In: Geological Association of Canada, Mineralogical Association of Canada, Program with Abstracts*, V. 9, p. 86.
- Malpas, J.G.  
 1978: Magma operation in the upper mantle: field evidence from ophiolite suites and application to the generation of oceanic lithosphere, *Philosophical Transactions of the Royal Society of London, Ser. A.*, V. 288, p. 527-546.
- Mantis, M.  
 1971: Paleontological evidence defining the age of the Troodos pillow lava series in Cyprus, *Kypriakos Logos*, #3, p. 202-208.
- Marshall, D.B. and McLaren, A.C.  
 1977: Deformation mechanisms in experimentally deformed plagioclase feldspars, *Journal Material Science*, V. 12, p. 893-903.
- Marshall, D.B. and Wilson, C.J.L.  
 1976: Recrystallization and peristerite formation in albite, *Contributions Mineralogy and Petrology*, V. 57, p. 55-69.
- Marshall, D.B., Vernon, R.H. and Hobbs, B.E.  
 1976: Experimental deformation and recrystallization of a peristerite, *Contributions Mineralogy and Petrology*, V. 57, p. 49-54.
- McBirney, A.R. and Noyes, R.M.  
 1979: Crystallization and layering of the Skaergaard Intrusion, *Journal of Petrology*, V. 20, #3, p. 487-554.
- McLelland, J., Lockhead, A. and Vyhnal, C.  
 1988: Evidence for multiple metamorphic events in the Adirondack Mountain, N.Y., *Journal of Geology*, V.96, p. 279-298.

- Mehegan, J.M. and Robinson, P.T.  
 1984: Regional geochemistry and pyroxene compositions of the Troodos ophiolite lavas: The volcanic evolution of Troodos, In: Geological Association of Canada, Mineralogical Association of Canada, Program with Abstracts, V. 9, p. 88.
- Meijer, A.  
 1980: Primitive arc volcanism and a boninite series: Examples from Western Pacific island arcs, In: The tectonic and geological evolution of Southeast Asian seas and islands, Ed.: D.E. Hayes, American Geophysical Union Geophysical Monograph, V. 23, p. 269-282.
- Menzies, M. and Allen, C.R.  
 1974: Plagioclase lherzolite-residual mantle relationships within two Eastern Mediterranean Ophiolites, Contributions to Mineralogy and Petrology, #45, p. 197-213.
- Mercier, J.C.C.  
 1976: Natural peridotites: chemical and rheological heterogeneity of the upper mantle, Ph.D. Thesis, State University of New York at Stony Brook, p. 718.
- Mercier, J.C.C. and Nicolas, A.  
 1975: Textures and fabrics of upper-mantle peridotites as illustrated by xenoliths from basalts, Journal of Petrology, V. 16, #2, p. 454-487.
- Michaelides, A.  
 1983: On the genesis of chromite deposits of the Troodos plutonic complex, Cyprus, Unpub. Ph.D. Thesis, Faculty of Physics and Mathematics, Dept. of Geology, Technical Highschool, Athens.
- Miyashiro, A.  
 1973: The Troodos ophiolite complex was probably formed in an island arc, Earth and Planetary Science Letter, V. 19, p. 218-224.
- Miyashiro, A.  
 1975a: Origin of the Troodos and other ophiolites: A reply to Hynes, Earth and Planetary Science Letters, V. 25, p. 217-222.
- Miyashiro, A.  
 1975b: Origin of the Troodos and other ophiolites: A reply to Moores, Earth and Planetary Science Letters, V. 25, p. 227-235.

- Moll, N.E.  
 1981: The structure and petrology of the gabbro unit and the mafic-ultramafic contact, Table Mountain, Bay of Islands complex, Newfoundland, Ph.D. Thesis, University of Washington.
- Moore, E.M., Robinson, P.T., Malpas, J. and Xenophontas, C.  
 1984: Model for the origin of the Troodos massif, Cyprus and other mid-east ophiolites, *Geology*, V. 12, p. 500-503.
- Moore, E.M.  
 1982: Origin and emplacement of ophiolites: Reviews of Geophysics and Space Physics, V. 20, p. 735-760.
- Moore, E.M. and Vine, F.J.  
 1971: The Troodos massif, Cyprus and other ophiolites as oceanic crust: evaluation and implications, *Phil. Trans. Roy. Soc. Lond. A*, 268, p. 443-466.
- Morse, S.A.  
 1969: The Kiglapait Layered Intrusion, Labrador, Geological Society of America, Memoir #112, p. 146.
- Murton, B.J.  
 1986: Anomalous oceanic lithosphere formed in a leaky transform fault: evidence from the Western Limassol Forest complex, Cyprus, *Journal of the Geological Society, London*, V. 143, p. 845-854.
- Neyens, M.  
 1986: Deformation at the crust-mantle interface, Table Mountain ophiolite massif, Newfoundland Unpublished M.Sc. Thesis, State University of Utrecht, The Netherlands, p. 87.
- Nicolas, A., and Prinzhofer, A.  
 1983: Cumulative or residual origin of the transition zone in ophiolite: Structural evidence, *Journal of Petrology*, V. 24, part 2, p. 188-206.
- Nicolas, A. and Jackson, M.  
 1982: High temperature dikes in peridotites: Origin by hydraulic fracturing, *Journal of Petrology*, V. 23, #4, p. 568-582.
- Nicolas, A. and Violette, J.F.  
 1982: Mantle flow at oceanic spreading centers: models derived from ophiolites, *Tectonophysics*, #81, p. 319-339.

- Nicolas, A., Boudier, F. and Bouchez, J.L.  
1980: Interpretation of peridotite structures from ophiolitic and oceanic environments, American Journal of Science, #280, p. 192-210.
- Nicolas, A. and Poirier, J.F.  
1976: Crystalline Plasticity and Solid State Flow in Metamorphic Rocks, J. Wiley Interscience, London.
- Nicolas, A., Boudier, F., and Boullier, A.M.  
1973: Mechanisms of flow in naturally and experimentally deformed peridotites, American Journal of Science, V. 273, p. 853-876.
- Nicolas, A. and Jackson, E.D.  
1972: Répartition en deux provinces des peridotites des chaînes alpines longeant la Méditerranée: implications tectoniques: Suisse Min. Pet. Bulletin, V.52, p. 479-495.
- Nicolas, A., Bouchez, J.L., Boudier, F. and Mercier, J.C.  
1971: Textures, structures and fabrics due to solid-state flow in some European lherzolites, Tectonophysics, #12, p. 55-86.
- Nicolas, A.  
1969: Une vue unitaire concernant l'origine des massifs ultrabasiques des Alpes occidentales internes, Académie Science Comptes Rendus, Paris, V.269, p. 1831-1834.
- Norman, R.E. and Strong, D.F.  
1975: The geology and geochemistry of ophiolitic rocks exposed at Mings Bight, Newfoundland, Canadian Journal of Earth Sciences, V.12, p. 777-797.
- Pallister, J.S. and Hopson, C.  
1981: Semail ophiolite plutonic suite: field relations, phase variations, cryptic variation and layering and a model of a spreading ridge magma chamber, Journal Geophysical Research, V.86, p. 2593-2644.
- Panayiotou, A., Michaelides, A. and Georgiann, E.  
1986: The Troodos chromite deposits of the Troodos ophiolite complex, In: Chromites, Theophrastus Publications.
- Pantazis, Th. M.  
1967: The geology and mineral resources of the Pharmakas-Kalavassos area, Cyprus Geological Survey Memoir, #8, p. 190.



- Pearce, J.A.  
 1980: Geochemical evidence for the genesis and eruptive setting of lavas from Tethyan ophiolites, *In: Panayiotou, A., (ed), Ophiolites: International Ophiolite Symposium, Cyprus, 1979, Proceedings, p. 261-272.*
- Pearce, J.A.  
 1975: Basalt geochemistry used to investigate past tectonic environments on Cyprus, *Tectonophysics, V.25, p. 41-67.*
- Pearce, J.A. and Cann, J.R.  
 1973: Tectonic setting of basic volcanic rocks determined using trace element analyses, *Earth and Planetary Science Letters, #19, p. 290-300.*
- Pearce, J.A. and Cann, J.R.  
 1971: Ophiolite origin investigated by discriminant analyses using Ti, Zr and Y, *Earth and Planetary Science Letters, #12, p. 339-349.*
- Peterman, Z.E., Coleman, R.G., and Hildreth, R.A.  
 1971: Sr87/Sr86 in mafic rocks of the Troodos massif, Cyprus, *United States Geological Survey Professional Paper 750-D, p. 157-161.*
- Poirer, J.P. and Nicholas, A.  
 1975: Deformation induced recrystallization due to progressive misorientation of subgrains with special reference to mantle peridotites, *Journal of Geology, V.83, p. 707-720.*
- Post, R.  
 1973: The flow of Mt. Barnette dunite, *Ph.D. Thesis, University of California, Los Angeles, p. 272.*
- Raleigh, C.B.  
 1965: Structural and petrology of an alpine peridotite on Cypress Island, Washington, USA, *Contributions to Mineralogy and Petrology, #11, p. 719-741.*
- Rathbone, P.A., Coward, M.P. and Harris, A.L.  
 1983: Cover and basement: A contrast in style and fabrics, *In: Contributions to the tectonics and geophysics of Mountain Chains, Ed.: R.D. Hatcher, H. Williams and I. Zeith, Geological Society of America Memoir #158, p. 213-223.*

- Rautenschlein, M., Jenner, G.A., Hertogen, J., Hofmann, A.W., Kerrich, R., Schmincke, H.U. and White, W.M.  
 1985: Isotopic and trace element composition of volcanic glasses from the Akaki Canyon, Cyprus: Implications for the origin of the Troodos Ophiolite, Earth and Planetary Science Letters, V.75, p. 369-383.
- Ricou, L.E.  
 1971: Le Croissant Ophiolitique Peri-Arabe, une Ceinture de Nappes Mises en Place au Crétacé Supérieur. Revue De Géographie Physique et de Géologie Dynamique (2), V.13, #4, p. 327-350.
- Ringwood, A.E.  
 1966: Chemical evolution of the terrestrial planets, Geochem. Cosmochim. Acta 30, p. 41-104.
- Robertson, A.H.F. and Woodcock, N.H.  
 1980: Tectonic setting of the Troodos massif in the east Mediterranean: In: Panayiotou, A., ed. Ophiolites: International Ophiolite Symposium, Cyprus, Panayiotou, A., ed. 1979, Proceedings p. 36-49.
- Robertson, A.H.F.  
 1977: The Kannaviou Formation, Cyprus: volcanoclastic sedimentation of a probable late Cretaceous volcanic arc, Journal of Geological Society of London, #134, p. 269-292.
- Robertson, A.H.F.  
 1976: Pelagic chalks and calciturbidites from the lower Tertiary of the Troodos massif, Cyprus, Journal of Sedimentary Petrology, V.46, #4, p. 1007-1016.
- Robertson, A.H.F.  
 1975: Cyprus umbers: basalt - sediment relationships on a Mesozoic ocean ridge, Geological Society of London Journal, V. 131, p. 511-531.
- Robertson, A.H.F., and Hudson, J.D.  
 1974: Pelagic sediments in the Cretaceous and Tertiary history of the Troodos massif, Cyprus, International Association Sedimentology Special Publication, #1, p. 403-436.
- Robinson, P.T., Panayiotou, A., Xenophontos, C., Constantinou, G., and Malpas, J.  
 1986: The Geology and tectonic setting of the Troodos ophiolite, Cyprus. (in prep.)

- Robinson, P.T., Melson, W.G., O'Hearn, T., Schmincke, H.U.  
 1983: Volcanic glass compositions of the Troodos ophiolite, Cyprus, *Geology*, V.11, p. 400-404.
- Rosencrantz, E.  
 1983: The structure of sheeted dikes and associated rocks in North Arm Mountain Massif, Bay of Islands ophiolite, and the intrusive process at oceanic spreading centers: *Canadian Journal of Earth Science*, V.20, p. 787-801.
- Saunders, A.D., Tarney, J., Marsh, H.G., and Wood, D.A.  
 1980: Ophiolites as ocean crust or marginal basin crust: A geochemical approach, *In*: Panayiotou, A., ed., *Ophiolites, International Ophiolite Symposium, Cyprus, 1979, Proceedings*, p. 193-204.
- Schmidt, E.R.,  
 1952: The structure and composition of the Merensky Reef and associated rocks of the Rustenburg Platinum Mine, *Transactions Geological Society of South Africa*, V.55, p. 233-280.
- Schmincke, H.U., Rautenschlein, M., Robinson, P.T., and Mehegan, J.M.  
 1983: Troodos extrusive series of Cyprus: A comparison with oceanic crust, *Geology*, V.11, p. 405-409.
- Searle, M.P.  
 1980: The metamorphic sheet and underlying volcanic rocks beneath the Semail Ophiolite in the Northern Oman Mountains of Arabia, Unpub. Ph.D. Thesis, Open University, England, p. 213.
- Secher, D.  
 1981: Les Iherzolites ophiolitiques de Nouvelle - Calédonie et leurs gisements de chromite, *These Doct. Spec. Univ. Nantes*.
- Seifert, K.E. and Verploeg, A.J.  
 1977: Deformational characteristics of experimentally deformed Adirondack anorthosite, *Canadian Journal of Earth Science*, V.14, p. 2706-2717.
- Shelley, D.  
 1979: Plagioclase preferred orientation in Foreshore Group Metasediments, Bluff, New Zealand, *Tectonophysics*, V.58, p. 279-290.
- Shelley, D.  
 1977: Plagioclase preferred orientation in Hoast Schist, New Zealand, *Journal of Geology*, V.85, p. 635-644.

- Shelton, A.W. and Gass, I.G.  
 1980: Rotation of the Cyprus microplate, In: Panayiotou, A. (ed.), Ophiolites: International Ophiolite Symposium, Cyprus, Proceedings, p. 61-65.
- Simonian, K.O. and Gass, I.G.  
 1978: Arakapas Fault Belt, Cyprus: A fossil transform fault, Geological Society America Bulletin, V.89, p. 1220-1230.
- Smewing, J.D., Simonian, K.O., and Gass, I.G.  
 1975: Metabasalts from the Troodos massif, Cyprus: Genetic Implications deduced from petrography and trace element geochemistry, Contributions Mineralogy Petrology, #51, p. 49-64.
- Smewing, J.D.  
 1975: Metamorphism of the Troodos massif, Cyprus, Unpubl. Ph.D. Thesis, Open University, England.
- Spooner, E.T.C.  
 1977: Hydrothermal model of the origin of the ophiolitic cupriferous pyrite ore deposits of Cyprus, Geological Society of London, Special Publication, #7, p. 58-71.
- Spray, J.G. and Roddick, J.C.  
 1981: Evidence for upper Cretaceous transform fault metamorphism in West Cyprus, Earth and Planetary Science Letters, V.55, p. 273-291.
- Staudigel, H., Gillis, K.M., and Robinson, P.T.  
 1984: Isotopic Composition of some Secondary Phases in the Troodos Ophiolite, Cyprus, In: Program with Abstracts, Geological Association of Canada, Mineralogical Association of Canada, V.19, p. 108.
- Swarbrick, R.E.  
 1980: The Mamonia Complex of S.W. Cyprus: a Mesozoic continental margin and its relationship to the Troodos Complex. In: Panayiotou, A. ed., Ophiolites: International Ophiolite Symposium, Cyprus, 1979, Proceedings p. 86-92.
- Talkington, R. and Malpas, J.  
 1980: Spinel phases of the White Hills peridotite, St. Anthony complex, Newfoundland: Part 1 occurrence and chemistry, In: Panayiotou, A. (ed.), Ophiolite: International Ophiolite Symposium, Cyprus, 1979, Proceedings, p. 607-619.

- Thayer, T.P.  
1980: Syncrystallization and subsolidus deformation in ophiolite peridotite and gabbro, *American Journal of Science*, V.280-A, p. 269-283.
- Tullis, J.A.  
1979: High temperature deformation of rocks and minerals, *Reviews of Geophysics and Space Physics*, V.17, #6, p. 1137-1154.
- Turner, W.M.  
1973: The Cyprian gravity nappe and the autochthonous basement of Cyprus, *In: Gravity and Tectonics*, K.A. DeJong and R. Scholten, Ed., Wiley and Sons, London, p. 287-301.
- Turner, W.M.  
1971: Geology of the Polis-Kathikas area, Cyprus, Ph.D. Thesis, University of New Mexico, p. 430.
- Varga, R.J. and Moores, E.M.  
1985: Spreading structure of the Troodos ophiolite, Cyprus, *Geology*, V.13, p. 846-850.
- Verosub, K.L. and Moores, E.M.  
1981: Tectonic rotations in extensional regimes and their paleomagnetic consequences for oceanic basalts, *Journal of Geophysical Research*, V.86, p. 6335-6349.
- Vernon, R.H.  
1975: Deformation and recrystallization of a plagioclase grain, *American Mineralogist*, V.60, p. 884-888.
- Wadsworth, N.J.  
1985: Layered intrusions - a fluid situation, *Geology Today*, Mar-Apr., p. 50-54.
- Wager, L.R., Brown, G.M., and Wadsworth, W.J.  
1960: Types of igneous cumulates, *Journal of Petrology*, #1, p. 73-85.
- Wager, L.R. and Deer, W.A.  
1939: Geological investigations in East Greenland, Part III, The petrology of the Skaergaard intrusion, Kangerdlugssuag, East Greenland, *Medd. om Gronland*, V.105, p. 352.
- Weiler, Y.  
1970: Mode of occurrence of pelites in the Kythrea flysch basin (Cyprus), *Journal of Sedimentary Petrology*, V.40, p. 1255-1261.

- White, S.  
1977: Geological significance of recovery and recrystallization processes in quartz, *Tectonophysics*, #39, p. 143-170.
- White, S.  
1976: The effects of strain on the microstructures, fabrics and deformation mechanisms in quartzites, *Phil. Trans. Roy. Soc. Lond. A*, #283, p. 69-86.
- White, S.  
1975: Tectonic deformation and recrystallization of oligoclase, *Contributions Mineralogy and Petrology*, V.50, p. 287-304.
- Wilson, R.A.M.  
1959: The geology of the Xeros - Troodos area, *Cyprus Geological Survey Memoir*, #1, p. 184.
- Wood, D.A., Joron, J.L., Marsh, N.G., Tarney, J. and Trevil, M.  
1980: Major and trace element variations in basalts from the North Phillippine Sea, drilled during D.S.D.P. Leg. 58: A comparative study of back-arc-basin basalts with lava series from Japan and mid ocean ridges, in Klein, G., DeVriers, Kobayashi, K. et.al, *Initial Reports of the D.S.D.P.*, V.58, Washington, DC, US Government Printing Office, p. 873-894.
- Woodcock, N.H. and Robertson, A.H.F.  
1977: Imbricate thrust belt tectonics and sedimentation as a guide to emplacement of part of the Antalya Complex, S.W. Turkey, *Proceedings 6th Coll. Geol. Aegean Region Izmir*.
- Xenophontos, C., and Afrodisis, S.  
An extension of the Arakapas Fault Belt into western Cyprus and its implications for the emplacement of the Troodos ophiolite (In. Prep.)
- Zwart, H.J.  
1958: La Faillede Mérens dans les Pyreneés Ariégeoises, *Society geological Bulletin of France*, V.8, p. 794-796.

## APPENDIX A

Microprobe analyses of the clinopyroxene, orthopyroxene, plagioclase and olivine phases for the layered olivine gabbro. C = core, R = rim, O = no description, Z = zone, Cr = Cr<sup>2+</sup>/Cr<sup>3+</sup> (Mol %), Cr = Cr<sup>2+</sup>/Cr<sup>3+</sup> (Mol %), An = anorthite component; Fo = forsterite component.

## A.1. CLINOPYROXENE

Identifier	Na	Mg	Al	Si	K	Ca	Ti	Cr	Mn	Fe	Ni	TOTAL	Mg <sup>2+</sup>	Cr <sup>2+</sup>
4560	O	16.67	2.11	52.68	-	23.31	.18	.05	.12	4.99	.08	100.57	85.61	.91
	O	17.09	1.34	53.92	-	23.50	.16	.08	.13	4.93	.02	101.29	86.06	1.46
	C	16.87	3.22	51.96	.02	21.66	.20	.06	.14	5.39	.03	99.37	84.79	1.36
	R	16.00	1.96	53.45	-	23.29	.20	.13	.17	5.29	.03	100.71	84.35	2.26
4561	C	16.18	1.88	53.84	-	23.54	.17	.12	.17	5.24	.05	101.34	85.24	2.08
	R	16.86	2.02	53.78	.01	22.93	.18	.12	.13	4.99	.01	101.21	85.76	2.20
	O	16.89	1.37	54.37	.01	22.55	.18	.05	.16	4.89	.05	100.67	86.02	.93
	O	16.82	1.23	53.43	.01	24.00	.12	.08	.17	4.52	.03	100.54	86.89	1.60
4563	O	16.16	1.53	53.50	-	23.12	.22	.13	.18	5.08	.03	100.11	84.99	2.32
	O	16.43	1.25	52.68	-	23.42	.15	.09	.16	4.75	.01	99.06	86.03	1.72
	C	15.60	2.19	53.27	-	22.81	.23	.10	.12	5.15	.01	99.59	84.37	1.78
	R	16.63	1.43	53.82	.01	22.72	.20	.13	.11	5.28	.04	100.55	84.88	2.27
4564	O	16.50	1.50	53.77	-	22.09	.20	.15	.10	5.07	-	99.48	85.29	2.72
	C	16.57	1.66	52.57	-	22.93	.21	.14	.16	5.33	.07	98.84	84.71	2.40
	O	16.27	1.75	53.93	-	23.60	.20	.10	.14	5.06	.10	101.08	85.13	2.35
	C	16.65	1.53	52.85	-	22.87	.20	.10	.17	5.41	.01	99.93	84.50	2.19
	O	16.22	1.94	53.01	-	22.89	.22	.05	.20	5.22	.05	99.99	84.70	.86
	R	16.42	1.59	53.45	-	22.69	.22	.09	.18	5.35	.01	99.89	84.76	1.56
	R	16.71	1.41	52.69	-	23.43	.20	.13	.12	4.96	.02	99.78	85.71	2.60
	C	16.48	1.57	53.04	-	21.90	.21	.08	.16	5.23	.02	98.79	84.88	1.40
	C	16.34	1.21	54.23	.01	22.74	.20	.11	.15	4.83	.04	100.04	85.77	2.07
4565	C	17.39	1.45	52.98	.01	20.45	.17	.11	.07	5.42	.05	98.83	84.64	1.82
	R	16.73	2.73	52.11	-	20.65	.12	.11	.12	5.31	.04	98.32	84.40	1.84
	C	16.52	1.27	53.82	-	22.15	.02	.14	.15	5.14	.05	99.46	85.13	2.44
	R	17.06	1.39	53.24	-	21.13	.02	.09	.14	5.59	.02	98.88	84.46	1.48
	C	16.47	1.64	53.79	.02	23.11	.22	.13	.17	5.40	.00	101.24	84.46	2.19
	C	17.35	1.87	53.19	.01	21.25	.20	.12	.17	6.26	.04	101.03	83.16	1.75



## APPENDIX A (Cont'd)

## 1.A. GLIOPTEROLITE (Cont'd)

Identifier	Na	Mg	Al	Si	K	Ca	Ti	Cr	Mn	Fe	Ni	TOTAL	Mg*	Cr*
4566														
O	.18	16.71	2.02	53.34	.01	23.12	.16	.11	.19	4.99	.05	100.90	85.44	1.99
O	.16	16.71	1.79	53.70	-	23.27	.18	.14	.18	5.29	.01	101.43	84.91	2.40
C	.22	16.48	1.87	52.91	.01	22.66	.18	.07	.16	5.19	.04	99.81	84.98	1.35
R	.23	16.61	1.74	53.47	.01	22.84	.18	.12	.15	5.31	.01	100.68	84.76	2.07
4567														
O	.20	16.38	1.70	52.50	-	22.30	.20	.13	.13	5.24	-	98.77	84.78	2.37
C	.13	16.53	2.04	53.76	-	23.23	.13	.11	.19	4.88	.02	101.04	85.78	2.04
R	.19	17.02	2.23	54.30	-	21.71	.12	.09	.14	5.45	.04	101.27	84.77	2.02
O	.15	16.44	1.36	54.70	.01	22.64	.16	.11	.18	4.82	-	100.58	85.87	2.07
4568														
C	.18	16.63	1.86	54.23	-	22.50	.22	.13	.08	5.48	-	101.30	84.40	2.20
C	.16	17.04	1.79	52.61	-	22.95	.26	.17	.11	5.52	-	100.62	84.61	2.84
C	.18	16.45	1.90	53.63	.01	22.29	.28	.18	.23	5.94	.05	101.15	85.15	2.73
4570														
O	.19	17.37	2.04	54.23	-	22.29	.19	.12	.16	4.70	-	101.27	86.81	2.32
O	.18	17.14	1.90	54.82	.01	21.37	.24	.08	.15	5.26	.05	101.21	85.30	1.39
C	.20	17.36	2.10	52.19	.01	21.81	.16	.09	.17	5.34	.05	99.47	85.27	1.53
R	.10	17.43	2.12	53.39	-	21.73	.20	.09	.22	5.39	.01	100.77	84.73	1.45
4571														
C	.19	16.63	1.78	53.73	-	23.17	.21	.15	.20	4.79	.02	100.87	86.07	2.82
R	.07	17.47	2.09	52.80	-	21.89	.17	.16	.14	6.29	-	101.08	85.19	2.33
O	.20	23.13	1.70	55.29	-	21.13	.17	.15	.18	8.11	.02	101.07	85.55	1.70
O	.21	16.60	1.70	53.46	-	23.21	.20	.14	.15	5.04	.04	100.75	85.44	2.53
4572														
C	.19	16.88	1.83	53.11	-	21.45	.23	.12	.17	5.42	.01	99.39	84.73	2.02
R	.14	16.80	1.57	53.98	-	22.98	.21	.05	.12	4.84	.01	100.71	86.08	.95
O	.18	16.47	1.78	53.79	-	22.33	.22	.17	.20	5.55	-	100.70	84.09	2.78
O	.13	16.73	1.79	53.21	-	22.23	.24	.12	.09	5.48	.07	100.10	84.47	2.02
O	.18	16.56	1.57	51.90	-	22.91	.18	.13	.19	5.32	.03	98.99	84.72	2.21
4573														
O	.16	16.90	1.83	54.14	-	21.09	.03	.07	.15	5.23	.03	99.63	85.21	1.22
O	.10	16.05	1.68	54.31	-	19.24	.03	.08	.17	6.40	.03	100.09	83.41	1.44
O	.09	16.80	1.18	54.42	-	22.73	.11	.08	.11	4.88	.01	100.22	86.48	1.57
O	.13	16.72	1.23	54.97	.01	22.74	.17	.12	.09	5.02	-	101.21	85.58	2.38
4574														
R	.24	16.57	1.84	53.15	-	22.47	.17	.09	.16	5.19	.03	99.93	85.05	1.58
C	.14	16.14	2.57	51.94	-	21.54	.14	.16	.11	5.45	.05	98.24	84.07	2.70
C	.14	16.88	1.27	53.53	.01	24.10	.23	.10	.11	4.80	-	101.16	84.23	2.49
R	.21	16.43	1.37	52.40	-	23.65	.21	.15	.20	4.63	-	99.26	86.34	2.92

## APPENDIX A (Cont'd)

1.A. GLIMMETHIONE (Cont'd)

Identifier	Na	Mg	Al	Si	K	Ca	Ti	Cr	Mn	Pb	NI	TOTAL	Mg*	Cr*
4375	C	.14	16.41	1.74	53.36	.02	21.80	.20	.08	.16	-	99.26	84.55	1.37
	R	.16	17.33	2.57	53.38	-	21.30	.22	.08	.12	-	100.55	85.11	1.34
	O	.12	17.18	1.75	53.73	-	21.89	.21	.07	.20	.01	100.37	85.48	1.22
	C	.13	16.68	1.58	54.16	-	21.91	.22	.11	.14	-	100.50	84.26	1.82
	C	.18	16.77	1.93	54.30	-	22.71	.20	.16	.14	-	101.36	85.79	3.31
4376	R	.19	16.96	1.82	54.27	-	22.20	.19	.16	.16	.07	100.48	86.64	3.11
	C	.10	17.50	1.88	52.45	-	22.05	.22	.13	.19	.04	100.12	84.99	2.14
	R	.18	16.96	1.93	53.96	.01	22.89	.22	.15	.11	.03	101.54	85.60	2.72
	C	.14	16.41	1.74	53.36	.02	21.80	.20	.08	.16	-	99.26	84.55	1.37
	R	.16	17.33	2.57	53.38	-	21.30	.22	.08	.12	-	100.55	85.11	1.36
4378	O	.12	17.18	1.75	53.73	-	21.89	.21	.07	.20	.01	100.37	85.45	1.22
	O	.13	16.68	1.58	54.16	-	21.91	.22	.11	.14	-	100.50	84.26	1.82
	C	.17	15.44	1.83	53.90	-	20.63	.20	.08	.13	.05	101.40	84.52	1.22
	R	.16	16.82	1.83	52.47	.01	22.66	.22	.10	.17	-	99.73	84.98	2.23
	C	.16	16.55	1.72	54.38	-	23.08	.22	.12	.18	-	101.50	85.26	2.14
4380	O	.21	16.82	1.82	54.37	.01	22.55	.19	.09	.14	.05	101.50	85.10	1.57
	C	.20	16.85	1.71	53.95	-	22.55	.20	.09	.22	.03	100.91	84.45	1.99
	R	.24	16.52	1.68	53.75	.02	21.26	.23	.13	.13	.02	99.56	84.04	2.14
	C	.29	17.35	1.61	53.10	-	21.98	.18	.10	.16	.04	100.37	84.72	2.13
	O	.18	16.95	1.64	54.33	-	22.24	.20	.09	.13	.02	100.83	85.68	1.63
4383	R	.12	17.33	1.78	54.20	-	21.38	.22	.04	.18	.02	101.08	84.13	.43
	C	.16	16.54	1.87	55.09	-	20.96	.22	.11	.14	.05	101.36	82.61	1.63
	O	.12	17.45	1.91	54.37	-	20.80	.09	.09	.20	.01	101.15	83.59	1.34
	O	.15	18.21	1.88	54.46	-	19.66	.18	.09	.12	.01	101.75	82.31	1.19
	C	.22	17.41	1.82	52.70	.01	21.31	.22	.11	.13	.05	100.15	83.41	1.64
4386	R	.20	17.44	1.73	53.81	-	21.58	.22	.10	.16	.07	101.10	84.32	2.04
	O	.15	16.82	1.72	53.69	.02	21.78	.11	.05	.17	.03	100.82	83.41	.76
	O	.18	16.74	1.69	52.73	-	21.45	.16	.07	.17	.07	99.30	83.18	1.04
	R	.22	16.72	1.59	54.20	-	21.54	.23	.11	.09	.04	99.84	85.46	2.01
	C	.25	16.98	1.79	53.39	-	21.90	.20	.11	.19	.05	99.96	85.60	1.25
4390	R	.18	16.69	1.45	53.72	-	22.15	.21	.13	.15	.08	99.99	85.07	2.27
	C	.10	17.31	1.78	52.23	-	21.11	.15	.09	.18	.03	98.66	84.45	1.44

APPENDIX A (Cont'd)

1.A. CLINOPTILOIDE (Cont'd)

Identifier		Na	Mg	Al	Si	K	Ca	Ti	Cr	Mn	Fe	Ni	TOTAL	Mg*	Cr*
4588	C	.22	16.88	1.96	52.90	-	22.46	.18	.09	.18	5.46	-	100.52	84.17	1.45
	R	.12	16.69	1.67	54.29	.01	22.56	.18	.11	.18	5.06	.04	100.91	84.45	1.97
	C	.09	17.3	1.82	53.70	.01	21.97	.20	.13	.12	5.29	.05	101.86	84.42	2.10
	C	.12	16.39	1.76	54.45	-	22.70	.18	.07	.15	5.45	.05	101.32	84.27	1.13
4589	C	.24	16.43	1.77	54.29	-	22.66	.28	.10	.15	5.56	-	101.46	84.04	2.18
	C	.19	16.75	1.86	53.45	-	21.41	.18	.16	.13	5.49	.07	99.68	84.45	2.66
	R	.16	17.41	1.78	53.39	.01	22.18	.23	.15	.22	5.71	.01	101.28	84.46	2.38
	C	.23	16.67	1.71	52.77	-	22.60	.21	.11	.18	5.35	.04	99.87	84.74	1.87
	R	.19	16.11	1.84	54.50	-	21.81	.20	.10	.14	5.61	-	100.51	83.66	2.12
	C	.01	18.05	2.20	53.30	.01	19.41	.23	.09	.16	6.45	.01	99.92	83.30	1.20
4590	O	.19	17.25	1.89	53.52	-	22.22	.11	.20	.20	5.60	.04	101.21	84.58	3.31
	O	.18	17.54	1.91	53.92	-	20.88	.20	.25	.20	5.48	.08	100.61	85.08	4.12
	R	.20	16.90	1.89	53.86	-	22.21	.18	.24	.18	5.91	.02	99.61	88.50	5.52
	C	.26	17.09	2.33	53.72	-	21.84	.22	.20	.20	5.54	.02	101.43	84.60	3.28
4591	O	.11	15.43	1.85	52.77	.01	22.34	.13	.21	.18	5.45	.02	98.50	83.46	3.50
	O	.16	16.97	2.02	53.02	-	20.43	.20	.24	.14	6.06	.03	99.26	83.30	3.64
	O	.24	16.22	1.81	52.98	-	22.73	.20	.10	.12	5.40	-	99.82	84.26	2.21
	O	.20	16.32	1.75	53.34	-	23.06	.21	.13	.18	5.48	-	100.69	84.15	2.16
	O	.22	15.95	1.87	51.86	-	22.65	.21	.13	.20	5.36	-	98.45	84.12	2.20
4592	C	.18	15.98	1.82	52.64	.01	23.16	.27	.25	.16	4.89	.05	99.41	85.34	4.63
	R	.18	16.43	1.43	52.50	-	22.75	.20	.15	.12	5.28	.04	99.07	84.73	2.61
	C	.16	17.79	1.91	52.77	.01	20.64	.23	.17	.13	6.13	.01	99.95	83.79	2.56
	C	.14	17.00	1.72	52.92	-	21.02	.20	.13	.15	5.55	-	98.84	84.51	2.14
4593	O	.20	17.58	1.82	54.77	-	20.99	.22	.04	.12	5.71	.04	101.48	84.58	.65
	O	.22	17.11	1.68	53.82	.03	20.32	.17	.07	.14	5.67	.04	99.25	84.31	1.13
	C	.21	16.32	1.82	53.66	-	23.00	.18	.08	.17	5.25	.03	100.72	84.71	1.38
	R	.18	16.52	1.46	54.28	-	23.88	.17	.07	.15	4.94	-	101.66	85.63	1.29
4595	C	.07	16.43	1.49	52.38	-	23.16	.16	.05	.14	5.18	-	99.05	84.97	.88
	R	.20	16.21	1.90	53.05	.01	22.52	.18	.08	.18	5.35	.02	99.70	84.37	1.36
	C	.20	16.59	1.68	53.76	-	21.53	.20	.10	.16	5.46	.02	99.70	84.42	2.17
	R	.12	17.15	1.62	52.43	-	22.56	.21	.15	.17	5.45	-	99.86	84.87	2.51
	C	.12	17.26	1.79	53.68	-	21.27	.20	.02	.11	5.76	-	100.21	84.23	.32
	R	.19	17.60	1.70	53.68	.02	21.19	.22	.11	.17	5.86	-	100.71	84.26	1.72

## APPENDIX A (Cont'd)

## I.A. GLIMPSPROBES (Cont'd)

Identifier	Na	Mg	Al	Si	K	Ca	Ti	Cr	Mn	Fe	Ni	TOTAL	Mg*	Cr*
4596	C	.25	16.88	1.49	52.57	-	22.30	.21	.09	4.71	.06	98.75	86.46	1.72
	R	.26	16.69	1.68	54.02	-	22.29	.23	.05	4.63	.07	99.91	86.38	.97
	C	.24	16.73	1.60	52.98	-	21.90	.16	.05	5.27	.03	99.17	84.87	.84
	R	.01	16.69	.68	54.11	.01	23.30	.09	.01	3.95	.05	99.05	88.28	.23

APPENDIX A (Cont'd)

A.2

OSTROPTERODON

Identifier		Na	Mg	Al	Si	K	Ca	Ti	Cr	Mn	Fe	Ni	TOTAL	Mg*
4572	O	-	30.07	1.36	56.27	.01	1.12	.06	-	.25	12.53	.04	99.71	81.05
	O	.02	28.64	1.18	55.10	-	1.60	.15	.06	.29	12.55	-	99.60	79.81
	O	-	29.39	1.10	56.72	-	1.18	.11	.05	.18	12.91	.01	101.65	80.22
	C	.01	28.62	1.04	55.39	-	1.53	.09	.08	.30	12.87	.05	99.97	79.85
	B	-	29.77	1.23	55.63	.01	1.18	.15	.06	.28	12.56	.05	100.92	80.86
4574	O	.07	24.27	7.97	51.60	-	3.84	.05	.07	.16	10.78	-	98.92	80.05
	R	.05	27.21	3.74	54.49	-	1.02	.07	.08	.31	12.08	.05	99.11	80.06
	C	.07	29.11	1.29	54.36	-	.81	.10	.05	.31	13.08	.01	99.21	79.86
	O	-	28.29	1.10	55.86	-	2.09	.09	.08	.15	12.69	.04	100.38	79.89
4588	C	-	29.45	1.20	56.59	-	1.25	.10	.06	.31	12.51	.04	101.50	80.75
	R	.01	28.77	1.18	55.61	.02	1.46	.10	.05	.16	12.53	.03	99.92	80.36
	O	.02	28.28	1.18	54.96	-	1.44	.10	.09	.30	13.13	.03	99.54	79.32
	O	.02	28.60	1.01	55.21	-	1.20	.11	.09	.34	12.86	-	99.45	79.85
4593	R	.01	28.25	1.19	55.03	.02	1.15	.12	.01	.29	12.54	.05	98.65	80.05

APPENDIX A (Cont'd)

A.3

PLAGIOCLASE

Identifier		Na	Mg	Al	Si	K	Ca	Ti	Cr	Mn	Fe	NI	TOTAL	An
4340	C	1.12	.03	33.29	45.95	.01	18.31	.02	.02	.04	.36	.01	99.14	95.20
	R	.98	.02	32.73	46.08	-	18.55	-	.05	.02	.31	.04	98.78	95.40
	O	1.04	.02	33.26	46.47	-	18.60	.01	.01	.01	.38	-	99.80	95.20
	O	1.05	.05	33.22	45.91	-	18.83	.03	.07	-	.38	-	99.54	95.20
4341	C	.99	-	33.20	46.27	-	19.21	.02	-	.03	.37	-	100.07	95.54
	R	.96	-	32.65	46.21	-	18.83	.01	.03	.02	.39	.01	99.13	95.58
	O	.97	.02	33.16	46.79	.01	18.58	-	.02	-	.30	.01	99.87	95.48
	O	.98	.02	33.22	46.57	-	18.78	.02	-	-	.32	.02	99.95	95.49
4343	O	1.07	.03	32.78	45.79	-	18.59	.01	.02	.03	.36	.07	98.74	95.06
	O	1.05	.04	33.22	45.75	.02	18.46	-	-	.01	.31	.01	98.88	95.10
	O	1.14	.02	32.81	45.68	-	18.71	-	.01	.02	.41	.03	98.84	96.77
	R	1.04	.01	32.80	46.04	.02	18.94	-	-	.01	.36	.03	99.26	95.26
	C	.89	.03	32.53	45.84	-	18.80	.01	-	-	.35	-	98.46	95.89
4344	C	1.12	.01	32.93	46.39	.01	18.13	-	-	.03	.36	-	98.96	95.26
	C	1.11	.05	32.43	45.78	-	18.99	-	-	.02	.39	.03	98.81	96.96
	R	.89	.02	33.20	46.34	.01	18.94	-	.02	-	.36	-	98.78	95.91
	O	1.02	.02	32.99	46.79	-	18.23	.02	-	.01	.41	-	99.51	95.20
4345	C	.89	-	32.87	45.48	.01	19.20	-	-	-	.33	.02	98.81	95.98
	R	1.30	-	33.30	46.88	.03	18.58	.01	.08	.01	.40	.05	100.65	96.04
	O	.94	.05	33.09	46.97	.01	18.63	-	.07	.07	.39	.05	100.26	95.63
	O	1.07	-	33.60	46.28	-	18.29	.05	-	.01	.38	.04	98.72	96.97
	O	1.04	.04	33.46	46.30	.02	18.86	.02	-	.06	.41	.04	100.23	95.20
4346	O	1.16	.02	33.11	46.04	.01	18.61	.03	.03	-	.36	-	99.37	96.64
	O	1.01	.04	32.70	46.50	.01	18.28	.01	-	-	.41	-	98.96	95.23
	C	1.27	.02	32.69	46.37	-	17.93	-	-	.01	.41	-	98.70	93.97
	R	.99	.07	33.24	46.25	-	18.17	.01	.01	-	.43	-	99.17	95.30
4347	R	1.31	.03	33.02	48.03	-	17.58	.02	.04	-	.39	.02	100.44	91.70
	C	1.15	.04	33.26	46.71	.01	18.24	.01	.02	.04	.32	.01	99.80	96.60
	O	.99	.03	33.46	46.79	.02	19.14	-	-	.03	.36	-	100.82	95.60
	O	1.15	.02	32.45	46.89	-	18.68	-	-	.04	.29	-	99.53	96.70

APPENDIX A (Cont'd)

43

PLASTOCLASE (Cont'd)

Identifier		Na	Mg	Al	Si	K	Ca	Ti	Cr	Mn	Fe	Ni	TOTAL	An
4568	O	1.17	.04	32.60	46.95	-	17.91	-	-	-	.36	.03	99.07	94.40
	O	1.05	.04	33.11	46.56	.02	18.41	-	-	-	.42	.03	99.63	96.40
	O	.94	.04	33.44	46.88	-	18.64	-	.02	.06	.46	.01	100.50	95.63
	O	1.13	.01	33.61	46.89	-	18.15	-	.03	.04	.28	.03	100.06	94.63
	O	.86	.04	33.13	47.24	.01	18.28	-	-	.01	.46	.07	100.10	95.90
4570	C	1.02	.01	33.59	47.28	.01	17.96	-	.01	-	.39	.05	100.31	95.10
	C	1.02	.04	33.73	46.32	-	18.11	.03	-	-	.39	-	99.65	95.10
	O	.94	.02	33.76	47.57	.01	17.96	-	-	.03	.42	.03	100.75	95.40
	O	.97	.04	33.84	45.87	-	18.68	.01	-	-	.36	.02	99.80	95.50
4571	C	1.06	.04	33.69	47.07	.01	18.65	-	-	.02	.33	.05	100.93	95.10
	R	.93	-	34.07	46.26	-	19.18	.03	.03	.01	.34	-	100.88	95.79
	C	.96	.04	33.35	46.84	.01	18.20	-	-	-	.15	.03	99.58	95.44
	R	1.04	.02	33.40	46.17	-	18.29	-	.04	-	.44	.03	99.45	95.10
	C	.95	.03	33.29	46.98	.01	18.31	.02	-	-	.41	.01	100.00	95.50
	C	.91	-	33.57	46.83	-	18.04	-	.01	-	.33	.03	100.52	95.81
	C	.82	-	33.32	46.76	.02	18.13	-	.05	.02	.32	-	99.45	96.06
	Z	.98	.02	33.88	46.91	-	18.52	.01	.02	.03	.37	.04	100.77	95.41
4572	O	.94	.04	33.44	46.60	.01	18.16	-	.01	.03	.28	.05	99.55	95.52
	C	1.07	.03	32.61	46.38	-	18.21	.01	-	.01	.21	.03	98.55	94.94
	R	1.15	-	32.64	46.10	.01	18.18	-	.04	.01	.40	-	98.54	94.58
	C	.92	.05	33.05	46.24	.01	18.07	.02	.01	.01	.30	.04	98.72	95.59
4574	C	1.20	.03	32.71	46.11	.01	18.45	.01	.01	-	.35	.03	98.41	94.43
	R	1.13	.02	33.04	45.70	.01	18.94	.01	.05	.04	.37	.01	99.31	94.86
	O	1.13	.04	31.98	45.81	-	19.09	.01	.02	-	.41	-	98.48	94.91
	O	1.30	.02	32.82	45.99	-	18.80	.01	-	-	.43	.05	99.43	94.09
4575	C	1.17	.03	32.89	45.20	.02	19.08	.03	.02	.01	.42	.01	98.87	94.74
	R	1.01	.02	33.01	46.09	-	18.65	-	.02	-	.31	.01	99.12	95.33
	C	1.16	.04	33.32	47.07	.01	18.26	.03	-	-	.30	-	100.19	94.54
	R	.79	.13	33.24	45.98	-	18.02	.01	-	-	.49	.05	98.73	96.18
	O	1.27	.01	33.03	47.50	.02	18.57	.03	-	.02	.41	-	100.84	94.17
4576	C	1.09	.02	32.91	46.71	.02	18.67	-	.02	-	.30	.03	99.79	96.98
	R	.91	-	32.80	46.71	-	19.13	-	-	-	.35	.03	99.94	95.87
	O	1.04	.02	33.64	47.38	-	18.43	-	-	.01	.38	-	100.91	95.14
	O	1.07	.02	32.72	45.91	-	18.61	-	-	.04	.36	.02	98.77	95.05



APPENDIX A (Cont'd)

**43**  
PLASTOCLASE (Cont'd)

Identifier		Na	Mg	Al	Si	K	Ca	Ti	Cr	Mn	Fe	Ni	TOTAL	As
4378	C	1.09	.02	33.76	47.73	-	18.49	-	.02	.01	.38	.04	101.55	94.93
	R	1.23	.02	33.90	46.17	.02	18.53	.02	-	-	.36	-	100.26	94.33
	O	.61	.04	33.69	47.23	-	18.18	-	.02	-	.30	.03	100.09	97.03
	O	1.09	.05	33.13	47.23	-	18.72	.01	-	.03	.35	.02	100.63	94.99
4380	C	1.14	.01	32.78	46.04	-	18.66	.03	-	.02	.29	.05	99.02	94.60
	R	1.05	-	32.49	46.70	.01	18.27	-	-	-	.40	.04	98.96	95.00
	C	1.19	.03	32.82	45.96	-	18.28	.01	.01	-	.33	.01	98.65	94.40
	C	1.16	.01	32.67	46.39	.02	17.90	-	.01	-	.30	.02	98.68	94.50
4383	C	.93	-	32.70	47.37	.01	18.00	.01	-	.03	.39	.03	99.47	95.30
	R	.94	.01	34.30	47.21	-	17.79	.01	-	-	.26	-	100.54	95.30
	O	.93	-	33.70	47.41	.01	18.16	-	-	-	.34	.03	100.57	95.60
	O	1.07	.03	33.36	47.51	.02	18.07	-	.02	-	.25	.05	100.37	94.90
4385	O	1.02	.01	32.80	46.34	-	18.93	-	-	-	.36	-	99.45	95.34
	C	1.06	.02	33.86	46.28	.01	18.37	-	.04	.01	.38	.01	100.03	95.04
	R	1.14	.03	33.95	47.21	-	18.43	.02	.01	-	.30	.04	101.12	94.70
	O	1.03	.01	33.38	46.17	-	18.09	.03	.02	.03	.42	.05	99.23	95.10
	C	1.08	.02	32.77	46.18	-	19.01	.02	-	-	.45	.03	99.36	95.10
	R	.73	-	32.35	45.73	-	19.36	-	.02	.03	.36	.01	98.60	96.70
	O	.85	.05	32.64	46.46	.01	18.63	-	-	-	.39	.04	99.07	96.00
	O	1.07	.04	32.25	46.91	.01	18.09	-	.02	-	.28	.01	98.66	94.90
4386												Br		
	C	1.00		35.52	45.72	.01	18.37				.42	.09	100.63	95.30
	R	1.02		35.78	46.04	.01	18.05				.39	-	101.79	95.20
	C	.80		34.36	45.86	-	18.82				.39	.05	100.29	96.30
	C	1.12		35.41	46.00	-	18.63				.29	.08	101.54	94.83
	R	1.17		35.45	45.61	.01	18.58				.37	.08	101.27	94.60
	R	1.04		35.23	44.04	-	18.32				.43	.04	101.11	95.11
	R	.98		34.13	46.12	-	18.09				.21	-	99.93	95.33
4388	C	1.10	.02	32.54	46.64	.01	18.36	-	-	.04	.35	-	99.05	94.80
	R	.91	.02	32.74	46.16	.01	18.68	.02	.02	.04	.39	.01	99.00	95.80
	C	.95	.02	32.88	46.16	.01	18.79	.02	.02	.04	.29	.01	99.18	95.60
	R	.67	.02	33.14	46.39	.01	18.24	-	.04	-	.29	.01	98.82	96.80
	C	1.09	-	32.69	46.20	-	19.12	.01	.01	-	.34	.05	99.50	95.10

## APPENDIX A (Cont'd)

## A.3

## PLAGIOCLASE (Cont'd)

Identifier		Na	Mg	Al	Si	K	Ca	Ti	Cr	Mn	Fe	Ni	TOTAL	An
4589	O	.90		33.96	45.70	.01	19.48					Sr		
	O	1.07		35.47	45.77	.01	19.07				.39	.39	101.44	95.99
	C	1.13	-	32.70	44.33	.01	18.56	-	.02	.01	.42	.03	101.84	95.10
	R	1.26	-	32.63	46.39	.01	18.34	.02	-	-	.38	.04	99.18	94.80
	C	1.07		34.77	45.84	-	18.86				.38	.01	99.23	94.14
	C	1.11		35.00	46.20	-	18.32				.34	.11	100.99	95.10
	R	.96		34.91	45.79	.01	19.07				.44	.18	101.16	94.78
4590											.39	-	101.13	95.60
	O	1.21	.02	32.46	47.28	.01	18.12	-	.01	-	.44	.03	99.58	94.30
	C	1.04	.02	33.49	47.47	-	18.55	-	.01	-	.40	.03	101.02	94.96
	R	.60	.02	33.41	46.01	-	19.36	-	-	.01	.44	.04	99.88	97.30
4592	O	1.04	.02	33.08	46.95	.02	17.58	.01	.03	-	.39	-	99.13	94.90
	O	.87	-	33.50	47.97	-	18.66	-	.04	.02	.36	.01	101.43	95.90
	C	1.09	.05	33.71	47.01	-	18.68	.01	-	.04	.27	-	100.87	95.00
	R	.94	.04	33.98	47.27	.01	17.89	.01	-	-	.34	-	100.47	95.50
4595	C	1.00	.05	33.55	47.06	-	18.07	.04	.02	.02	.40	-	100.21	95.20
	O	.88	.02	33.89	46.54	.01	18.44	-	-	-	.35	.04	100.17	95.90
	C	1.00	.05	32.18	47.03	-	18.20	.01	.02	.02	.39	-	98.89	95.20
	R	.86		35.15	44.59	-	18.92				.36	Sr .06	99.95	96.04
4596	C	.83		35.14	46.31	.01	18.84				.44	Sr .12	101.69	96.16
	R	.97		35.02	45.98	-	18.94				.41	Sr .05	101.38	95.56
	R	1.02		33.98	45.98	-	18.82				.30	Sr .10	100.21	95.50
	R	1.00		35.04	46.21	.01	19.00				.38	Sr -	101.64	95.44
	C	.43		35.02	45.51	-	19.93				.33	Sr .06	101.29	98.10
	R	.71		34.82	45.85	.01	18.38				.34	Sr .04	100.13	96.61
4596												Sr		
	O	1.03		34.59	45.61	.01	19.49				.36	.03	101.13	95.44
	O	.86		34.82	45.88	.01	19.11				.35	.05	101.07	96.08
	O	.80		34.50	45.34	-	19.77				.30	.23	100.95	96.47
	O	.99		34.40	44.91	.02	19.78				.32	-	100.41	95.66
4596	O	.59		34.89	45.41	-	19.60				.43	-	100.92	97.35

APPENDIX A (Cont'd)

A.4

OLIVINE

Identifier		Na	Mg	Al	Si	K	Ca	Ti	Cr	Mn	Fe	Ni	TOTAL	Fe
4570	O	-	41.36	-	39.98	-	.04	-	.02	.31	19.84	.12	101.66	78.79
4571	C	.03	41.09	-	39.48	-	.05	.01	.03	.27	18.84	.12	99.94	79.53
	R	.05	41.63	-	39.74	.01	.02	-	.02	.34	19.52	.14	101.47	79.16
	C	.04	42.75	-	39.25	-	.02	-	-	.20	19.02	.09	101.36	80.02
	O	.07	41.09	.16	40.00	.01	.05	-	-	.27	18.77	.07	100.49	79.59
4575	O	-	42.50	-	39.66	-	.02	.01	-	.25	18.98	.11	101.53	79.96
	O	.01	42.46	-	39.73	.01	.03	-	.03	.29	17.86	.08	101.51	80.90
	R	.07	42.35	.04	39.67	-	.02	.02	.02	.25	18.61	.11	101.14	80.20
	C	.01	42.25	-	40.09	-	.03	-	-	.25	18.84	.15	101.63	79.98
	C	-	40.49	-	38.32	.01	.02	.02	-	.21	19.47	.12	98.66	78.75
	R	.01	40.23	-	38.55	-	.02	.02	.03	.25	19.44	.14	98.68	78.66
4578	C	.05	41.59	.02	39.89	-	.04	-	.05	.23	19.01	.14	101.03	79.58
	C	.01	40.70	.02	39.16	-	.03	-	-	.26	19.79	.07	100.04	78.56
	C	.02	40.05	.02	39.43	-	.02	-	.03	.21	19.75	.13	99.66	78.32
	R	.01	39.84	-	38.86	-	.06	-	.03	.26	19.28	.13	98.46	78.64
	C	-	40.91	-	38.39	-	.02	.04	.02	.28	19.50	.14	99.30	78.89
	R	.01	40.62	-	38.93	-	.02	-	.03	.27	19.78	.05	99.71	78.53
	C	-	40.30	-	38.55	.01	.02	-	.03	.21	19.84	.17	99.13	78.35
	R	.04	40.70	.02	39.21	-	.02	-	-	.31	19.95	.11	100.36	78.42
	R	-	40.36	-	39.02	-	.04	.02	.03	.29	19.73	.10	99.60	78.47
4581	C	.02	40.82	-	38.24	-	.02	-	.03	.29	19.34	.12	98.88	78.99
	C	-	40.45	-	38.92	.01	.04	.03	-	.27	19.47	.16	99.36	78.73
4590	C	-	41.18	-	38.98	-	.04	-	-	.30	19.56	.13	100.19	79.00
	R	.02	41.10	-	39.09	-	.03	.02	-	.24	18.91	.12	99.54	79.50
	C	-	40.13	.04	39.34	-	.02	-	-	.27	19.42	.17	99.39	78.60
	O	.02	40.99	-	39.58	-	-	-	-	.30	19.52	.10	100.50	78.90
4592	C	.01	40.41	-	38.83	.01	.02	.02	-	.32	19.43	.10	99.16	78.80
	R	.03	41.07	-	39.39	.01	.02	-	.03	.27	20.56	.14	101.52	78.06
	C	.03	40.34	-	38.47	-	.04	.02	.05	.27	20.33	.12	99.68	77.95
	R	-	40.22	.13	37.91	-	.01	-	-	.28	20.30	.08	98.95	77.93
	O	.03	40.59	-	39.10	.02	.04	-	.05	.21	20.46	.18	100.69	77.94
	C	-	40.13	-	38.59	.01	.04	-	.04	.27	20.07	.14	99.29	78.08
	R	.03	40.42	-	38.57	.01	.02	-	.01	.27	20.25	.15	99.73	78.05

## APPENDIX A (Cont'd)

AA OLIVINE (Cont'd)

Identifier	Na	Mg	Al	Si	K	Ca	Ti	Cr	Mn	Fe	Mi	TOTAL	Po
4393	.03	39.63	.02	39.07	-	.02	-	-	.27	19.75	.14	98.95	78.10
C	-	41.27	-	39.27	-	.04	-	.02	.27	19.51	.14	100.52	79.03
a	-	40.73	-	39.13	-	-	-	-	.30	19.48	.15	99.79	78.04
C	-	41.09	-	38.87	.01	.04	-	.05	.26	19.42	.09	99.82	79.04
R	-	41.41	-	38.63	-	.02	.01	.02	.27	19.57	.14	100.24	79.03
O	.06	40.60	-	39.00	.02	.02	-	.02	.31	19.93	.13	100.09	78.59
O	.06	40.64	-	39.03	-	.01	.02	.02	.26	19.84	.11	99.95	78.49

APPENDIX A (Cont'd)

A.5

BOWLING DATA

Sample	Phase	#	Mg	Cr	Mn	Fe	Ni	Ca	Na
4575	Oliv.	1	44.99	-	.33	19.49	.11		
		2	45.02	.03	.30	18.73	.21		
		3	45.06	.02	.23	17.43	.09		
		4	44.86	.04	.27	18.89	.08		
		5	45.97	.01	.20	19.02	.19		
		6	44.11	-	.25	19.08	.05		
4590	Oliv.	1	44.48	-	.29	19.05	.17		
		2	45.26	-	.19	19.68	.13		
		3	44.81	-	.26	19.99	.10		
		4	44.57	-	.27	19.16	.17		
		5	44.43	-	.27	19.62	.14		
		6	44.36	-	.27	19.61	.15		
4590	Cpx.	1		.12	.16				.18
		2		.16	.23				.18
		3		.20	.11				.26
		4		.21	.13				.31
		5		.21	.19				.87
		6		.21	.11				.33
		7		.15	.18				.29
		8		.16	.20				.17
	<u>NI</u>			<u>3.54</u>	<u>2.42</u>				<u>3.55</u>
4592	Cpx.	1		.13	.18				.20
		2		.21	.16				.32
		3		.16	.09				.23
		4		.13	.19				.23
		5		.11	.13				.27
		6		.09	.16				.22
	<u>NI</u>			<u>3.33</u>	<u>1.93</u>				<u>.95</u>
4590	Plag.	1				.38		1.16	16.88
		2				.45		1.17	16.72
		3				.50		1.41	17.01
		4				.45		1.05	16.64
		5				.38		1.19	17.21
		6				.38		1.54	17.14

## APPENDIX A (Cont'd)

A.5

## SOWING DATA (Cont'd)

Sample	Phase	#	Mg	Cr	Mn	Fe	Ni	Co	Na
4588	Plag.	7				.39		1.19	17.07
		8				.44		1.36	17.30
						<u>1.27</u>		<u>1.23</u>	<u>1.20</u>
		1				.30		1.27	17.67
		2				.28		1.07	17.71
		3				.33		1.38	17.36
	Plag.	4				.30		1.20	17.36
		5				.36		1.18	17.56
		6				.32		1.29	17.64
						<u>.97</u>		<u>1.01</u>	<u>2.76</u>
		1				.22		1.70	17.73
		2				.36		1.34	17.49
4568	Plag.	3				.44		1.46	16.91
		4				.43		1.47	16.99
		5				.45		1.80	17.91
		6				.44		1.17	16.13
		7				.47		.98	17.45
						<u>2.44</u>		<u>2.14</u>	<u>2.58</u>
	Plag.	1				.38		1.34	18.46
		2				.38		.97	17.99
		3				.33		1.48	18.01
		4				.39		1.41	17.84
		5				.32		1.41	17.95
		6				.40		1.29	17.74
4596	Plag.	7				.39		1.54	17.88
		8				.33		1.29	17.80
						<u>1.04</u>		<u>1.27</u>	<u>1.02</u>
	Plag.	1				.32		1.66	16.83
		2				.33		1.45	16.91
		3				.38		1.64	16.83
		4				.34		1.45	16.79
		5				.45		1.56	17.33
		6				.38		1.16	17.60
4565	Plag.	7				.39		1.30	17.58
		8				.38		1.37	17.57
						<u>1.36</u>		<u>1.13</u>	<u>1.89</u>
	Plag.	1				.32		1.66	16.83
		2				.33		1.45	16.91
		3				.38		1.64	16.83
		4				.34		1.45	16.79
		5				.45		1.56	17.33
		6				.38		1.16	17.60

# APPENDIX B

Microprobe mineral analysis (wt. %) of clinopyroxene, orthopyroxene, olivine and plagioclase phases within layered olivine and hypersthene gabbro and transition zone lithologies of the older suite.  $Mg'$ ,  $Ca'$ ,  $Fe'$  (Mol %),  $Mg^{\#} = Mg \div (Mg + Fe \text{ (Mol \%)}) \times 100$  for the sample average, A = Average, An (Mol%), Fe (Mol%), Code: N = neoblasts, P = strained porphyroclast, R = rim, C = core, O = no description, Oik = oikocryt, Z = inclusion.

## B.1. LAYERED OLIVINE GABBRO

### B.1.1. Clinopyroxene

Sample	Code	Na	Mg	Al	Si	X	Ca	Ti	Cr	Mn	Fe	Ni	TOTAL	Average
139	O	.18	17.63	2.39	52.61	-	19.55	.16	.14	.14	5.66	.05	98.51	$Mg' = 51.55$
	O	.11	17.23	1.88	53.34	-	21.12	.07	.10	.12	5.30	-	99.28	$Ca' = 43.20$
	A	.14	17.43	2.13	52.98	-	20.33	.11	.12	.13	5.48	.03	98.88	$Fe' = 5.25$ $Mg^{\#} = 85.00$
102	O	.20	17.71	2.10	54.21	-	19.95	.13	.09	.13	5.71	-	100.23	$Mg' = 51.45$
	O	.27	17.29	2.16	53.68	.01	20.74	.15	.08	.16	5.93	-	100.45	$Ca' = 42.97$
	A	.23	17.50	2.13	53.94	-	20.34	.13	.08	.14	5.82	-	100.32	$Fe' = 5.57$ $Mg^{\#} = 84.28$
102	O	.20	17.34	2.14	53.09	.01	20.62	.23	.07	.23	5.88	.03	99.83	$Mg' = 50.85$
	O	.30	16.78	2.12	53.16	-	20.18	.18	.10	.12	5.32	-	98.45	$Ca' = 43.68$
	O	.29	17.04	1.86	53.61	-	20.34	.13	.10	.15	5.43	.07	99.02	$Fe' = 5.47$
	A	.26	17.05	2.04	53.29	-	20.38	.18	.09	.16	5.61	.03	99.08	$Mg^{\#} = 84.42$
102	O	.18	18.35	2.10	52.60	-	18.18	.20	.09	.13	6.65	.03	98.50	$Mg' = 55.05$ $Ca' = 39.20$ $Fe' = 5.74$ $Mg^{\#} = 83.09$
	O	.21	16.94	2.00	54.04	.01	20.93	.18	.13	.04	5.65	-	100.14	$Mg' = 50.44$ $Ca' = 44.79$ $Fe' = 4.78$ $Mg^{\#} = 84.28$
102	O	.33	17.51	2.08	53.63	.01	21.80	.38	.09	.18	5.55	.12	101.67	$Mg' = 50.48$ $Ca' = 44.84$ $Fe' = 4.64$ $Mg^{\#} = 84.93$
	O	.10	18.34	1.57	53.92	-	19.79	.13	.04	.18	6.26	.02	100.35	$Mg' = 51.01$
132	O	.21	16.78	1.69	53.19	-	21.84	.08	.04	.22	5.33	-	99.37	$Ca' = 43.46$
	A	.15	17.55	1.63	53.55	-	20.81	.10	.04	.20	5.79	-	99.83	$Fe' = 5.54$ $Mg^{\#} = 84.58$



APPENDIX B (Cont'd)

B.1. LAYERED OLIVINE GABBRO (Cont'd)

B.1.1. Clinopyroxene

Sample	Code	Na	Mg	Al	Si	K	Ca	Ti	Cr	Mn	Fe	Ni	TOTAL	Average
152	O	.25	17.19	1.78	51.97	-	21.74	.12	.04	.17	5.48	.04	98.77	Hg' = 49.24
	O	.23	16.92	1.80	53.52	-	22.23	.03	.05	.15	5.42	-	100.35	Ca' = 45.61
	A	.24	17.05	1.79	52.74	-	21.98	.07	.04	.16	5.45	.02	99.53	Fe' = 5.15 Hg** = 84.79
152	O	.25	17.03	1.77	53.35	-	22.27	.11	.04	.16	5.39	.02	100.40	Hg' = 48.94
														Ca' = 45.98
														Fe' = 5.07 Hg** = 84.90
265	O	.18	17.03	1.83	53.76	-	20.80	-	.10	.20	5.13	-	99.01	Hg' = 50.62
														Ca' = 44.43
														Fe' = 4.95 Hg** = 85.54
102	C	.18	17.41	2.91	54.10	-	20.72	.21	.04	.18	5.59	-	101.03	Hg' = 51.34
														Ca' = 43.86
														Fe' = 4.80 Hg** = 84.74
081	O	.20	16.87	2.02	53.32	-	21.21	-	.07	.18	5.85	.06	99.78	Hg' = 49.65
	O	.19	17.04	1.86	53.12	-	21.63	.11	.07	.13	5.18	.04	100.16	Ca' = 45.07
	A	.20	16.95	1.93	53.62	-	21.41	.05	.07	.15	5.51	.05	99.95	Fe' = 5.27 Hg** = 84.57
081	O	.18	16.89	1.99	53.14	-	20.78	.16	.08	.13	5.98	.03	99.37	Hg' = 50.35
														Ca' = 44.51
														Fe' = 5.14 Hg** = 83.42
008	O	.18	18.00	2.00	53.77	-	19.75	-	.02	.20	6.09	-	99.99	Hg' = 52.35
	O	.09	17.85	1.95	54.25	-	20.11	.02	.02	.22	6.05	-	100.34	Ca' = 41.82
	A	.13	17.92	1.97	54.00	-	19.92	-	.02	.20	6.07	-	100.23	Fe' = 5.83 Hg** = 84.03

## APPENDIX B (Cont'd)

## B.1. LATEX OLIVINE GARNET (Cont'd)

## B.1.1 Clinopyroxene

Sample	Code	Na	Mg	Al	Si	K	Ca	Ti	Cr	Mn	Fe	NI	TOTAL	Average
008	O	.16	17.95	1.83	53.73	-	19.84	.08	.02	.16	3.82	.07	99.97	Mg = 32.03 Ca = 41.80 Fe = 5.58 Mg = 84.60
037	O	.13	16.75	1.79	52.99	.01	19.59	.21	.14	.23	7.64	.05	99.51	Mg = 49.78
	O	.13	16.43	1.64	53.41	-	19.14	.32	.09	.10	9.85	.04	101.15	Ca = 41.73
	A	.13	16.59	1.71	53.20	-	19.36	.26	.11	.16	8.75	.04	100.30	Fe = 8.50 Mg = 77.16

APPENDIX B (Cont'd)

B.1. LAYERED OLIVINE CASSID (Cont'd)

B.1.2 Orthopyroxene

Sample	Code	Na	Mg	Al	Si	K	Ca	Ti	Cr	Mn	Fe	Ni	TOTAL	Average
139	Oik	-	30.29	1.21	56.74	-	1.51	-	-	.29	11.38	-	101.42	Mg' = 85.55
	Oik	.04	30.21	1.28	56.52	-	2.48	.05	.05	.21	10.82	-	101.87	Ca' = 4.26
	A	.02	30.25	1.24	56.63	-	2.10	.02	.02	.25	11.10	-	101.61	Fe' = 10.20
265	Oik	.02	29.61	1.34	56.47	-	2.64	-	.04	.27	10.64	.04	101.07	Mg' = 84.65 Ca' = 5.42 Fe' = 9.92
272	O	-	29.08	1.17	53.83	-	.53	-	.02	.29	13.76	.08	98.75	Mg' = 85.04
	O	.02	28.52	1.15	53.71	-	.86	-	-	.28	14.36	.03	98.94	Ca' = 1.49
	A	.01	28.79	1.16	53.76	-	.70	-	-	.28	14.06	.05	98.82	Fe' = 13.47
081	O	-	29.80	1.27	55.64	-	1.04	-	.02	.22	12.80	.07	100.87	Mg' = 87.07 Ca' = 2.18 Fe' = 10.75
008	O	.02	30.82	1.35	55.62	-	1.28	.05	.02	.30	11.29	.03	100.77	Mg' = 86.71
	O	.01	30.59	1.31	55.55	-	1.56	-	.04	.23	11.36	.06	100.71	Ca' = 2.88
	A	.01	30.70	1.32	55.60	-	1.42	.02	.02	.27	11.32	.04	100.73	Fe' = 10.41
037	O	.01	31.89	1.55	56.36	-	2.06	.03	.23	.20	9.18	.03	101.53	Mg' = 87.75 Ca' = 4.07 Fe' = 8.21

APPENDIX B (Cont'd)

B.1. LAYERED OLIVINE GABBRO (Cont'd)

8.1.3 Olivine

Sample	Code	Na	Mg	Al	Si	K	Ca	Ti	Cr	Mn	Fe	Ni	TOTAL	Average
061	O		41.35	-	39.14	-	-	-	-	.28	20.37	.07	101.22	Fe = 78.09
	O		41.38	-	38.59	-	-	-	-	.22	20.98	.15	101.33	
	A		41.36	-	38.87	-	-	-	-	.25	20.68	.11	101.27	
061	O		40.62	-	38.97	-	-	-	-	.30	20.61	.13	100.63	Fe = 77.58
	O		40.82	-	38.23	-	-	-	-	.28	21.32	.12	100.76	
	A		40.71	-	38.60	-	-	-	-	.29	20.96	.12	100.68	
008	O		43.21	-	34.25	-	-	-	-	.24	19.18	.06	101.93	Fe = 80.05
008	O		42.95	-	39.41	-	.01	-	-	.19	18.41	.08	101.05	Fe = 80.87
	O		43.48	.02	39.46	-	-	-	-	.23	18.00	.11	101.30	
	A		43.21	-	39.44	-	-	-	-	.21	18.21	.09	101.18	
265	O		42.39	.57	39.48	-	-	-	-	.26	18.28	.13	101.10	Fe = 80.52
	O		41.82	-	38.64	-	.01	-	-	.24	17.99	.19	98.88	
	A		42.10	.28	39.05	-	-	-	-	.25	18.14	.16	99.98	
272	O		41.18	-	38.03	-	-	-	-	.30	19.00	.15	99.20	Fe = 79.91
	O		42.38	-	38.79	-	-	-	-	.25	18.64	.13	100.18	
	A		42.01	-	38.44	-	-	-	-	.27	18.82	.14	99.68	
372	O		41.83	.02	37.81	-	-	-	-	.38	18.71	.09	98.84	Fe = 80.18
	O		43.26	.02	38.32	-	-	-	-	.30	18.77	.15	100.81	
	A		42.54	.02	38.06	-	-	-	-	.34	18.74	.12	99.81	
152	O		42.05	.02	39.28	-	.03	-	-	.34	19.83	.03	101.61	Fe = 78.81
	O		40.71	.09	38.38	-	.02	-	.03	.31	19.84	.05	99.43	
	A		41.38	.04	38.86	-	.02	-	-	.34	19.83	.04	100.49	
152	O		43.74	-	38.39	-	.01	-	-	.20	18.40	.03	100.77	Fe = 79.06
	O		40.80	.09	38.76	-	.04	-	.01	.29	19.59	.05	99.61	
	A		42.27	.04	38.57	-	.02	-	-	.25	18.99	.04	100.18	
102	O		40.51	.02	38.60	-	-	-	-	.32	19.07	.17	98.70	Fe = 79.10

## APPENDIX B (Cont'd)

## B.1. LATHEED OLIVINE CARBIDE (Cont'd)

## B.1.3 Olivine

Sample	Code	Na	Mg	Al	Si	K	Ca	Ti	Cr	Mn	Fe	Ni	TOTAL	Average
139	O		42.11	-	39.28		-	-	-	.36	18.60	.15	100.50	Po = 80.13
081	O		41.13	-	39.43		.01	-	-	.25	20.30	.12	101.24	
	O		41.48	-	39.76		-	-	-	.16	20.30	.04	101.75	
	A		41.31	-	39.60		-	-	-	.21	20.30	.08	101.50	Po = 78.37

APPENDIX B (Cont'd)

B.1. LAYERED OLIVINE GABBRO (Cont'd)

Plagioclase

Sample	Code	Na	Mg	Al	Si	K	Ca	Ti	Cr	Mn	Fe	Ni	TOTAL	Average
139	Z	1.35	.02	32.91	46.84	-	17.26	-	-	-	.35	.01	98.75	An = 93.41
102	O	1.33	.06	32.07	47.38	-	16.93	-	-	.02	.39	-	98.18	An = 93.37
152	O	1.21	.05	32.71	46.94	-	17.81	.02	.04	.05	.44	-	99.27	An = 94.22
152	Z	1.00	.06	32.93	46.32	-	17.52	-	-	.03	.63	.05	98.54	An = 95.09
265	Z	.98	.02	33.69	45.89	.01	17.50	-	-	-	.35	.03	98.47	An = 95.18
265	O	.88	.06	33.27	46.65	-	16.87	-	-	-	.29	-	98.02	An = 95.49
272	O	.50	.03	33.85	45.13	-	18.93	-	-	-	.35	-	98.79	An = 97.69
081	O	.86	.03	33.85	45.53	-	17.94	-	-	.03	.37	.07	98.67	An = 95.86
008	O	.86	.03	33.06	45.88	-	18.48	-	-	.02	.46	-	98.77	An = 96.06
	O	.78	.12	32.73	45.99	.05	17.59	-	-	.05	.47	-	97.79	
	A	.82	.07	32.89	45.94	.03	18.03	-	-	.04	.45	-	98.25	
008	O	.88	.07	32.80	46.07	.01	17.61	-	-	-	.45	-	97.89	An = 95.67
008	O	.97	-	33.90	45.27	-	17.92	-	-	-	.44	-	98.51	An = 96.06
	O	.69	.04	33.82	45.34	-	18.20	.02	-	.03	.37	-	98.70	
	A	.82	.02	33.86	45.40	-	18.06	-	-	.01	.41	-	98.61	
037	O	.79	.02	33.28	45.53	-	18.38	-	-	-	.34	-	98.54	An = 96.23





APPENDIX B (Cont'd)

B.2. LAYERED HYPERSTHENE GABBRO (Cont'd)

B.2.1 Clinopyroxene

Sample	Code	Na	Mg	Al	Si	K	Ca	Ti	Cr	Mn	Fe	Ni	TOTAL	Average
266	O	.13	15.55	1.92	51.88	-	18.95	.07	.03	.20	9.01	.05	97.79	Mg <sup>2+</sup> = 48.95 Ca <sup>2+</sup> = 42.86 Fe <sup>2+</sup> = 8.18 Mg <sup>2+</sup> = 75.46
266	O	.15	15.94	1.94	53.52	-	20.35	-	.03	.14	5.93	.07	98.07	Mg <sup>2+</sup> = 49.38 Ca <sup>2+</sup> = 45.31 Fe <sup>2+</sup> = 5.31 Mg <sup>2+</sup> = 82.72
267	O	1.46	16.82	7.93	51.28	.01	16.12	.75	.07	.17	6.30	.01	100.03	Mg <sup>2+</sup> = 55.38
	O	1.27	16.36	7.86	50.75	-	16.15	.48	.10	.09	6.32	-	99.59	Ca <sup>2+</sup> = 38.52
	O	1.37	16.61	7.96	50.70	-	15.85	.56	.09	.18	6.21	.07	99.60	Fe <sup>2+</sup> = 6.09
	O	1.32	16.46	7.97	50.14	-	16.00	.63	.11	.06	6.42	.05	99.17	Mg <sup>2+</sup> = 82.38
	A	1.36	16.56	7.93	50.72	-	16.03	.66	.09	.15	6.31	.03	99.84	
267	O	.14	17.72	1.41	53.96	-	21.18	.12	.07	.14	5.36	-	100.70	Mg <sup>2+</sup> = 51.37 Ca <sup>2+</sup> = 44.13 Fe <sup>2+</sup> = 5.28 Mg <sup>2+</sup> = 85.68
267	O	.16	17.39	1.73	54.19	.01	21.80	.05	.05	.14	5.42	-	100.95	Mg <sup>2+</sup> = 49.99
	O	.16	16.98	1.81	53.60	-	21.77	-	.07	.13	4.87	.01	99.44	Ca <sup>2+</sup> = 45.56
	O	.21	17.30	1.75	53.21	-	21.95	-	.07	.16	5.58	-	100.23	Fe <sup>2+</sup> = 4.45
	A	.18	17.22	1.76	53.68	-	21.84	.01	.06	.14	5.29	-	100.21	Mg <sup>2+</sup> = 85.29
270	O	.11	14.61	1.53	52.66	-	21.74	.03	.03	.25	8.59	.04	99.59	Mg <sup>2+</sup> = 44.21 Ca <sup>2+</sup> = 47.28 Fe <sup>2+</sup> = 8.51 Mg <sup>2+</sup> = 75.19
269	O	.15	15.91	1.50	52.50	-	22.66	.08	.02	.13	6.27	.05	99.25	Mg <sup>2+</sup> = 46.68 Ca <sup>2+</sup> = 47.57 Fe <sup>2+</sup> = 5.95 Mg <sup>2+</sup> = 81.89



APPENDIX B (Cont'd)

B.2. LAYERED HYPERSTHENE GABBRO (Cont'd)

B.2.1 Clinopyroxene

Sample	Code	Na	Mg	Al	Si	K	Ca	Ti	Cr	Mn	Fe	Ni	TOTAL	Average
402	O	.20	15.92	1.54	53.53	-	22.41	.21	-	.16	6.52	.02	100.51	Hg' = 46.62 Ca' = 47.16 Fe' = 6.22 Hg <sup>++</sup> = 81.30
209	O	.14	16.12	1.84	52.94	-	21.90	.39	-	.26	7.03	-	100.64	Hg' = 46.46
	O	.28	15.68	2.10	53.74	.01	22.71	.26	.01	.27	6.86	.04	101.95	Ca' = 46.83
	A	.20	15.90	1.98	53.34	-	22.31	.32	-	.26	6.94	.02	101.28	Fe' = 6.69 Hg <sup>++</sup> = 80.32
209	O	.18	15.96	2.07	52.18	.01	21.95	.22	-	.16	6.59	-	99.33	Hg' = 47.11 Ca' = 46.56 Fe' = 6.34 Hg <sup>++</sup> = 81.18
209	O	.38	15.12	1.84	52.79	.01	22.14	.20	.01	.19	7.43	.03	100.14	Hg' = 45.57 Ca' = 47.95 Fe' = 6.49 Hg <sup>++</sup> = 78.38
267	O	.26	17.20	1.98	53.25	-	22.98	.07	.12	.14	4.95	.08	101.03	Hg' = 48.49
	O	.23	16.93	1.96	53.54	.01	22.77	.04	.10	.21	5.31	-	101.19	Ca' = 46.72
	A	.25	17.06	1.96	53.44	-	22.87	.05	.11	.17	5.13	.04	101.08	Fe' = 4.79 Hg <sup>++</sup> = 85.60
267	O	.10	16.90	2.20	52.39	-	22.11	.25	.13	.14	5.48	.05	99.75	Hg' = 49.12
	O	.12	17.06	2.45	52.37	-	21.99	.18	.13	.13	5.19	-	99.61	Ca' = 45.84
	A	.11	16.98	2.33	52.38	-	22.05	.21	.13	.13	5.34	.02	99.64	Fe' = 5.03 Hg <sup>++</sup> = 85.00
267	O	.13	16.34	2.05	52.62	.01	22.45	.07	.12	.11	5.26	.03	99.38	Hg' = 48.20
	O	.24	16.84	2.78	51.23	-	22.63	.20	.05	.16	5.42	.01	99.56	Ca' = 46.78
	A	.18	16.69	2.41	51.92	-	22.54	.14	.08	.13	5.34	.02	99.46	Fe' = 5.02 Hg <sup>++</sup> = 84.77

### **D.2. LATENT REPRESENTATION GAMING (Cont'd)**

## 2.2.1 Ciphertexts

Sample	Code	Na	Mg	Al	Si	K	Ca	Ti	Cr	Mn	Fe	NI	TOTAL	Average
267	O	.21	17.26	1.95	52.93	-	21.67	.16	.04	.16	5.48	-	99.87	Mg' = 49.23
	O	.22	17.04	1.86	53.08	-	22.35	.23	.13	.16	5.35	.04	100.66	Ca' = 45.67
	A	.21	17.13	1.91	53.01	-	22.11	.19	.08	.16	5.42	.07	100.23	Fe' = 5.10
														Ni <sub>geo</sub> = 85.00
267	O	.19	17.08	1.86	53.11	-	21.57	.05	.13	.08	5.15	.08	99.30	Mg' = 50.15
														Ca' = 45.51
														Fe' = 4.33
														Ni <sub>geo</sub> = 85.53

APPENDIX B (Cont'd)

B.2. LAYERED HYPERSTHENE GABRO (Cont'd)

B.2.2 Orthopyroxene

Sample	Code	Na	Mg	Al	Si	K	Ca	Ti	Cr	Mn	Fe	Ni	TOTAL	Average
268	O	.01	29.25	.97	55.20	-	.36	-	-	.31	12.64	-	98.74	Mg' = 87.10
	O	-	30.12	.91	55.52	-	.58	-	-	.18	12.40	.05	99.75	Ca' = 1.02
	A	-	29.65	.94	55.36	-	.47	-	-	.25	12.52	.02	99.25	Fe' = 11.89
266	O	.02	25.38	1.14	54.61	-	.77	.07	.01	.31	18.83	-	101.14	Mg' = 79.26 Ca' = 1.73 Fe' = 19.01
266	O	.03	24.72	1.48	53.26	-	.80	-	-	.20	18.07	.02	98.58	Mg' = 79.54
	O	.07	25.45	1.00	53.23	-	.84	.02	.01	.31	18.29	.05	99.25	Ca' = 1.87
	A	.05	25.08	1.23	53.24	-	.82	-	-	.25	18.18	.04	98.89	Fe' = 18.59
065	O	.04	27.46	1.25	54.49	-	1.37	.03	.04	.29	16.23	-	101.20	Mg' = 82.98 Ca' = 2.92 Fe' = 14.10
065	O	.02	27.64	1.02	54.40	-	1.14	.01	.04	.33	16.04	.02	100.66	Mg' = 82.61
	O	-	28.18	.82	53.36	-	.71	.05	.05	.20	16.15	-	99.51	Ca' = 1.98
	A	.01	27.90	.91	53.88	-	.93	.02	.04	.27	16.09	-	100.04	Fe' = 15.41
402	O	.01	27.18	.95	54.55	-	1.00	.04	-	.38	16.20	-	100.31	Mg' = 81.94 Ca' = 2.17 Fe' = 15.90
402	O	-	27.58	1.08	54.25	-	1.05	-	-	.29	16.48	.05	100.79	Mg' = 82.24
	O	-	27.84	1.11	54.92	.01	.89	.05	-	.38	16.07	-	101.27	Ca' = 2.09
	A	-	27.71	1.10	54.59	-	.98	.02	-	.33	16.27	.02	101.03	Fe' = 15.67
402	Z	.04	27.64	1.04	55.70	-	.67	.06	-	.33	15.87	.05	101.41	Mg' = 83.31
	Z	.03	27.20	1.13	55.96	-	.61	.09	-	.25	15.50	-	98.78	Ca' = 1.34
	A	.03	27.63	1.09	54.83	-	.64	.08	-	.29	15.69	.03	100.10	Fe' = 15.34
209	O	-	27.05	1.20	55.05	-	1.64	.07	.01	.20	16.04	.06	101.32	Mg' = 82.45 Ca' = 3.59 Fe' = 13.97

APPENDIX B (Cont'd)

3.2. LAYERED HYPERSTHENE GABBRO (Cont'd)

3.2.2. Orthopyroxene

Sample	Code	Na	Mg	Al	Si	K	Ca	Ti	Cr	Mn	Fe	Wt	TOTAL	Average
209	O	-	27.58	1.11	54.66	-	1.46	-	.01	.30	16.90	.01	101.63	Mg = 82.65 Ca = 3.14 Fe = 14.20
209	O	.02	26.96	2.43	52.88	-	1.22	.03	-	.39	16.11	-	100.04	Mg = 81.48 Ca = 2.65 Fe = 15.86
209	O	.01	27.48	1.75	54.50	.01	1.22	.05	-	.14	16.23	-	101.38	Mg = 83.33 Ca = 2.66 Fe = 14.00
269	O	.02	27.54	1.23	54.85	-	.64	-	.04	.23	15.72	.07	100.34	Mg = 83.07
	O	-	27.49	1.25	54.59	-	.67	-	.05	.19	16.14	-	100.39	Ca = 1.43
	A	.01	27.51	1.24	54.72	-	.66	-	.05	.21	15.93	.03	100.35	Fe = 15.50
269	O	.04	26.87	1.16	54.02	-	.63	-	.02	.31	16.04	-	99.08	Mg = 82.90
	O	-	27.77	1.22	54.79	-	.63	-	.03	.29	16.12	.08	100.93	Ca = 1.37
	A	.02	27.46	1.20	54.52	-	.63	-	.02	.30	16.09	.05	100.27	Fe = 15.73
269	O	-	27.25	.96	54.26	-	.32	-	.01	.27	16.15	.01	99.23	Mg = 83.33 Ca = .70 Fe = 15.97

APPENDIX B (Cont'd)

B.2. LAYERED HYPERSTHENE GABBRO (Cont'd)

B.2.3. Plagioclase

Sample	Code	Na	Mg	Al	Si	K	Ca	Ti	Cr	Mn	Fe	Ni	TOTAL	Average
268	O	.83	.03	33.34	44.93	-	19.11	-	-	-	.29	-	98.54	An = 96.22
	O	.79	.04	33.86	45.23	-	18.29	-	-	-	.36	.04	98.61	
	A	.81	.04	33.59	45.08	-	18.70	-	-	-	.33	-	98.58	
267	O	.89	-	34.32	45.53	-	18.70	-	-	-	.45	-	99.90	An = 95.97
	O	.85	.03	33.75	44.25	-	18.38	-	-	-	.29	.04	97.63	
	A	.87	.01	34.04	44.89	-	18.54	-	-	-	.37	.03	98.77	
267	O	1.00	.02	33.43	45.39	-	18.40	-	-	.03	.35	-	98.63	An = 95.37
	O	.94	.01	33.30	44.13	-	18.09	-	-	.04	.39	-	98.91	
	A	.98	.01	33.37	45.76	-	18.25	-	-	.03	.37	-	98.77	
267	O	.74	.01	33.55	45.61	-	18.31	-	-	.02	.39	-	98.64	An = 96.48
266	O	.82	.03	33.53	45.91	-	17.36	-	-	.03	.55	.04	98.27	An = 95.91
266	O	.89	.02	33.27	45.91	-	17.04	-	-	.03	.53	.03	97.72	An = 95.48
065	O	1.24	-	33.02	45.97	-	17.80	-	-	-	.53	.02	98.54	An = 94.07
065	O	1.43	-	33.11	45.99	-	17.38	-	-	.03	.51	.03	98.50	An = 92.98
264	O	.87	.04	33.88	45.95	-	17.35	-	-	.02	.48	.01	98.60	An = 95.67
402	Z	1.04	-	33.81	45.92	-	16.94	.01	-	.01	.46	.03	98.22	An = 94.73
402	Z	.96	.04	33.32	46.82	-	16.96	-	-	-	.58	-	98.68	An = 95.12
402	O	1.21	.02	33.19	46.13	-	17.16	-	-	-	.55	-	98.27	An = 94.01
209	Z	1.22	.01	33.30	45.64	.02	17.95	.01	-	-	.39	-	98.64	An = 91.10
209	O	2.48	.04	32.17	46.26	.07	17.11	-	-	.04	.45	.04	98.85	An = 87.62
267	O	.98	.04	33.55	45.06	.01	18.42	-	-	.02	.42	.08	98.58	An = 95.41
267	O	.86	-	33.35	45.03	-	18.96	-	.01	-	.16	.04	98.60	An = 96.05

## APPENDIX B (Cont'd)

## B.3. TRANSITION ZONE

## B.3.1 Orthopyreneane

Sample	Code	Na	Mg	Al	Si	K	Ca	Ti	Cr	Mn	Pb	Ni	TOTAL	Average
407A-A	N	-	32.52	.64	58.92	-	.36	-	.28	.14	5.88	.01	98.74	Mg = 93.74 Ca = .74 Pb = 5.52
407A-A	N	.03	34.66	.56	57.68	-	1.85	.01	.27	.16	5.96	.01	101.20	Mg = 91.90 Ca = 3.52 Pb = 4.58
407A-A	N	.04	32.37	.35	56.58	-	1.790	.01	.27	.14	5.71	.09	100.43	Mg = 91.31 Ca = 3.44 Pb = 5.25
407A-A	N	.05	35.10	.73	57.19	.02	1.91	.05	.27	.19	6.13	.04	101.69	Mg = 91.23
407A-A	N	.05	34.02	2.62	56.69	-	1.86	.03	.24	.18	5.85	.08	101.61	Ca = 3.59
407A-A	A	.05	36.52	1.68	56.94	.01	1.89	.04	.26	.19	5.99	.06	101.65	Pb = 5.18
407A-A	P	.14	34.68	1.27	56.81	-	1.94	.04	.26	.17	6.14	-	101.46	Mg = 91.07 Ca = 3.66 Pb = 5.27
407A-A	P	.04	34.14	.87	57.75	-	1.98	.04	.32	.17	5.85	-	101.16	Mg = 91.09 Ca = 3.80 Pb = 5.11
407A-A	P	.04	34.68	.61	58.29	-	1.87	.04	.24	.19	5.25	.05	101.26	Mg = 91.87 Ca = 3.55 Pb = 4.58
407A-A	N	-	34.63	.65	57.50	-	1.86	.02	.24	.15	6.20	-	101.25	Mg = 91.16 Ca = 3.52 Pb = 5.32
407A-A	N	-	35.03	.55	57.33	.01	1.82	-	.30	.16	6.10	.05	101.36	Mg = 91.39 Ca = 3.41 Pb = 5.19



APPENDIX B (Cont'd)

B.3. TRANSITION ZONE (Cont'd)

B.3.1 Orthopyroxene

Sample	Code	Na	Mg	Al	Si	K	Ca	Ti	Cr	Mn	Fe	Ni	TOTAL	Average
407A-A	H	.03	34.74	.64	57.94	.01	1.84	.01	.34	.14	5.98	-	101.68	Mg <sup>2+</sup> = 91.35
	H	.04	31.48	1.42	59.43	.02	1.92	-	.34	.09	5.22	.07	100.04	Ca <sup>2+</sup> = 3.72
	A	.03	33.11	1.04	58.68	.01	1.88	-	.34	.11	5.60	.04	100.84	Fe <sup>2+</sup> = 4.92
407A-A	H	.04	34.91	.64	57.68	.01	1.91	.01	.39	.18	6.07	.03	101.87	Mg <sup>2+</sup> = 91.22 Ca <sup>2+</sup> = 3.59 Fe <sup>2+</sup> = 5.19
407C-A	H	-	35.55	.61	57.34	-	1.54	-	.22	.17	6.14	.21	101.79	Mg <sup>2+</sup> = 93.84 Ca <sup>2+</sup> = 2.94 Fe <sup>2+</sup> = 4.61
407C-A	H	.03	34.60	.65	58.13	-	1.45	-	.22	.11	5.97	.05	101.20	Mg <sup>2+</sup> = 92.08 Ca <sup>2+</sup> = 2.77 Fe <sup>2+</sup> = 5.15
407C-A	H	-	34.62	.65	57.82	-	1.57	-	.20	.09	5.76	-	100.72	Mg <sup>2+</sup> = 92.56 Ca <sup>2+</sup> = 3.02 Fe <sup>2+</sup> = 4.42
407C-A	H	.03	35.20	.61	57.27	-	1.34	-	.22	.17	6.01	.04	100.89	Mg <sup>2+</sup> = 92.32 Ca <sup>2+</sup> = 2.53 Fe <sup>2+</sup> = 5.16
407C-A	H	.06	34.63	.61	57.63	-	1.61	.02	.29	.14	6.03	.08	101.10	Mg <sup>2+</sup> = 91.74 Ca <sup>2+</sup> = 3.06 Fe <sup>2+</sup> = 5.20
407C-A	H	.03	33.00	1.94	56.56	.02	1.71	-	.29	.14	5.91	.03	99.65	Mg <sup>2+</sup> = 91.28 Ca <sup>2+</sup> = 3.40 Fe <sup>2+</sup> = 5.33
407C-A	H	.04	35.02	.66	57.36	.03	1.80	-	.29	.18	6.18	.08	101.63	Mg <sup>2+</sup> = 91.35 Ca <sup>2+</sup> = 3.37 Fe <sup>2+</sup> = 5.28

APPENDIX B (Cont'd)

B.3. TRANSITION ZONE (Cont'd)

B.3.1 Orthopyroxene

Sample	Code	Na	Mg	Al	Si	K	Ca	Ti	Cr	Mn	Fe	Ni	TOTAL	Average
407C-D	P	.02	34.82	.61	58.02	-	1.81	.01	.24	.16	5.95	.05	101.71	Mg <sup>2+</sup> = 91.32
	P	.03	34.94	.58	57.52	-	2.04	-	.27	.15	5.95	.13	101.60	Ca <sup>2+</sup> = 3.57
	P	-	35.08	.53	57.59	-	1.84	-	.24	.16	6.08	-	101.52	Fe <sup>2+</sup> = 5.11
	A	.02	34.95	.57	57.71	-	1.90	-	.25	.16	5.99	.06	101.61	
407C-D	N	.04	34.24	.59	58.32	.02	1.93	-	.27	.09	6.19	.10	101.81	Mg <sup>2+</sup> = 91.01 Ca <sup>2+</sup> = 3.68 Fe <sup>2+</sup> = 5.31
407C-D	N	-	34.08	.64	57.40	-	2.00	-	.27	.20	5.71	-	100.29	Mg <sup>2+</sup> = 91.13 Ca <sup>2+</sup> = 3.85 Fe <sup>2+</sup> = 5.02
407C-D	N	-	34.71	.84	56.86	-	1.95	-	.23	.18	6.02	.18	100.96	Mg <sup>2+</sup> = 91.14 Ca <sup>2+</sup> = 3.68 Fe <sup>2+</sup> = 5.17
407C-D	N	.02	35.14	.68	56.09	-	1.94	.03	.35	.16	5.70	.10	100.32	Mg <sup>2+</sup> = 91.48 Ca <sup>2+</sup> = 3.67 Fe <sup>2+</sup> = 4.85

APPENDIX B (Cont'd)

B.3. TRANSITION ZONE (Cont'd)

B3.2. Olivine (interstitial and enclosing orthopyroxene phase)

Sample	Code	Na	Mg	Al	Si	K	Ca	Ti	Cr	Mn	Fe	Ni	TOTAL	Average
407C-A	C		48.22	.78	41.69		-	-	-	.16	9.60	.16	100.62	Fe = 90.23
	R		49.16	-	40.70		.01	-	-	.13	9.63	.17	99.80	Fe = 90.37
	A		48.69	.39	41.19		-	-	-	.14	9.61	.16	100.20	Fe = 90.30
407C-O	R		49.43	-	40.24		-	-	-	.16	8.84	.15	98.82	Fe = 90.88
	C		49.36	.04	41.38		-	-	-	.11	9.34	.13	100.34	Fe = 90.41
	A		49.39	.02	40.80		-	-	-	.13	9.08	.14	99.56	Fe = 90.68
407C-O	O		49.39	-	39.33		.04	.01	-	.07	9.21	.13	98.18	Fe = 90.44
	O		48.63	-	41.25		-	-	-	.11	9.42	.20	99.41	Fe = 90.30
	A		49.01	-	40.29		.02	-	-	.09	9.32	.17	98.90	Fe = 90.37
407C-O	O		48.25	.02	40.93		-	-	-	.17	9.00	.15	98.52	Fe = 90.22
	O		48.42	.04	39.82		-	-	-	.21	9.45	.13	98.06	Fe = 90.23
	A		48.33	.04	40.38		-	-	-	.19	9.22	.14	98.29	Fe = 90.22

## APPENDIX B (Cont'd)

## B.3. TRANSITION ZONE (Cont'd)

## B.3.3. Clinopyroxene (interstitial to orthopyroxene phase)

Sample	Code	Na	Mg	Al	Si	K	Ca	Ti	Cr	Mn	Fe	Ni	TOTAL	Average
407C-0	0	.11	20.16	.96	56.77	.01	22.53	-	.69	.11	2.53	-	101.85	Mg = 56.21 Ca = 43.53 Fe = 2.26 Mg = 93.40

# APPENDIX C

Microprobe mineral analysis (wt.%) of olivine, clinopyroxene, orthopyroxene and plagioclase phases within Mchrlite-Lherzolite, Pyroxenite and Gabbro lithologies of the Younger Suite. Mg', Ca', Fe' (Mol %) for the sample average, An (Mol %), Fo (Mol %), and  $Mg^* = Mg \times 100 / (Mg + Fe \text{ (Mol \%)})$ , C = core, R = rim, I = xenocryst inclusion, Oih = Oihocryst, O = no description, and A = Average.

## C.1. MCHRLITE-LHERZOLITE

### C.1.1. Olivine

Sample	Code	Na	Mg	Al	Si	K	Ca	Ti	Cr	Mn	Fe	Ni	TOTAL	Average
273	O		41.60	-	38.78		-	-	-	.16	17.94	.12	98.61	Fo = 80.48
	O		41.37	-	38.40		.01	-	-	.27	17.93	.13	98.10	
	A		41.48	-	38.59		-	-	-	.22	17.93	.12	98.33	
173	O		38.13	.04	37.90		-	-	-	.30	23.93	.12	100.42	Fo = 73.66
	O		38.27	.04	38.77		-	-	-	.24	23.55	.11	100.98	
	O		37.64	-	38.78		-	-	-	.30	24.56	.15	101.43	
	A		37.92	.02	38.55		-	-	-	.29	24.15	.13	101.05	
173	I		38.63	.04	37.97		-	-	-	.24	23.60	.15	100.62	Fo = 74.47
173	O		38.63	.04	37.74		-	-	-	.27	22.72	.17	99.56	Fo = 75.18
132	C		40.11	-	37.83		-	-	-	.26	19.55	.16	97.92	Fo = 78.36
	R		40.64	.02	38.52		-	-	.02	.30	19.84	.04	99.40	
	A		40.37	.02	38.17		-	-	-	.28	19.70	.10	98.63	
183	O		45.82	-	39.67		-	.01	-	.22	13.01	.09	98.82	Fo = 86.20
173	C		38.92	.02	38.73		-	-	-	.29	22.52	.14	100.61	Fo = 73.32
	R		38.71	.11	38.64		-	-	-	.19	22.79	.12	100.55	
	A		38.82	.06	38.68		-	-	-	.24	22.66	.13	100.58	
173	C		37.58	.02	38.86		-	-	-	.29	23.05	.14	99.94	Fo = 74.40
	R		37.76	-	38.84		-	-	-	.30	23.16	.08	100.14	
	A		37.67	-	38.84		-	-	-	.30	23.10	.11	100.02	
173	I		37.93	-	38.87		-	-	-	.33	22.66	.10	97.88	Fo = 74.88
173	R		36.43	.02	36.39		-	-	-	.32	22.86	.10	99.78	Fo = 74.82
	C		36.66	.04	36.77		-	-	.01	.30	23.28	.16	100.99	
	A		38.12	.04	38.91		-	-	-	.31	22.86	.14	100.39	

APPENDIX C (Cont'd)

C.1. WERRELLITE-LABRADORITE (Cont'd)

C.1.1 Olivine

Sample	Code	Na	Mg	Al	Si	K	Ca	Ti	Cr	Mn	Fe	Mi	TOTAL	Average
213	O		47.45	.02	39.76		.04	-	.02	.22	12.34	.08	99.93	
	O		47.56	-	40.00		.04	-	-	.25	12.60	.17	100.63	
	A		47.50	-	39.88		.04	-	-	.23	12.47	.13	100.25	Fe = 87.16
213	Z		48.05	.02	40.18		.07	-	-	.11	11.84	.21	100.52	
	Z		47.42	-	39.85		.02	-	-	.15	12.10	.14	99.68	
	A		47.73	-	40.01		.05	-	-	.13	11.99	.17	100.09	Fe = 87.64
073	O		46.16	.02	39.67		-	-	-	.21	13.64	.15	99.85	
	O		47.23	-	40.03		-	-	-	.27	13.95	.16	101.63	
	A		46.69	-	39.84		-	-	-	.23	13.79	.15	100.71	Fe = 85.78
073	O		46.77	-	39.91		-	-	-	.19	13.76	.24	100.88	
	O		46.40	-	39.74		-	-	-	.22	13.92	.24	100.53	
	A		46.59	-	39.82		-	-	-	.21	13.84	.24	100.70	Fe = 85.71
271	O		39.79	-	38.63		-	-	-	.29	20.20	.18	99.09	
	O		40.90	.02	38.02		-	-	-	.37	21.02	.08	100.41	
	A		40.34	-	38.32		-	-	-	.33	20.41	.13	99.73	Fe = 77.71
273	O		42.74	.02	39.27		-	-	-	.27	18.13	.11	100.54	
	O		42.70	.02	38.66		.02	-	-	.26	18.19	.07	99.93	
	A		42.72	.02	38.96		-	-	-	.27	18.16	.09	100.22	Fe = 80.74
273	O		43.56	-	39.48		-	-	-	.23	18.36	.11	101.73	
	O		43.18	-	38.95		-	-	-	.15	18.26	.08	100.63	
	A		43.37	-	39.21		-	-	-	.19	18.30	.09	101.16	Fe = 80.85
068	O		41.91	.90	39.31		.01	-	-	.16	18.48	.17	100.93	
	O		41.78	.19	37.96		-	-	-	.20	18.80	.12	99.06	
	A		41.84	.55	38.64		-	-	-	.18	18.64	.15	100.00	Fe = 80.00
068	O		42.34	.99	39.88		.02	-	-	.21	17.72	.12	101.28	Fe = 80.98

## APPENDIX C (Cont'd)

## G.1. NICKELITE-LIMBOLITE (Cont'd)

## C.A.1 Olivine

Sample	Code	Na	Mg	Al	Si	K	Ca	Ti	Cr	Mn	Fe	Ni	TOTAL	Average
048	0		42.79	.02	36.46		-	-	-	.24	18.50	.11	100.11	
	0		42.16	-	39.26		-	-	-	.19	17.97	.06	99.79	
	A		42.48	-	38.93		-	-	-	.21	18.23	.08	99.94	Fe = 88.11
132	0		41.30	.07	39.41		.01	-	-	.26	20.73	.10	101.89	
	0		41.06	.11	37.53		.02	-	-	.30	21.43	.11	100.55	
	0		41.31	.57	36.22		-	-	-	.21	19.97	.07	98.35	
	0		40.42	.04	38.61		-	-	-	.24	20.98	.13	100.61	
	0		41.13	.04	38.89		-	-	-	.31	20.78	.12	101.27	
	A		41.08	.14	38.26		-	-	-	.27	20.78	.10	100.64	Fe = 86.28
132	0		40.33	-	39.65		-	-	-	.24	20.02	.01	100.26	Fe = 86.43
132	0		41.23	.02	39.56		-	.02	-	.24	20.45	.03	101.55	Fe = 78.22
132	0		41.15	-	36.89		-	-	-	.25	20.78	.05	99.13	
	0		40.60	.02	39.50		-	-	-	.23	19.41	.03	100.00	
	A		40.87	-	38.20		-	-	-	.24	20.20	.04	99.55	Fe = 78.88
183	0		43.80	-	40.33		-	-	-	.17	13.13	.18	99.60	
	0		46.59	.07	40.97		-	-	-	.17	13.38	.15	101.24	
	A		46.20	.02	40.64		-	-	-	.17	13.21	.16	100.40	Fe = 86.01
183	0		47.28	-	40.00		-	-	-	.21	13.39	.16	101.05	
	0		44.71	.02	38.78		-	-	-	.21	13.73	.07	97.32	
	A		46.00	-	39.39		-	-	-	.21	13.56	.11	99.26	Fe = 81.80

APPENDIX C (Cont'd)

C.1. WERLITE-LAURELITE (Cont'd)

C.1.2 Clinopyroxene

Sample	Code	Na	Mg	Al	Si	K	Ca	Ti	Cr	Mn	Fe	Ni	TOTAL	Average
073	O	.09	17.92	1.82	53.70	-	21.07	.09	.07	.10	4.02	.06	98.92	Mg' = 52.14 Ca' = 44.05 Fe' = 3.81 Mg* = 88.80
073	O	.09	17.96	1.82	53.58	-	20.91	-	.15	.12	4.03	.09	98.75	Mg' = 52.58 Ca' = 43.99 Fe' = 3.43 Mg* = 88.82
073	O	.11	18.72	2.11	51.72	-	18.53	-	.21	.09	4.96	.09	96.53	Mg' = 55.65 Ca' = 39.58 Fe' = 4.77 Mg* = 87.05
213	Z	.06	18.79	1.26	53.86	-	22.14	-	.40	.08	2.81	-	99.42	Mg' = 52.27
	Z	.03	19.08	.03	54.41	-	23.71	-	.05	.12	2.04	.05	99.84	Ca' = 45.48
	A	.04	18.94	.78	54.13	-	22.93	-	.23	.10	2.45	.03	99.62	Fe' = 2.24 Mg* = 93.23
213	Z	.09	18.47	1.43	53.84	-	22.19	-	.49	.11	3.02	.06	99.70	Mg' = 52.16 Ca' = 45.03 Fe' = 2.81 Mg* = 91.60
213	Z	.09	22.99	1.11	56.84	-	12.27	-	.05	.10	3.65	-	97.10	Mg' = 69.67 Ca' = 26.72 Fe' = 3.61 Mg* = 91.80
213	O	.05	18.29	2.15	53.61	-	21.61	-	.37	.13	3.39	.07	99.68	Mg' = 53.05
	O	.05	18.77	2.12	54.25	-	20.89	.02	.60	.15	3.46	.03	100.14	Ca' = 43.71
	A	.05	18.53	2.14	53.93	-	21.25	-	.39	.14	3.42	.05	99.89	Fe' = 3.24 Mg* = 90.60



APPENDIX C (Cont'd)

G.1. WHEELITE-LAWRENOLITE (Cont'd)

C.1.2 Clinopyroxene

Sample	Code	Na	Mg	Al	Si	K	Ca	Ti	Cr	Mn	Fe	Ni	TOTAL	Average
048	Z		16.05	1.89	53.27		21.67	.08	.18	.14	4.74	.03	98.04	Mg' = 46.38
	Z		15.98	1.96	52.25		22.04	.10	.19	.14	4.82	.01	97.48	Ca' = 46.94
	A		16.01	1.92	52.76		21.85	.09	.18	.14	4.78	.02	97.75	Fe' = 4.67 Mg'' = 85.66
048	O		16.13	1.88	53.22		21.63	.04	.16	.17	4.88	.08	98.36	Mg' = 48.73
														Ca' = 46.47
														Fe' = 4.81 Mg'' = 85.61
132	O		16.59	1.72	53.96		19.43	.13	-	.18	6.35	.04	98.38	Mg' = 50.84
														Ca' = 42.79
														Fe' = 6.36 Mg'' = 82.32
132	O		18.35	1.72	51.84		18.59	.16	-	.18	6.61	.06	97.41	Mg' = 54.05
														Ca' = 39.56
														Fe' = 6.40 Mg'' = 83.10
048	O	.18	20.76	1.96	53.87	-	16.22	-	.25	.18	7.14	-	100.56	Mg' = 60.46
	O	.10	20.99	2.82	53.76	-	15.20	.08	.16	.13	7.40	.03	100.67	Ca' = 52.70
	A	.13	20.87	2.39	53.81	-	15.71	.04	.21	.16	7.27	.01	100.61	Fe' = 6.84 Mg'' = 83.65
048	O	.10	16.84	1.59	53.34	.01	22.23	.07	.35	.12	4.33	.07	99.05	Mg' = 49.27
	O	.21	17.00	1.76	53.29	-	22.07	.03	.25	.16	4.71	.03	99.50	Ca' = 46.39
	A	.16	16.91	1.67	53.30	-	22.15	.05	.30	.14	4.52	.05	99.25	Fe' = 4.37 Mg'' = 86.95
048	O	.16	17.05	1.80	53.12	-	21.18	.05	.27	.09	4.03	-	98.65	Mg' = 49.87
	O	.05	16.82	1.80	53.51	.01	21.90	.07	.21	.17	4.50	-	99.04	Ca' = 45.60
	A	.10	16.93	1.80	53.31	-	21.54	.06	.24	.13	4.71	-	98.82	Fe' = 4.53 Mg'' = 86.51

APPENDIX C (Cont'd)

C.1. WEHLITE-LIMBSOLITE (Cont'd)

C.1.2. Clinopyroxene

Sample	Code	Na	Mg	Al	Si	K	Ca	Ti	Cr	Mn	Fe	Ni	TOTAL	Average
068	O	.14	17.38	2.13	50.96	-	20.94	.02	.27	.16	5.13	-	97.11	Mg' = 50.95 Ca' = 44.11 Fe' = 4.94 Mg <sup>2+</sup> = 85.79
068	O	.18	17.15	2.05	52.78	-	21.64	.07	.26	.16	4.95	.02	99.26	Mg' = 52.41
	O	.14	19.66	1.80	54.01	-	20.00	.02	.29	.18	5.68	-	101.77	Ca' = 42.62
	A	.16	18.40	1.93	53.39	-	20.82	.05	.27	.17	5.31	-	100.48	Fe' = 4.96 Mg <sup>2+</sup> = 86.06
068	O	.14	17.41	1.93	52.55	-	20.13	-	.32	.16	7.90	.05	97.60	Mg' = 50.85
	O	.09	17.11	1.94	53.06	-	22.01	.13	.21	.15	4.46	-	99.18	Ca' = 44.61
	A	.11	17.26	1.93	52.80	-	21.07	.06	.27	.15	4.69	.03	98.38	Fe' = 4.34 Mg <sup>2+</sup> = 86.76
183	O	.09	19.12	2.52	53.73	-	19.65	-	.70	.10	4.10	-	100.00	Mg' = 53.45
	O	.18	17.70	2.55	53.05	-	21.50	-	.73	.13	3.49	.01	99.34	Ca' = 42.94
	A	.13	18.40	2.53	53.39	-	20.57	-	.71	.11	3.79	-	99.64	Fe' = 3.61 Mg <sup>2+</sup> = 89.64
183	O	.14	17.53	1.99	52.34	-	22.34	.03	.54	.04	3.71	-	98.66	Mg' = 50.41 Ca' = 46.16 Fe' = 3.43 Mg <sup>2+</sup> = 89.38
183	O	.16	18.23	2.41	51.68	-	22.38	.03	.37	.14	3.22	.06	98.68	Mg' = 51.67
	O	.07	17.52	1.18	52.97	-	23.29	-	.26	.06	3.07	-	98.43	Ca' = 47.41
	A	.11	17.88	1.79	52.32	-	22.83	.02	.32	.10	3.14	.03	98.54	Fe' = .92 Mg <sup>2+</sup> = 91.02
132	Z	.23	17.88	1.96	53.38	.01	20.02	.22	.07	.13	5.73	.03	99.65	Mg' = 51.77
	Z	.13	17.81	1.85	52.86	-	21.13	.28	.04	.16	5.53	-	99.79	Ca' = 42.90
	A	.18	17.84	1.90	53.11	-	20.57	.25	.05	.15	5.63	.01	99.69	Fe' = 5.53 Mg <sup>2+</sup> = 84.95

APPENDIX C (Cont'd)

G.1. WEIRLITE-LIMONOLITE (Cont'd)

C.1.2 Clinopyroxene

Sample	Code	Na	Mg	Al	Si	K	Ca	Ti	Cr	Mn	Fe	Ni	TOTAL	Average
132	O	.11	17.30	1.91	53.66	-	21.07	.23	.07	.15	5.40	.05	99.95	Mg' = 49.78
	O	.14	16.71	1.51	53.72	-	21.89	-	.08	.14	5.16	-	99.36	Ca' = 45.17
	A	.13	17.00	1.70	53.68	-	21.47	.12	.07	.14	5.28	.03	99.63	Fe' = 5.05 Mg'' = 85.15
132	O	.19	16.86	1.78	53.53	-	21.92	.22	.02	.12	5.37	-	100.01	Mg' = 49.07
														Ca' = 45.85
														Fe' = 5.08 Mg'' = 84.83
132	O	.14	17.20	1.80	53.22	-	21.75	.18	.05	.16	4.94	.07	99.61	Mg' = 49.53
	O	.05	16.84	1.77	52.72	-	22.18	.14	.08	.15	4.57	.05	98.55	Ca' = 45.93
	A	.10	17.02	1.78	53.02	-	21.96	.16	.07	.15	4.76	.06	99.07	Fe' = 4.55 Mg'' = 86.43
173	O	.25	18.09	1.74	51.82	-	20.16	.09	.21	.14	5.85	-	98.36	Mg' = 53.36
	O	.30	18.51	1.73	53.80	.01	18.72	.17	.13	.20	6.59	-	100.15	Ca' = 40.73
	A	.27	18.30	1.73	52.80	-	19.44	.13	.16	.17	6.21	-	99.23	Fe' = 5.92 Mg'' = 84.00
173	O	.17	16.48	2.08	52.66	-	21.32	.23	.05	.07	5.73	-	98.82	Mg' = 48.90
	O	.26	16.29	1.88	52.67	-	21.09	.39	.08	.18	5.79	-	98.63	Ca' = 45.51
	A	.21	16.38	1.98	52.67	-	21.21	.31	.13	.13	5.76	-	98.71	Fe' = 5.60 Mg'' = 83.52
173	Z	.23	16.76	2.56	50.60	-	19.75	.09	.25	.23	6.68	-	97.15	Mg' = 50.56
														Ca' = 42.81
														Fe' = 6.63 Mg'' = 81.72
173	O	.18	16.80	2.00	52.86	.01	21.40	.17	.13	.17	5.47	.04	99.23	Mg' = 52.10
	O	.24	18.81	2.23	53.61	.01	18.50	.17	.12	.11	7.00	.02	100.82	Ca' = 41.97
	A	.21	17.80	2.11	53.23	.01	19.95	.17	.12	.14	6.23	.03	100.01	Fe' = 5.93 Mg'' = 83.58

# APPENDIX C (Cont'd)

## C.1. WEIRLITE-LAWSONITE (Cont'd)

### C.1.2 Clinopyroxene

Sample	Code	Na	Mg	Al	Si	K	Ca	Ti	Cr	Mn	Fe	NI	TOTAL	Average
173	Z	.22	17.79	2.28	54.03	-	19.18	.24	.13	.21	7.58	-	101.63	Mg' = 52.24 Ca' = 40.84 Fe' = 7.28 Mg'' = 81.00
273	Z	.21	17.63	1.86	53.28	-	21.74	.01	.24	.09	5.12	-	100.18	Mg' = 50.50 Ca' = 44.75 Fe' = 4.74 Mg'' = 85.99
273	O	.17	17.22	2.16	52.52	-	20.71	.06	.16	.14	4.88	-	98.02	Mg' = 49.97
	O	.05	17.48	.34	54.13	-	23.94	.07	.04	.12	3.20	.03	99.41	Ca' = 46.21
	A	.11	17.35	1.25	53.31	-	22.33	.07	.09	.13	4.04	.01	98.68	Fe' = 3.82 Mg'' = 88.44
271	O	.18	16.86	1.85	53.36	-	21.66	.02	.02	.16	5.64	-	99.73	Mg' = 49.54
	O	.12	16.83	1.62	53.37	-	21.38	-	-	.17	5.53	-	99.02	Ca' = 45.31
	A	.14	16.84	1.72	53.36	-	21.52	-	-	.16	5.58	-	99.38	Fe' = 5.35 Mg'' = 84.32

APPENDIX C (Cont'd)

C.1. WENKITE-LIMBOLITE (Cont'd)

C.1.1 Orthopyroxene

Sample	Code	Na	Mg	Al	Si	K	Ca	Ti	Cr	Mn	Fe	Ni	TOTAL	Average
173	Oik		30.03	.67	56.68		.02	.03	-	.32	10.43	.01	98.19	Mg <sup>2+</sup> = 88.10
	Oik		28.03	1.13	55.51		.35	.06	.07	.19	12.87	.03	98.25	Ca <sup>2+</sup> = .40
	A		29.03	.90	56.10		.19	.05	.04	.26	11.45	.02	98.22	Fe <sup>2+</sup> = 11.50
173	O		27.10	1.18	55.59		.28	.02	-	.32	13.46	-	97.94	Mg <sup>2+</sup> = 85.30
	O		27.34	1.06	54.31		.21	.07	.03	.32	14.30	.05	97.70	Ca <sup>2+</sup> = .54
	A		27.21	1.12	54.95		.24	.05	-	.32	13.88	.03	97.78	Fe <sup>2+</sup> = 14.14
073	O	.02	32.50	1.28	56.18	-	.67	.04	.05	.13	8.88	.05	99.80	Mg <sup>2+</sup> = 90.21
	O	-	33.33	1.37	56.38	-	.86	-	.06	.22	8.73	.08	101.04	Ca <sup>2+</sup> = 1.97
	A	.01	32.91	1.32	56.28	-	.77	-	.05	.17	8.80	.06	100.39	Fe <sup>2+</sup> = 7.82
213	Oik	.05	33.74	.88	57.15	-	.50	.03	.19	.14	7.60	-	100.29	Mg <sup>2+</sup> = 91.35
	Oik	-	32.74	.57	57.33	-	1.74	-	.19	.15	6.30	.07	99.10	Ca <sup>2+</sup> = 2.24
	A	.02	33.24	.73	57.23	-	1.13	-	.19	.14	6.95	.04	99.67	Fe <sup>2+</sup> = 6.21
213	Oik	.01	34.41	.84	57.79	-	1.33	-	.14	.17	7.07	-	101.96	Mg <sup>2+</sup> = 92.08
	Oik	.06	34.43	1.07	56.76	.01	1.12	-	.23	.11	6.96	.01	101.26	Ca <sup>2+</sup> = 1.90
	A	.04	34.77	.96	51.27	-	1.22	-	.19	.14	7.01	-	101.60	Fe <sup>2+</sup> = 6.02
068	O		29.57	1.31	56.24		.46	-	.07	.20	11.98	.03	99.88	Mg <sup>2+</sup> = 87.56 Ca <sup>2+</sup> = 1.00 Fe <sup>2+</sup> = 11.46
068	O		29.34	1.40	55.99		.64	-	.11	.31	11.90	.09	97.78	Mg <sup>2+</sup> = 87.10 Ca <sup>2+</sup> = 1.34 Fe <sup>2+</sup> = 11.53
132	O		40.52	-	38.80		.02	.01	-	.28	19.91	.05	99.58	Mg <sup>2+</sup> = 86.28 Ca <sup>2+</sup> = .04 Fe <sup>2+</sup> = 13.68
132	O		40.48	-	38.02		-	.01	.02	.15	20.39	.08	99.15	Mg <sup>2+</sup> = 86.10 Ca <sup>2+</sup> = 0.00 Fe <sup>2+</sup> = 13.89

APPENDIX C (Cont'd)

C.1. WEILLITE-LAWSONITE (Cont'd)

C.1.3 Orthopyroxene

Sample	Code	Na	Mg	Al	Si	K	Ca	Ti	Cr	Mn	Fe	Ni	TOTAL	Average
068	O	.01	30.04	1.25	54.90	-	1.14	.02	.10	.14	10.25	.09	97.94	Mg' = 87.72
	O	.04	31.26	1.17	56.06	-	1.18	.07	.10	.26	11.09	.03	101.27	Ca' = 2.39
	A	.02	30.65	1.21	55.48	-	1.16	.05	.10	.20	10.67	.05	99.60	Fe' = 9.90
068	O	.05	30.76	1.30	55.43	-	1.41	.05	.13	.24	11.36	-	100.73	Mg' = 87.72
	O	.02	30.03	1.24	55.50	-	.70	.02	.10	.21	12.00	.07	99.89	Ca' = 2.16
	A	.04	30.39	1.27	55.46	-	1.05	.03	.11	.22	11.67	.03	100.29	Fe' = 10.82
132	O	-	29.80	1.13	55.72	-	.83	-	.03	.22	12.88	-	100.61	Mg' = 87.41 Ca' = 1.75 Fe' = 10.84
132	O	-	29.87	1.13	53.57	-	.84	.02	.03	.23	13.00	.01	98.71	Mg' = 86.12 Ca' = 1.74 Fe' = 12.13
273	O	.01	30.66	1.21	56.28	-	.96	-	.08	.22	11.12	.06	100.61	Mg' = 87.19
	O	-	26.16	5.69	53.09	.01	.81	.07	.05	.25	10.71	.12	96.98	Ca' = 1.94
	A	-	28.42	3.47	54.68	-	.88	.03	.07	.23	10.91	.09	98.79	Fe' = 10.87
273	O	-	31.15	1.54	56.04	-	1.05	.02	.08	.20	11.02	.01	101.11	Mg' = 86.71
	O	.07	30.82	1.50	55.82	-	2.19	.01	.07	.25	11.09	.06	101.88	Ca' = 3.26
	A	.02	30.98	1.52	55.93	-	1.62	.01	.07	.22	11.05	.04	101.46	Fe' = 10.03

## APPENDIX C (Cont'd)

## C.1. WEIRLITE-LARSENOLITE (Cont'd)

## C.1.4 Plagioclase

Sample	Code	Na	Mg	Al	Si	K	Ca	Ti	Cr	Mn	Fe	Ni	TOTAL	Average
048	0	.82	.04	32.89	45.20	.01	18.07	-	.01	.01	.39	-	97.43	An = 94.44
	0	.80	.01	33.17	45.14	-	18.13	.01	-	-	.33	-	97.61	
	0	.61	.03	33.95	44.97	-	18.04	-	.02	-	.25	.06	97.94	
	A	.74	.02	33.33	45.11	-	18.09	-	-	-	.32	-	97.62	
048	0	1.00	.06	32.87	44.78	-	17.79	.07	-	.01	.30	-	96.88	An = 92.52
	0	.85	.05	32.82	44.66	.01	17.98	.04	-	.06	.41	-	96.88	An = 93.90
132	0	.89	.03	33.17	45.99	-	18.39	.02	-	.02	.39	.04	98.95	An = 93.49
132	2	1.09	.01	32.97	45.48	-	17.90	-	-	.01	.34	.04	97.83	An = 91.97
132	0	.84	-	32.01	44.87	.01	17.53	-	-	.03	.29	-	95.58	An = 93.56
173	0	.98	.01	32.34	45.57	.01	17.78	-	-	.01	.39	.01	97.00	An = 92.64
173	0	1.15	.02	32.67	45.41	.01	17.71	-	-	.01	.41	.04	97.44	An = 94.47
173	0	1.05	-	32.38	45.47	-	18.29	-	-	.01	.26	.03	97.49	An = 91.92
173	0	1.14	.02	32.55	45.33	.01	17.77	-	-	-	.43	.02	97.27	An = 91.37
173	0	.85	.05	32.20	45.73	.01	17.71	-	-	-	.45	.03	97.04	An = 93.54
173	0	.97	-	33.04	45.40	-	18.25	.01	-	.07	.37	.02	98.11	An = 92.88
273	0	.83	.04	33.04	44.01	-	18.16	-	-	-	.34	-	96.42	An = 93.83
273	2	.83	.05	32.64	45.18	-	18.02	-	-	.03	.36	.03	97.16	An = 93.78
273	2	1.07	.04	32.84	44.01	.02	17.80	.03	-	-	.36	.02	96.20	An = 92.04
271	0	.81	-	33.53	45.33	-	18.34	-	-	.06	.41	-	98.27	An = 96.15

APPENDIX C (Cont'd)

C.2. YOUNGER SUITE - PYROXENITE

C.2.1 Clinopyroxene

Sample	Code	Na	Mg	Al	Si	K	Ca	Ti	Cr	Mn	Fe	Ni	TOTAL	Average
281	O	.07	24.05	.83	53.85	-	14.82	.04	.39	.11	3.02	.05	101.22	Mg' = 66.20 Ca' = 29.32 Fe' = 4.49 Mg'' = 89.52
281	O	.09	20.50	.73	54.79	-	20.52	.03	.36	.07	2.94	-	100.04	Mg' = 56.09
	O	.13	19.55	.68	54.08	-	20.62	-	.36	.09	2.50	.01	98.02	Ca' = 41.41
	A	.11	20.02	.70	54.43	-	20.57	.01	.36	.08	2.72	-	99.01	Fe' = 2.49 Mg'' = 92.90
281	O	.04	19.17	.76	53.64	-	21.63	-	.37	.07	2.62	.01	98.30	Mg' = 54.57
	O	.09	19.72	.71	54.22	-	20.98	.04	.32	.09	2.81	.04	99.02	Ca' = 42.94
	A	.06	19.45	.73	53.93	-	21.30	.02	.35	.08	2.71	.02	98.65	Fe' = 2.49 Mg'' = 92.75
281	O	.13	21.03	.76	54.76	-	19.79	-	.29	.07	3.01	.07	99.91	Mg' = 56.47
	O	.12	20.05	.68	54.43	-	21.73	-	.33	.07	2.59	.04	100.04	Ca' = 41.02
	A	.13	20.54	.72	54.60	-	20.76	-	.31	.07	2.80	.05	99.97	Fe' = 2.51 Mg'' = 92.89
207	O	.24	18.49	2.16	53.29	-	21.01	-	.59	.16	4.00	.01	99.97	Mg' = 52.36
	O	.11	18.08	2.21	53.30	-	21.73	-	.55	.11	3.77	-	99.87	Ca' = 43.99
	A	.18	18.28	2.18	53.28	-	21.37	-	.57	.13	3.88	-	99.88	Fe' = 3.65 Mg'' = 89.35
207	O	.23	22.85	1.72	56.92	.02	12.64	.03	-	.10	3.68	.01	98.22	Mg' = 68.53
	O	.33	21.93	2.04	56.54	.02	12.22	.02	-	.11	4.55	.05	97.80	Ca' = 27.36
	A	.28	22.39	1.88	56.73	.02	12.44	.02	-	.10	4.12	.03	98.01	Fe' = 4.11 Mg'' = 90.65
246	O	.12	16.22	2.96	52.53	-	20.27	.06	.31	.13	3.57	.02	101.18	Mg' = 50.75 Ca' = 45.57 Fe' = 3.68 Mg'' = 89.00



APPENDIX C (Cont'd)

C.2. TOUCHER SUITE - PYROXENITE (Cont'd)

C.2.1 Clinopyroxene

Sample	Code	Na	Mg	Al	Si	K	Ca	Ti	Cr	Mn	Fe	Ni	TOTAL	Average
246	O	.11	16.68	4.93	52.39	-	20.62	-	.33	.09	3.54	-	98.70	Mg' = 53.35
	O	.13	18.84	1.99	53.25	-	21.34	-	.32	.14	3.44	-	99.43	Ca' = 43.43
	O	.12	17.76	3.46	52.82	-	20.98	-	.32	.11	3.49	-	99.07	Fe' = 3.23
	A													Mg = 90.70
246	O	.09	19.26	1.77	56.91	.01	20.25	-	.25	.17	3.35	-	102.06	Mg' = 53.44
	O	.07	18.45	1.89	51.45	-	22.30	-	.32	.09	3.54	-	98.12	Ca' = 43.33
	O	.08	18.85	1.83	54.18	-	21.27	-	.29	.13	3.45	-	100.09	Fe' = 3.21
	A													Mg = 90.68
246	O	.06	19.21	.87	55.52	-	20.42	.07	.21	.15	3.62	-	100.06	Mg' = 54.74
	O	-	19.93	1.01	54.73	-	21.23	.07	.35	.09	3.82	.05	101.29	Ca' = 41.85
	O	.02	19.57	.94	55.12	-	20.82	.03	.28	.12	3.71	.02	100.64	Fe' = 3.40
	A													Mg = 90.38
246	O	.08	20.64	.97	55.53	-	19.50	-	.36	.11	4.31	.05	101.54	Mg' = 57.24
														Ca' = 38.86
														Fe' = 3.90
														Mg = 89.50
161	O	.23	17.57	1.20	53.88	.03	23.16	.05	.15	.14	3.24	-	99.64	Mg' = 49.45
	O	-	17.30	.73	53.82	-	23.24	.06	.21	.13	3.29	.05	98.83	Ca' = 47.47
	O	.14	17.05	1.09	54.61	.10	22.95	-	.18	.13	3.22	.06	99.54	Fe' = 3.07
	A	.12	17.30	1.00	54.09	.04	23.11	.03	.18	.13	3.25	.01	99.26	Mg = 90.46
161	Z	.09	18.23	1.24	54.66	-	22.91	.03	.11	.07	3.41	.06	100.82	Mg' = 50.62
	Z	.13	17.87	1.36	53.27	-	22.94	.03	.22	.15	3.51	.09	99.58	Ca' = 46.19
	A	.11	18.05	1.30	53.94	-	22.92	.03	.16	.11	3.46	.08	100.19	Fe' = 3.19
														Mg = 90.28
161	O	.05	17.81	.71	54.77	-	23.84	.05	.16	.15	3.11	.02	100.68	Mg' = 49.31
	O	.12	17.70	.56	54.29	-	23.95	.07	.11	.13	3.36	-	100.30	Ca' = 47.71
	O	.09	17.63	.70	54.01	-	23.78	.03	.15	.13	3.22	.08	99.80	Fe' = 2.98
	A	.09	17.71	.65	54.15	-	23.85	.05	.13	.14	3.23	.03	100.23	Mg = 90.71

# APPENDIX C (Cont'd)

## C.2. YOUNGER SUITE - PYROXENITE (Cont'd)

### C.2.1 Clinopyroxene

Sample	Code	Na	Mg	Al	Si	K	Ca	Ti	Cr	Mn	Fe	NI	TOTAL	Average
407C-A	O	.07	22.63	.90	55.25	-	16.50	-	.41	.13	3.42	-	99.32	Mg' = 58.28
	O	.07	18.49	.91	54.59	-	21.98	.02	.44	.14	2.53	.09	99.26	Ca' = 39.11
	A	.07	20.57	.91	54.92	-	19.24	-	.43	.14	2.97	.04	99.29	Fe' = 2.71 Mg = 92.50
407C-A	O	.08	20.41	.98	54.99	-	19.43	-	.42	.08	2.94	.02	99.35	Mg' = 57.64
	O	.09	20.30	.91	53.86	.02	19.47	.02	.45	.13	3.01	.03	98.27	Ca' = 39.59
	A	.08	20.35	.94	54.43	-	19.45	-	.43	.10	2.97	.03	98.79	Fe = 2.76 Mg = 92.40
407C-A	O	.06	26.48	.73	56.06	-	12.71	-	.37	.09	4.62	-	101.14	Mg' = 71.36 Ca' = 24.61 Fe' = 4.03 Mg = 91.08
407C-A	O	.05	28.89	.79	55.94	-	8.44	-	.43	.11	4.84	.06	99.55	Mg' = 68.22
	O	.13	20.44	.94	55.02	-	20.00	-	.40	.12	2.94	.04	100.03	Ca' = 28.26
	A	.09	24.70	.86	55.49	-	14.24	-	.41	.11	3.89	.05	99.85	Fe' = 3.51 Mg = 91.88
407C-A	O	-	20.07	.89	55.01	.02	21.25	-	.49	.10	2.83	.09	100.75	Mg' = 55.88
	O	.10	20.57	1.24	54.75	.01	20.70	-	.55	.07	3.09	.01	101.09	Ca' = 41.46
	A	.05	20.32	1.07	54.88	.02	20.98	-	.52	.09	2.96	.05	100.92	Fe' = 2.66 Mg = 92.44
407C-A	O	.10	19.51	.93	54.19	.01	21.29	-	.55	.09	2.57	.07	99.30	Mg' = 54.59
	O	.09	19.89	.94	54.13	.01	21.88	-	.51	.15	2.65	.02	100.26	Ca' = 43.00
	A	.09	19.71	.93	54.16	.01	21.59	-	.53	.12	2.61	.04	99.78	Fe' = 2.40 Mg = 93.08
407C-A	O	.09	19.81	.84	53.91	-	21.76	-	.70	.12	2.69	.05	99.96	Mg' = 54.51 Ca' = 43.03 Fe' = 2.46 Mg = 92.90

APPENDIX C (Cont'd)

C.2. YOUNGER SUITE - PYROXENITE (Cont'd)

C.2.1 Orthopyroxene

Sample	Code	Na	Mg	Al	Si	K	Ca	Ti	Cr	Mn	Fe	Wt	TOTAL	Average
281	O	-	35.29	.31	57.59	-	1.43	-	.19	.20	6.02	-	101.44	Mg' = 92.37
	O	.01	35.31	.47	55.98	-	1.06	-	.22	.11	5.93	.06	99.16	Ca' = 2.34
	A	-	35.29	.49	56.88	-	1.24	-	.20	.14	5.97	.03	100.25	Fe' = 5.09
281	O	-	34.62	.50	57.53	.01	1.39	-	.20	.09	6.03	.03	100.40	Mg' = 92.16
														Ca' = 2.46
														Fe' = 5.18
281	O	.03	34.47	.44	55.23	-	1.46	-	.15	.25	6.09	.09	98.72	Mg' = 92.13
	O	.03	35.32	.51	57.57	-	1.46	-	.14	.20	5.75	-	100.99	Ca' = 2.75
	A	.03	35.15	.47	56.40	-	1.46	-	.14	.23	5.92	.05	99.85	Fe' = 5.12
246	O	-	31.10	1.71	55.24	-	1.84	-	.19	.20	8.77	.01	99.06	Mg' = 88.16
														Ca' = 3.75
														Fe' = 8.09
246	O	-	31.90	1.60	57.12	-	1.68	-	.19	.30	8.95	.07	101.81	Mg' = 89.26
	O	.02	33.29	1.20	56.75	-	.99	.01	.16	.24	9.16	.03	101.84	Ca' = 2.62
	A	.01	32.59	1.40	56.93	-	1.33	-	.18	.27	9.05	.05	101.81	Fe' = 8.12
246	O	-	32.83	1.97	55.83	-	1.13	-	.16	.25	8.28	.02	100.46	Mg' = 89.99
	O	.06	33.07	1.84	53.89	-	1.21	-	.20	.24	8.98	-	99.51	Ca' = 2.30
	A	.03	32.95	1.91	54.86	-	1.17	-	.18	.24	8.63	.01	99.99	Fe' = 7.70
161	O	-	32.70	1.00	56.82	-	1.18	-	.09	.20	9.39	.10	101.47	Mg' = 90.04
	O	.01	33.17	1.05	57.39	-	1.20	.01	.09	.20	8.64	.05	101.81	Ca' = 2.11
	O	.01	32.69	1.09	55.69	-	.85	.07	.10	.16	8.43	.05	99.09	Fe' = 7.85
	A	-	32.84	1.05	56.63	-	1.07	-	.09	.18	8.82	.06	100.75	
161	O	.02	32.77	.99	57.14	-	1.16	-	.10	.20	8.55	.05	101.00	Mg' = 89.76
	O	.04	33.27	.89	58.15	-	1.27	-	.11	.25	8.65	.04	102.62	Ca' = 2.41
	O	.06	32.80	1.05	57.28	.01	1.30	-	.13	.21	9.29	-	102.14	Fe' = 7.83
	A	.04	32.94	.98	57.52	-	1.23	-	.11	.21	8.83	.02	101.88	

APPENDIX C (Cont'd)

C.2. YOUNGER SUITE - PYROXENITE (Cont'd)

C.2.2 Orthopyroxene

Sample	Code	Na	Mg	Al	Si	K	Ca	Ti	Cr	Mn	Fe	Ni	TOTAL	Average
161	O	.04	33.64	1.06	56.79	-	.60	.03	.13	.18	9.07	.06	101.60	Mg' = 91.71 Ca' = 1.18 Fe' = 7.19
161	O	.04	32.69	1.11	55.66	-	1.41	-	.13	.23	8.64	-	99.89	Mg' = 90.29 Ca' = 2.79 Fe' = 6.91
161	O	-	32.32	1.18	56.79	-	1.04	-	.13	.18	8.91	.01	100.55	Mg' = 89.78
	O	.03	32.71	.80	56.78	.01	1.06	.03	.13	.32	9.34	.04	101.26	Ca' = 1.98
	A	.01	32.91	.98	56.79	-	1.05	.01	.14	.25	9.13	.03	100.91	Fe' = 8.24

APPENDIX C (Cont'd)

C.2. YOUNGER SUITE - PYROXENITE (Cont'd)

C.2.3 Olivine

Sample	Code	Na	Mg	Al	Si	K	Ca	Ti	Cr	Mn	Fe	Ni	TOTAL	Average
207	0		45.34	-	39.80		.01	-	-	.21	15.60	.09	101.05	
	0		44.59	.04	40.09		-	-	-	.26	14.69	.19	99.88	
	0		45.27	-	39.35		.04	.01	-	.25	15.95	.11	100.96	
	A		45.06	-	39.75		.01	-	-	.24	15.41	.13	100.59	Fe = 83.90
207	0		45.22	-	34.59		.02	-	-	.27	15.83	.12	101.05	
	0		44.91	-	39.83		.04	-	-	.14	15.66	.09	100.66	
	0		45.06	-	39.71		.03	-	-	.21	15.75	.10	100.86	Fe = 83.60
	A													
407C-A	0		49.43	.05	38.40		-	-	-	.13	9.60	.11	97.71	Fe = 90.15
	0		48.95	-	38.57		-	-	-	.12	9.34	.12	97.10	Fe = 90.33
	0		48.77	.02	39.71		-	-	-	.21	9.69	.15	98.55	Fe = 89.96
	0		49.41	.02	39.46		-	.01	-	.21	9.67	.16	98.95	Fe = 90.08
	A		49.09	.02	39.58		-	-	-	.21	9.68	.15	98.73	Fe = 90.02
407C-A	0		49.61	-	41.28		-	-	-	.14	10.16	.08	101.27	Fe = 89.78
407C-A	0		47.84	-	40.43		-	-	-	.14	8.96	.11	97.49	Fe = 90.84
407A-A	0		48.94	.02	41.84		-	-	-	.14	9.09	.08	100.11	Fe = 90.53
	0		48.86	.02	40.32		-	-	-	.17	9.10	.14	98.63	Fe = 90.51
	A		48.89	.02	41.08		-	-	-	.15	9.09	.11	99.34	Fe = 90.55
407A-A	0		49.00	-	40.95		.01	-	-	.16	8.80	.17	99.10	Fe = 90.81
	0		49.85	-	38.69		-	-	-	.19	9.48	.12	98.33	Fe = 90.36
	0		48.72	.04	40.98		-	-	-	.13	9.21	.23	99.31	Fe = 90.43
	A		49.18	-	40.21		-	-	-	.15	9.16	.17	98.88	Fe = 90.51

## APPENDIX C (Cont'd)

## C.2. YOUNGER SUITE - PYROXENITE (Cont'd)

## C.2.4 Plagioclase

Sample	Code	Na	Mg	Al	Si	K	Ca	Ti	Cr	Mn	Fe	BI	TOTAL	Average
161	0	.75	.02	33.43	44.71	-	18.45	-	-	-	.19	-	99.77	An = 96.49
161	0	.91	.04	31.27	49.36	.01	18.56	-	-	.04	.25	-	100.42	An = 95.75
161	0	.66	.85	33.14	44.04	-	17.56	.06	-	.11	2.28	.01	98.50	An = 96.69

APPENDIX C (Cont'd)

C.3. YOUNGER SUITE - CARBON

C.3.1 Plagioclase

Sample	Code	Na	Mg	Al	Si	K	Ca	Ti	Cr	Mn	Fe	Ni	TOTAL	Average
415	O	.63	.04	32.97	44.47	-	18.48	-	-	.01	.45	-	97.55	An = 96.99
073	O	.70	.04	32.66	44.25	-	17.85	-	-	.01	.37	.04	95.92	An = 94.66
073	O	.67	.04	32.93	45.18	.01	18.23	-	-	-	.30	.01	97.37	An = 94.48
285	O	.41	.03	33.44	44.37	-	17.65	-	-	-	.55	.01	96.46	An = 97.94
193	O	1.44	-	33.63	46.32	-	17.14	-	-	.04	.53	.02	99.12	An = 92.97
193	O	1.50	-	32.25	46.60	-	17.66	-	-	-	.67	.03	98.73	An = 92.86
193	C	1.15	.03	32.38	44.61	-	17.86	-	-	.01	.56	-	96.60	An = 94.49
193	R	7.33	.02	24.73	58.88	.14	8.22	-	-	.01	.25	-	99.59	An = 55.35
193	R	5.78	.01	26.36	55.36	.02	10.36	-	-	-	.39	.01	98.30	An = 66.48
193	C	1.21	.07	32.34	46.62	-	17.54	-	-	-	.64	.03	98.45	An = 94.12
257	O	.59	.03	33.40	45.11	-	19.28	-	-	.03	.33	.01	98.78	
	O	.57	.01	33.46	44.52	.02	19.56	-	-	-	.32	.05	98.52	
	A	.58	.02	33.43	44.82	.01	19.41	-	-	-	.32	.03	98.61	An = 97.41
257	Z	.55	.02	33.49	44.32	.02	19.88	-	-	.03	.41	-	98.72	An = 97.56
257	O	.71	.05	33.43	44.68	.01	19.45	-	-	.03	.48	.03	98.86	
	O	.55	.04	31.88	43.24	-	19.37	-	-	.04	.53	.05	95.73	
	A	.63	.05	32.64	43.96	-	19.41	-	-	.04	.50	.04	97.27	An = 97.15

APPENDIX C (Cont'd)

C.3. YOUNGER SUITE - CABARO (Cont'd)

C.3.2 Clinopyroxene

Sample	Code	Na	Mg	Al	Si	K	Ca	Ti	Cr	Mn	Fe	Ni	TOTAL	Average
073	O	.16	17.90	1.73	52.46	-	19.91	-	.05	.15	4.32	.03	96.72	Mg' = 53.23 Ca' = 42.55 Fe' = 4.23 Mg* = 88.07
205	O	.26	15.23	3.16	50.67	-	21.37	.32	.06	.23	7.33	.02	98.65	Mg' = 45.53
	O	.18	14.90	1.66	52.47	.01	22.23	.19	.05	.21	7.02	.04	98.95	Ca' = 47.36
	A	.21	15.06	2.40	51.57	-	21.80	.25	.05	.22	7.11	.03	98.77	Fe' = 7.10 Mg* = 78.90
285	O	.78	17.98	4.16	52.80	.07	10.41	.21	.04	.18	10.96	.10	97.68	Mg' = 61.90 Ca' = 25.90 Fe' = 12.20 Mg* = 74.52
285	O	.33	18.73	2.80	53.80	.09	10.69	.10	.01	.13	9.95	.05	96.66	Mg' = 63.20 Ca' = 25.90 Fe' = 10.80 Mg* = 77.03
285	O	.53	19.14	2.81	53.71	.06	10.13	.06	.01	.26	10.33	.05	97.09	Mg' = 64.22 Ca' = 24.48 Fe' = 11.31 Mg* = 76.74
257	O	.10	17.46	1.57	52.93	.01	21.65	.06	.05	.17	4.58	-	98.58	Mg' = 49.54
	O	.16	16.89	1.09	52.29	-	22.02	.25	.13	.18	6.49	-	99.49	Ca' = 45.24
	A	.13	17.18	1.33	52.61	-	21.83	.16	.09	.17	5.53	-	99.04	Fe' = 5.23 Mg* = 84.70



## APPENDIX B (Cont'd)

## C.3. TUNICER SUITE - GAMBRO (Cont'd)

## C.3.3. Orthopyroxene

Sample	Code	Na	Mg	Al	Si	K	Ca	Ti	Cr	Mn	Fe	NI	TOTAL	Average
285	O	.01	31.73	.93	55.98	.01	1.38	.02	.02	.27	11.42	.05	102.00	Mg = 86.80
	O	.02	30.59	1.49	55.92	-	1.39	.06	.04	.27	11.50	.05	101.34	Ca = 2.76
	A	.01	31.16	1.21	55.95	-	1.38	.04	.03	.27	11.55	.05	101.66	Fe = 10.47
257	O	-	31.28	1.80	55.76	-	1.76	.02	.08	.15	10.36	.12	101.32	Mg = 87.30
	O	.01	31.50	1.39	56.23	-	1.73	.04	.08	.22	10.05	.09	101.35	Ca = 3.49
	A	.01	31.39	1.59	56.00	-	1.75	.03	.08	.19	10.21	.11	101.34	Fe = 9.20

## APPENDIX C (Cont'd)

## C.3. YOUNGER SUITE - GABARO (Cont'd)

## C.3.4 Norablanda

Sample	Code	Na	Mg	Al	Si	K	Ca	Ti	Cr	Mn	Fe	Ni	TOTAL
193	C	.91	15.59	4.04	51.11	.26	10.68	1.22	-	.21	13.59	.04	97.63
	C	.56	15.01	3.35	51.79	.12	11.68	.05	-	.17	15.13	.02	97.68
	R	.01	18.94	1.20	50.95	.02	1.73	.16	.02	.51	20.57	-	94.11
257	C	.35	19.50	3.47	52.38	.16	11.81	-	.08	.16	8.32	.01	96.24

# APPENDIX D

Microprobe mineral analysis (wt.%) of the Amphibole phase within Mafic-Dike (Sample 187).

## Amphibole

Sample	Code	Na	Mg	Al	Si	K	Ca	Ti	Cr	Mn	Fe	Ni	TOTAL
187		.67	18.16	3.64	53.37	.04	10.92	.05	.03	.19	10.21	.02	97.29
187		.91	17.89	4.12	52.85	.04	10.89	.23	-	.27	10.50	.06	97.75
187		.79	18.02	3.88	53.11	.04	10.90	.14	-	.22	10.36	.04	97.49
187		.79	17.93	3.68	53.27	.04	10.80	.03	.09	.11	10.63	.05	97.42
187		.57	18.23	2.89	55.25	.04	11.48	.25	.05	.16	9.56	.01	98.48
187		.57	18.00	4.29	53.71	.04	9.86	.15	.09	.25	11.11	.03	98.09
187		.22	19.60	1.28	55.41	.01	11.09	.05	.44	.21	9.02	.04	97.39

# APPENDIX E

Mafic Dikes - FeO\* - Total Fe

## E.1. MAJOR ELEMENTS - MAFIC DIKES

Sample	SiO <sub>2</sub>	TiO <sub>2</sub>	Al <sub>2</sub> O <sub>3</sub>	FeO*	MnO	MgO	CaO	Na <sub>2</sub> O	K <sub>2</sub> O	P <sub>2</sub> O <sub>5</sub>	LOI	TOTAL
047A	52.40	.30	11.70	5.40	.07	14.26	12.12	1.25	.04	.03	3.24	100.81
055	53.20	.40	14.40	8.38	.11	6.90	8.26	3.22	.17	.01	4.74	99.79
062	56.70	.23	9.74	6.79	.09	12.96	8.46	2.99	.17	.02	2.46	100.61
066	52.90	.23	11.60	5.54	.07	14.07	11.44	1.50	.10	-	3.46	100.93
141	54.60	.22	9.33	8.07	.14	12.88	9.34	2.75	.11	-	1.56	99.02
147	52.00	.22	12.70	8.03	.15	12.00	12.64	1.00	.12	-	1.52	100.33
155R	55.60	.18	8.62	8.66	.13	12.60	10.08	2.56	.08	-	1.60	100.11
187	54.60	.23	10.20	7.83	.13	12.61	9.92	2.68	.11	.03	1.76	100.10
188	54.80	.09	8.89	7.83	.14	14.43	9.86	2.24	.04	.03	2.50	100.89
218	50.60	.20	10.90	8.66	.14	13.72	9.90	1.11	.25	-	3.08	98.56
230	52.60	.22	13.40	3.85	.05	11.91	14.46	1.88	.04	.02	2.23	100.67
231	55.60	.20	10.00	5.89	.07	14.62	10.68	2.54	.11	-	2.34	100.05
240	56.50	.15	7.11	6.62	.13	15.95	9.96	2.37	.09	-	1.90	100.58
270	44.20	.49	9.58	17.18	.22	14.09	10.66	.18	.02	.01	3.62	100.25
401	52.40	.25	11.40	6.62	.09	12.64	10.36	1.78	.09	-	2.94	98.57
4502	54.00	.32	11.40	4.88	.07	12.00	11.22	2.88	.10	.03	3.46	100.36
4503	50.00	.36	14.30	8.08	.13	9.26	9.00	2.84	1.59	.01	4.17	99.74
4504	51.00	.26	11.50	4.38	.06	14.87	12.54	1.37	.05	-	3.31	99.34
4505	52.50	.30	11.40	4.60	.05	15.12	12.54	1.23	.05	.01	2.65	100.43
4506	51.50	.28	10.80	5.39	.07	15.82	11.72	1.38	.04	-	3.01	100.01
4507	50.20	.34	12.60	6.67	.11	13.81	10.48	1.92	.05	.11	3.90	100.19
4508	54.20	.26	10.50	8.52	.13	12.04	9.08	1.98	.21	.01	3.42	100.35
4509	57.80	.34	14.30	7.89	.10	6.34	5.84	5.16	.18	.01	2.69	100.65
4510	50.70	.20	7.92	8.25	.12	18.84	9.00	.98	.10	-	4.26	100.37
4510A	50.70	.20	7.84	8.28	.12	19.02	8.86	1.02	.13	.02	4.13	100.54
4511	54.30	.20	8.36	8.58	.14	14.43	7.56	2.61	.06	.06	4.22	100.52
4512	52.90	.20	10.70	8.51	.14	13.06	11.06	.70	.09	.03	2.41	99.80
4513	52.30	.22	10.80	8.70	.14	13.16	9.44	1.33	.23	-	3.83	100.15
4514	50.20	.24	10.90	7.84	.11	16.94	9.04	.93	.48	.02	3.70	100.42
4515	52.00	.24	10.10	7.59	.11	13.71	8.30	1.37	1.09	.01	4.02	98.54
4516	55.00	.25	12.30	4.35	.08	11.23	9.56	3.45	.13	.02	2.66	99.03
4525	53.20	.32	14.50	9.27	.15	8.92	11.60	1.60	.06	.01	.66	100.29
4526	51.90	.18	16.60	5.47	.09	11.00	10.82	2.16	.32	-	3.04	99.58
4527	55.70	.28	11.80	7.29	.09	10.37	11.32	.63	.18	.01	1.93	99.60
4528	53.10	.26	10.60	8.35	.14	12.87	9.70	1.94	.13	.03	3.14	100.26

APPENDIX E (Cont'd)

Mafic Dikes

E.1. MAJOR ELEMENTS - MAFIC DIKES (Cont'd)

Sample	SiO <sub>2</sub>	TiO <sub>2</sub>	Al <sub>2</sub> O <sub>3</sub>	FeO*	MnO	MgO	CaO	Na <sub>2</sub> O	K <sub>2</sub> O	P <sub>2</sub> O <sub>5</sub>	LOI	TOTAL
4531	56.30	.34	13.90	4.19	.04	8.08	10.16	4.30	.13	.03	2.11	99.58
4532	47.60	.26	9.82	9.17	.15	17.50	10.36	.74	.05	-	5.02	100.67
4537	51.60	.26	10.60	5.21	.07	16.28	9.70	1.70	.12	.03	4.02	99.59
4545	55.60	.20	7.91	8.02	.15	13.89	9.46	2.16	.25	-	2.82	100.46
4501	51.80	.38	15.20	9.73	.14	7.30	7.74	4.01	.27	.08	3.62	100.27
Sample duplicates												
4512	53.10	.20	10.70	8.45	.14	12.91	11.00	.69	.09	-	2.46	99.74
4514	50.30	.20	11.00	7.69	.10	17.13	9.36	1.02	.24	-	3.64	100.68
4515	47.50	.31	14.20	10.83	.18	9.91	13.12	.84	.07	-	1.48	100.44
4516	55.10	.23	13.30	4.35	.05	10.25	11.96	2.31	.47	.03	1.42	99.47

\* NOTE - Sample 4501 collected from aphyric dike which intrudes poikilitic wehrlite pluton in the Limassol Forest Massif.

Appendix E-1'

Major Elements - Diabase Dikes from Sheeted Dike Complex

077A	58.80	.92	13.70	11.37	.08	2.67	4.68	4.52	.08	.05	2.28	99.15
089	54.60	.69	14.70	9.28	.12	5.33	8.36	4.27	.42	.03	2.58	98.38
092-1B	60.00	.93	14.20	10.28	.05	2.67	6.58	3.31	.20	.04	.56	98.82
092-2B	57.10	.96	14.30	11.37	.09	4.37	7.24	3.08	.21	.05	.86	99.63
096	55.40	.96	15.00	11.90	.05	4.69	9.18	2.44	.13	.03	.46	100.24

APPENDIX E (Cont'd)

Mafic Dikes - All analysis (ppm) except Ba' values (wt.%)

E.2. TRACE ELEMENTS - MAFIC DIKES (Cont'd)

Sample	Pb	Th	U	Rb	Sr	Y	Zr	Nb	Zn	Cu	Ni	La	Ti	Ba	V	Co	Cr	Ga
047A	-	4	1	-	87	9	20	2	3	7	275	-	-	-	190	21	750	8
055	3	1	-	4	145	9	13	3	18	14	39	-	-	-	266	45	86	15
062	10	4	-	1	77	8	11	4	11	9	124	-	-	-	198	15	826	8
064	10	5	-	1	80	8	13	5	6	8	258	-	-	-	188	6	825	11
141	4	6	-	2	122	41	46	5	4	5	11	1	-	21.95	383	39	31	20
147	5	10	-	1	42	8	12	4	39	15	103	2	-	20.05	194	4	504	11
155B	3	4	-	3	18	7	11	5	26	9	90	-	-	5.89	202	-	785	11
187	-	-	-	-	64	21	11	5	23	7	109	-	-	-	209	23	764	15
188	-	-	-	-	23	4	13	3	42	12	237	-	-	.88	204	8	1035	6
218	-	4	-	6	40	6	8	2	25	7	181	2	-	-	234	14	779	10
230	3	3	-	-	91	7	11	3	3	9	133	-	-	-	193	5	430	11
231	2	3	-	-	103	7	8	4	14	7	156	-	-	7.36	158	3	1035	8
240	11	6	-	2	39	6	9	3	31	6	206	-	-	6.72	185	4	1459	8
270	3	7	-	3	13	1	9	6	74	38	129	-	-	12.28	773	5	993	12
401	-	-	-	-	127	12	12	3	15	3	179	1	-	-	223	19	684	9
4502	-	6	-	4	126	13	-	-	-	-	143	-	.26	1	228	22	588	7
4503	-	-	-	9	123	7	1	2	36	61	64	-	.37	30	228	29	217	12
4504	-	-	-	-	97	10	-	-	-	-	219	-	.24	12	178	29	685	7
4505	-	1	1	-	88	14	-	2	-	-	262	-	.27	6	196	19	821	10
4506	-	9	6	3	76	15	-	1	-	-	258	-	.24	15	198	49	995	10
4507	-	8	-	4	147	1	-	1	4	-	217	-	.27	17	195	35	633	7
4508	-	6	-	-	76	14	-	-	3	-	98	-	.24	18	256	27	709	5
4509	-	-	3	5	94	14	-	1	1	-	70	-	.34	11	250	27	71	11
4510	-	-	10	5	26	9	-	-	8	-	258	-	.20	23	191	19	1014	2
4510A	-	4	3	-	26	12	-	1	7	-	282	-	.20	19	188	35	979	4
4511	-	2	-	2	47	11	-	1	18	-	149	-	.23	18	223	16	891	4
4512	-	9	3	9	32	6	-	-	6	-	151	-	.22	21	226	43	756	9
4513	-	-	-	6	50	8	-	4	14	-	147	-	.24	31	238	26	701	9
4514	-	18	-	11	39	7	-	2	2	-	387	-	.25	20	196	40	1025	7
4515	-	7	-	5	78	9	-	1	-	-	139	-	.22	24	212	39	715	8
4516	-	2	-	-	56	12	-	1	5	-	124	-	.25	1	252	9	557	8
4525	-	10	2	3	33	16	-	-	42	52	62	-	.31	31	226	20	151	14
4526	-	5	-	-	124	14	-	3	6	2	95	-	.18	26	181	24	281	8
4527	-	3	-	-	39	11	-	-	1	24	47	-	.26	13	252	32	320	11
4528	-	-	3	6	45	15	-	4	27	4	110	-	.21	20	217	25	767	8
4531	-	4	2	-	154	17	-	-	-	-	44	-	.31	17	249	23	207	9

# APPENDIX E (Cont'd)

## Mafic Dikes

### E.2. TRACE ELEMENTS - MAFIC DIKES (Cont'd)

Sample	Pb	Th	U	Rb	Sr	Y	Zr	Nb	Zn	Cu	Ni	La	Ti	Ba	V	Ce	Cr	Ga
4532	3	-	-	2	145	13	-	2	23	-	327	-	.22	29	232	24	1094	6
4537	-	10	4	4	80	9	-	-	1	-	369	-	.27	3	208	16	1028	7
4543	-	2	-	8	89	5	-	2	38	5	109	-	.16	12	210	14	926	8
45501	-	10	2	3	128	22	-	7	-	-	-	-	.38	29	328	23	59-	14

#### Sample Duplicates

4512	-	3	-	7	40	10	-	1	7	-	152	-	.22	18	227	19	728	8
4513	6	3	-	3	54	6	8	4	63	95	44	3	-	-	295	14	61	13
4516	5	8	2	4	64	11	10	3	8	9	85	-	-	6.66	195	16	384	12
4514	-	8	-	3	57	8	13	2	11	6	423	-	-	1.37	192	6	1029	9

#### Appendix E-2'

### Trace Element - Diabase Dikes from Sheeted Dike Complex

077A	3	4	-	2	99	32	59	4	8	8	-	3	-	-	162	47	10	17
089	4	4	-	4	124	26	50	4	14	8	18	-	-	12.00	314	33	33	17
092-18	-	-	-	2	108	30	54	2	-	12	2	2	-	-	160	65	10	16
092-28	4	14	2	-	100	32	52	4	-	-	17	-	-	-	367	54	25	13
096	10	3	6	3	122	41	50	5	3	4	10	6	-	-	390	63	31	15

# APPENDIX E (Cont'd)

## Mafic Dikes

### E.2. TRACE ELEMENTS - MAFIC DIKES (Cont'd)

#### E.2.1

#### Standards for Trace Element Analysis

Data: 1984 - February

Standard	Pb	Th	U	Rb	Sr	Y	Zr	Nb	Zn	Cu	Ni	La	Ti	Ba	V	Ce	Cr	Ga
AGV-1	35	10	-	65	652	23	233	17	81	66	14	34	1	1285	141	129	15	35
G2	32	31	-	166	460	10	308	14	86	31	9	128	-	2492	48	210	22	28
GSP-1	54	103	3	247	225	22	488	30	95	48	11	148	1	1408	58	421	16	21
GSP-1	54	103	-	251	228	20	499	29	101	38	7	125	1	1388	57	408	13	24
BCR-1	15	11	-	49	328	43	191	14	123	25	18	20	2	552	427	140	40	13
W-1	4	1	-	19	184	26	96	12	84	114	77	35	1	144	259	109	126	21

Data: 1984 - August - November (4501-4545)

BCR-1	1	13	2	55	348	48	183	13	116	20	16	21	2.20	759	399	76	47	22
AGV-1	19	4	3	68	680	22	238	13	80	67	13	40	1.06	1114	121	105	25	23



## APPENDIX F

### ANALYTICAL EQUIPMENT

Major element analyses were obtained by atomic absorption spectrometry (AA) using a Perkin-Elmer digitized spectrometer. The analyses were performed by G. Andrews, Department of Earth Sciences, Memorial University. Sample sets of 24 were run including duplicate samples. A sample weight of 0.1000 g was analyzed. The samples were dissolved in a solution of 5 ml HF, 50 ml saturated  $H_3BO_3$  and 145 ml  $H_2O$  heated on a steam bath for approximately 12 hours prior to analysis.  $P_2O_5$  was determined by colourimetry and loss on ignition (LOI) was determined after heating approximately 1.5 g of sample at  $1000^{\circ}C$  for 3 hours in a muffle furnace.

Trace element analyses were performed using a Phillips 1450 X-ray fluorescence spectrometer autocalibrated against international rock standards C-2 and PCC-1. Powdered rock samples weighing 10 g were mixed with 1.3 g of phenol formaldehyde binder, pressed into pellets under 50 MPa for 1 minute and fused for 10-12 minutes at  $200^{\circ}C$ .

Mineral analyses were obtained using a fully automated JEOL JXA-50A wavelength dispersive electron microprobe with Krisel control, equipped with three spectrometers and a Digital Equipment Corporation PDP-11 computer with a teleprinter. The microprobe was operated with a beam current of 22 nanoamps and an accelerating voltage of 15 kV. Counts were made every 30 seconds or a maximum of 60,000. A beam diameter of 1-2 micrometers was used for all minerals. Bence-Albee corrections were used in data reduction and analyses were performed using a variety of calibrations based upon the appropriate standards. Values of the homogeneity index calculated with each set of analyses provided a qualitative means of determining whether analytical differences recorded between and within grains (e.g: zoning of crystals) were valid in comparison with the analytical capability of the equipment.

32 88

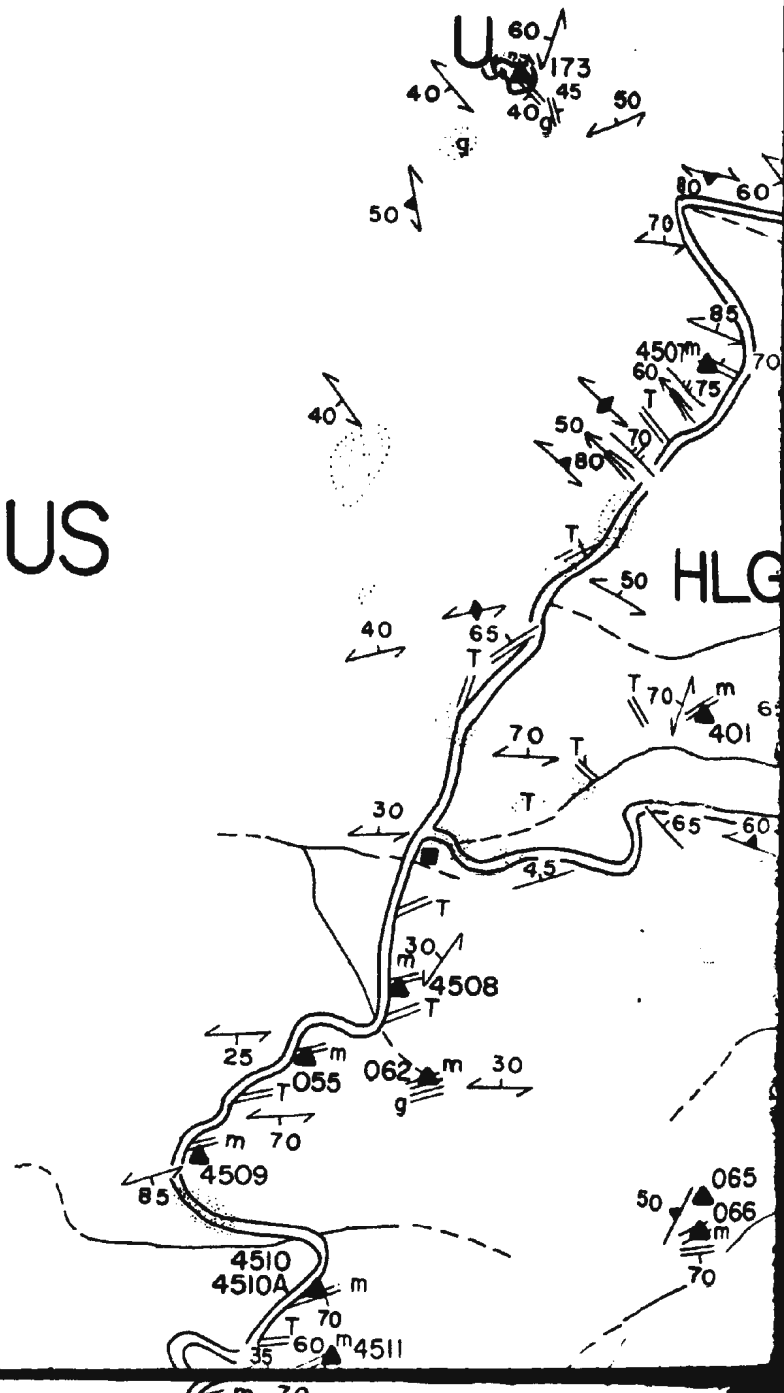
# GEOLOGICAL MAP of the PLUTONIC COMPLEX, N.W. TROC

GEOLOGY by S.M.DUNSWORTH, 1983-84

# MAP

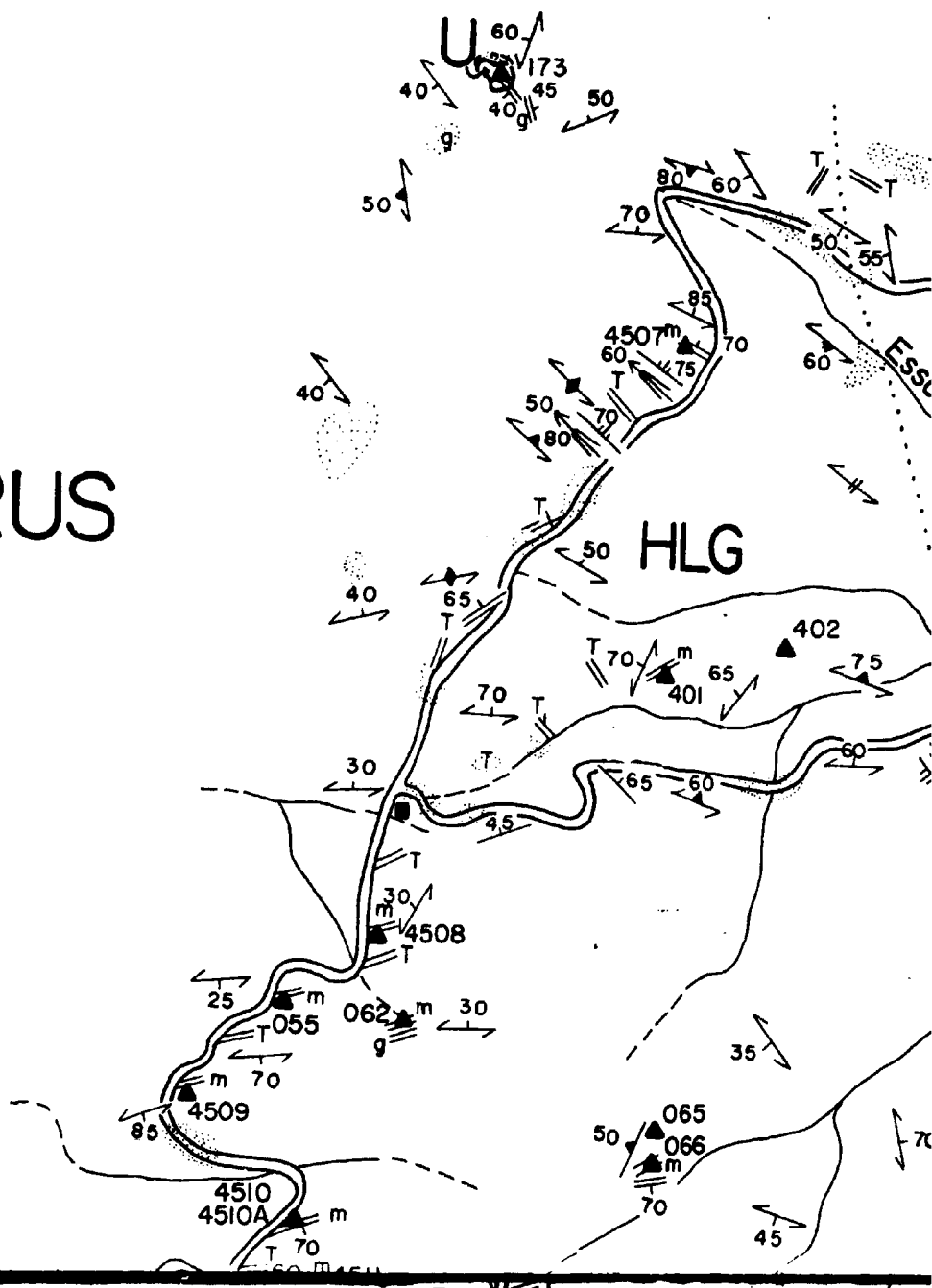
W. TROODOS, CYPRUS

TH, 1983-84



ROODOS, CYPRUS

84



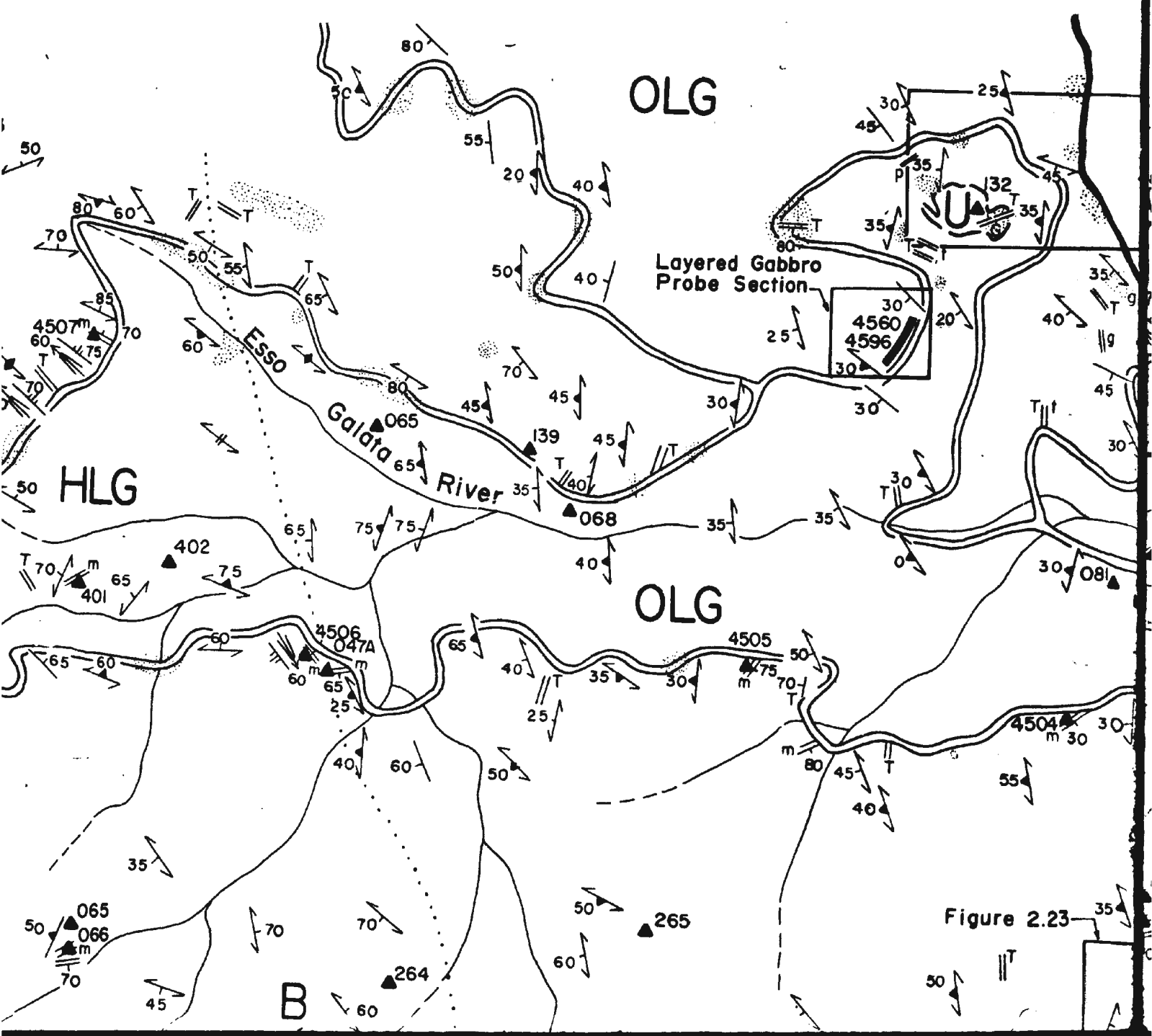


Figure 2.23

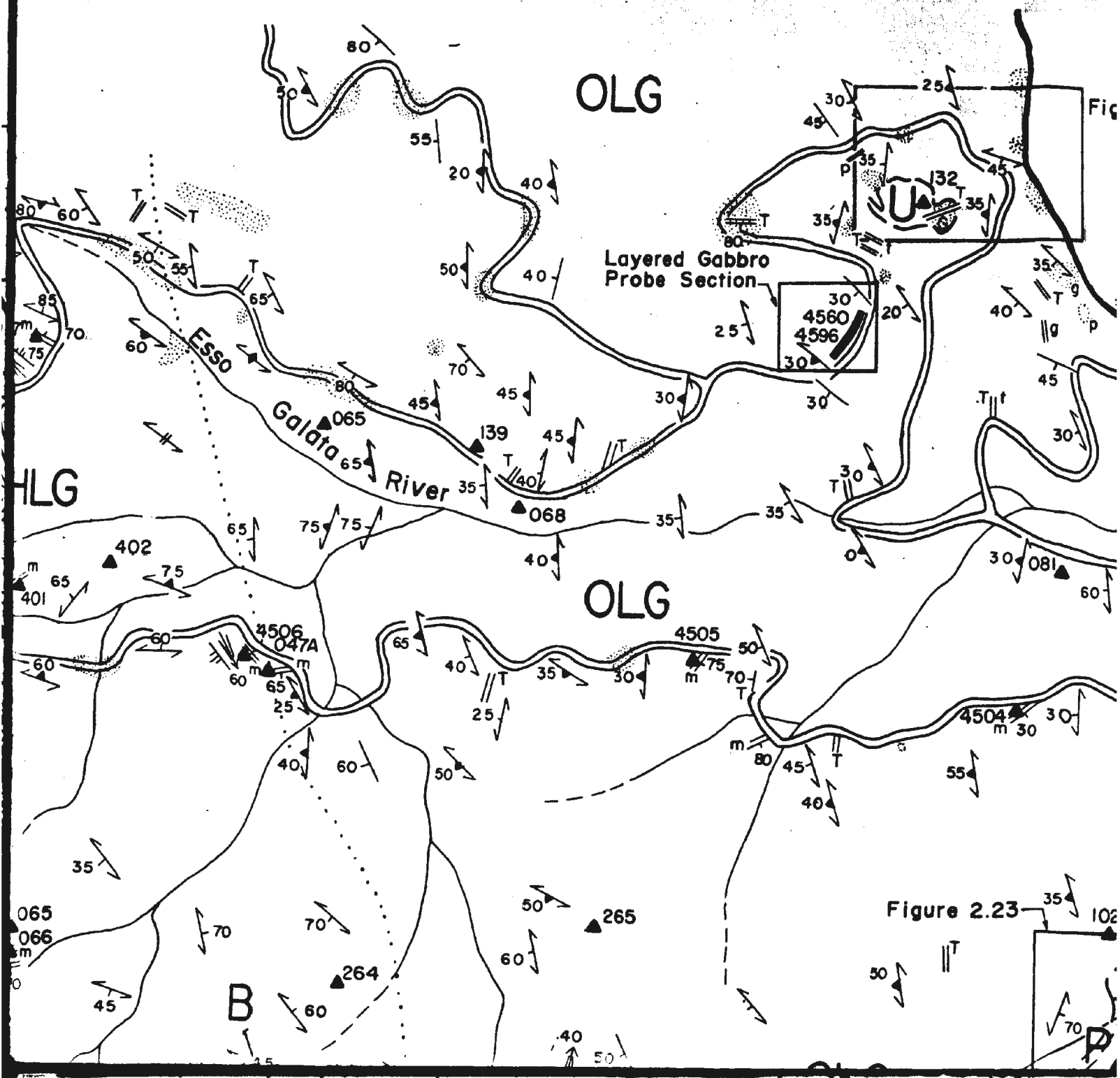
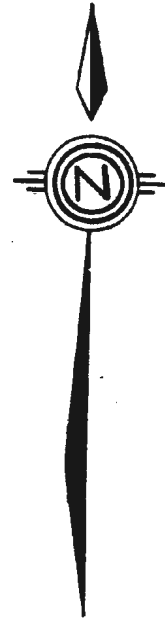
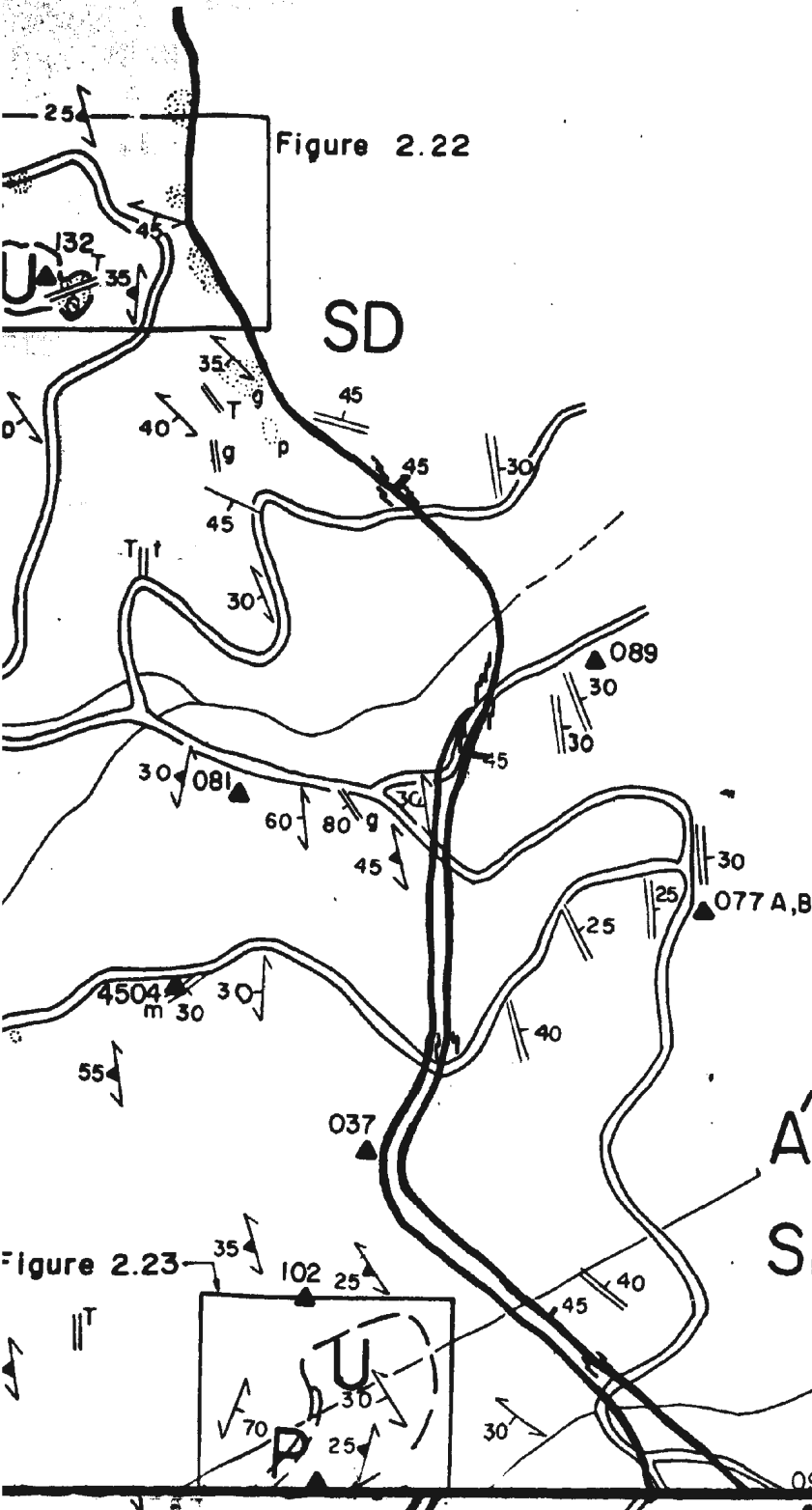
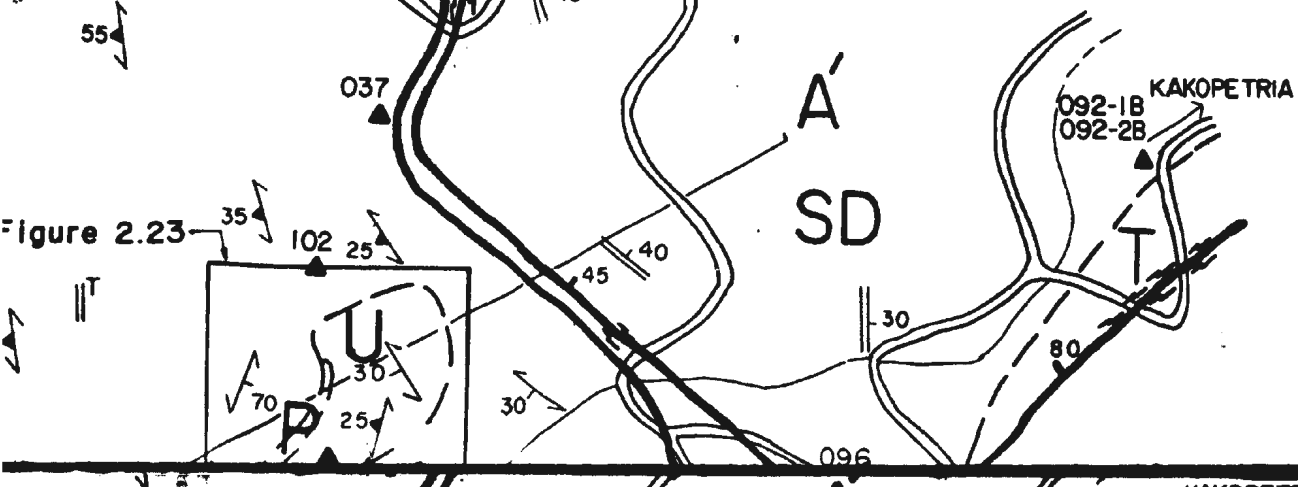


Figure 2.22

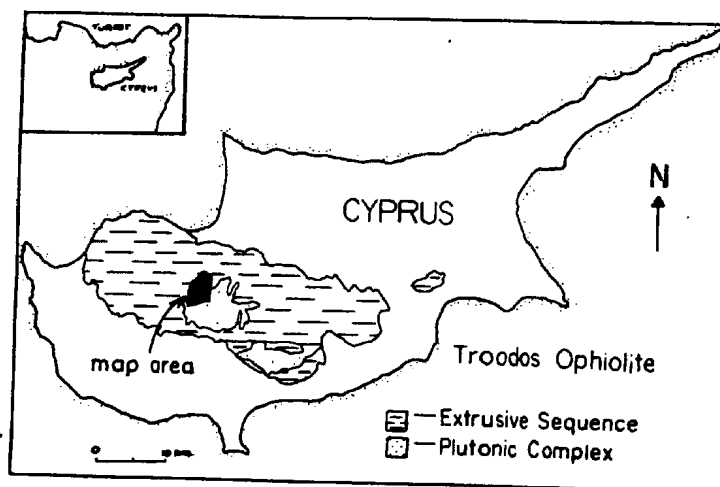
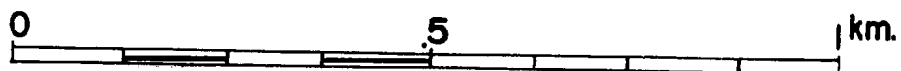


34°  
59'

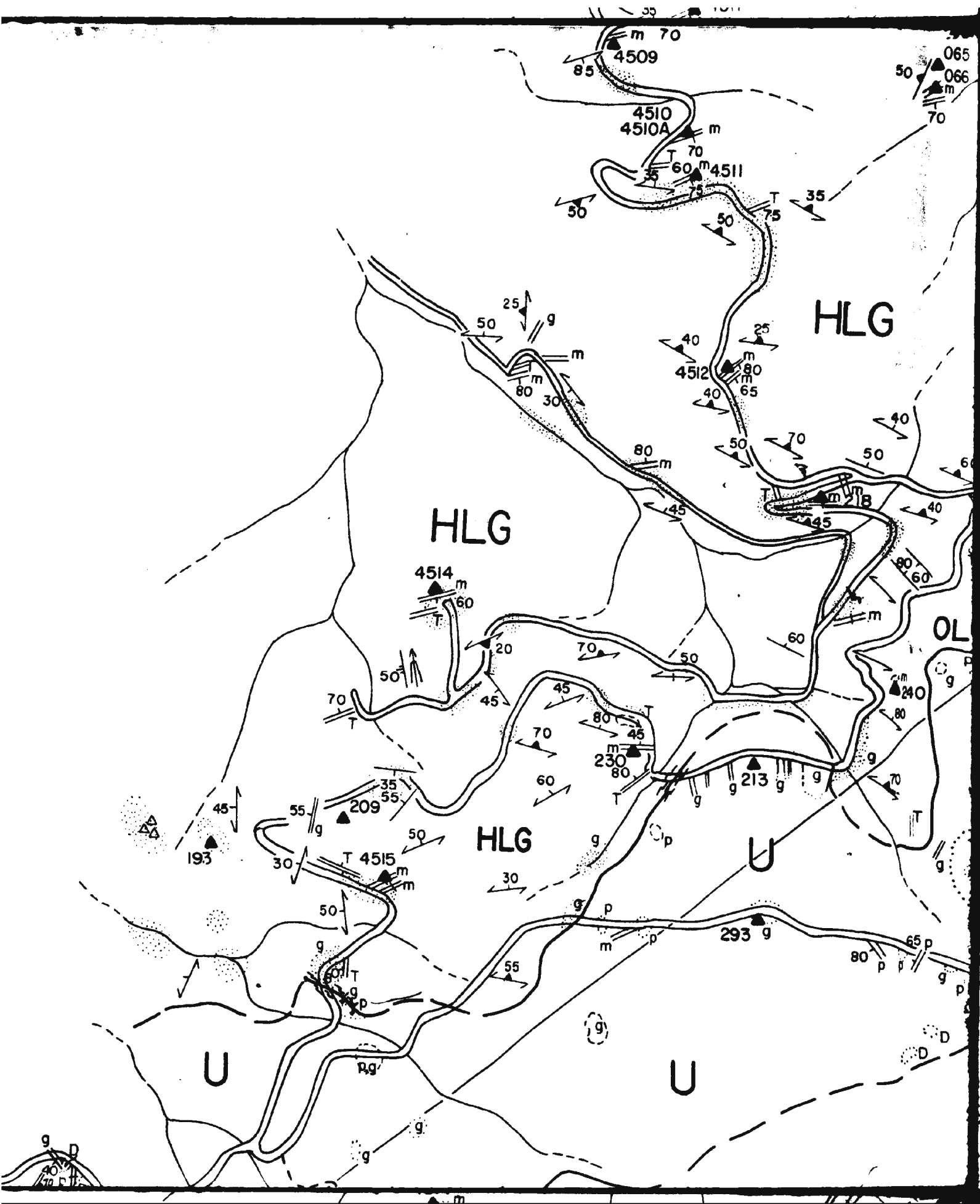
Figure 2.23

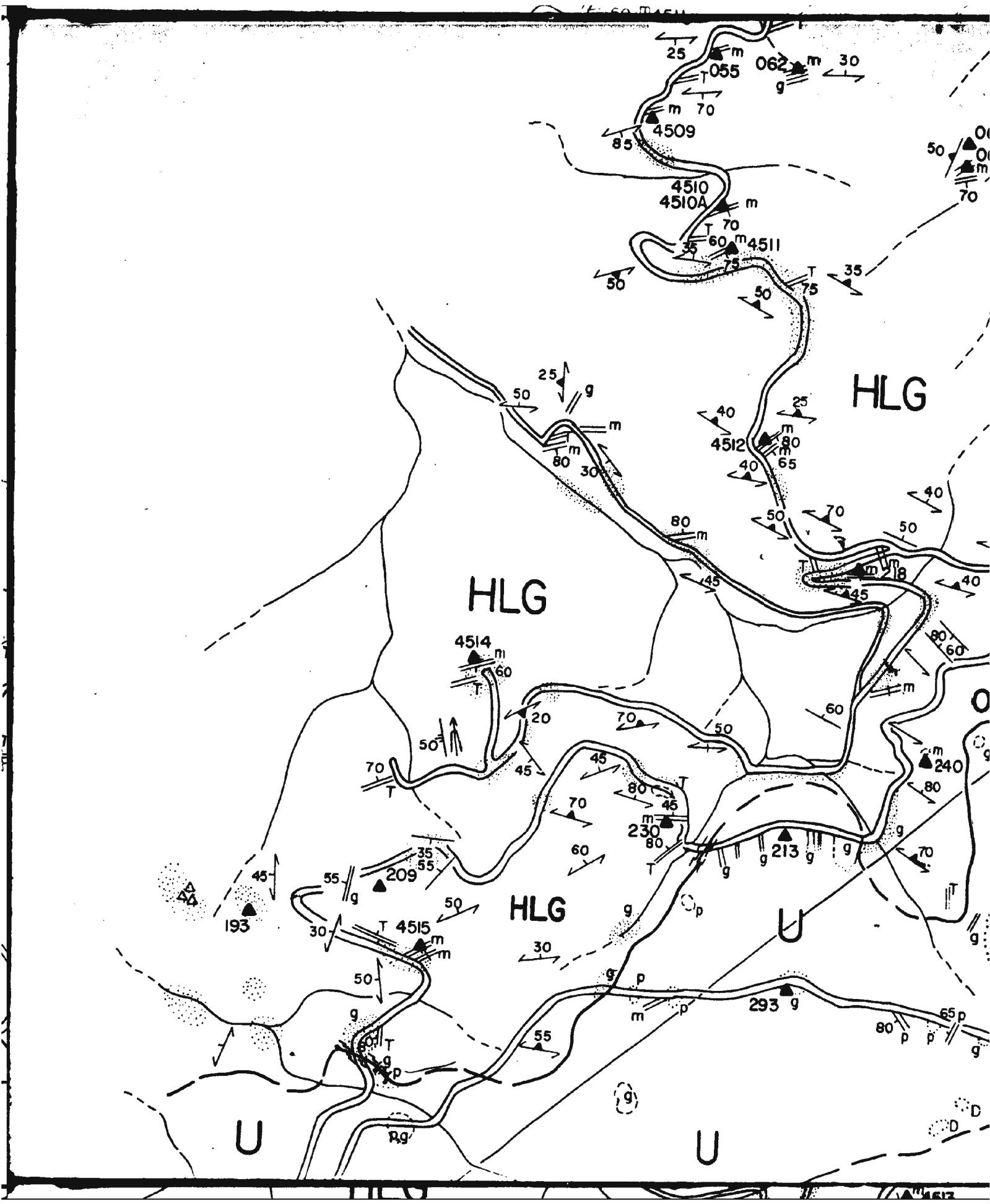


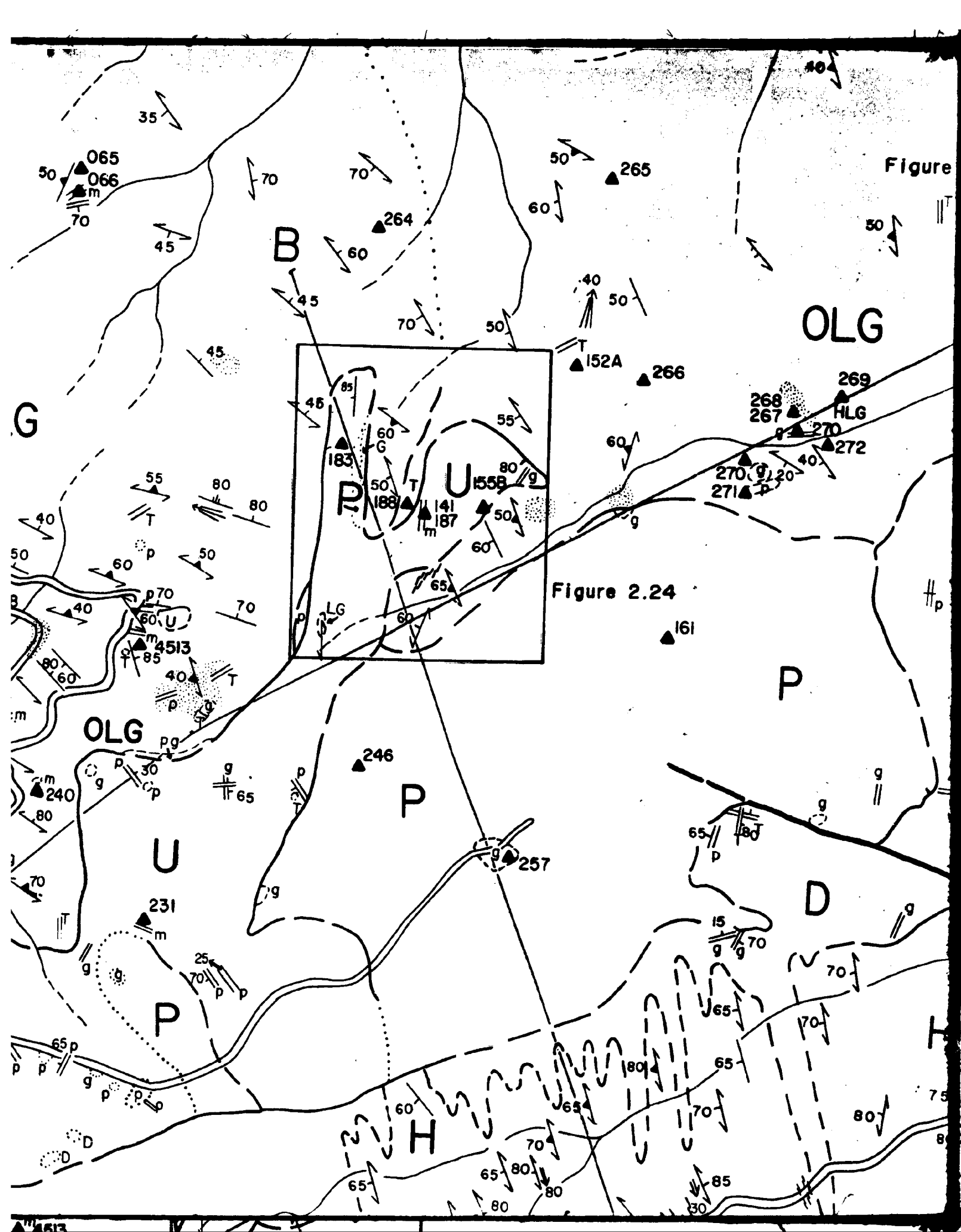
SCALE - 1:7,500

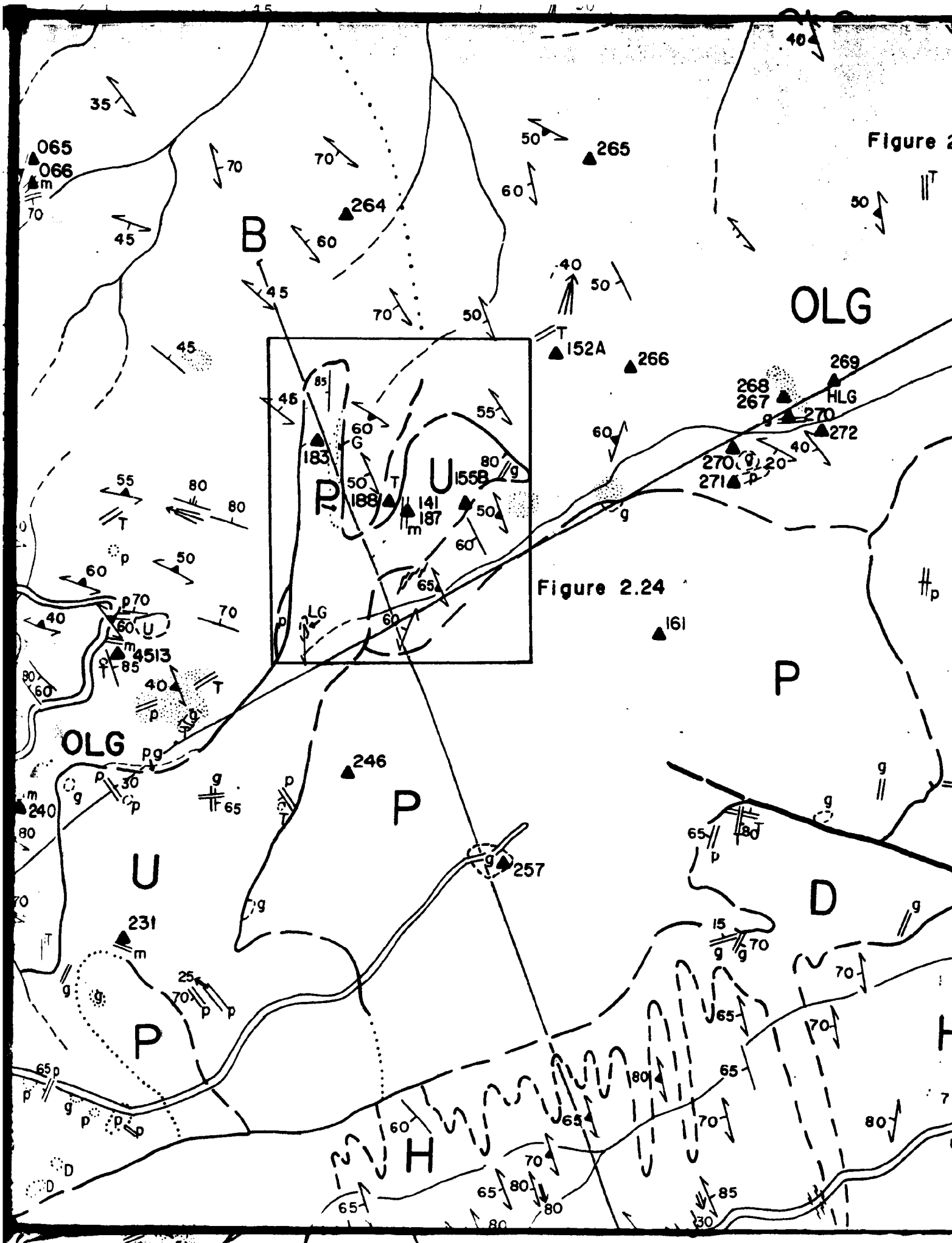


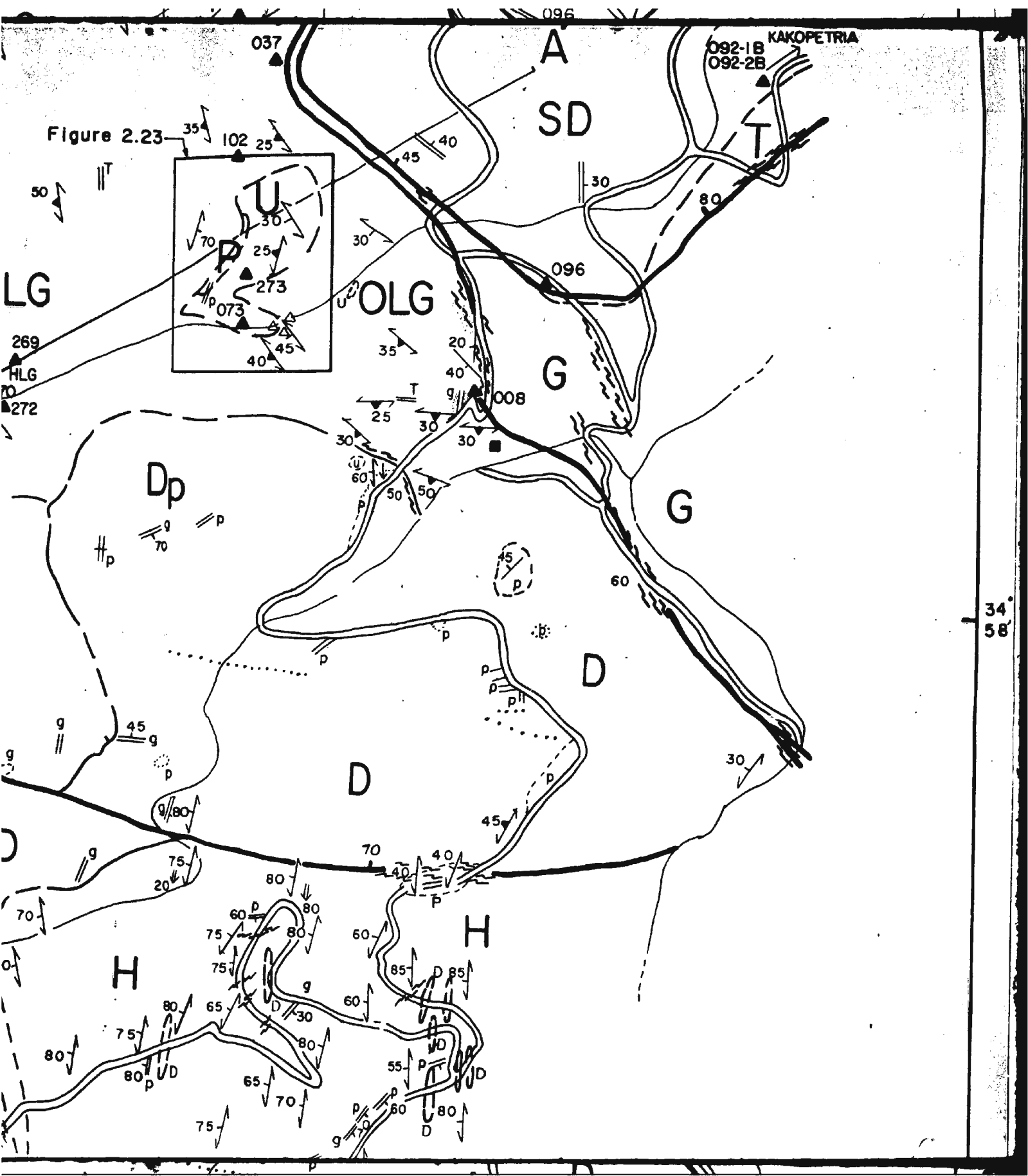




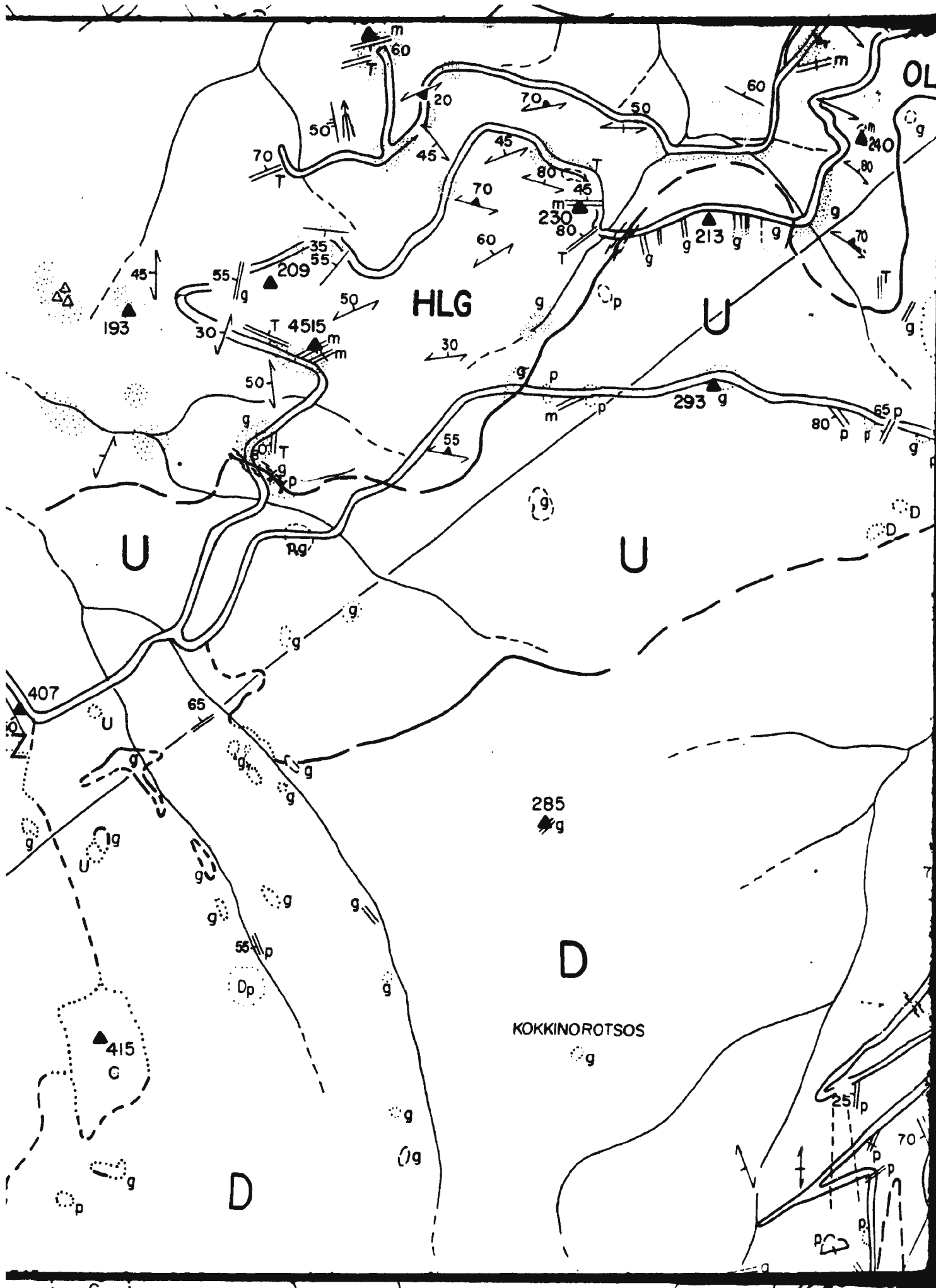


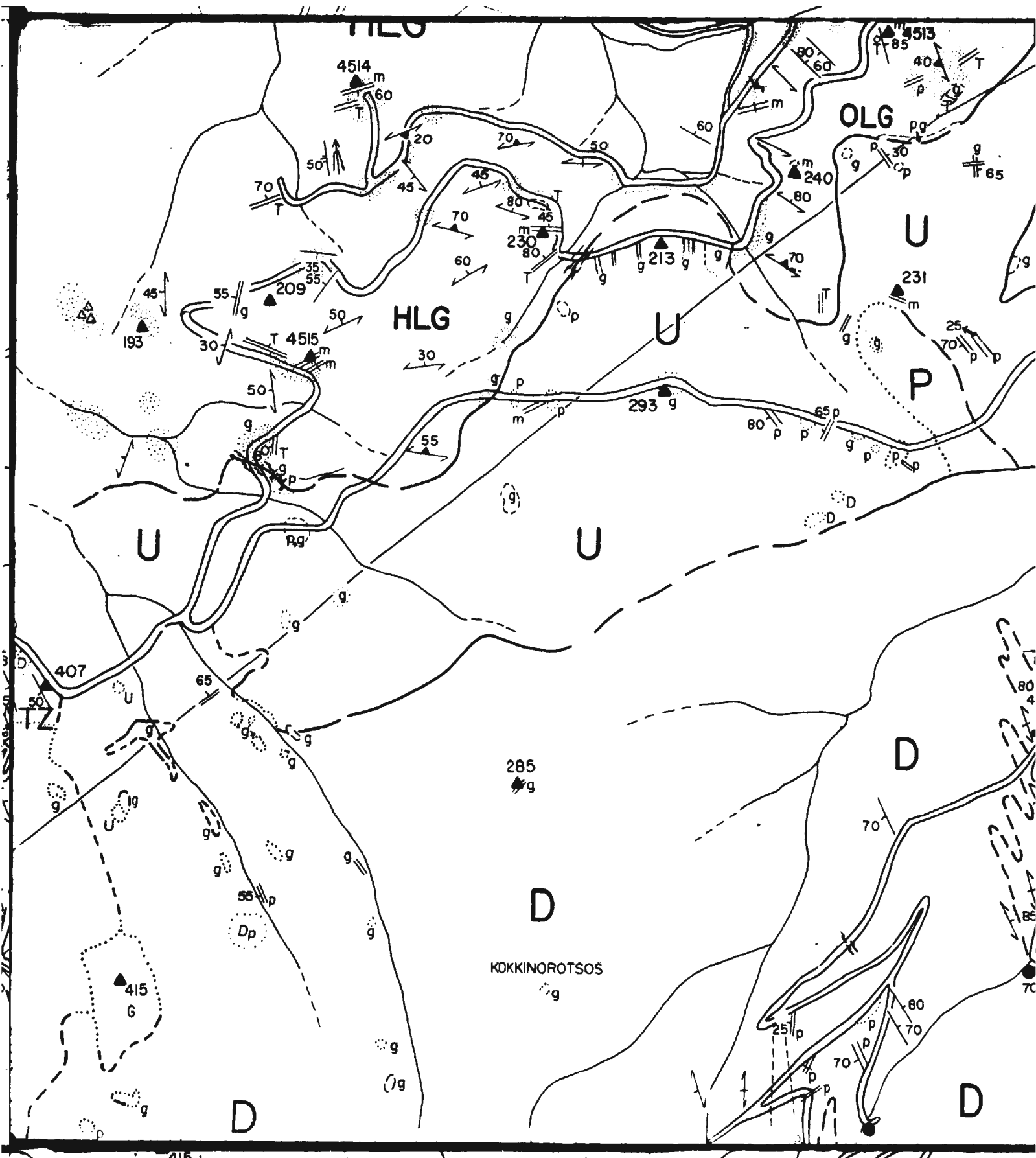




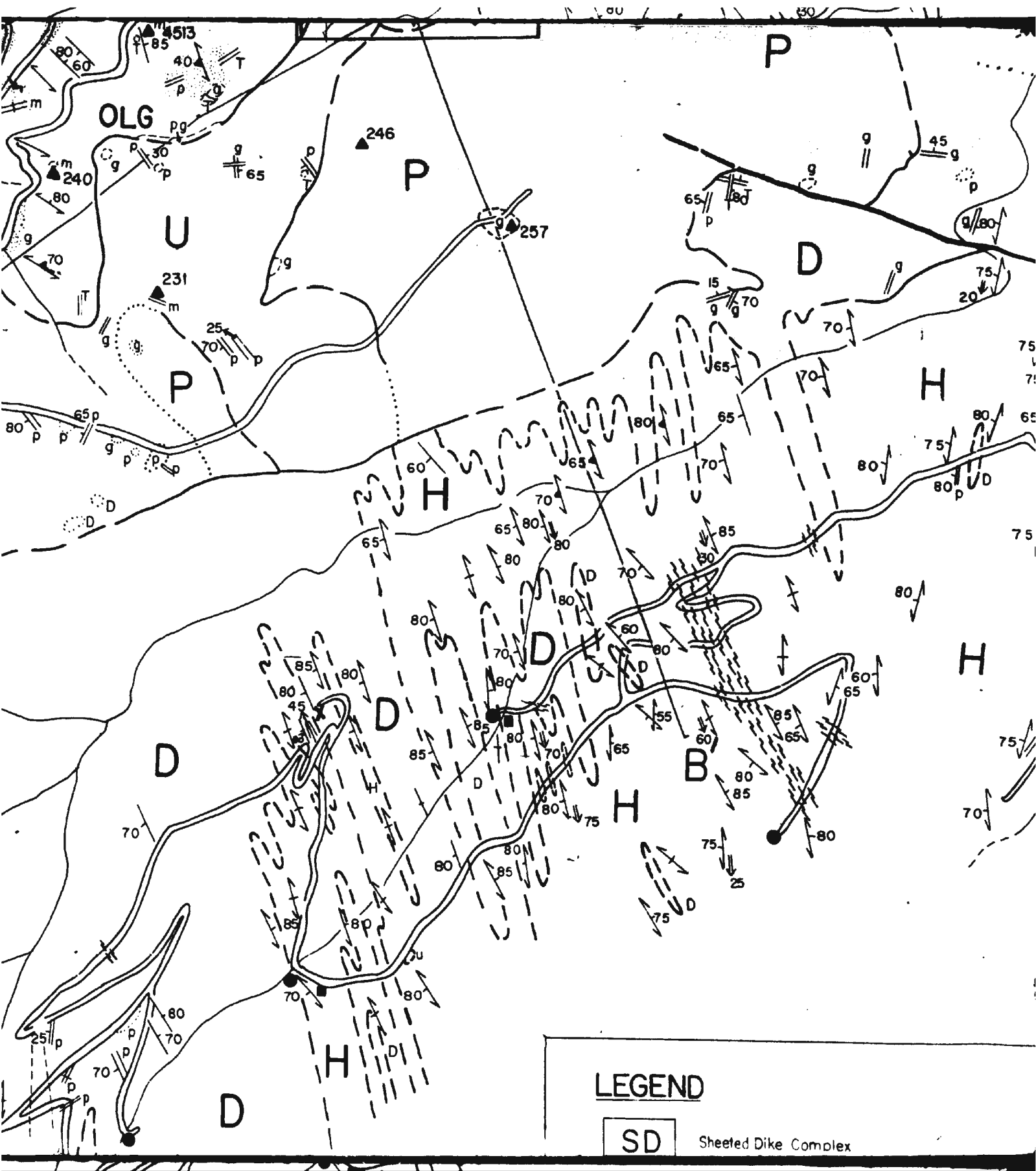


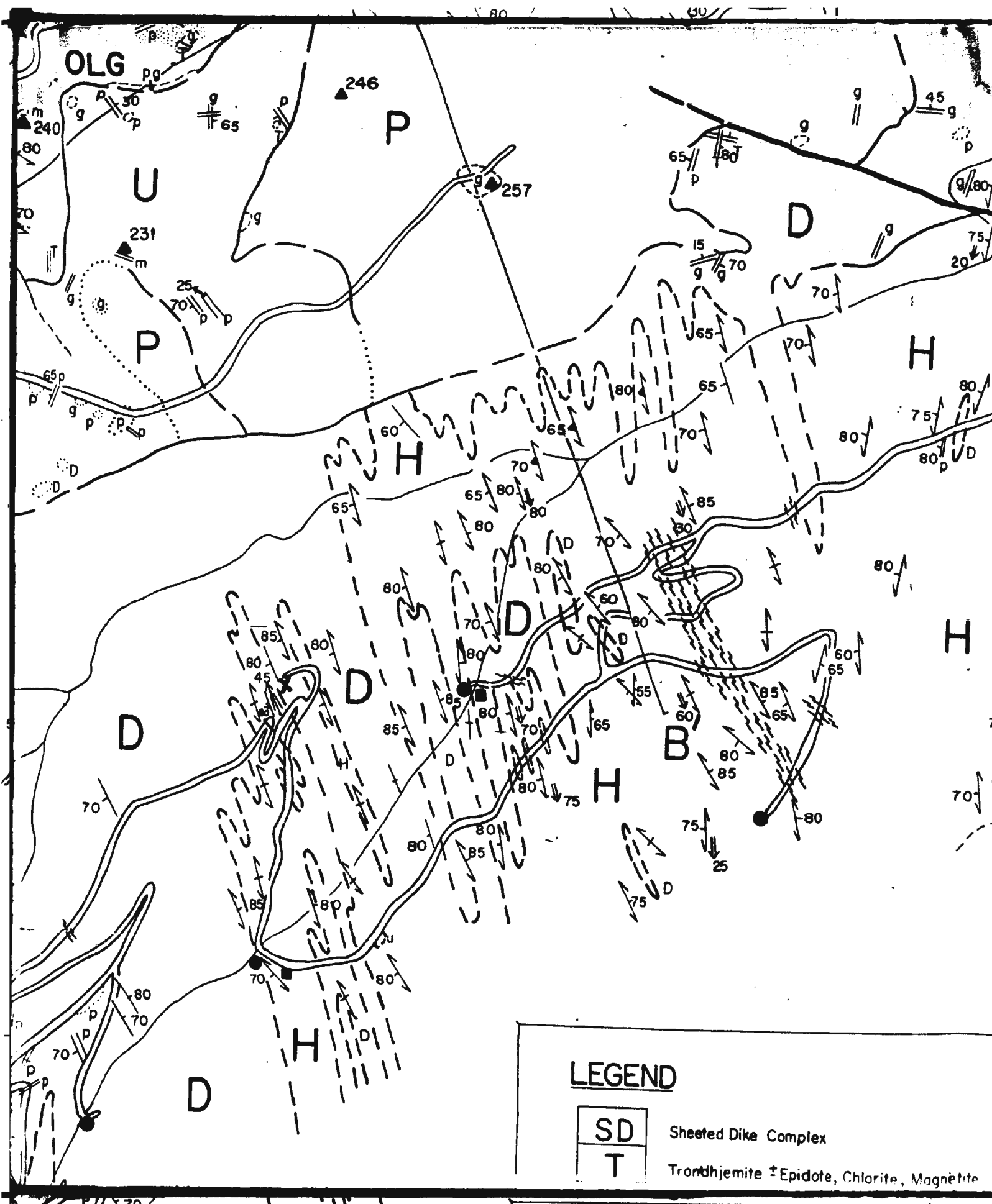


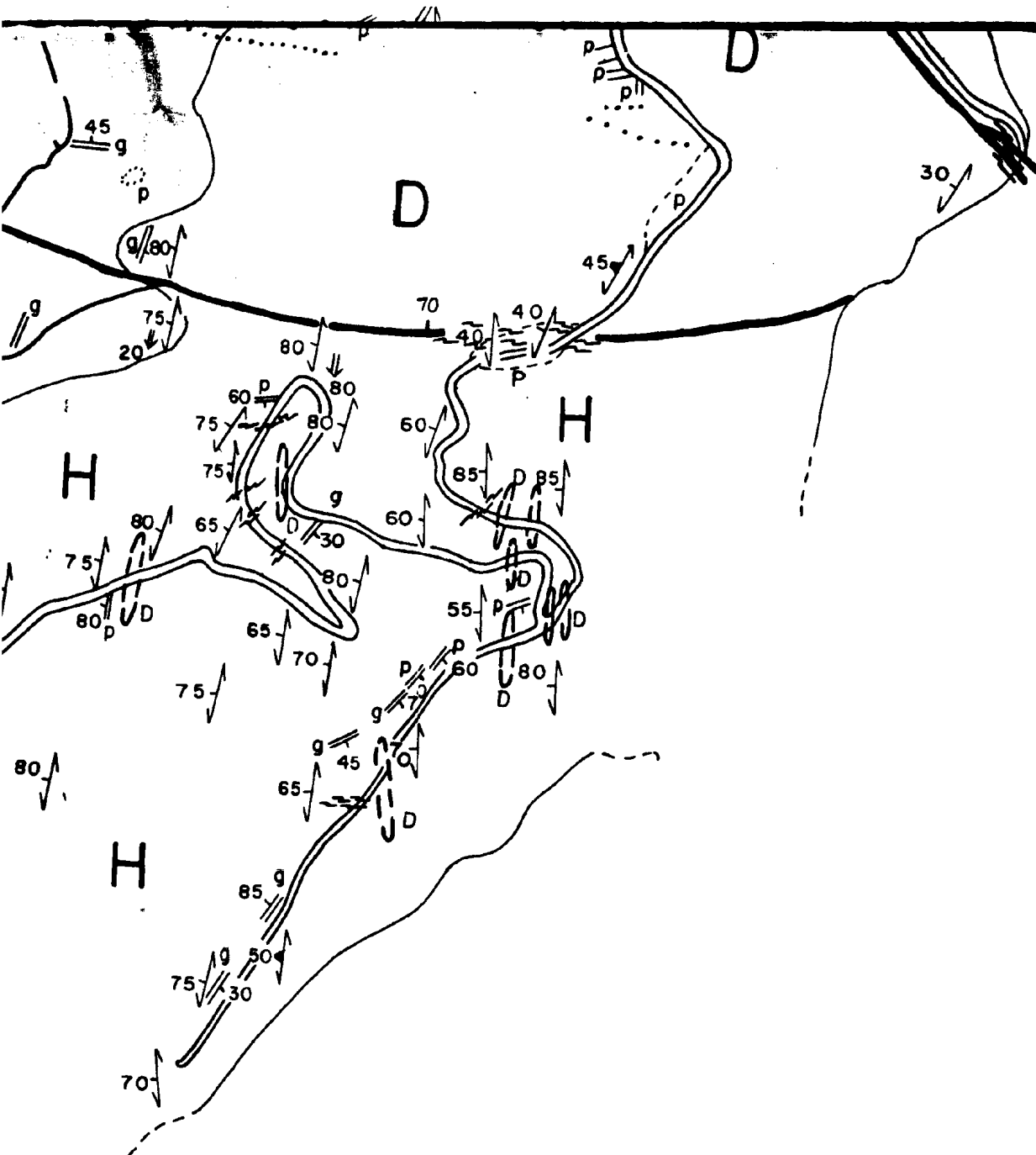





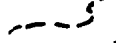






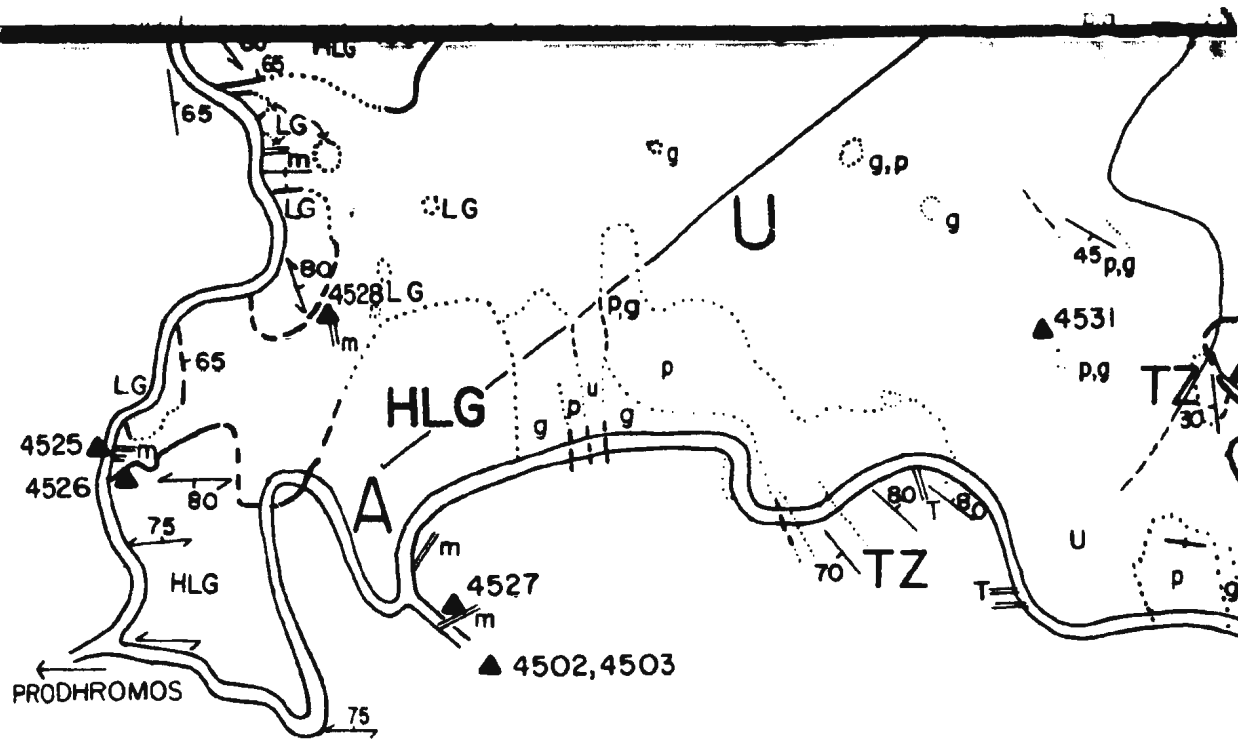


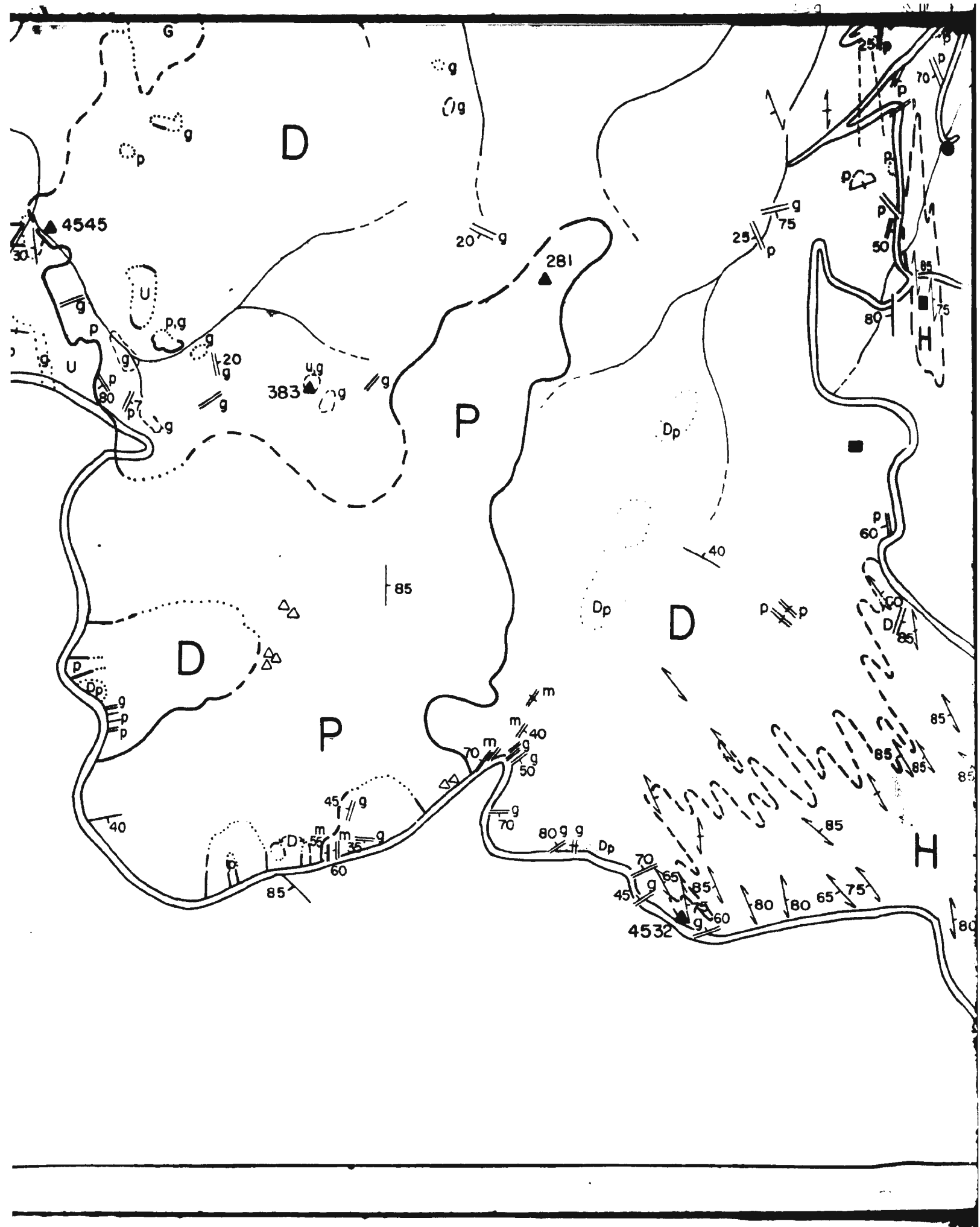
# SYMBOLS

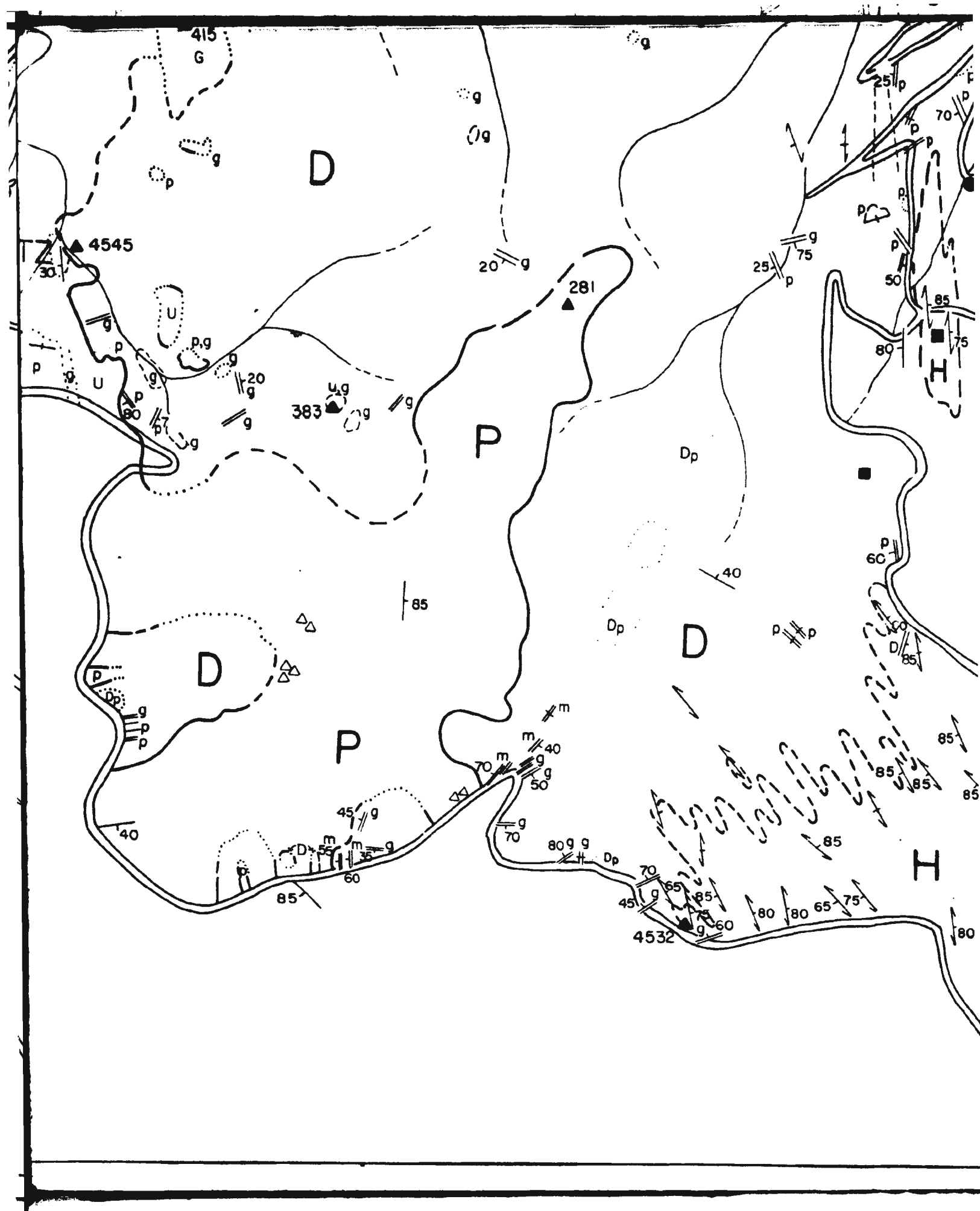
 Lithological Contact = Defined  
 Inferred

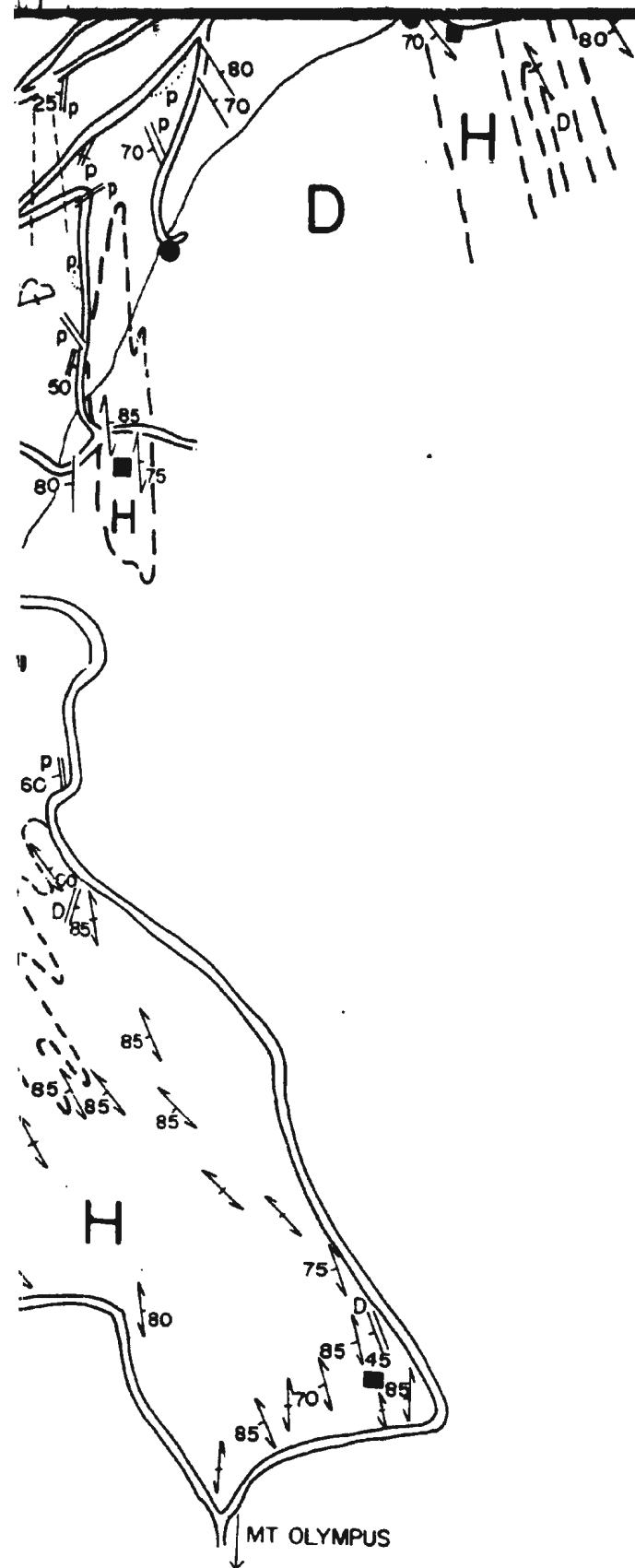
orite, Magnetite

34°  
57'

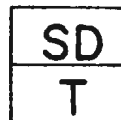








## LEGEND



Sheeted Dike Complex

Trondhjemite  $\pm$  Epidote, Chlorite, Magnetite

## EARLY SUITE



Mixed Gabbro Zone - diffuse layered gabbro  
medium to pegmatitic  
hornblende gabbro



Hypersthene Layered Gabbro



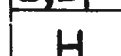
Olivine Layered Gabbro



Transition Zone = recrystallized pyroxenite  
(Opx.)



Dunite, Dunite with clinopyroxene



Harzburgite Tectonite

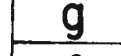
## LATER SUITE(S)



Dikes = Microgabbro



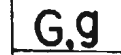
Trondhjemite



Gabbro = medium to pegmatitic



Pyroxenite = medium to pegmatitic



Gabbro - pyroxene  $\pm$  hornblende



Pyroxenite - clinopyroxene  $\pm$  websterite



Cumulate Ultramafics = Harzburgite, Lherz  
and Websterite  $\pm$  D





# SYMBOLS



Lithological Contact = Defined  
Inferred  
Gradational



Fault = Defined  
Inferred



Shear Zone



Cumulate Layering



Dike Attitude = in Sheeted Dike and  
Plutonic Complexes



Foliation = Inclined  
Vertical



Foliation, Layering



Lineation



Isoclinal Fold



Xenoliths = along intrusive contacts



Road

Stream



Building



Mine Adit



Chrome Prospect



Sample Location

lorite, Magnetite

se layered gabbro with  
im to pegmatitic pyroxene-  
lende gabbro

bro

allized pyroxenite ± olivine  
(opx.)

roxene

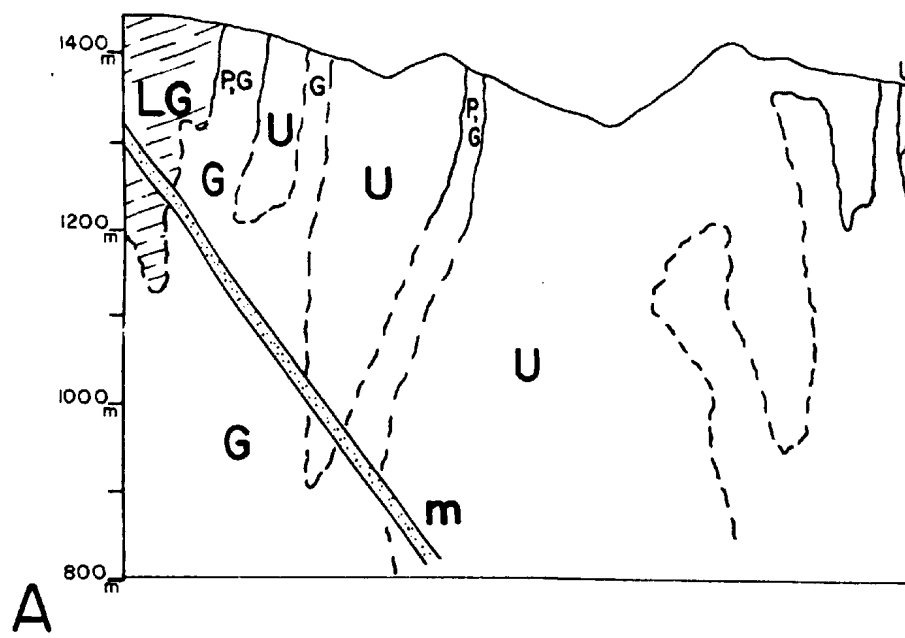
pegmatitic

n to pegmatitic

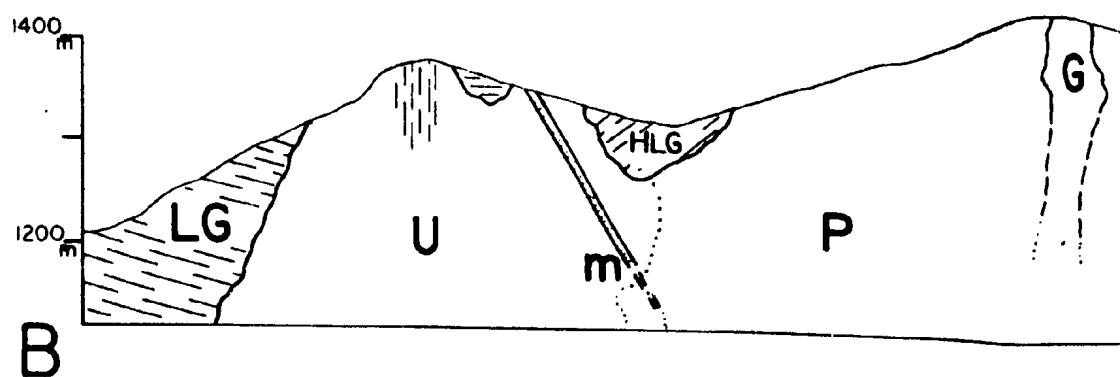
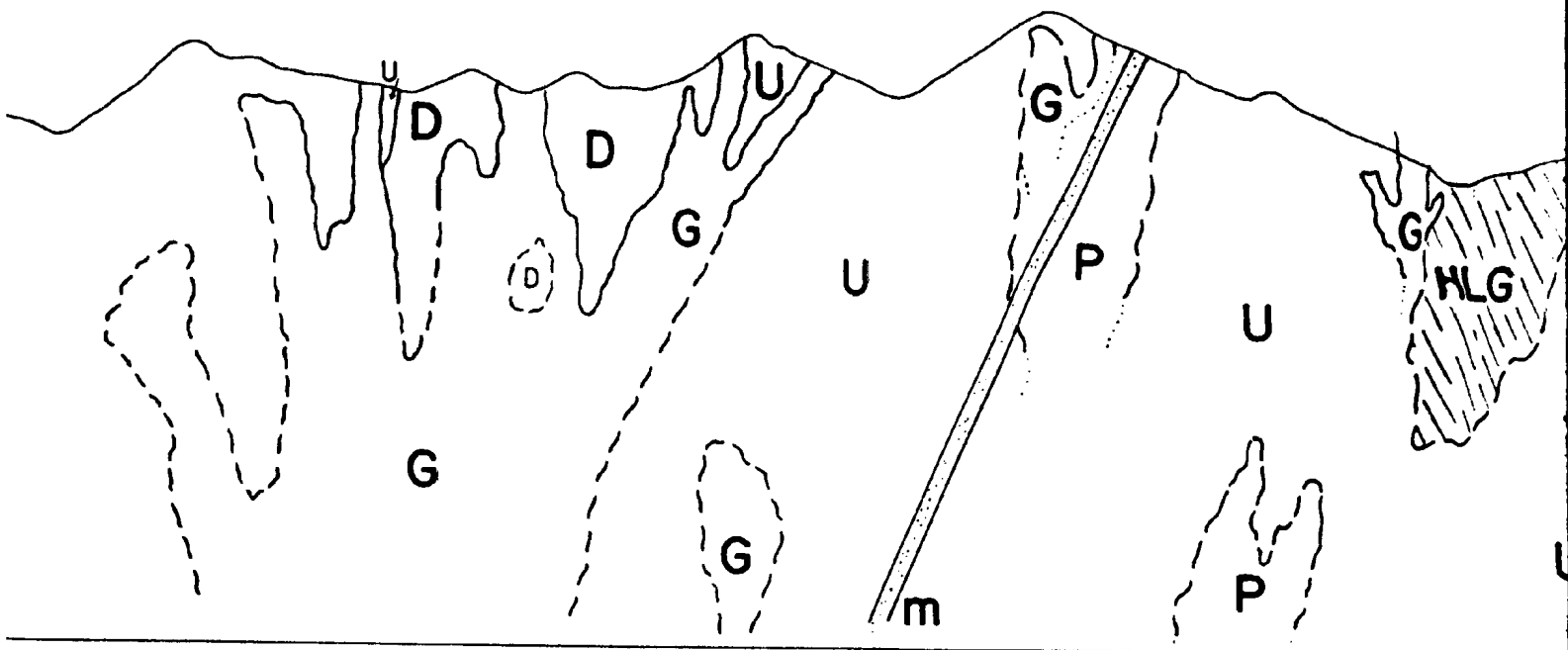
de

± websterite

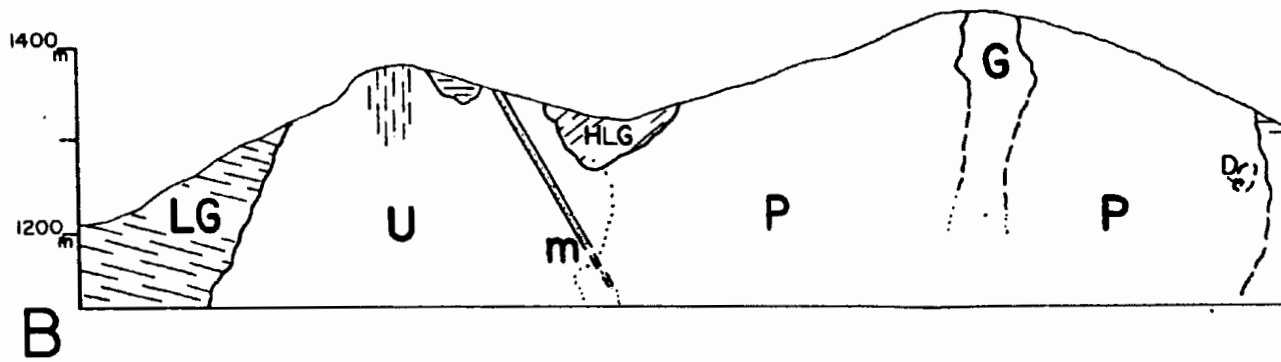
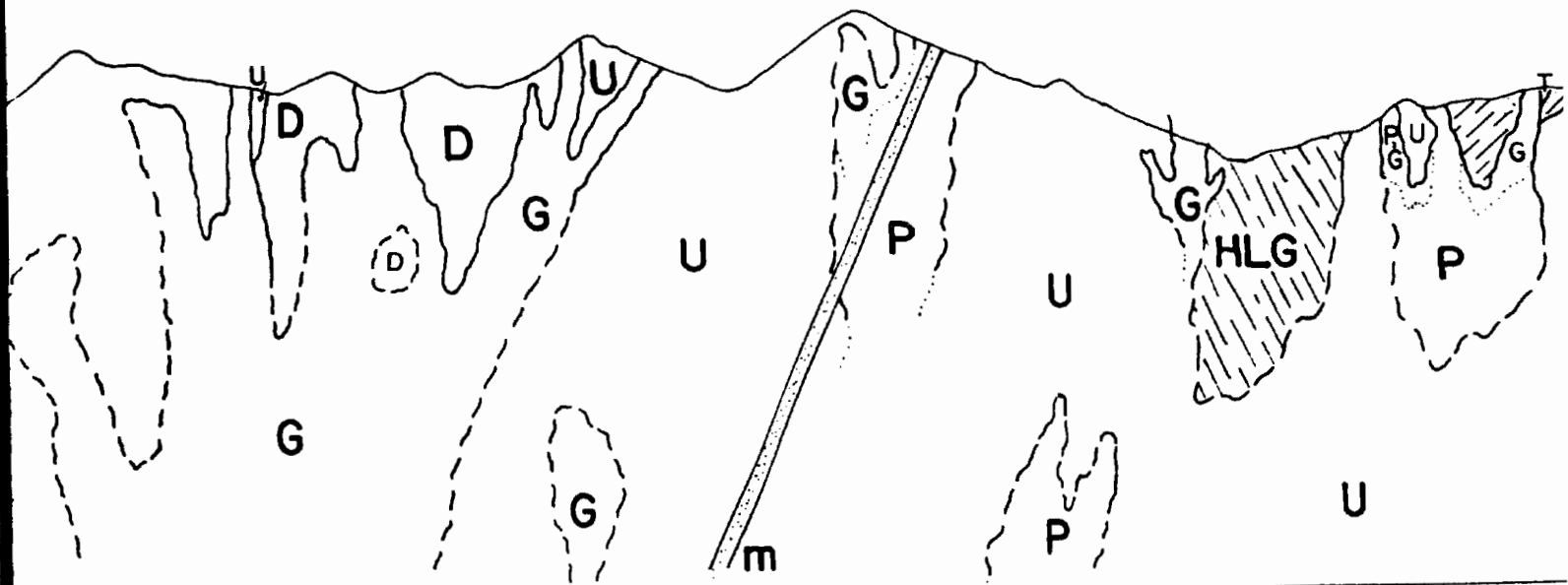
larzburgite, Lherzolite, Wehrlite  
nd Websterite ± plagioclase



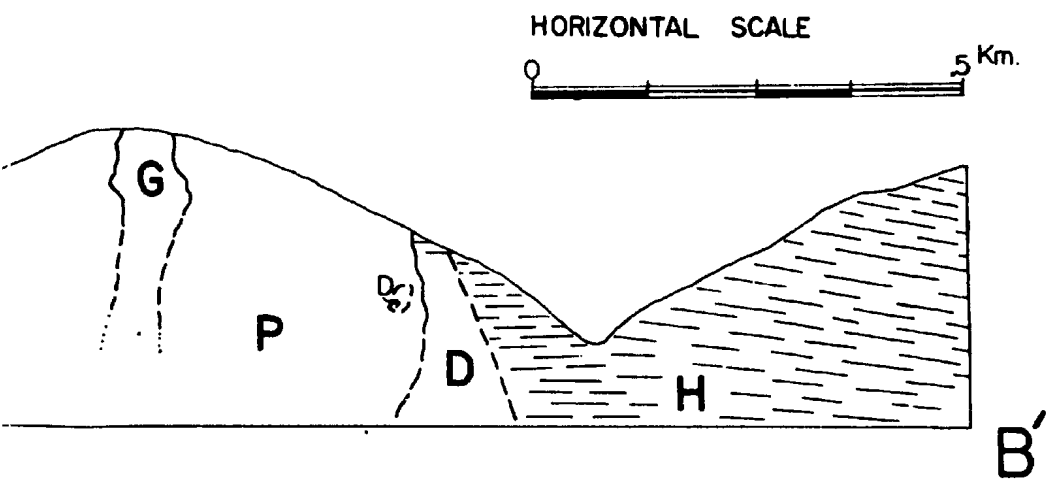
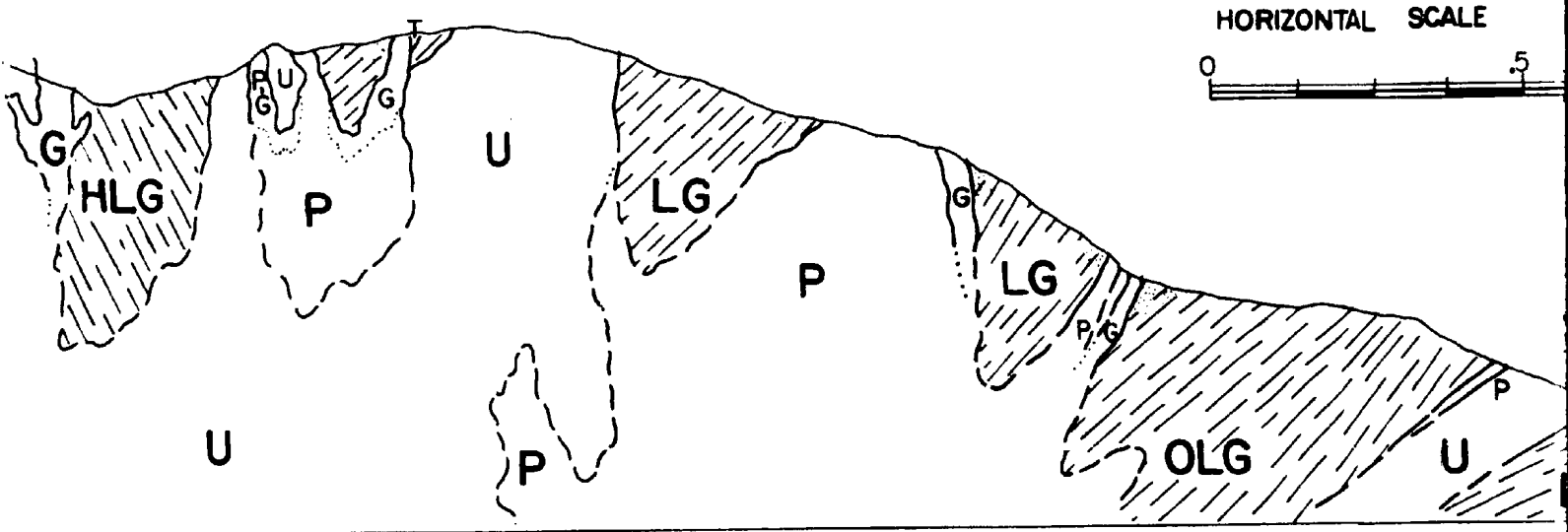
# GEOLOGICAL CRO



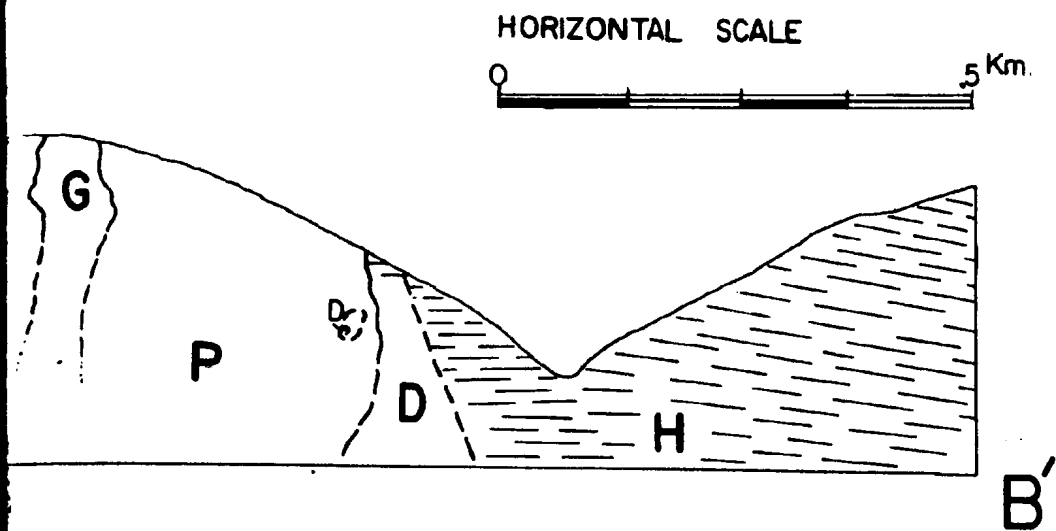
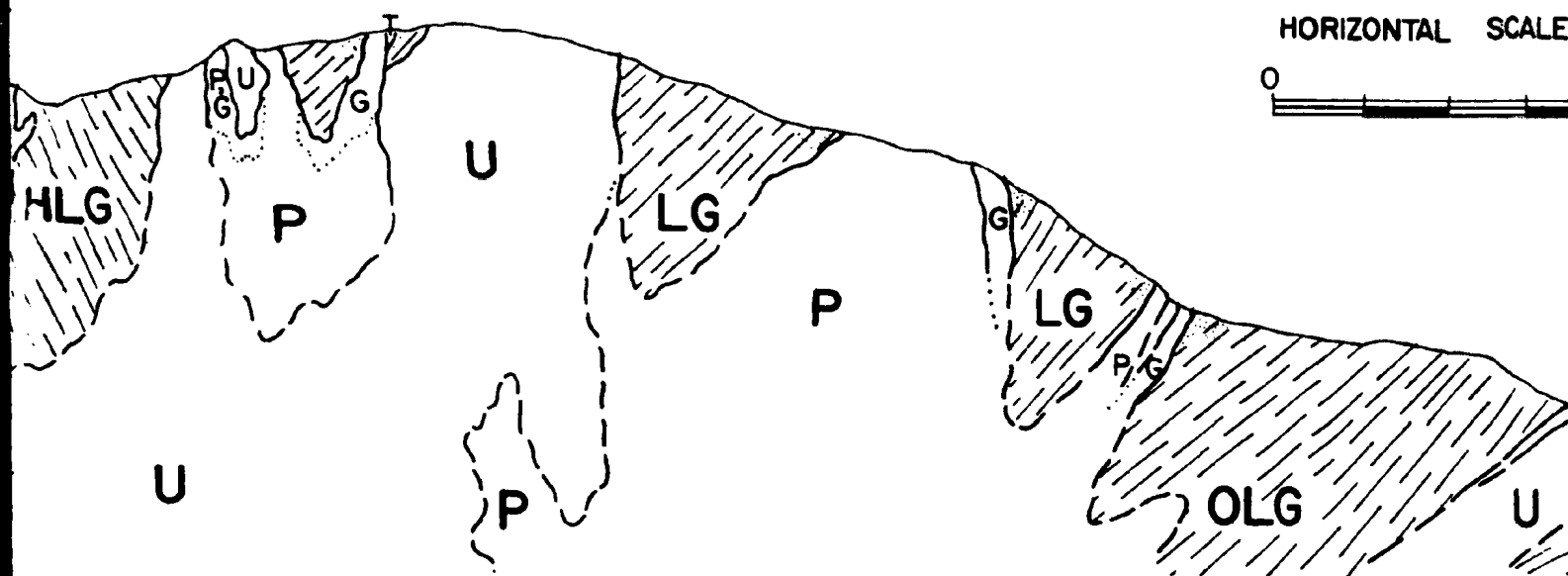
# GEOLOGICAL CROSS SECTION



# CROSS SECTIONS



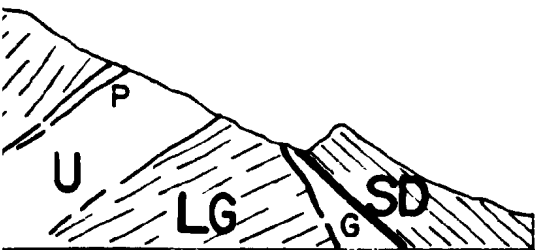
# CROSS SECTIONS



SCALE

.5

Km.



A'





